

SOLIDIFICATION ANALYSES AND HEAT TREATMENT OF MODIFIED AND REFINED Al-Si ALLOYS -A STUDY

Thesis

Submitted in partial fulfillment of the requirements for the degree of

DOCTOR OF PHILOSOPHY

by

VIJEESH V



**DEPARTMENT OF METALLURGICAL AND MATERIALS
ENGINEERING**

**NATIONAL INSTITUTE OF TECHNOLOGY KARNATAKA,
SURATHKAL, MANGALURU – 575025**

JUNE 2016

DECLARATION

by the

Ph. D. RESEARCH SCHOLAR

I hereby *declare* that the Research Thesis entitled “**Solidification Analyses and Heat Treatment of Modified And Refined Al-Si Alloys -A Study**” which is being submitted to the **National Institute of Technology Karnataka, Surathkal** in partial fulfillment of the requirements for the award of the Degree of **Doctor of Philosophy** in Metallurgical and Materials Engineering is a bonafide report of the research work carried out by me. The material contained in this **Research Thesis** has not been submitted to any University or Institution for the award of any degree.

VIJEESH V

Register No. **MT11F04**

Department of Metallurgical and Materials Engineering
National Institute of Technology Karnataka, Surathkal

Place: NITK Surathkal, Srinivasnagar

Date:

C E R T I F I C A T E

This is to *certify* that the Research Thesis entitled “**Solidification Analyses and Heat Treatment of Modified And Refined Al-Si Alloys -A Study**” submitted by **VJJEESH V** (Register Number: **MT11F04**) as the record of the research work carried out by him, is accepted as the **Research Thesis** submission in partial fulfillment of the requirements for the award of degree of **Doctor of Philosophy**.

Research Guide

Prof. K. Narayan Prabhu

Professor,

Dept. of Metallurgical and Materials Engineering,

NITK, Surathkal.

Chairman – DRPC
(Signature with Date and Seal)

ACKNOWLEDGEMENT

I express my sincere gratitude to Dr. K. Narayan Prabhu, Professor and former Head, Department of Metallurgical and Materials Engineering, NITK, Surathkal for allowing me to carry out the research work under his supervision and guiding me in the right direction throughout the project work. I also thank him for providing me the excellent experimental facilities during the project work.

I am grateful to Dr. Jaganath Nayak, Professor and Head and Department of Metallurgical and Materials Engineering, NITK, Surathkal and RPAC member for permitting me to use the laboratory facilities. I also thank to Dr. Uday Bhat, Associate Professor, Department of Metallurgical and Materials for allowing me to operate and use the XRD instrument. I also like to extend my gratitude to Dr. Ravishankar K.S for his support provided during the research work.

I profusely thank Dr. K. Rajendra Udupa, Professor and former Head, Department of Metallurgical and Materials Engineering, NITK, Surathkal and Dr. N. K.Udayashankar, Professor and former Head, Department of Physics, NITK, Surathkal and member, RPAC for their critical comments and suggestions during the research work.

I thank the Director and administration of National Institute of Technology Karnataka, Surathkal for permitting me to pursue my research work at the Institute.

My heartfelt thanks are also to all faculty members of the Department whose useful suggestions have helped me a lot.

I sincerely thank Dr. Satyanarayan, Associate Professor, Department of Mechanical Engineering, Alvas Engineering college, Moodabidre, for his help during surface roughness analysis and microstructure studies. I also extend my thanks to Dr. Ramesh, Assistant Professor, Shastra University, Tamil Nadu, for his valuable suggestions during casting experiments.

I thank my colleagues Ms. Mrunali Sona Mr. Vignesh Nayak, Mr. Sudheer Rajagopalan, Mr. Pranesh Rao and Mr. Sanjay Tikle of the Casting Research Center, Department of Metallurgical and Materials Engineering, NITK, Surathkal for their help, suggestions and cooperation.

I also thank Ms. Rashmi Banjan for her support in connection with usage of scanning electron microscope.

I am also obliged to Mr. Vasant, Mrs. Sharmila, Mr. Sundar Shettigara, Mrs. Vinaya, Mr. Giriyappa, Mr. Ramachandra, Mr. Lokesh, Mr. Yashwanth, Mr. Satish, Mr. Dinesh and all technical and non-technical staff of Metallurgical and Materials Engineering Department for their whole hearted help during the course of my work.

I wish to thank Mr. Harishankar, Mr. Sunil Jose, Mr. Balaji, Mr. Amarnath, Mr. Ramakrishna Devananda, Mr. Abu Baker Siddique, Mr. Srinivasan, Mr. Mahesh, Mr. Avin, Mr. Pradeep Bhagawath and Mr. Kiran Bhat, M. Tech students for their support and cooperation during the research work. I also wish to thank Mr. Arun Ashok Rao, Final year B.Tech. student at NITK for his help during the thesis work.

A special thanks to Dr. Rijesh M, Assistant Professor, Amal Jyothi Engineering College, Kottayam, Kerala and former research scholar, Department of Metallurgical and Materials Engineering, NITK, Surathkal, Mr. Abinav K Nair, Research scholar, Department of Chemical Engineering, NITK and Mr. Gibin George, Research scholar, Department of Metallurgical and Materials Engineering, NITK, Surathkal for their encouragement and help during my project work.

I would like to thank Mrs. Melby Chacko, Mrs. Akshatha Patil, Dr. Kripa Suvarana, Mr. Arun Augustin, Mr. Prasanth, Mrs. Jayalakshmi and Dr. Prakrithi Sreenath for their help and support during my project work. I also thank all my friends of NITK for their support and cooperation during my stay in the institute hostel.

I am greatly indebted to my parents and brothers, for their love, constant encouragement, patience and support. I would also like to extend huge, warm thanks to my wife Mrs. Pooja M. My Son Anirudh Krishna who was born before this thesis was completed deserves lots of love and appreciation for cheering me up with his beautiful smile.

Finally, I thank all those who directly / indirectly helped me to complete the research work.

VIJEESH V

Abstract

The present work involved the study of the effect of addition of cerium (Ce), phosphorus (P) and strontium (Sr) on cooling curve parameters, heat transfer characteristics, microstructure and mechanical properties of Al-8Si, Al-13Si, Al-14Si and Al-22%Si alloys. Melt treated alloys were solidified against sand base and against stainless steel, brass, and copper chills to assess the effect of cooling rate on silicon morphology. Thermal analysis parameters of melt treated alloys were determined by recording the temperature of the liquid metal solidifying against the chill. The addition of Ce significantly influenced both primary and eutectic phase nucleation temperatures and increased the undercooling temperatures. Newtonian and Fourier analysis techniques were used for the calculation of solid fraction and latent heat of solidification. The heat flux across the casting/chill interface was estimated using inverse modeling technique. The interfacial heat flux between the chill and the alloy increased with Ce and Sr melt treatment and decreased on addition of P. The effect of melt treatment and chilling on microstructure was assessed by measuring (i) the grain size (ii) roundness of eutectic silicon (iii) fineness of primary silicon. Ce treated alloys solidified against sand base at a slow cooling rate resulted in refinement of eutectic silicon along with the formation of Al-Si-Ce ternary intermetallic compound. The addition of Ce to alloys solidified against chills resulted in complete modification of the eutectic silicon. The addition of Ce also resulted in fine equiaxed grains in Al-8Si alloys and refined the primary silicon in hypereutectic Al-Si alloys. The addition of Ce simultaneously modified and refined both primary and eutectic phases, whereas, Sr and P modified eutectic silicon and refined primary silicon respectively. On addition of Ce, P and Sr there was a significant improvement in the mechanical properties of the alloys. The combined addition of Ce with Sr to Al-Si alloys resulted in further improvement of mechanical properties. Al-8Si, Al-14Si and Al-22Si alloys were subjected to T6 heat treatment. The ageing temperature and time were selected based on a series of trial experiments. The tensile strength of all untreated alloys increased when subjected to heat treatment, whereas, the heat treatment had deleterious effect on the mechanical properties of melt treated alloys except on P treated alloys.

Keywords: Melt treatment, thermal analyses, Newtonian and Fourier analysis, heat transfer, hypereutectic Al-Si alloys, eutectic silicon, primary silicon, modification, refinement.

CONTENTS

<i>List of Tables</i>	<i>iv</i>
<i>List of Figures</i>	<i>v</i>
<i>Nomenclature</i>	<i>xiv</i>
CHAPTER 1: INTRODUCTION	1
1.1 Scope of the present investigation	1
1.2 Objectives	3
1.3 Contents of the Thesis	4
CHAPTER 2: LITERATURE REVIEW	5
2.1 Aluminum silicon alloys	5
2.2 Melt treatment of Al-Si alloys	9
2.2.1 Grain Refinement	9
2.2.2 Modification	14
2.2.3 Simultaneous addition of refiner and modifier	19
2.2.4 Melt treatment by Rare Earth (RE) addition	20
2.2.5 Effect of cerium (Ce) on Al-Si alloys	23
2.3 Rapid Solidification	25
2.4 Heat Treatment	29
2.4.1 Solution treatment	30
2.4.2 Quenching	35
2.4.3 Ageing	35
2.5 The combined effect of modification/refinement and heat treatment on Al-Si alloys	38
2.6 Assessment of modification/Refinement	40
2.6.1 Computer Aided Cooling Curve Analysis (CACCA)	41
2.7 Heat transfer studies	48
2.8 Summary of Literature	50
CHAPTER 3: MATERIALS AND METHODS	52
3.1. Materials	52

characteristics of Al-13Si alloy	150
5.4.3 Effect of Ce and P melt treatment on microstructure	
characteristics of Al-14Si alloy	155
5.4.4 Effect of Ce and P melt treatment on microstructure	
characteristics of Al-22 Si alloy	161
5.5 Effect of Ce and Sr/P on the mechanical properties of Al-Si alloys	166
5.5.1 Al-8Si alloys	166
5.5.2 Al-13Si alloys	170
5.5.3 Al-14Si alloys	173
5.5.4 Al-22Si alloys	176
5.6 Effect of T6 heat treatment on the mechanical properties of melt treated	
Al-Si alloys	178
5.7 Effect of combined additions on thermal parameters, microstructure and	
tensile properties of Al-Si alloys	190
5.8 Role of Ce in simultaneous refinement and modification of Al-Si	
alloys	193
CHAPTER 6: CONCLUSIONS	198
REFERENCES	202
LIST OF PUBLICATIONS	220
BIODATA	222

List of Tables

Table No.	Caption	Page No.
3.1	Composition of Alloys used for experiments	52
3.2	List of experiments carried out	56
4.1	Effect of melt treatments on peak heat flux transients of Al-8Si alloy	68
4.2	Effect of melt treatment on heat flux transients of Al-13Si alloy	69
4.3	Effect of melt treatment on heat flux transients of Al-14Si alloy	69
4.4	Effect of melt treatment of Al-22Si on various heat flux transients	70
4.5	The effect of melt treatment on tensile properties of Al-8Si alloy	80
4.6	The effect of melt treatment on tensile properties of Al-13Si alloy	81
4.7	The effect of melt treatment on tensile properties of Al-14Si alloy	82
4.8	The effect of melt treatment on tensile properties Al-22Si alloy	83
5.1	Cooling curve analysis of Al-8% Si alloy	86
5.2	Cooling curve analysis of Al-13Si alloy	97
5.3	Cooling curve analysis of Al-14% Si alloy	103
5.4	Cooling curve analysis of Al-22% Si alloy	112
5.5	Latent heat calculated using different methods	124
5.6	Effect of various melt treatment on the latent heat of Al-8Si alloy	129
5.7	Effect of various melt treatment on the latent heat of Al-13Si alloy	132
5.8	Effect of various melt treatment on the latent heat of Al-14Si alloy	135
5.9	Effect of various melt treatment on the latent heat of Al-22Si alloy	138
5.10	Eutectic Si particle characteristics of Al-8 Si alloy	147
5.11	Eutectic silicon particle characteristics of Al-13Si alloy	152
5.12	Eutectic silicon characteristics of Al-14Si alloy	158
5.13	Eutectic silicon characteristics of Al-22Si alloy	164
5.14	Effect of combined additions on the solidification parameters of slowly cooled Al-Si alloys	191
5.15	Ultimate tensile strength of copper mold solidified Al-Si alloys before and after various melt treatment	193

List of Figures

Table No.	Caption	Page No.
2.1	Al-Si binary phase diagram	6
2.2	Optical micrograph of an as cast hypoeutectic Al-Si alloy	6
2.3	Microstructure of eutectic alloy	7
2.4	As-cast microstructure of Hypereutectic Al-Si alloy	8
2.5	Grain refinement of Al-7Si alloy (a) unrefined (b) refined with Al-3Ti-3B	10
2.6	Microstructure of (a) unrefined and (b) phosphorous refined hypereutectic alloy	11
2.7	Silicon particle characteristic of hypereutectic Al-Si alloy with varying P addition (a) number of particle per unit length (b) silicon equivalent diameter	12
2.8	Microstructures of the Al-Si alloy in the as-cast condition: (a) unmodified (b) modified with strontium	14
2.9	Twinning mechanism of silicon growth (a) faceted Growth of silicon (b) Step growth of silicon	15
2.10	DAS as function of cooling rate	25
2.11	Microstructure of an Al-16Si alloy showing primary and eutectic Si phases (a) slowly solidified (b) DC cast at 4.34 mm/s	27
2.12	(a) Effective diameter of primary silicon (b) SDAS as a function of cooling rates	28
2.13	Steps involved in heat treatment process	29
2.14	Dissolution of Cu particles (a) eutectic Al ₂ Cu (b) blocky Al ₂ Cu	33
2.15	Spheroidization of eutectic silicon during solution treatment (a) 50 min (b) 400 min, at 540°C	34
2.16	Illustration of Friedel effect and Orowan mechanism (a) shearing (b) bypassing	36
2.17	Response of Al-Si alloys to natural ageing	38
2.18	Cooling curve, first derivative curve and characteristic parameters of Al-Si alloy	42

2.19 Effect of grain refinement on the α -Al dendrite nucleation temperature	43
2.20 Effect of eutectic silicon modification on cooling curve of A356 alloy	44
2.21 Relationship between modification level and temperature depression with Sr content	46
2.22 Cooling curve, derivative curve and eutectic base of hypereutectic Al-Si alloy	47
2.23 The effect of modification on heat flux transient	49
3.1 Schematic sketch of solidification setup (a) with chill (b) without chill	53
4.1 Cooling curves of Al-8%Si alloys with varying Ce content solidified on (a) unchilled (b) copper chilled alloys	57
4.2 Cooling curves of Al-8%Si alloys with varying Ce content solidified on (a) brass and (b) stainless steel chills	58
4.3 Cooling curves of Al-8%Si alloys with varying Sr content solidified on (a) unchilled (b) copper (c) brass and (d) stainless steel chills	59
4.4 Cooling curves of Al-13%Si alloys with varying Ce content solidified on (a) unchilled (b) copper (c) brass and (d) stainless steel chills	60
4.5 Cooling curves of Al-13%Si alloys with varying Sr content solidified on (a) unchilled (b) copper (c) brass and (d) stainless steel chills	61
4.6 Cooling curves of Al-14%Si alloys with varying Ce content solidified on (a) crucible cooled (b) cast iron (c) brass (d) copper chills	62
4.7 Cooling curves of Al-14%Si alloys with varying P content solidified on (a) crucible cooled (b) cast iron (c) brass (d) copper chills	63
4.8 Cooling curves of Al-22%Si alloys with varying Ce content solidified on (a) crucible cooled (b) cast iron (c) brass (d) copper chills	64
4.9 Cooling curves of Al-22%Si alloys with varying P content solidified on (a) crucible cooled (b) SS (c) brass (d) copper chills	65
4.10 Temperature-time curves at different locations from interface in the copper chill	66
4.11 Variation of heat flux and chill surface temperature with time	67
4.12 Effect of chill material on casting/chill interfacial heat flux transients	67
4.13 Microstructure of untreated and unchilled Al-8% alloy	71

4.14 Microstructure of untreated and chilled Al-8% alloy	71
4.15 Micrographs of Al-8%Si alloy solidified on different chills	
(a) untreated -copper chill (b) 0.5 wt.% Ce- Cu chill (c) 0.04 wt.% Sr- copper chill	
(d)) untreated -brass chill (e) 1.0 wt.% Ce- brass chill (f) 0.04 wt.% Sr- brass chill	
(g) Untreated SS chill (h) 1.5 wt.% Ce- SS chill (i) 0.04 wt.% Sr- SS chill	72
4.16 Macrostructures of Ce treated alloy (a) untreated (b) 0.5%	
(c) 1.0% (d) 1.5%Ce	73
4.17 Micrographs of Al-13%Si alloy (a) unchilled-untreated	
(b) unchilled- Ce treated (c) unchiled-P treated (d) untreated -copper chill	
(e) copper chilled-Ce (f) copper chilled-P treated (g) brass chilled- untreated	
(h) Ce- brass chill (i) brass chilled-P treated(j) SS chilled-untreated	
(k) SS chilled-Ce treated (l)SS chilled- P	75
4.18 Micrographs of Al-14%Si alloy (a) unchilled-untreated	
(b) unchilled- Ce treated (c) unchiled-P treated (d) untreated -copper chill	
(e) copper chilled-Ce (f) copper chilled-P treated (g) brass chilled- untreated	
(h) Ce- brass chill (i) brass chilled-P treated (j) SS chilled-untreated	
(k) SS chilled-Ce treated (l) SS chilled- P treated	76
4.19 Micrographs of Al-22%Si alloy (a) unchiled-untreated	
(b) unchilled- Ce treated (c) unchiled-P treated (d) untreated -copper chill	
(e) copper chilled-Ce (f) copper chilled-P treated (g) brass chilled- untreated	
(h) Ce- brass chill (i) brass chilled-P treated(j) SS chilled-untreated	
(k) SS chilled-Ce treated (l)SS chilled- P treated	77
4.20 Stress-strain curve of Al-8Si alloy solidified against sand	
(a) untreated (b) 2 wt.% Ce treated	78
4.21 Stress-strain curve of Al-8Si alloy solidified on copper mold	
(a) untreated (b) 1.5 wt.% Ce treated	79
5.1 Cooling and first derivative curve for Al–8%Si alloy	84
5.2 Variation of α -Al nucleation temperature with varying content of	
(a) Ce (b) Sr	88
5.3 Variation of α -Al minimum nucleation temperature with varying	
content of (a) Ce (b) Sr	88

5.4 Variation in degree of undercooling of α -Al with varying content of (a) Ce (b) Sr	89
5.5 Variation of eutectic nucleation temperature with varying content of (a) Ce (b) Sr	91
5.6 Variation of eutectic minimum nucleation temperature with varying content of (a) Ce (b) Sr	91
5.7 Variation in degree of undercooling of eutectic with varying content of (a) Ce (b) Sr	92
5.8 Eutectic growth temperature differences versus cooling rate for varying content of (a) Ce (b) Sr	93
5.9 Illustration of dendrite coherency temperature (DCT) determined from cooling curves	95
5.10 The Effect of melt treatment on (a) dendrite coherency temperature (b) fraction solid at DCP	95
5.11 Variation of eutectic nucleation temperature with varying content of (a) Ce (b) Sr	98
5.12 Variation of eutectic minimum temperature with varying content of (a) Ce (b) Sr	99
5.13 Variation of eutectic undercooling of Al-13Si alloy with addition of varying content (a) Ce (b) Sr	99
5.14 Eutectic growth temperature differences versus cooling rate for varying content of (a) Ce (b) Sr	101
5.15 Variation of primary silicon nucleation temperature with varying content of (a) Ce (b) P	104
5.16 Variation of primary silicon minimum nucleation temperature with varying content of (a) Ce (b) P	104
5.17 Variation of primary silicon undercooling of Al-14Si alloy with the addition of varying content (a) Ce (b) Sr	106
5.18 Variation of eutectic silicon nucleation temperature in Al-14Si alloy with varying content of (a) Ce (b) P	108
5.19 Variation of eutectic minimum nucleation temperature in Al-14Si alloy	

with varying content of (a) Ce (b) P	109
5.20 Variation of eutectic undercooling of Al-14Si alloy with varying content (a) Ce (b) P	109
5.21 Eutectic growth temperature differences versus cooling rate for varying content of (a) Ce (b) P	110
5.22 Variation of primary silicon nucleation temperature in Al-22Si alloy with varying content of (a) Ce (b) P	113
5.23 Variation of primary silicon minimum nucleation temperature in Al-22Si alloy with varying content of (a) Ce (b) P	114
5.24 Variation of primary silicon undercooling of Al-22Si alloy with the addition of varying content (a) Ce (b) P	114
5.25 Variation of eutectic nucleation temperature in Al-22Si alloy with varying content of (a) Ce (b) P	116
5.26 Variation of eutectic minimum nucleation temperature in Al-22Si alloy with varying content of (a) Ce (b) P	117
5.27 Variation of eutectic undercooling in Al-22Si alloy with varying content of (a) Ce (b) P	117
5.28 Eutectic growth temperature differences versus cooling rate for varying content of (a) Ce (b) P	118
5.29 First derivative curve fitted with (a) linear data base line (b) Fourier base line	122
5.30 Comparison of fraction solid calculated using Newtonian and Fourier analysis for Al-8Si alloy	123
5.31 Diffusivity and specific heat of the alloy as a function of temperature	125
5.32 Enthalpy as a function of fraction solid	125
5.33 Variation in solid fraction formed during solidification of Al-8Si alloy with varying content of (a) Ce (b) Sr	127
5.34 Variation in diffusivity of Al-8Si alloy with varying content of (a) Ce (b) Sr	127
5.35 Variation in specific heat of Al-8Si alloy with varying content of (a) Ce (b) Sr	128

5.36 Variation in latent heat evolved during the solidification of Al-8Si alloy with varying content of (a) Ce (b) Sr	128
5.37 Variation in solid fraction formed during solidification of Al-13Si alloy with varying content of (a) Ce (b) Sr	130
5.38 Variation in diffusivity of Al-13Si alloy with varying content of (a) Ce (b) Sr	130
5.39 Variation in specific heat of Al-13Si alloy with varying content of (a) Ce (b) Sr	131
5.40 Variation in latent heat evolved during the solidification of Al-13Si alloy with varying content of (a) Ce (b) Sr	131
5.41 Variation in solid fraction formed during solidification of Al-14Si alloy with varying content of (a) Ce (b) P	133
5.42 Variation in diffusivity of Al-14Si alloy with varying content of (a) Ce (b) P	133
5.43 Variation in specific heat of Al-8Si alloy with varying content of (a) Ce (b) P	134
5.44 Variation in latent heat evolved during the solidification of Al-14Si alloy with varying content of (a) Ce (b) P	134
5.45 Variation in solid fraction formed during solidification of Al-22Si alloy with varying content of (a) Ce (b) P	136
5.46 Variation in diffusivity of Al-22Si alloy with varying content of (a) Ce (b) P	137
5.47 Variation in specific heat of Al-22Si alloy with varying content of (a) Ce (b) P	137
5.48 Variation in latent heat evolved during the solidification of Al-22Si alloy with varying content of (a) Ce (b) P	138
5.49 Variation of heat flux with time for copper chilled Al-8Si alloy	139
5.50 Variation of peak heat flux with varying content of addition (a) Ce (b) Sr	140
5.51 Variation of peak flux of Al-13Si alloy with varying content of (a) Ce (b) Sr	141

5.52 Variation of peak heat flux of Al-14Si alloy with varying content of (a) Ce (b) P	141
5.53 Variation of peak heat flux of Al-22Si alloy with varying content of (a) Ce (b) P	142
5.54 Variation of grain size in Al-8Si alloys with (a) Ce (b) Sr	143
5.55 EDS analysis of the intermetallic formed due to the addition of Ce	144
5.56 Variation of eutectic silicon particle characteristic with varying content of (a) Ce (b) Sr	148
5.57 Correlation between dimensionless thermal analysis parameter and roundness factor of eutectic Si in Al-8Si alloy	150
5.58 Variation of silicon particle characteristic with (a) Ce (b) Sr	153
5.59 Microstructures of Al-13Si alloy (a) Ce modified (b) Sr modified	154
5.60 Correlation between dimensionless thermal analysis parameter and roundness factor of eutectic Si in Al-13 Si alloy	154
5.61 Variation of primary silicon characteristic with varying content of (a) Ce (b) P	156
5.62 Variation of eutectic silicon characteristic with varying content of (a) Ce (b) P	159
5.63 Correlation between dimensionless thermal analysis parameter and roundness factor of eutectic in Al-14Si alloy	161
5.64 Variation of primary silicon size with varying content of (a) Ce (b) P	163
5.65 Variation of eutectic silicon characteristic with varying content of (a) Ce (b) P	165
5.66 Correlation between thermal analysis parameter, ΔT_G and primary silicon characteristic parameter in Al-22 Si alloy	165
5.67 Variation of ultimate tensile strength with melt treatment (a) with Ce (b) with Sr	167
5.68 Variation of ultimate tensile strength with melt treatment (a) Ce (b) Sr	167
5.69 SEM micrographs of fractured surface (a) untreated (b) Ce treated (c) Sr treated	169
5.70 Effect of varying content of addition on the hardness of the alloy	

(a) Ce (b) Sr	169
5.71 Variation of ultimate tensile strength with melt treatment	
(a) with Ce (b) with Sr	171
5.72 Variation of percentage of elongation with melt treatment	
(a) with Ce (b) with Sr	171
5.73 Variation in Ce intermetallic morphology with cooling rate	
(a) copper chilled (b) SS chilled	172
5.74 Effect of varying content of addition on the hardness of the alloy	
(a) Ce (b) Sr	172
5.75 Variation of ultimate tensile strength with melt treatment	
(a) with Ce (b) with P	173
5.76 Variation of percentage of elongation with melt treatment	
(a) with Ce (b) with P	174
5.77 Effect of varying content of addition on the hardness of the alloy	
(a) Ce (b) P	174
5.78 Variation of ultimate tensile strength with melt treatment	
(a) with Ce (b) with P	176
5.79 Variation of ultimate tensile strength with melt treatment	
(a) with Ce (b) with P	177
5.80 Effect of varying content of addition on the hardness of the alloy	
(a) Ce (b) Sr	177
5.81 Effect of T6 heat treatment on the UTS of treated Al-8Si alloys	
(a) Ce treated (b) Sr treated	179
5.82 Effect of T6 heat treatment on the ductility of treated Al-8Si alloys	
(a) Ce treated (b) Sr treated	179
5.83 Effect of T6 heat treatment on the hardness of melt treated Al-8Si alloys	180
5.84 Microstructure of Al-8Si alloys (a) before and (b) after T6 heat treatment	180
5.85 Micrographs of tensile fracture surfaces of heat treated Al-8Si alloys (a) untreated (b) Ce treated (c) P treated	182

5.86 Effect of T6 heat treatment on the UTS of treated Al-14Si alloys	
(a) Ce treated (b) P treated	183
5.87 Effect of T6 heat treatment on the ductility of treated Al-8Si alloys	
(a) Ce treated (b) P treated	184
5.88 Effect of T6 heat treatment on the hardness of melt treated Al-14Si alloys	184
5.89 Microstructure of Al-14Si alloy (a) before and (b) after T6 heat treatment	185
5.90 Micrographs of tensile fracture surfaces of heat treated Al-14Si alloys (a) untreated (b) Ce treated (c) P treated	186
5.91 Effect of T6 heat treatment on the UTS of treated Al-22Si alloys (a) Ce treated (b) P treated	187
5.92 Effect of T6 heat treatment on the ductility of treated Al-22Si alloys (a) Ce treated (b) P treated	188
5.93 The effect of T6 heat treatment on the hardness of melt treated Al-8Si alloys	188
5.94 Microstructure of Al-14Si alloy (a) before and (b) after T6 heat treatment	189
5.95 Micrographs of tensile fracture surfaces of the heat treated Al-22Si alloys (a) untreated (b) Ce treated (c) P treated	189
5.96 Effect of combined additions on the microstructures of (a) Al-8Si alloy (b) Al-13Si alloy (c) Al-14Si alloy (d) Al-22Si alloy	192
5.97 (a) Al-Ce- Si ternary phase diagram (b) Calculated Al corner of Al–Ce–Si liquidus surface	194
5.98 EDAX analysis of Ce intermetallic in Al-8Si alloys	196
5.99 EDAX analysis of Ce intermetallic in Al-13Si alloys	196
5.100 EDAX analysis of Ce intermetallic in Al-14Si alloys	197
5.101 EDAX analysis of Ce intermetallic in Al-22Si alloys	197

Nomenclature

Symbol	Description
α	Thermal diffusivity, m^2/s
C_P	Specific heat, J/kgK
K	Thermal conductivity, W/mK
ρ	Density, kg/m^3
α - Al	Primary aluminum
$T_N(\alpha)$	α - Aluminum nucleation temperature, K
$T_{\min}(\alpha)$	α - Aluminum minimum nucleation temperature, K
$T_G(\alpha)$	α - Aluminum growth temperature, K
$T_N(\text{Eut})$	Eutectic nucleation temperature, K
$T_{\min}(\text{Eut})$	Eutectic minimum nucleation temperature, K
$T_G(\text{Eut})$	Eutectic growth temperature, K
T_S	Solidus temperature, K
ΔT_{UN}	Undercooling, K
ΔT_G	Change in growth temperature, K
$\Delta T_G / \Delta T_{\text{UN}}$	Dimensionless thermal parameter
UTS	Ultimate tensile strength, MPa

CHAPTER 1

INTRODUCTION

Aluminum-Silicon (Al-Si) alloys are the most versatile materials, comprising 85% to 90% of the total aluminum cast parts produced for the automotive and aerospace industry. Depending on the Si concentration, the Al-Si alloys fall into three major categories: hypoeutectic (<12% Si), eutectic (12-13% Si) and hypereutectic (14-25% Si) [Sigworth 2013]. The cast microstructure of untreated hypoeutectic Al-Si alloys consists of pro-eutectic aluminum dendrites and flake or needle like eutectic silicon in a eutectic matrix, whereas, hypereutectic alloys consists of coarse and segregated primary silicon along with modified eutectic. The mechanical properties of the cast Al-Si alloys are significantly degraded by the presence of such microstructures. The enhancement in the mechanical properties is generally achieved by transforming the eutectic silicon into fine fibrous form (modification process) and/or by refining the pro-eutectic phases (refinement process) [Liu et al. 2011] [Onyia et al. 2013]. Most commonly, group II elements like Na and Sr are used to modify eutectic silicon and Al-Ti-B and P master alloys to refine grains in the hypoeutectic and hypereutectic alloys respectively. Apart from chemical modification/refinement, chilling and heat treatment also plays an important role in the mechanical property enhancement [Ceylan et al. 1997]. The spheroidization of the silicon during heat treatment process influences the mechanical properties as equally as chemical treatments [Crowell, N and Shivkumar, S 1995]. But, spheroidization is greatly influenced by the size and morphology of the silicon prior to the heat treatment process.

1.1 Scope of the Present Investigation

Since both the melt treatment process (refinement and modification) are important and are carried out simultaneously, the interaction between modifiers and the grain refiners would affect the efficiency of the process. Studies have shown that the combined addition of common modifiers and refiners to Al-Si alloys mutually

poisoned the beneficial effect of each treatment. The combined addition of Sr and B resulted in the formation of SrB_6 . On the other hand, the addition of Sr along with P resulted in the formation of AlP. As the mechanical properties of the alloy are greatly dependent on the aluminium grain size and morphology of eutectic silicon, it is very important to simultaneously refine and modify both phases. In the recent past, the melt treatment of Al-Si alloys using rare earth elements has gained attention due to their ability in refining and modifying the α -Al and eutectic silicon in Al-Si alloys. Few studies carried out using misch-metal containing 50-55 wt. % of cerium also showed significant influence on the microstructure of Al-Si alloys. However, the effect of addition of elemental Ce to Al-Si alloy melt on cooling curve parameters and heat transfer characteristics were not yet been investigated.

Computer aided cooling curve analysis (CACCA) is an online tool that can be effectively used to assess the quality of the casting. Conventionally, the degree of modification and grain refinement are assessed by destructive sampling followed by metallographic examination of the structure. The cooling curve in conjunction with the first derivative curve is used to determine and analyze different solidification characteristics. The alloy solidification characteristics change with modification, refinement and cooling rate and their effects are reflected on the cooling curve parameters. Hence, by accurately measuring and analyzing the changes in the cooling curve parameters, one can assess the changes brought about by melt treatment and cooling rates. Similarly, the modification process effects the heat flux transients between the casting/mold. The assessment of heat flux transients during solidification would be useful for solidification modeling. The effect of Ce/ P melt treatment on heat flux transients of Al-Si alloys has not yet been assessed.

Solidification of Al-Si alloys begins with the nucleation and growth of pro-eutectic α -aluminum phase in hypoeutectic and primary silicon in hypereutectic Al-Si alloys. The size and distribution of these phases would control the size and distribution of porosity, intermetallic and eutectic phases in the casting. Fine and evenly distributed primary and eutectic phases are known to improve the tensile strength of the alloy. Hence, direct chill casting technique can be employed to produce refined

microstructure in Al-Si alloys without any chemical modification. The further refinement of microstructure can be brought by the conjunction of melt treatment and chilling. The present investigation is also aimed at the study of combined effect of modification/refinement melt treatment and chilling on the microstructure. The mechanical properties of the Al-Si alloys are greatly dependent on the morphology and distribution of the eutectic Si. The spheroidization of eutectic Si during heat treatment also improves the mechanical properties of the alloy. Since both modification process and spheroidization process transforms the morphology of Si into fine globular structure, the assessment of influence of silicon modification on heat treatment parameters and mechanical properties would be an interesting topic for investigation.

1.2 Objectives

- 1) To carry out modification and refinement of hypoeutectic, eutectic and hypereutectic Al-Si alloys by the addition of Ce, Sr and P.
- 2) To evaluate the melt quality of Al-Si alloys by computer aided cooling curve analysis (CACCA) technique by the measurement of thermal analysis parameters and to correlate them with the morphology of Si and fineness of grains.
- 3) To estimate the latent heat and solid fraction using Newtonian and Fourier analysis techniques.
- 4) To determine and assess the effect of melt treatment on dendrite coherency point of alloys
- 5) To assess the effect of melt treatment on heat transfer characteristics of alloys.
- 6) To investigate the effect of varying concentration of Ce, Sr and P additions on the microstructure characteristics of Al-Si alloys.
- 7) To assess the effect of varying concentration of modifier/refiner additions on the mechanical properties.
- 8) To investigate the combined effect of chilling, melt treatment and ageing on the morphology of the eutectic silicon and mechanical properties.

To meet the objectives of the present work following research methodologies were selected.

- Type of alloy: hypo, eutectic, hypereutectic Al-Si alloys
- Melt treatment: unmodified, modified and refined with strontium, phosphorus and cerium
- Chill materials: EC grade copper, C360 grade brass and Type 304 stainless steel
- Casting conditions: Without chill, with chill, gravity die-cast and metallic molds
- Heat treatment: T6 treatment.

1.3 Contents of the Thesis

A detailed review of the literature on Al-Si alloys, melt treatment of Al-Si alloys and their importance on microstructure, cooling curve parameters and mechanical properties is presented in Chapter 2. The details of experimental set-up and methodology of the investigation are presented in Chapter 3. The results of the experiments carried out are given in Chapter 4. In Chapter 5, interpretation of experimental results, analysis of results of cooling curve parameters, assessment of latent heat of the alloys using Fourier and Newtonian analyses, influence of melt treatment on diffusivity, fraction solid, specific heat and dendrite coherency point of the alloys, microstructure characteristics, mechanical properties of the alloys before and after heat treatment are discussed. The conclusions drawn based on the results and discussion are presented in Chapter 6.

CHAPTER 2

LITERATURE REVIEW

Aluminum-silicon (Al-Si) alloys are the aluminum-base alloys with silicon as the major additive. Al-Si alloys are among the most useful aluminum casting alloys because of their high fluidity, high resistance to corrosion, low shrinkage and low coefficient of thermal expansion. They have wide spread applications in automotive, marine, electrical and aircraft industry. These alloys usually contain about 2 to 25 wt. % of silicon, along with some amount of impurities of the order of 1.5 % to 2 %. The silicon content of most widely used alloys is found in the range of 3-22 %. Copper, nickel, zinc, magnesium, and other alloying element, are added depending upon the use of the alloy [Mondolfo 2013].

2.1 Aluminum Silicon Alloys

The melting point of the aluminum decreases with the addition of silicon to it, similarly, the addition of aluminum to silicon also lowers the liquidus temperature of silicon. A considerable amount of silicon is soluble in solid aluminum at higher temperatures. The maximum solubility of 1.65 weight percent was observed at the eutectic temperature. However, the aluminum has negligible solubility in silicon. As the concentration of silicon increases, the lowering liquidus curves from the either side meet at 12.6 wt. percent of silicon as shown in Figure 1. Based on this point and silicon content, the Al-Si alloys are classified into three major categories as hypoeutectic, eutectic and hypereutectic Al-Si alloys [Sigworth 2013].

➤ Hypoeutectic Al-Si alloys

The Al-Si alloys having silicon content in the range of 3-10 (wt. %) are termed as hypoeutectic alloys. These alloys are most commonly used for general applications.

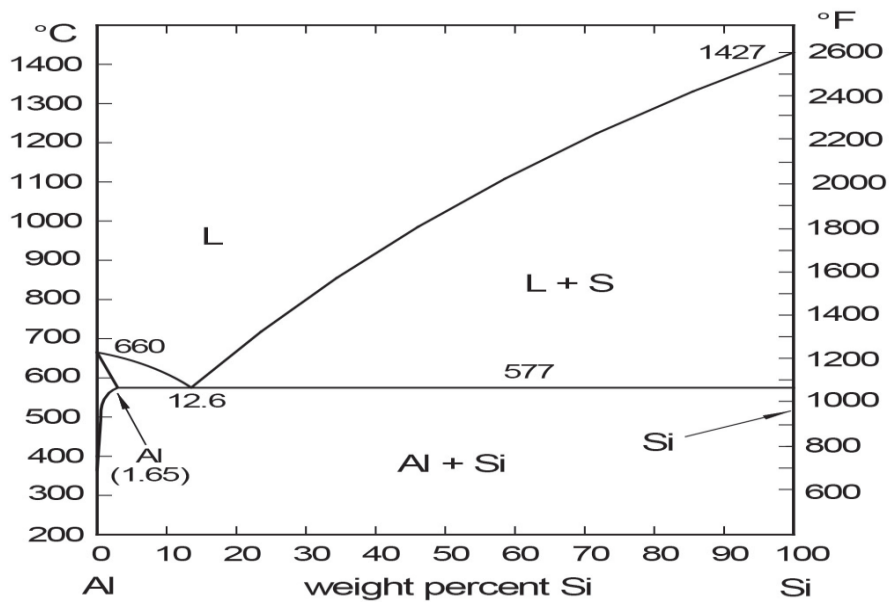


Figure 2.1 Al-Si binary phase diagram [Sigworth 2013]

Alloys with 3-5% silicon are used for rotors, vessels, valve bodies, large fan blade fittings etc. Alloys with 5-10% Si are mainly used in their cast form in critical components like pistons, valve lifters, cylinder liners, engine blocks, etc [Nogita et al. 2010]. The microstructure of hypoeutectic Al-Si cast alloys consists of two main constituents: primary aluminum and (Al + Si) eutectic as indicated in the Figure 2.2.

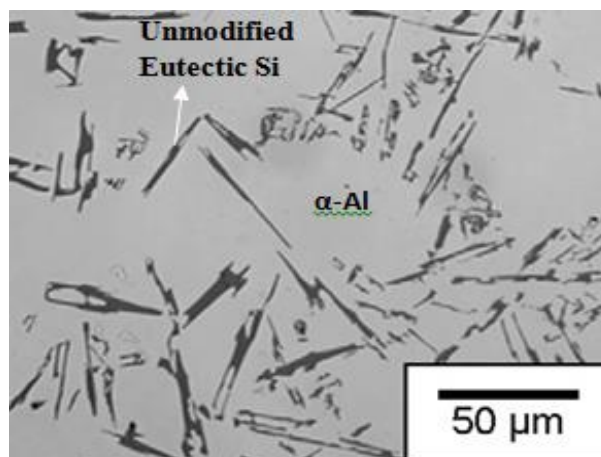


Figure 2.2 Optical micrograph of an as cast hypoeutectic Al-Si alloy [Nogita et al. 2010]

The physical and mechanical properties of hypoeutectic alloys are dependent on the size and shape of these two phases. Generally, the quality and properties of the Al-Si alloy castings are improved by two melt treatment processes namely ‘grain refinement and modification’. Grain refinement is a process by which the columnar α -Al grains are transformed into fine equiaxed structure by the addition of grain refiners like Ti-B master alloys to the melt, whereas, modification is a process of transforming acicular eutectic silicon into fine fibrous form by the addition of group II elements like Na, Sr [Kashyap and Chandrashekar 2001] [Liu et al. 2011] [Onyia et al. 2013]. The fine grains along with modified fine fibrous Si is desired for improved mechanical and physical properties [Closset and Gruzleski 1982].

➤ **Eutectic Al-Si alloys**

The alloys having silicon content in the range of 11-13 wt. % are termed as eutectic alloys. Eutectic alloys with high degree of fluidity and low shrinkage on solidification are generally used for application where strength is not a criterion such as domestic cookware, pump castings. The alloy microstructure basically consists of long acicular (lamellar) eutectic Si coupled along primary aluminum as shown in the Figure 2.3. The addition of eutectic modifiers such as Sr and Na are found to enhance the mechanical properties to a larger extent by modifying the eutectic silicon into fine fibrous structure [Lu et al. 2004].

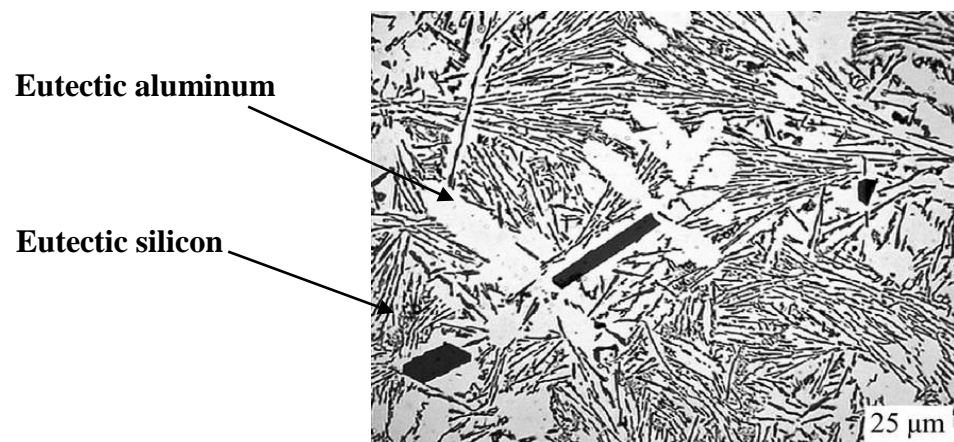


Figure 2.3 Microstructure of eutectic alloy [Suárez-Peña and Asensio-Lozano 2006]

➤ Hypereutectic Al-Si alloys

The hyper-eutectic alloys are the alloys with silicon content above eutectic composition, more specifically in the range of 15% to 23%. Hypereutectic alloys with low density, high specific stiffness, high-temperature resistance, wear resistance, and low coefficient of thermal expansion is of great interest in transportation industry. The alloy is mainly considered because of its ability in replacing cast iron in automobile engine parts. Some of the major applications of hypereutectic Al-Si alloy include high-performance automobile engine parts such as connecting rods, rocker arms, cylinder, pistons and valve retainers. Figure 2.4 shows a typical microstructure of hypereutectic Al-Si alloy, the phases present are termed as primary silicon particles, eutectic silicon and α -aluminum dendrites.

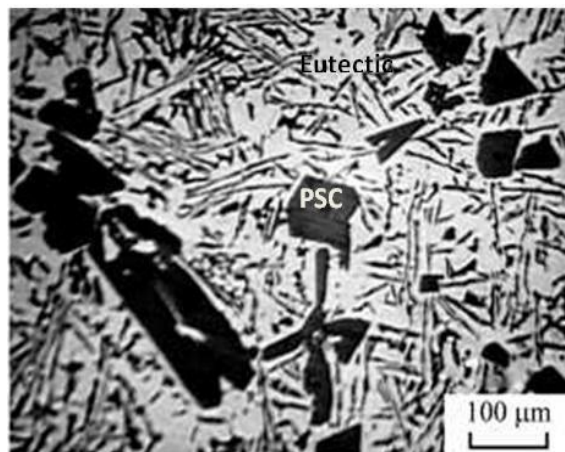


Figure 2.4 As-cast microstructure of Hypereutectic Al-Si alloy [Ouyang et al. 2007]

The microstructure of the alloy depends on the nucleation and cooling rates during solidification. The morphology of primary silicon crystals depends on solidification parameters such as freezing rate, temperature gradient in the liquid, and composition of the liquid. Generally, the cast microstructure of the hypereutectic Al-Si alloy consists of coarse and segregated primary silicon crystals and needle like eutectic silicon. Such microstructures have a harmful effect on the extrudability, machinability, strength and ductility of the alloy. For better mechanical properties and wear resistance, a uniform distribution of primary silicon particles are desired.

Refinement of commercial hypereutectic alloys were normally done by adding phosphorus containing master alloy into the melt [Zuo et al. 2009]. The addition of phosphorous to the melt effectively refines the primary silicon in sand and permanent mold-castings [Hernández and Sokolowski 2005].

2.2 Melt Treatment of Al-Si Alloys

The physical and mechanical properties of aluminum castings can be altered by altering the size and shapes of the constituents in the alloy microstructure. Some of the common ways to alter the size and shape of the phases in Al-Si alloys are modification [Lu and Hellawell 1987], grain refinement [Mohanty and Gruzleski 1996], primary silicon refinement by rapid cooling [Zuo et al. 2009], mechanical vibration [Abu-Dheir et al. 2005] and spray forming [Ojha et al. 2008]. Among all, the additions of modifiers/refiners are found to be more effective and economical than any other process. An overview of melt treatment techniques is given below:

2.2.1 Grain refinement

A large fraction of hypoeutectic Al-Si alloy microstructure consists of primary α -Al, which influences the properties and quality of the casting. The microstructure of sand cast and gravity cast alloy consists of large columnar structured α -Al, which degrades the properties of the alloy. Generally, the casting quality and mechanical properties of the hypoeutectic alloy are improved by the process is known as ‘Grain Refinement’. In the process the primary α -Al is transformed into equiaxed structure by the addition of grain refiners [Mohanty and Gruzleski 1996]. The effect of addition of refiner to Al-7Si alloy on the macrostructure is shown in Figure 2.5. A fine grained structured is obtained by the addition of Al-3Ti-B. A fine equiaxed α -Al has several benefits such as high yield strength, high toughness, improved machinability, excellent drawability etc.

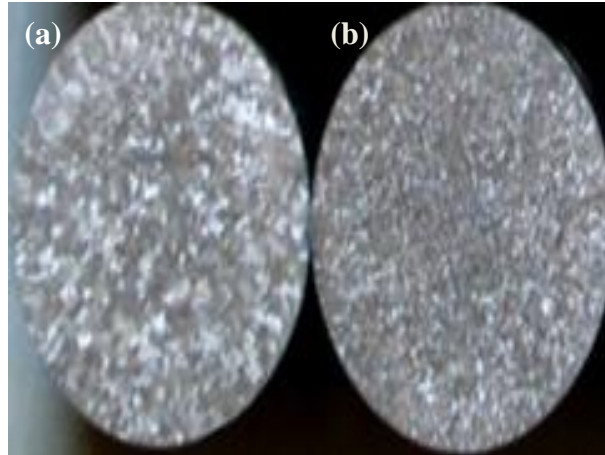


Figure 2.5 Grain refinement of Al-7Si alloy (a) unrefined (b) refined with Al-3Ti-3B
[Wang et al. 2012]

The concept of grain refinement in Al-Si alloys was borrowed from the melt treatment techniques adopted for wrought alloys. In pure aluminum and wrought alloys, the grain refining is carried out using Al-5Ti-B master alloys. When added, the master alloy dissolves and Ti particles segregate on the TiB_2 formed earlier, to take part in the nucleation process [Ghadimi et al. 2013]. But, when added to Al-Si alloys the refining efficiency of Al-5Ti-B was reduced due to the presence of Si. At high Si content, Ti reacts with Si to form titanium-silicide and coats on to the surface of $TiAl_3$ and prevent it from nucleating aluminum during solidification [Wang et al. 2012]. Studies have shown that the grain refining efficiency of Al-Ti-B in Al-Si alloys can be improved by decreasing the Ti content and by increasing B content in the master alloy. Kori et al. (2000) compared the grain refining efficiency of Al-5Ti-B, Al-3Ti-3B and Al-B and reported that the Al-B showed better grain refining efficiency than the other two master alloys. Sritharan and Li (1997) reported that Al-Ti-B master alloys are better grain refiners when the Ti-B ratio is greater than 2.2. Chen et al. (2012) studied the effect of Al-3B on the grain refinement and tensile properties of Al-7Si-Mg alloy and found that the addition of 0.01vol% of Al-3B significantly improved the grain refinement and tensile properties of the alloy.

The exact mechanism of grain refinement by Al-B in Al-Si alloys is not known till now. Among several proposed theories, the theory put forward by Sigworth and Guzowski (1985) known as Boride theory and the Al-B eutectic theory by Mohanty

and Gruzleski (1996) are most convincing. According to the Boride theory, the α -Al are thought to nucleate on the AlB_2 particles introduced by the Al-B master alloys, as AlB_2 particle has a lower crystallographic discrepancy of 4.96% with α -Al. However, even though it is a strong refiner in Al-Si alloys, Al-B was not known to refine grains in pure aluminum. This led Mohanty and Gruzleski to propose Al-B eutectic theory. According to this theory, in the presence of boron, the α -Al will co-precipitate at higher temperature through a eutectic reaction and nucleation of α -aluminum as fine grains occurs on the pre-existing α -Al.

Unlike in hypoeutectic Al-Si alloys, the Al-Ti-B or Al-B master alloys are not applicable for the grain refinement of hypereutectic Al-Si alloys. The presence of high mass percent of Si (>13%) poisons the effect of $TiAl_3$ by forming titanium silicide. The refinement of commercial hypereutectic Al-Si is done by adding phosphorous master alloy into the melt. The added phosphorous effectively refines the coarser primary silicon formed due to slow solidification rates. The process of improving the properties of hypereutectic Al-Si alloy by phosphorous addition was patented by (Stern-Rainer 1933) in 1933. Figure 2.6 illustrates the change in the morphology of primary silicon due to the addition of phosphorous [Wu et al. 2009].

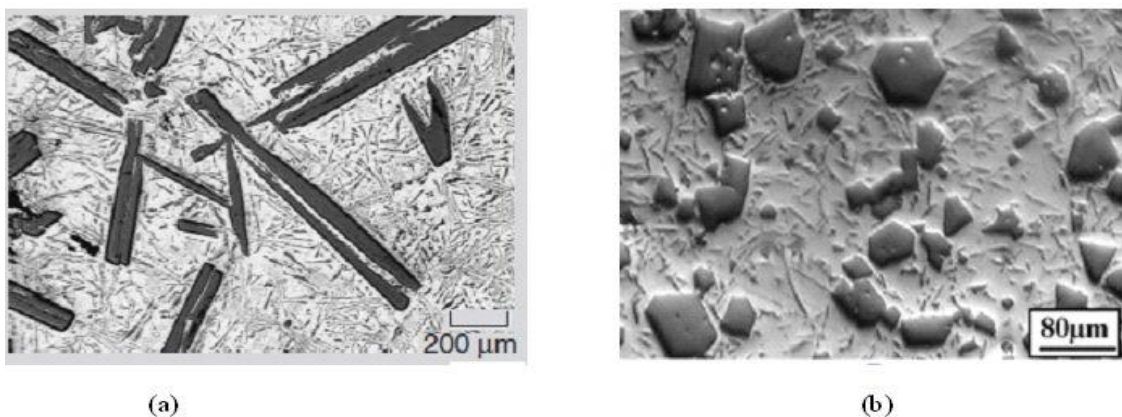


Figure 2.6 Microstructure of (a) unrefined and (b) phosphorous refined hypereutectic alloy [Hernández and Sokolowski 2005] [Wu et al. 2009]

Similarly, Figure 2.7 shows the effect of phosphorous treatment on the primary silicon particle characteristic. The number of primary silicon particles per unit area increases

with a decrease in its size due to phosphorous addition. The phosphorous treatment led to the significant improvement in mechanical properties along with reduction in primary silicon size [Dwivedi et al. 2005] [He et al. 2010].

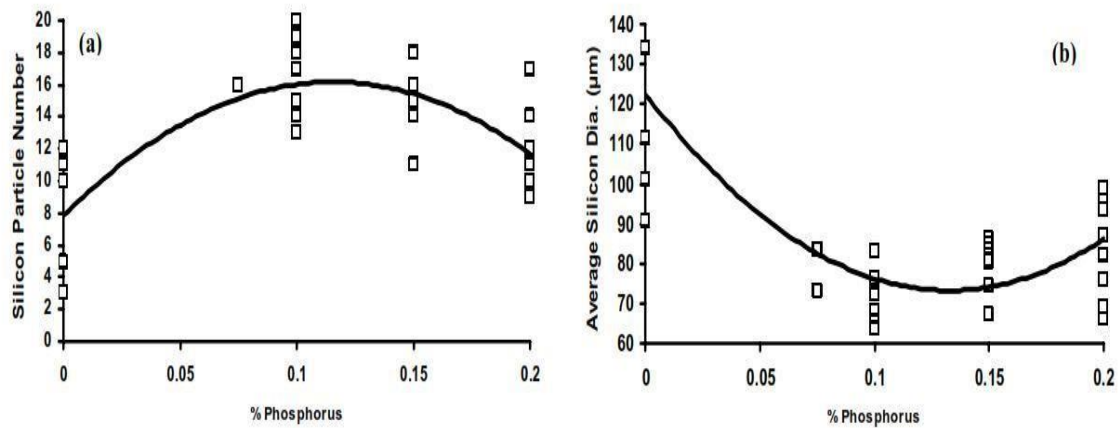


Figure 2.7 Silicon particle characteristic of hypereutectic Al-Si alloy with varying P addition (a) number of particle per unit length (b) silicon equivalent diameter [Ghomashchi 2004]

The mechanism of phosphorus refinement in hypereutectic alloy is as follows. The added phosphorus will react with the Al present in the melt to form a stable compound, 'AlP' with a melting point higher than 982°C ($\text{Al}_{(l)} + \text{P}_{(l)} \rightarrow \text{AlP}_{(s)}$). Both AlP and Si are cubic crystals with very similar lattice parameters (Si 5.42 Å, AlP 5.45 Å). Thus, during solidification the primary silicon nucleates heterogeneously on the solid AlP particles with a cube-cube orientation relationship and refines the primary silicon. Thermal analysis studies have revealed that the addition of phosphorus significantly increases the precipitation temperature of primary silicon and thereby heterogeneously nucleating primary silicon at high temperature with a regular faceted crystals [Zhang Ying et al. 2007] [Zuo et al. 2009].

The addition of phosphorous is of vital importance in most casting technologies of hypereutectic Al-Si alloys. The phosphorus was either added directly to the melt in the form of red phosphorus, phosphate salt or as Cu-P, Al-Cu-P and Al-Fe-P master alloys. Due to the environmental problems caused by the direct application of

phosphorus and because of the low recovery rates, the direct use of phosphorus salt was stopped. Cu-P and Al-Cu-P master alloys were more stable but needed higher temperatures to be effective. Al-Fe-P master alloys were discarded due the presence of Fe content which is considered to be an impurity [Zhang et al. 2008] [Zuo et al. 2009]. This led to the development of Al-P series master alloy without any impurities. There are two ways by which AlP compounds precipitate in the melt on addition of Al-P series master alloy and act as heterogeneous nucleant for primary silicon. When P is added to the melt as master alloy, the AlP dissociates into Al and P. Due to the potential difference in the P content of the melt P start dissolving into the melt. This continues till the solubility limit of P in Al-Si melt is reached, for that temperature.

Later during solidification, as the temperature decreases the solubility of P also decreases in the melt. The dissolution reaction is reversed to form AlP from the precipitated P. The newly formed AlP is much smaller in size and will be homogeneously distributed in the melt than the externally added P. As a result, the primary silicon heterogeneously nucleates on the precipitated AlP with cube-cube orientation relationship. Second method is to add master alloy with pre-existing AlP, which nucleates primary silicon with random orientation relationship. These two mechanisms of AlP relationship with primary silicon depends on the P content in the Al-Si and Al-P series master alloys [Lescuyer et al. 1998].

The effectiveness of refinement and homogeneous distribution primary silicon depends on the uniformity of AlP compounds in the melt. Due to the low wettability in Al melt, the AlP compounds generally segregate and float on the surface of the melt. It is also more likely that the AlP compounds get adsorbed on to the inner walls of the molds. To avoid these difficulties the Al-P series master alloys are added with Si. The Si plays an important role in improving the effectiveness of the Al-P series master alloys [Li et al. 2011].

2.2.2 Modification

The modification of eutectic silicon is done by melt treating the alloy with group II elements like sodium, potassium, rubidium, calcium, strontium, barium, lanthanum and ytterbium. Among them, only sodium and strontium find any significant industrial use. Strontium master alloys are the most common modifier used in industry as it is more effective and less volatile compared to others. The amount of modifiers required to achieve complete modification depends on the alloy composition. Alloys with high silicon content would require more concentration of modifying agent. Typical retained sodium levels are in range 0.005-0.01% and 0.02% strontium is sufficient to modify 7% Si alloy such as 356 alloys. The eutectic alloy such as 413 alloys would require concentration up to 0.04% Sr.

During solidification, the atoms of Sr restrict the growth of the eutectic silicon and thus modify the acicular silicon into fine fibrous form [Lu and Hellawell 1987]. The effect of modification on eutectic silicon is shown in Figure 2.8. The Si modification occurs by inducing twins in the growing silicon and is known as Twin Plane Re-Edge (TPRE) mechanism. The silicon in the unmodified alloy grow either with minimum or no twins, whereas, the treated silicon will be heavily twinned.

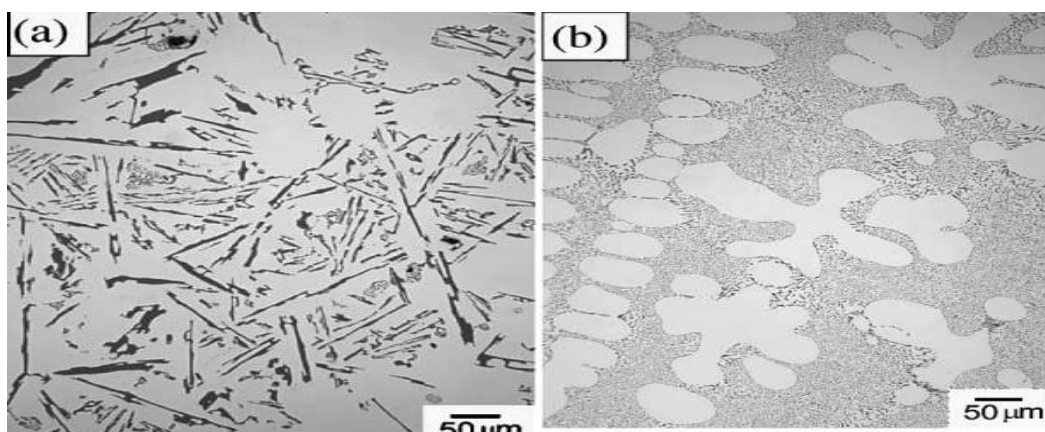


Figure 2.8 Microstructures of the Al–Si alloy in the as-cast condition: (a) unmodified (b) modified with strontium [Nogita and Dahle 2003]

During the solidification of unmodified Al-Si alloy, Si being a non-metal freezes in a faceted manner i.e. it forms crystals which are bounded to definite crystallographic planes. The silicon grows only in certain specific crystallographic directions. The crystallography exhibited by the plate-like form of silicon is illustrated in the Figure 2.9 (a). The silicon crystals grows only in the $\langle 112 \rangle$ direction forming large flat faces along $\langle 111 \rangle$ planes. A very important feature of the silicon crystallization is that twins are easily formed. These crystallographic defects occur when large groups of atoms uniformly shift position across a plane in the crystal structure, known as twin plane. A self-perpetuating groove of 141° at the solid/liquid interface is produced across $\langle 111 \rangle$ planes due to the silicon twins. Subsequently, the crystallization of the silicon occurs by the addition of atoms to form steps which move across the solid liquid interface as shown in the Figure 2.9 (b) [Hamilton and Seidensticker 1960] [Lu and Hellawell 1987].

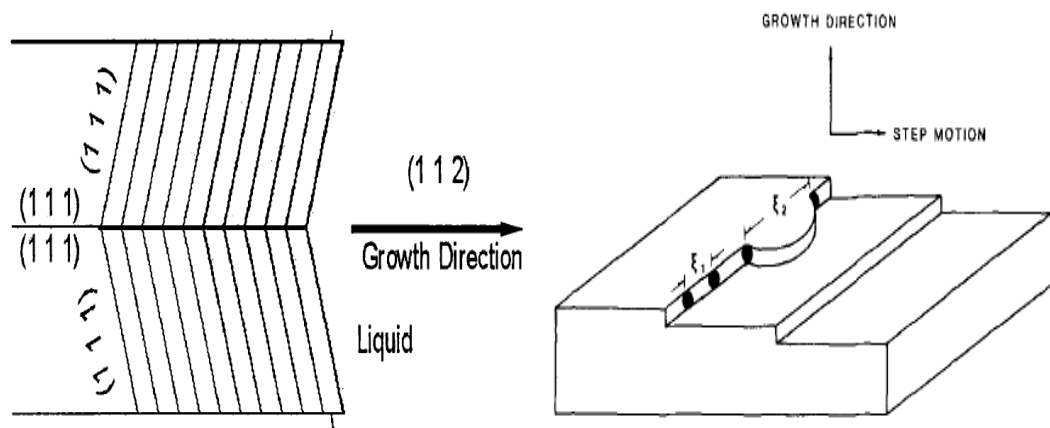


Figure 2.9 Twinning mechanism of silicon growth (a) faceted growth of silicon (b) Step growth of silicon [Lu and Hellawell 1987] [Hamilton and Seidensticker 1960]

The modifier additions are known to hinder the growth of the faceted silicon by inducing more twins. Lu and Hellawell (1987) carried out a detailed study on the efficiency of the various modifiers on the eutectic silicon by observing induced twinning using transmission electron microscopy. They found that the maximum twinning occurs when the ratio of atomic radius of the modifying agent and atomic radius of Si is closer to 1.65. It is believed that the modifier (impurity) atom adsorbs

on to the solid liquid interface to promote twining by displacing a {111} monolayer growth step to the alternative stacking steps and is called as “Impurity Induced Twining”. Several elements are known to modify the eutectic silicon in Al-Si alloys but the efficiency of the modification depends on the atom radius of the modifier.

Qiyang et al. (1991) found that the modification had no effect on the latent heat of fusion, hence proposed that the modification is a kinetic problem rather than a thermodynamic one. They proposed that the addition of Na enhanced the nucleation temperature of primary phase and thereby nucleated it at higher temperature. Subsequently, the eutectic aluminum nucleates and grows epitaxially from the primary phase ahead of Si as the growth of eutectic silicon is restricted by Na. At this condition, Si can only grow by twining between the dendrites of Al.

Several theories have been proposed to explain the mechanism of modification. Basically, there are two classes of theories namely, restricted nucleation theory and restricted growth theory. According to the restricted nucleation theory, the modifier either neutralizes the heterogeneous nucleant (AIP) of silicon or it reduces the diffusion coefficient of Si in melt, so that less number of Si atoms agglomerates for nucleation. Thus, modifying the eutectic silicon by enhancing the undercooling required for nucleation. According to restricted growth theory, modification of the eutectic silicon occurs by adsorption of modifier atom into the twin reentrant groove of the crystalizing silicon. As a result, growth of the silicon is hindered to produce a modified of fine fibrous eutectic silicon.

Few studies supporting the restricted growth theories are given here.

- In 1924 Edward and Archer proposed that the growth obstruction of silicon is brought by finely dispersed Na that separated out from the melt during solidification of the Na treated Al-Si alloy [Xiufang et al. 2001].
- Ransley and Neufled (1947) found that the sodium rich compounds ($\text{NaAlSi}_{1.25}$ and $\text{NaAlSi}_{1.33}$) decreased the growth of silicon phase.

- Winegard et al. (1951) suggested that the addition of chemical modifier decreases the interfacial tension between solid aluminum and solid silicon and thus increases the interface angle between the solids. The solidifying aluminum blocks the growth of silicon causing modification of the eutectic structure as well as significant undercooling.
- (Hanna et al. 1984) studied the effect of sodium based alkali flux on the modification of Al-Si alloys and concluded that the restriction in silicon growth would be the primary mechanism of silicon modification rather than the nucleation affect.
- Glenister and Elliott (1981) proposed that the strontium restricted the growth of the silicon phase by making them grow more isotropically along the planar interface.

Some studies based on the restricted nucleation theory are mentioned here.

- Kim and Heine (1963) found that the addition of modifier (Na) reduced the nucleation temperature of silicon, while the unmodified silicon was obtained at higher temperature. Based on the observations they proposed a growth-temperature/phase shape relation for Al-Si eutectic. As the morphology of the silicon was dependent on the temperature at which it grows.
- Ghosh and Kondic (1963) proposed that the Na addition reduced the growth of silicon by reducing the diffusion rate of silicon in the melt and this led to the lower nucleation temperature during solidification (Gigliotti and Colligan 1972).
- (Parkhutik et al. (1983) reported that the addition of surface active elements leads to the suppression of the nucleation centres of the eutectic silicon to slow the growth of the silicon. In the process the aluminium phase outstrips the growth of silicon to block them from liquid.
- Flood and Hunt (1981) carried out the quenching experiments with Na added eutectic Al-Si to study the effect of addition on nucleation and growth of silicon. They suggested that the change may be the result of non-faceted Si growth at high velocities or in the presence of Na.

According to Shankar et al. (2004) the presence of Fe in the Al-Si alloys also play an important role in the nucleation of eutectic phases. Commercial Al-Si alloys invariably contains significant amount of Fe, which combines with Al and Si to form intermetallic's (α or β -AlSiFe) depending on the concentration of Fe in the melt. They proposed that in the unmodified alloys, the eutectic silicon nucleates on the β -(Al, Si, Fe) particles prior to the nucleation of eutectic aluminum. This leads to the free growth of Si into the melt forming large acicular silicon, whereas, the addition of modifiers alters the nucleation of β -(Al, Si, Fe) to nucleate the eutectic aluminum before silicon. As a result, the eutectic silicon is forced to grow in between the Al dendrites acquiring a fibrous, broom like morphology. The ability of silicon to twin easily aids this growth pattern to proceeds with the twin plane re-entrant edge mechanism.

The beneficial effect of modification is not achieved at its full scale as it is often associated with an increase in porosity when compared to unmodified alloy. Modification alters the porosity level from macroscopic shrinkage to redistributed micro porosity. The effect of Sr on the porosity varies with the Si content of the Al-Si system. Sr has high affinity towards the oxygen and thus reacts to form oxides. These oxides formed due to the addition of Sr play an important role in the formation of pores. Moreover, it is highly impossible to remove these oxides by degassing the melt [Liu et al. 2003].

The effect of modification on porosity is more noticeable in the sand cast alloys, a large number of isolated pores are observed throughout the casting due to the addition of Sr. Careful observation of porosity at different location of microstructure revealed that the pores were formed after a significant solidification of eutectic silicon [Lee and Sridhar 2000]. The pores formed due to Sr modification were associated with the reaction of Sr with the environmental moisture [Miresmaeili et al. 2005]. The addition of Na also increases the volume percentage of porosity in the casting but lower compared to the Sr [McDonald et al. 2004].

2.2.3 Simultaneous addition of refiner and modifier

Since the mechanical properties of Al-Si alloys are highly dependent on the aluminum grain size and morphology of eutectic Si, it is very important to simultaneously refine and modify both the phases to maximize the mechanical properties. But, studies show that the simultaneous modification and grain refinement treatment had negative effect on the mechanical properties as the modifiers interact with grain refiners to poison each other. As a result, both modification and grain refining efficiency of the additions are lost.

Li et al. (2002) studied the combined effect of Al-3Ti-4B and Al-10Sr on the microstructure of Al-Si-Cu alloy and reported that the combined addition resulted in coarser α -Al grain. They also found that the duration of effective Sr modification was significantly shortened due to the formation of SrB₆. They were of the opinion that the mutual poisoning was due to formation of SrB₆ in the alloy.

Nogita et al. (2003) studied the effect of boron and Sr interaction on the silicon morphology of hypoeutectic Al-Si alloy. They reported that the level of Sr available for modification decreased with increase in B content. The reduction in modification was due to the interaction between Sr-B to form a compound. The interaction between Sr and B had no effect on the nucleation temperature of primary aluminum.

Lu and Dahle (2006) studied the interaction between varying concentration of Sr and Al-Ti-B master alloy. They found that the interaction became more noticeable as the addition level of the grain refiner increased. The microstructure studies revealed that the interaction had significant effect on the modification of eutectic silicon. The possible mechanism they proposed was an interaction between AlB₂ and Sr to form SrB₆ particles, thus reducing the modification efficiency of Sr.

Prasada Rao et al. (2006) reported that the grain refining and modification efficiency of Al-Ti-C-Sr decreased with increase in holding time. At longer holding time, the

modification effect was found to be fading, however the grain refinement was retained.

Liao et al. (2007) studied the combined effect of Sr and B addition on Al-Si alloys and found that the Sr and B mutually poisoned each other to nullify its effects. The combined addition of Sr and B resulted in the formation a compound with 3:4 atom ratios of Sr and B. As a result, the modification and grain refinement was decreased.

Golbahar et al. (2014) carried out Sr modification on grain refined Al-Si-Mg alloys to study the interaction between modifier and grain refiner. The interaction between Sr and B led to the decrease of TiB_2 in the melt necessary for grain refinement leading to coarser grain structure.

The addition of eutectic modifier such as Na or Sr to hypereutectic Al-Si alloys was also known to neutralize the effect of phosphorus. When added to the melt, Sr reacts with phosphorous to form strontium phosphide and Na reacts to form Na_3P , compounds which are more stable than aluminum phosphide. This leads to coarsening of the primary silicon phase and deterioration of mechanical properties [Cisse et al. 1975].

Kim (2007) found that the addition of Sr to Al-20 wt. % Si changes the growth mode of primary silicon. The primary silicon was transformed into a non-faceted from faceted crystal. Faraji et al. (2009) reported that the addition of Sr to P treated hypereutectic Al-19Si alloy would suppress the formation of primary silicon. On addition of Sr, the primary silicon nucleation temperature was decreased by 40K, subsequently, decreasing the primary silicon cuboids formed per unit area.

2.2.4 Melt treatment by rare earth (RE) addition

The melt treatment of Al-Si alloys using rare earth elements has gained attention in the recent past due to their ability in modifying and refining the Al-Si alloys. Kowata, et al. (1994) were among the first few researchers who investigated the influence of rare earth in Al-Si alloys. Their primary aim was to find a eutectic modifier, which

does not interact with P refinement in hypereutectic Al-Si alloys. They investigated the effect of rare earth (45%Ce, 31%La, 15%Nd, and 5% Pr) addition on the refinement of primary silicon crystals in Al-20 wt. %Si hypereutectic alloys. They concluded that the primary silicon crystals could be refined with the addition of rare earth elements to Al-Si melt. Xian and Jun (1994) reported that the addition of rare earths elements modified eutectic silicon in hypereutectic Al-Si alloys. They were of the opinion that the refinement obtained by the addition of rare earth elements and sulfur in Al-23%Si was better than phosphorus refinement.

Chang et al. (1998) studied the effect of cooling rate and RE addition on Al-21 wt % Si alloy. The alloy was solidified in a wedge shaped cast iron mold at various cooling rates. They reported that the RE addition brought simultaneous refinement of both primary and eutectic silicon. The refinement of primary silicon increased with increase in cooling rate and the RE content. Subsequently, (12-17°C and 2-7°C) depression in the nucleation temperatures of primary silicon and eutectic silicon was observed with the addition. They were of the opinion that the decrease in nucleation temperature and growth of silicon was mainly due to the decrease in the diffusion rate. Further, studies by Chang et al. (1998) on RE modified Al-Si using electron probe micro-analyzer (EPMA) and convergent beam electron diffraction (CBED) in the transmission electron microscope (TEM) revealed that the RE elements were segregated between the primary Si crystals. The suppression of the TPRES growth mechanism in primary silicon and modification of the eutectic silicon was due to the change in surface energy at solid-liquid interfacial energy brought by RE addition.

CHEN et al. (2007) studied the complex modification of P and RE on Al-20Si-1.6Cu-0.7Mn-0.6Mg alloys solidified in a permanent mold preheated to 250°C. They reported that the addition of RE along with P resulted in refinement and modification of primary and eutectic Si. The primary silicon was refined to 23.3µm from 64.4µm and eutectic silicon was modified to fine fibrous form with an average size of 5.3µm. Subsequently, the refinement and modification improved the tensile strength and elongation of the alloy by 20 and 40% respectively.

Ouyang et al. (2007) investigated the effect of La addition on Al-18% Si alloy solidified on a preheated metal mold. The La master alloy was added in combination with P. The simultaneous modification of primary and eutectic silicon was achieved on combined addition of La and P. The morphology of eutectic silicon changed from long needle-like structure to short rod-like structure.

Ganfeng et al. (2010) found that the optimal addition of rare earth element (Er) to Al-17% Si and Al-25% Si alloys would yield a modified microstructure. The size of the primary silicon decreased with Er addition and the mechanical properties was found to be highest at the optimal concentration of Er addition.

As the addition of RE could bring simultaneous refinement and modification to hypereutectic Al-Si alloys, the researchers were interested in knowing its ability in refining and modifying hypoeutectic and eutectic Al-Si alloys. Tang and Mao (2000) investigated the effect of RE on Al-12Si-Cu and Al-7Si-Mg alloys. They found that the alloy microstructure was simultaneously refined and modified with the addition of RE. Moreover, the fading effect was less in RE added alloys. The RE treated alloys showed better mechanical properties than the Sr treated alloys. Although, the RE addition could influence the microstructure of hypoeutectic Al-Si alloy, the exact role of added RE was uncertain. Chang et al. (2001) speculated that the change in growth kinetics could be the main reason for structural modification.

Nogita et al. (2004) studied the effects of individual rare earth elements (La, Ce, Pr, Nd, Sm, Eu, Gd, Tb, Dy, Ho, Er, Tm, Yb and Lu) on eutectic modification of Al-10Si alloy. The thermal analysis and microstructural analysis indicated that all RE elements had some influence on eutectic silicon. Among all, Europium was the only element to yield fully modified eutectic silicon. Even though Yb had similar atomic ratio of (r/r_{Si}) as that of Eu and close to that of ideal atomic ratio of 1.65, Yb did not yield fully modified fine fibrous eutectic silicon structure.

Sebaie et al. (2008) investigated the influence of Mish-Metal (MM) alloy (10%Ce, 7%La, 1%Nd, 1%Pr, 1%others, rest Al) on the eutectic Si particle characteristics of

A319.1, A356.2 and A413.1 Al–Si casting alloys. The results revealed that the addition of MM partially modified the eutectic silicon, however, the MM modification was more effective at higher cooling rates.

Contradicting the previous literature on the effect of RE on hypoeutectic Al-Si alloys Zhu et al. (2011) reported that the tensile strength and ductility of the alloy decreased even though the eutectic silicon was fully modified. They studied the influence of misch-metal (MM) addition on microstructure and tensile properties of A356 alloy. The decrease in properties was mainly due to grain coarsening effect. It was found that a Ce- rich misch-metal was formed due to addition and it hindered the refinement of grains.

2.2.5 Effect of cerium (Ce) on Al-Si alloys

Since about 50-55 wt.% of mish-metal composition consist of cerium, it would be beneficial to study the individual effect Ce on the Al-Si alloys. Ce was found to have positive effect on the structural modification of Al-Si alloys. Moreover, according to [Lu and Hellawell 1987] the modification by chemical addition occurs by inducing twin in the silicon (Twin Plane Re-Edge (TPRE) mechanism). The maximum twining occurs when the ratio of atomic radius of the modifying agent and atomic radius of Si is closer to 1.65. The radii ratio (R_{ce}/R_{Si}) for cerium against silicon is 1.56, which is very much similar to the radii ratio of sodium. The (R_{Na}/R_{Si}) of sodium was 1.58, yet sodium produced fully modified structure at an addition of very low concentration of 0.01 Wt.%. Hence, similar to sodium, cerium could be also an ideal eutectic silicon modifier. Few available literatures on Ce treatment of Al-Si alloys are given below.

Anasyida et al. (2010) reported that the addition of Ce to Al-12Si-4Mg resulted in a formation of a needle shaped Al-Ce intermetallic phase. As a result there was a significant improvement in the micro hardness and wear resistance of the alloy. Voncina et al. (2012) investigated the influence of Ce on grain refining performance on A380 alloy. The alloy was treated with nominal concentrations (0.05% max) of

pure cerium at varying cooling rates (10, 100, 300, 350 K/ min). The results showed that the addition of Ce yielded smaller α -aluminum than in unmodified alloy.

Chen et al. (2013) investigated the effect of Ce and Sr addition on the nucleation kinetics of α -aluminum. Ce being a surface active element alters the surface energy of the melt and decrease the activation energy for nucleation of α -aluminum. Asmael et al. (2013) studied the effect of Ce addition on near eutectic Al-11.7% Si alloy. The melt treated with elemental pure cerium at 750 °C and solidified in a preheated ceramic mold showed a decrease in the nucleation and growth temperatures, along with the modification of silicon particle on addition of Ce.

Zhang et al. (2006) reported that the addition of Ce to Al-18Si alloy transformed the primary silicon from coarse branched shape to fine faceted shape. They observed that the eutectic silicon away from the primary silicon was effectively modified by the Ce addition than the silicon nearer to the primary silicon.

Dai and Liu (2009) studied the combined and individual effect of P, B and Ce on Al-30%Si and found that Ce has moderate effect on primary and eutectic silicon. The alloy was solidified in preheated (473K) permanent mold of dimension $\Phi 35\text{mm} \times 75\text{mm}$. They also found that the addition of Ce along with B had good modification effect on eutectic Si due to the large undercooling effect.

Kores et al. (2010) studied the effect of Ce addition on cast iron mold solidified Al-17 % Si alloy and reported that the addition of 1% Ce resulted in the refinement of primary and eutectic silicon. The primary silicon nucleation temperature decreased from 686 °C to 591.9 °C on Ce addition. But, this was contradictory to the results obtained by Wesis and Loper (1987). In their studies, they reported that cerium did not refine primary silicon but it moderately affected the eutectic silicon.

Recently, Li et al. (2013) reported that the Ce could significantly refine and modify primary and eutectic silicon. They studied the effect of Ce addition on the microstructure and tensile properties of Al-20%Si alloy. The alloy was solidified in a 200°C preheated permanent steel mold of 20mm inner diameter and 50 mm length.

The addition of cerium refined the primary silicon size from 94 μm to 33 μm and transformed eutectic silicon to fine fibrous form. The addition also led to the improvement in tensile strength and elongation.

2.3 Rapid Solidification

The solidification in hypoeutectic Al-Si alloys begins with the nucleation and growth of aluminum dendrite network. The primary and secondary dendrite arm spacing (DAS and SDAS) controls the size and distribution of porosity and intermetallic in the casting. The finer DAS leads to fine and evenly distributed porosity, intermetallic. The tensile strength of the alloy is significantly influenced by DAS [Shabestari and Moemeni 2004]. By properly controlling the casting parameters like pouring temperature, casting velocity and cooling rate, rapid solidification technique can be employed to produce refined microstructure in Al-Si alloys without any chemical modification [Ceylan et al. 1997]. Shabestari and Malekan (2005) reported that the DAS have logarithmic linear relationship with solidification rates, as shown in the Figure 2.10. They reported that the cooling rate have direct influence on solidification parameters. The liquidus temperature, undercooling temperature and solidification range increased and recalcence temperature decreased with increase in cooling rate. The DAS decreased by about 60% with 10% increase in cooling rate. The increasing cooling rates refined the eutectic silicon and intermetallic present in the alloy.

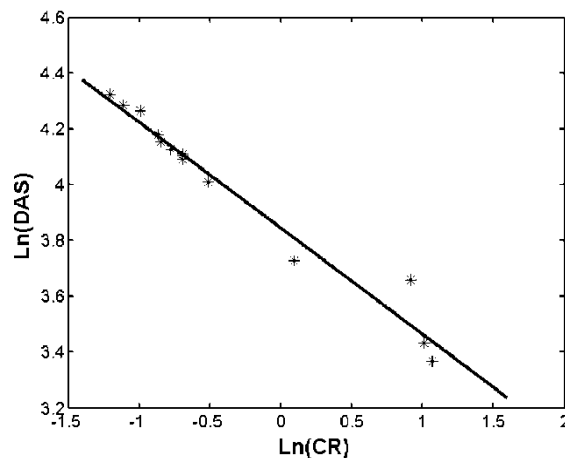


Figure 2.10 DAS as function of cooling rate (Shabestari and Malekan 2005)

Nguyen (2005) was of the opinion that the material strength and other mechanical properties of the Al-Si alloys can be enhanced by increasing the solidification rates. Conley et al. (2000) reported that the high cooling rates would result in the reduction in porosity. The sizes of the pores in the casting were smaller and evenly distributed when compared with slowly cooled alloys.

Dobrzański et al. (2006) studied the effect of cooling rate on the thermal characteristics of Al-9Si-Cu alloy and found that the cooling rate has significant influence on the nucleation temperatures of various phases in the alloy. The increase in aluminum nucleation temperatures would lead to an increased number of nuclei available for nucleation, resulting in fine grains and SDAS.

Aguilera-Luna et al. (2014) studied the effect of cooling rate on the Al-Si eutectic alloy and reported that by increasing the cooling rate from 0.5 to 4°C/s decreases the SDAS from 60 to 26 μm. The increased cooling rate also resulted in the modification of eutectic silicon by 1.5 levels. A similar kind of decrease in DAS in Al-Si-Cu with increased cooling rate was reported by Xiaowu et al. (2012)

Hosseini et al. (2013) studied the effect of cooling rate on solidification parameters of LM13 alloy and reported that the nucleation temperature of the alloy increased with cooling rate. As the cooling rate was increased from 1.1 to 5.6 °C/s, the nucleation temperature was raised by 12.9°C. The microstructure of the alloy was significantly influenced by the increase in cooling rate. The SDAS was decreased to 18.7μm from 50 μm when the cooling rate was increased from 1.1-50 °C/s. The increasing cooling rate also led to the refinement of eutectic microstructure by decreasing the distance between parallel eutectic layers. They also reported that the increasing cooling rate resulted in the reduction of interdendritic porosity and improvement in mechanical properties.

Size refinement of primary silicon in hypereutectic Al- Si base alloys is a key requirement for meeting property targets and can be achieved by inoculation with phosphorus, as is routinely applied in conventional foundry practice. Studies show

that the refinement can also be achieved by properly controlling casting parameters such as pouring temperature, casting velocity and cooling rate. Various techniques such as chill casting, rapid solidification or melt overheating are employed to produce refined microstructure in the hypereutectic Al-Si alloys without chemical modification [Yu et al. 2009] [Yamagata et al. 2008] .

Yu et al. (2009) observed a typical microstructure of fine primary Si particles with fully developed Al dendritic halos in the direct chill (DC) cast of hypereutectic Al-Si alloys without chemical modification as shown in the Figure 2.11. Yamagata et al. (2008) studied the effect of cooling rates on the microstructures of Al-20% Si die cast alloy. They found that the primary silicon size and secondary dendrite arm spacing (SDAS) decreases with increase in cooling rates. Figure 2.12 (a, b) illustrates the influence of cooling rates on primary silicon diameter and secondary dendrite arm spacing.

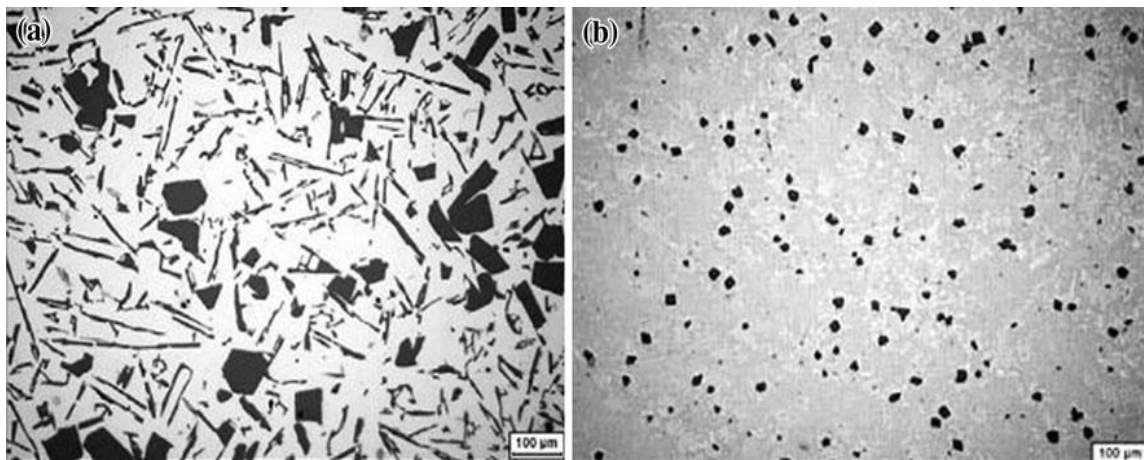


Figure 2.11 Microstructure of an Al-16Si alloy showing primary and eutectic Si phases (a) slowly solidified (b) DC cast at 4.34 mm/s [Yu et al. 2009]

Studies carried out by Sulzer (1960), Mandal et al. (1991) and Kaneko et al. (1978) reveal that the further refinement in primary silicon can be achieved by the addition of phosphorous to the alloys solidified at high cooling rates. In order to relate the primary silicon distribution and cooling rates, Kyffin et al. (2001) derived a relationship for mean inter-particle spacing of primary silicon and number of silicon

per unit area. In the absence of chemical refiners, the mean particle was related to cooling rate as $\lambda T^{1/3} = 256 \pm 24 \mu\text{m}(\text{K/s})^{1/3}$. As compared with casting alloys, the properties of rapidly solidified hypereutectic Al-Si alloys are greatly improved because of the refining of the silicon phase and increase in solubility of alloy elements.

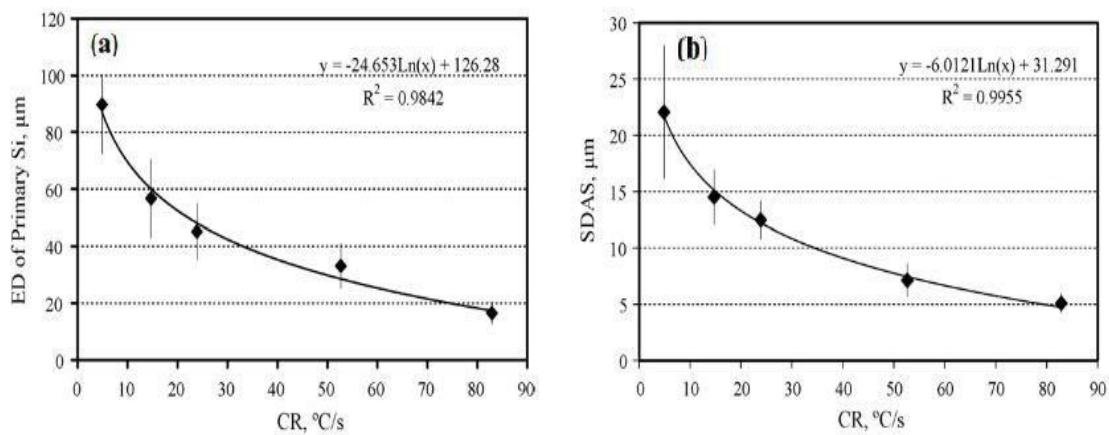


Figure 2.12 (a) Effective diameter of primary silicon (b) SDAS as a function of cooling rates [Yamagata et al. 2008]

In addition to the above, the parameters such as melt temperature, holding time and under-cooling also affect the primary silicon particles. After studying the effect of under-cooling on morphology of primary silicon, Kang et al. (2005) reported that primary silicon transformed from star-like to massive Si with increase in under-cooling. Xu et al. (2006) found that morphologies of primary silicon strongly depend on solidification conditions and found that the morphology of primary silicon changed from star-like and other irregular shape to octahedral with the elevation of melt temperature. Analysis of the results revealed that the cooling rate below a critical value (3.75°C/s) will hardly affect the morphologies of primary silicon. Korojy and Fredriksson (2009) reported that morphology of primary silicon changed from octahedral faceted shape to the plate-like shape with an increase in melt super heat temperature. Kasprzak et al. (2009) reported that high melt temperatures had a positive effect on the size and distribution of the primary Si crystals. They found that,

pouring of melt close to liquidus temperatures resulted in coarse primary silicon in spite of the initial high melt temperature.

2.4 Heat Treatment

The mechanical properties of cast Al–Si–Cu–Mg alloys depend mainly on the alloy composition and the parameters of the casting process. Further improvement in the mechanical properties of cast components would be bought by heat treatment. The presence of elements like Mg, Cu in the alloy makes it heat treatable by forming precipitates. Heat treatment process involves heating and cooling of the alloy to form homogenized precipitates in the matrix and is known as ‘precipitation- hardening’.

Various heat treatment cycles, e.g. different combinations of temperatures and times are used depending on the casting process and the alloy composition to achieve desired mechanical properties [Sjölander and Seifeddine 2010]. Generally, T6 heat treatment process is applied to sand, permanent mold and gravity die-cast Al–Si alloys. Figure 2.13 shows the stages involved in heat treatment of aluminum alloys and are as follows:

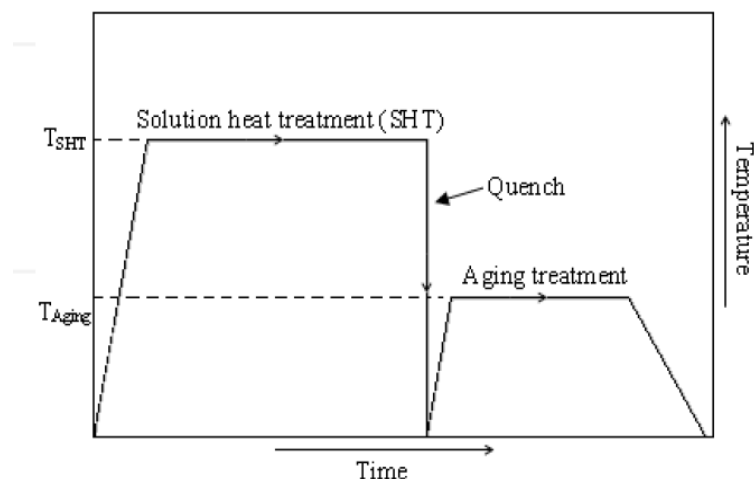


Figure 2.13 Steps involved in heat treatment process (Mohamed and Samuel 2012)

1. Solution treatment, relatively subjected to high temperature, to dissolve Cu- and Mg-rich particles formed during solidification and to achieve homogeneous concentration of the alloying elements in solid solution.
2. Quenching, cooling rapidly to room temperature, to obtain a supersaturated solid solution of solute atoms and vacancies.
3. Age hardening, causes precipitation of solute atoms from the supersaturated solid solution, either at room temperature (natural ageing) or at an elevated temperature (artificial ageing).

The aluminum association has standardized the definition and nomenclature applicable to thermal practices. The standardized temper designations applicable to castings are:

T0 (formerly T2, T2x): annealed (thermally stress relieved)

T4: solution heat treated and quenched

T5: artificially aged

T6: solution heat treated, quenched and artificially aged

T7: solution heat treated, quenched and over aged

T8: cold reduced before ageing to improve yield strength (bearing only)

The mechanical properties after heat treatment largely depend on the precipitation of non-equilibrium phases during aging and the changes occurring in Si particles due to solution treatment. The response of the aluminum alloys towards heat treatment depends on the presence and distribution of Cu and Mg precipitates in the alloy. Al-Si-Cu-Mg alloys and Al-Si-Mg alloys generally have high response towards heat treatment than Al-Si-Cu alloys [Mohamed and Samuel 2012].

2.4.1 Solution treatment

The dendritic solidification of aluminum alloys will result in the segregation of solute elements between the dendrites and have an adverse effect on the mechanical properties. The aim of solution treatment is to obtain a homogenized super saturated structure and to maintain the saturated structure through quenching, followed by

precipitation hardening. By carrying out solution treatment following benefits can be achieved in Al-Si-Cu-Mg alloys:

- 1) Homogenization of the casting
- 2) Dissolution of Cu and Mg intermetallic phases into the matrix
- 3) Spheroidization of eutectic Si particles

Solution treatment is carried out by subjecting the alloy to an isothermal temperature below the eutectic temperature for certain duration of time. The strength of the alloy increases with the increase in solutionizing temperature, as the solubility of the alloy increases with temperature. But, the increase in solution temperature is limited due to the presence of Cu and Mg in the alloy, which lowers the eutectic temperature of the binary Al-Si alloy. Therefore care should be taken while selecting the temperature to avoid the incipient melting of the phases in the alloy. The incipient melting lowers the mechanical properties of the alloy [Samuel 1998]. Conventionally, the solutionizing temperature of Al-Si-Cu-Mg alloys is maintained around 495°C to avoid the melting of Cu rich phases. The time required for homogenization is dependent on the solution temperature and dendrite arm spacing of the alloy. Generally, the homogenization of the alloy takes place within 1 hour of solution treatment, whereas, spheroidization takes longer time. Isothermal treatment for shorter time would lead to an inadequate dissolution of the phases, and longer solution treatment would result in the use of more energy. Moreover, prolonged exposure may lead to coarsening of micro-constituents and result in deleterious effect on the mechanical properties. Hence, adequate time has to be given for solution treatment.

The availability of the secondary phases for precipitation hardening directly depends on the dissolution of those phases during solution treatment. However, all the phases present in the alloy do not dissolve during the solution treatment. Particles like $\text{Al}_5\text{Mg}_8\text{Si}_6$ and $\text{Al}_5\text{Cu}_2\text{Mg}_8\text{Si}_6$ are hard to dissolve, whereas, phases like $\beta\text{-Mg}_2\text{Si}$ and $\theta\text{-Al}_2\text{Cu}$ dissolve comparably easily [Moustafa et al. 2003]. However, the complete dissolution of Al_2Cu is not possible in high copper content alloys [Prasad and Dan 1991]. In such cases, solution treatment with longer time would be adopted for

complete dissolution [Lasa and Rodriguez-Ibabe 2002]. To maximize the mechanical properties it is very important to achieve complete dissolution of Mg and Cu phases, as undissolved Cu and Mg phases are not available for strengthening.

The homogenization depends on the composition, size, shape and distribution of phases formed during solidification. During homogenization, the atoms detach from the phases and diffuse through the matrix to decrease the concentration gradient. Hence the homogenization is also influenced by the microstructure of alloy, generally dendrite arm spacing (DAS) and nature of the diffusing atom. The diffusion rates of the phases are greatly dependent on the solution temperature and the time of holding.

The dissolution of Mg containing phases like Mg_2Si is faster than the Cu phases (Al_2Cu). On addition of Mg to Al-Si alloys, Mg combines with silicon and iron to form Mg_2Si and π -Fe intermetallic. Studies show that the dissolution of Mg_2Si phases in A356 alloy with low Mg content was completed in less than 4 min and homogenization was completed within 15 min. However, the dissolution and homogenization time increased with the increase in Mg content [Rometsch et al. 1999]. Moreover, the transformation of π -Fe phase into β -Fe phase and Mg was dependent on the concentration of Mg in alloy, lower the Mg content, faster the transformation [Rometsch et al. 2001].

The dissolution of Al_2Cu depends on the size and morphology of the phase formed during the solidification. In as-cast condition the Al_2Cu can be present in different shapes, as block-like Al_2Cu , as eutectic Al_2Cu or mixture of both types. On solution treatment, the Al_2Cu particles dissolve and fragment into smaller size. The spheroidization and dissolution takes place by radial diffusion of Cu into matrix (Han et al. 2008). Studies show that blocky Al_2Cu particles are harder to dissolve compared to eutectic Al_2Cu particles as it does not fragment. When exposed for longer time, the blocky particles dissolve by spheroidization and diffusion and is illustrated in the Figure 2.14. The dissolution of Al_2Cu takes longer time compared to Mg-phases, as the diffusion of Cu in Al matrix is slow and also because of solution treatment temperature, Cu containing alloys are exposed to lower temperature to avoid the incipient melting of the Cu phase. The dissolution of 75% of Al_2Cu phase in 319.2 alloys would take about 8h at 515°C and 24h 505°C [Samuel et al. 1996].

The presence of Mg in the alloy would lead to the formation of blocky Al_2Cu phase between the eutectic Si and Q- $\text{Al}_5\text{Cu}_2\text{Mg}_8\text{Si}_6$. The Q phase is believed to be grown from the blocky Al_2Cu phase during the last stages of solidification. The coarseness of the Q phase increases with the increase in Mg content [Samuel et al. 1998]. The response of these phases to solution treatment depends on the composition and solution treatment temperature and time. Lasa and Rodriguez-Ibabe (2002) studied the effect of solution treatment on the Al-Si-Mg-Cu alloy and found that the Q phase did not change during the solution treatment. Yet in another study they reported that the dissolution of Q phase would occur at high temperatures. The phase started to dissolve when the temperature is increased to 530°C . The area fraction of Q phase increased by dissolving Mg_2Si in an alloy for low Cu and high Mg concentrations. The time needed for Al-Si-Cu-Mg alloys are shorter than the Al-Si Cu alloys. The time required to obtain uniform concentration of Cu in Al-7Si-3.5Cu was about 8h at 490°C and in the presence of Mg it was shortened to 4h [Han et al. 2008].

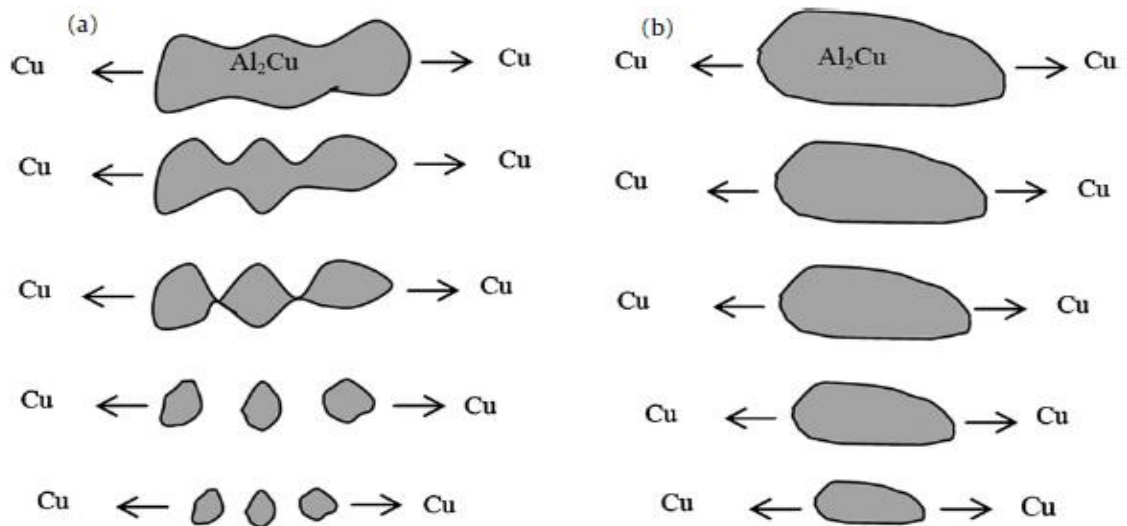


Figure 2.14 Dissolution of Cu particles (a) eutectic Al_2Cu (b) blocky Al_2Cu [Sjolander and Seifeddine 2010]

In addition to the dissolution and homogenization, the solution treatment also results in spheroidization of eutectic Si. The morphology of the eutectic Si has significant

influence on the mechanical properties of the alloy. In untreated alloys, the eutectic Si is present as large flakes and acts as crack initiators affecting the strength and ductility of the alloy. The morphology of eutectic Al-Si alloys can be altered either by chemical modification or by solution treatment. The granulation or spheroidization of Si takes place in two stages

- 1) Fragmentation or dissolution of eutectic silicon branches
- 2) Spheroidization of separated branches

During solution treatment, the unmodified Si particles break and separate into small segments retaining same morphology. Then the fragmented segments spheroidize into fine globular Si as shown in the Figure 2.15. The time required for spheroidization of eutectic Si depends on the solution temperature and the morphology of the eutectic Si. Finer eutectic Si would lead to faster spheroidization of silicon [Sjolander and Seifeddine 2010]. Ogris et al. (2002) reported that the modification had positive influence on the solution treatment. The time required for solution treatment decreased with Sr modification. Shivkumar et al. (1990) optimized the solutionizing time for Sr modified A356 as 3-6 h at 540°C. Similarly, the time required for complete spheroidization in Sr treated 319 alloys at 495°C was in the range of 8-16h (Crowell and Shivkumar (1995)).

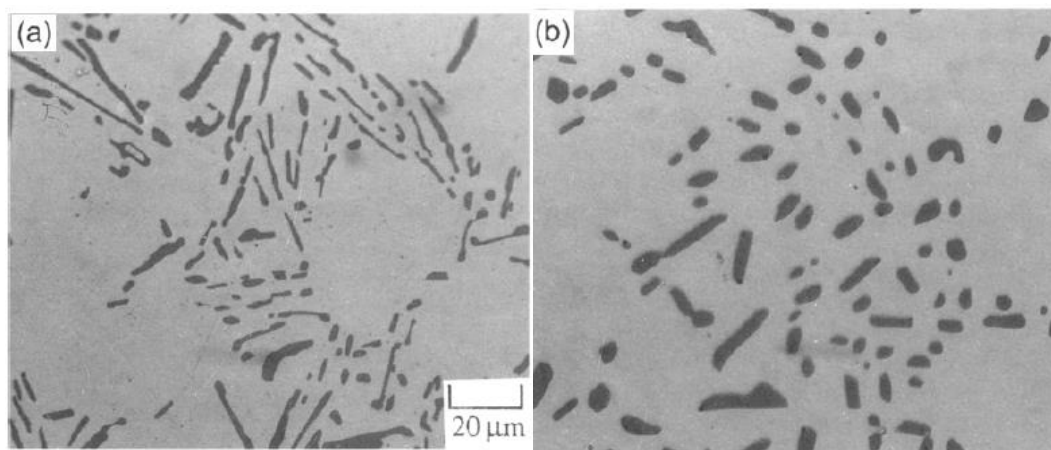


Figure 2.15 Spheroidization of eutectic silicon during solution treatment (a) 50 min (b) 400 min, at 540°C [Shivkumar et al. 1990]

2.4.2 Quenching

The objective of quenching is to retain dissolved solutes in the solid solution at room temperature and make it available for precipitation hardening during ageing.

If the quenching rate is sufficiently high, the solutes will be retained in solid solution along with high number of vacancies. On the other hand, at slow quenching rates the particles would precipitate on the grain boundaries or dislocations, resulting in the reduction of super-saturation of solute. Subsequent ageing will lead to lower hardness and tensile properties [Benardin 1995]. Various quenchants and quenching processes are used for the heat treatment of aluminum alloys, and cooling characteristics of few quenchants are reviewed by [Totten et.al 2003]. Among all, cold water (10-32 °C) is regularly used in industry in order to maximize the mechanical properties. When distortion or cracking is encountered, either hot water (60-70 °C) or a polymer quenchant is used [Xiao et al. 2010].

The drawback with cold water (10-32 °C) cooling is that it occasionally produces unacceptable distortion due to high thermal gradients. The thermal gradients are also produced due to the variations in the section size. [Tanner et al. 2004]. Generally, this problem is avoided by quenching in hot water (60-70 °C). Comparably, slower quenching rate will reduce the thermal gradients and eliminate the possibility of cracking. However, the slower cooling rate would reduce the mechanical properties and corrosion resistance of the alloy [Jolly 2005].

2.4.3 Ageing

The objective of the ageing is to obtain a homogeneous distribution of precipitates to improve the strength of the alloy. The strength of the heat treated alloy depends on the ability of the precipitates in stopping the movement of dislocations. The size, shape and coherency of the precipitates with matrix would influence its ability in stopping the dislocation movement. The interaction of precipitates with the dislocation can be explained by Friedel effect and Orowan mechanism. The mechanisms are illustrated in the Figure 2.16.

According to Friedel effect if the precipitates are small and too hard, the moving dislocations can shear the precipitates. On the other hand, if the precipitates are large and harder the moving dislocations can easily bypass the precipitates (Orowan mechanism). The strength of the alloy will be at its peak when there is an equal chance for both the mechanisms to occur simultaneously, i.e. the movement of dislocation occur by both shearing as well as by bowing [Sjölander and Seifeddine 2010].

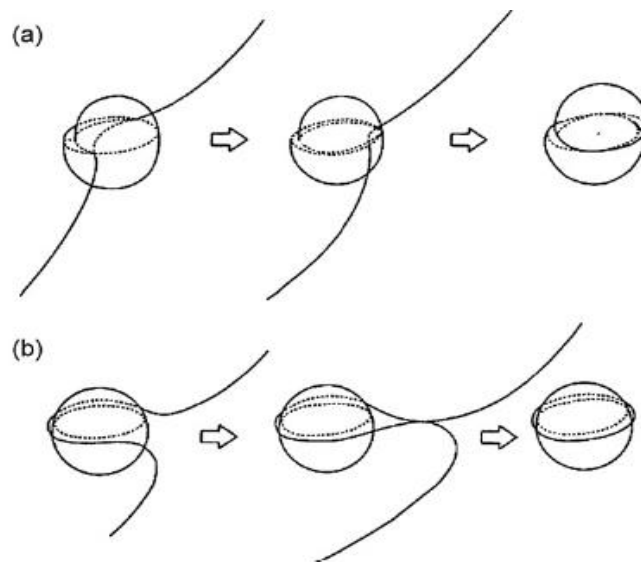


Figure 2.16 Illustration of Friedel effect and Orowan mechanism (a) shearing (b) bypassing [Sjölander and Seifeddine 2010]

After solution and quench treatments the matrix contains high concentration of supersaturated solute atom and vacancies. On ageing these atoms diffuse out from the matrix to evolve as clusters known as Guinier-Preston (GP) zones. GP zones are finely dispersed across the matrix and are coherent to the matrix. This phenomenon was first observed by Aldra in 1906. He found that the hardness of the alloys containing Mg, Cu and other trace elements increased with time at room temperature [Sjölander and Seifeddine 2010]. The process was later termed as precipitation hardening. The formation of GP zones are directly influenced by the concentration of

solutes in the matrix after quenching and the diffusion rate of the particular precipitate in the matrix. The diffusion of atoms through matrix is limited at the room temperature. Hence, the ageing of Al-Si alloys is generally done at the elevated temperatures. Based on the ageing temperature there are two types of ageing treatment.

- 1) Natural ageing- at room temperature for longer time
- 2) Artificial ageing- at elevated temperature, normally in the range of 150-210°C.

The precipitation hardening of Mg containing Al-Si alloys start by the formation of finely dispersed clusters (GP zone) consisting of Mg and Si. The zones grow and develop into needle shaped β'' phase, which is in coherent with the matrix. The growing needles becomes semi-coherent β' and end up in non-coherent stable β platelets. The strength of the alloy increases as the concentration of the Mg increases in the alloy.

The presence of Cu in Al-Si alloys results in the formation of GP zones consisting of Cu atoms at the room temperature. As the temperature is increased to 100°C, the GP zones dissolves and forms coherent θ'' (known as GP2) an ordered tetragonal arrangement of Al and Cu atom. After Pro-longed ageing time a meta-stable θ' phase is heterogeneously nucleated on the dislocations by dissolving θ'' . The difference in the thermal expansion between primary Al and Si particles would lead to the formation of large concentrations of dislocations in Al-Si-Cu alloys. These low energy dislocation sites would act as heterogeneous nucleation sites for θ' phase and with ageing time, a stable and incoherent θ (Al_2Cu phase) is formed. However, the precipitation of θ (Al_2Cu phase) was slower compared to the precipitation of Mg phases. Möller et al. (2007) and Reif et al. (1997) studied the effect of ageing time on the hardness of the Al-Si-Cu, Al-Si-Cu-Mg or Al-Si-Mg alloys and found that the Al-Si-Cu alloys respond slowly to the room temperature ageing, whereas, Mg added alloys harden quicker, corresponding results are shown in the Figure 2.17.

The presence of Cu and Mg in Al-Si alloys would lead to many precipitates depending on the composition of the alloy and the thermal treatments. An peak aged Al-Si-Cu-Mg alloys would contain β'' (Mg₂Si), θ' (Al₂Cu) and Q-Al₅Cu₂Mg₈Si₆ depending on the treatment given.

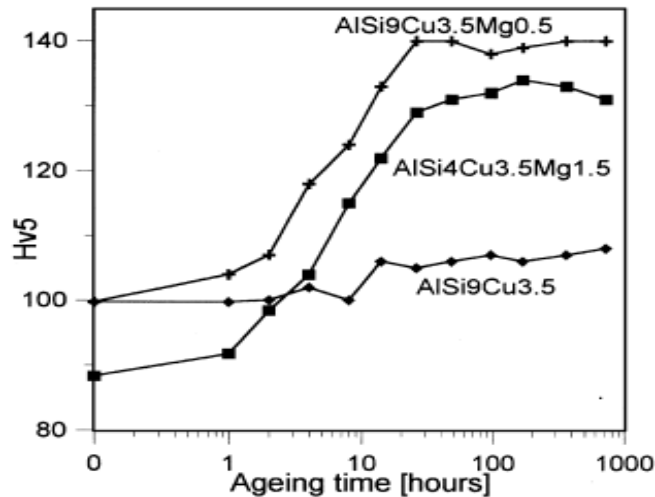


Figure 2.17 Response of Al-Si alloys to natural ageing (Reif et al. 1997)

2.5 The combined effect of modification/refinement and heat treatment on Al-Si alloys

The mechanical properties of the Al-Si alloy are greatly dependent on the morphology of the eutectic Si present between the dendrites. The chemical modifications of eutectic Si by trace elements like Sr or Na were found to improve the mechanical properties significantly. Similarly, the spheroidization of eutectic Si during heat treatment also plays an important role in improving the mechanical properties of the Al-Si alloy. Since, both the processes (modification and spheroidization) transforms the morphology of Si into fine globular structure, the influence of silicon modification on heat treatment parameters and mechanical properties has been documented by several studies. But, most of the results contradict each other.

Shivkumar et al. (1990) studied the effect of Sr modification on the solution temperature of A356 alloys. They reported that the modification had significant effect on the solution temperature and found to decrease of solution temperature. The modification process increased the spheroidization rate and decreased the coarsening rate of Si. But, conjunction of modification and heat treatment had negative impact on the mechanical properties of the alloy. A study by Samuel (1998) also revealed that the strength of the solution treated Sr treated alloy was apparently lower than the solution treated unmodified alloy.

Zhu et al. (2012) studied the effect T6 heat treatment on the rare earth (MM) added A356 alloy and found that the MM addition resulted in the better spheroidization than the unmodified alloy. The mechanical properties improved with the heat treatment irrespective of the prior treatment. However, the MM modified alloys showed better strength than the unmodified alloys.

Wang et al. (2003) studies on the influence of Sr and Na modification on solution treatment parameters revealed that the modification increased the incipient melting temperature of the alloy. The Sr treatment increased the solution temperature of the alloy. Ogris et al. (2002) reported that the spheroidization of Sr treated alloy was completed in shorter time than the unmodified alloy.

Tash et al. (2007) reported that the modified eutectic Si exhibits higher coarsening rate than the unmodified alloys. They were of the opinion that the negative effect of Sr modification was due to the presence of Mg in the alloy. The modification of 356 and 319 alloys had no effect on the ageing temperature. Sebaie et al. (2008) reported that the heat treatment of unmodified alloys resulted in coarsening of the Si particles and Sr modification resulted in better spheroidization.

Osorio et al. (2007) concluded from their studies that the combination of modification and heat treatment did not yield ant significant improvement in the strength of the Al-9Si alloy. Almost similar ultimate tensile strength was obtained with unmodified, modified and modified heat treated alloys. Moldovan et al. (2007) studied the effect

of heat treatment on the Al-Ti-B-Sr modified Al-7Si-0.3Mg alloys and found that the mechanical properties were significantly improved due to modification and heat treatment.

Ma et al. (2010) studied the influence of ageing treatments and Sr modification on the hardness of Al-11Si-2.5Cu-Mg alloys. They found that the addition of Sr decreased the hardness of the artificially aged samples and Sr modification also counteracted the hardness achieved by the addition of Mg. The precipitation characteristics and hardness were found to be influenced by the cooling rate during solidification for unmodified alloys, whereas, the precipitation in the Sr modified alloys remained inactive towards the varying cooling rate.

In another study Ma et al. (2010) revealed that the solution treatment effect in the Sr treated alloys varied with the cooling rate. They reported that the increase in Sr content decreased the roundness effect due solution treatment as the roundness begun to diminish at higher Sr levels. The rate of spheroidization was higher in the Sr treated alloys, whereas, coarsening was higher in the unmodified alloys.

Sebaie et al. (2008) studied the effect of Sr, MM modification, cooling rate and heat treatment on the eutectic Si characteristics of A319.1 and A413 alloys. They reported that the Sr modification resulted in higher hardness than in A319.1 and lower hardness in A413 alloys than the respective unmodified alloys at varying cooling rates. In both the alloys, MM addition and heat treatment had deleterious effect on the hardness of the alloy.

2.6 Assessment of Modification/Refinement

Traditionally the quality of casting is assessed by destructive sampling and by metallographic examination of the structure. But, these conventional processes are time consuming, expensive and inaccurate. Moreover these methods cannot be used for online prediction of the melt quality. Non-destructive Evaluation (NDE) techniques are known to overcome these problems by providing rapid and reliable

results. NDE methods of evaluation of melt quality are broadly classified as computer aided cooling curve analysis (CACCA), electrical conductivity measurements and ultrasonic techniques (Xiang et al. 2005).

2.6.1 Computer aided cooling curve analysis (CACCA)

CACCA is an online prediction tool that can be used effectively to determine the wide range of thermo-metallurgical information related to metals or alloys. The process involves measuring the temperature history of the sample with respect to time and determining the thermal characteristics, fraction solid and latent heat during melting or solidification [Shabestari 2010]. An accurate CACCA technique can be used to quantify grain size, dendrite coherency point (DCP), level of silicon modification, low melting point of secondary eutectics, temperature of phase transformation, heat release during phase transformation, fraction of solid phases, liquidus and solidus temperature and non-equilibrium cooling conditions, eutectic temperature.

In CACCA analysis, the temperature of the sample is measured continuously as it solidifies from molten state to solid state. The measured temperature is then plotted against time elapsed during solidification to acquire the cooling curve. Figure 2.18 shows a typical cooling curve of an Al-Si alloy, along with respective nomenclatures. The first derivative of the cooling curve provides information about the cooling rate of the sample. The cooling curve in conjunction with the derivative curve can be used to determine and analyze different solidification characteristic parameters.

The Al-Si alloy cooling curve are generally influenced by,

- Chemical composition and trace elements
- Grain refinement
- Eutectic silicon modifiers

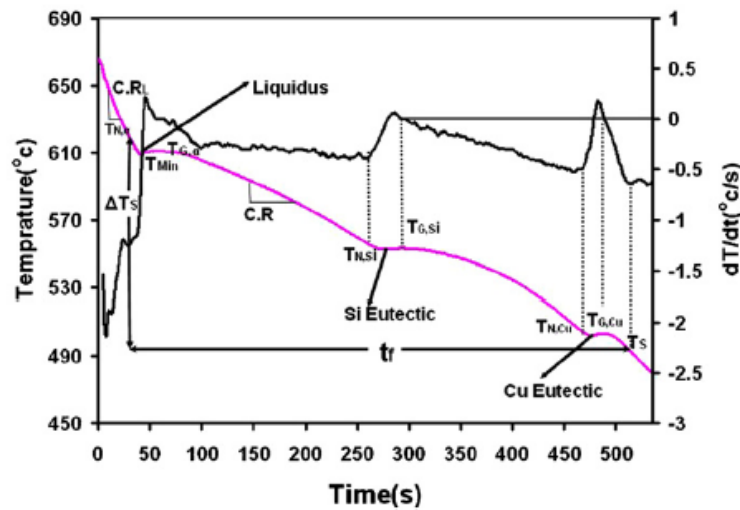


Figure 2.18 Cooling curve, first derivative curve and characteristic parameters of Al-Si alloy [Shabestari and Malekan 2010]

where,

- $T_{Al, \min}$ and $T_{Al, \max}$ are the minimum and maximum temperatures from which the recalescence ΔT_{Al} is calculated for the nucleation of the primary (Al) phase.
- $T_{e, \min}$ and $T_{e, \max}$ the minimum and maximum temperatures, from which the recalescence ΔT_e is calculated for the eutectic reaction.
- Times related to parameters are t_e , and t_{coales} , i.e. the duration of the eutectic plateau and the time difference between the minimum temperature for (Al) nucleation and eutectic transformation.

Theoretically, cooling curve of a pure metal contains a plateau as it freezes at a unique temperature. The solid solution alloys freezes over a range of temperatures and thus changing the slope of the cooling curve. However, the eutectic alloys freezes in the same fashion as that of pure metals, whereas, hypo and hypereutectic alloys exhibit primary phase solidification over a range of temperature followed eutectic freezing. Majority of the casting alloys are multi-component and contain several phases which affect the shape of the cooling curve and causes inflection in the cooling curve with their nucleations. These points can be easily detected as it appear as peaks on the first derivative curves [Niklas et al. 2011].

The CACCA technique can be effectively used as an online prediction/control tool for aluminum grain size in hypoeutectic alloys. It can also be used to predict the size and morphology of primary silicon and eutectic silicon in hypereutectic alloys. Since the liquidus temperature of the alloy is greatly influenced by the grain refiners, the prediction of grain refinement is done by analyzing the change in the liquidus parameters of the cooling curve. Thus the quality of the casting can be analyzed in advance before the start of solidification.

Shabestari and Malekan (2010) investigated the effect of Al-5Ti-1B grain refinement on the solidification characteristic of 319 alloys. The addition of grain refiner significantly affected the solidification characteristic of the alloy. The liquidus temperature increased with increase in the concentration of grain refiner as shown in Figure 2.19. The CACCA was also used for the calculation of change in latent heats of the alloy with grain refinement.

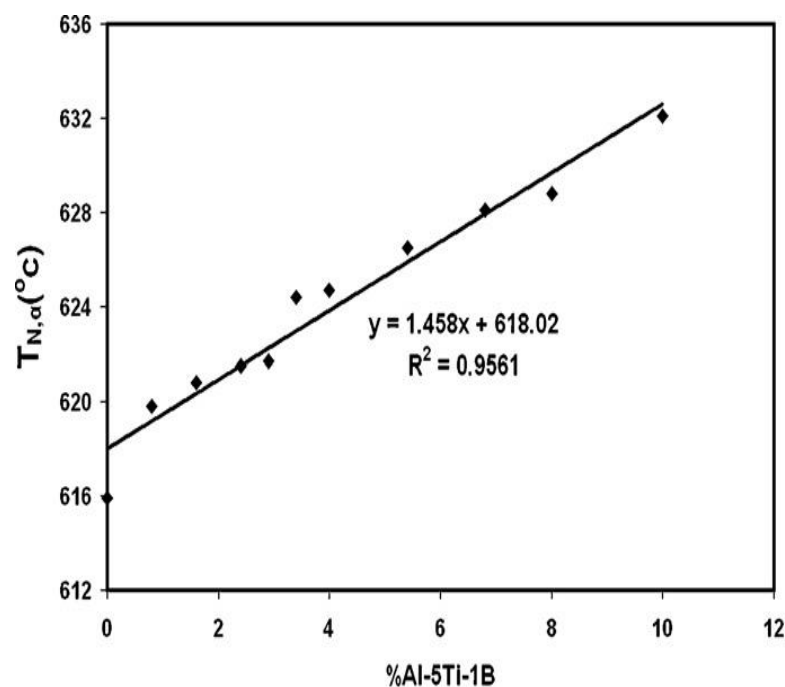


Figure 2.19 Effect of grain refinement on the α -Al dendrite nucleation temperature (liquidus temperature) [Shabestari and Malekan 2010]

The eutectic silicon modification level in Al-Si is generally evaluated by destructive sampling and the structure is assessed microscopically with standard charts of the American Foundry Society (AFS). This qualitative procedure is dependent on the experience of the operators and can introduce human errors on metallographic analysis. Moreover, the structures depicted in the AFS chart do not always resemble those in actual practice. Most importantly the procedure is time consuming expensive and inaccurate. It cannot be used for online prediction of the eutectic modification level [Djurdjevic et al. 2001]. CACCA technique can be effectively used to evaluate the degree of Si modification prior to the solidification. Figure 2.20 shows the effect of eutectic silicon modification on the cooling curve of the Al-Si alloy.

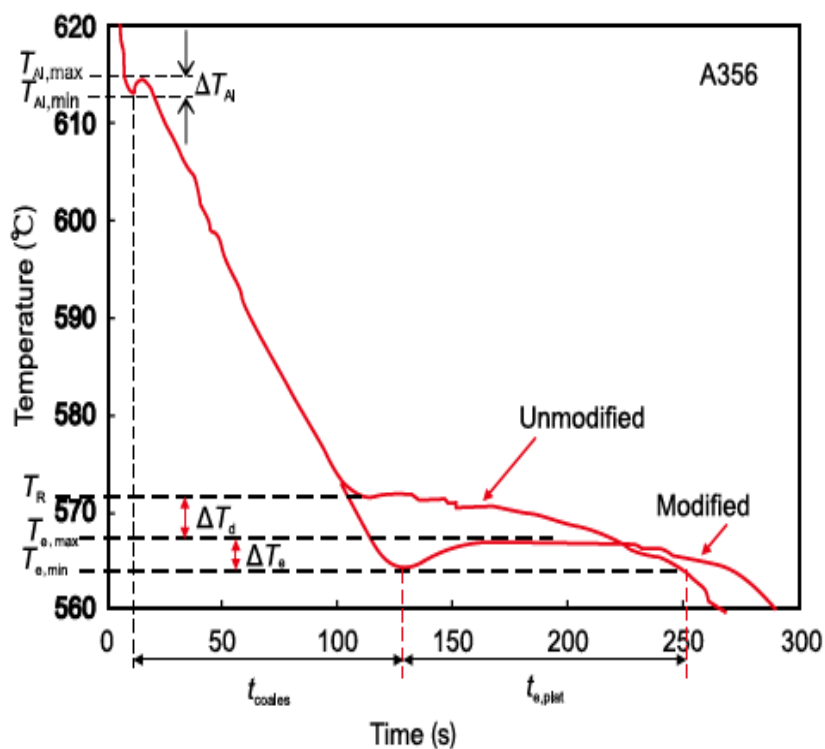


Figure 2.20 Effect of eutectic silicon modification on cooling curve of A356 alloy
[Niklas et al. 2011]

Modification treatment brings following changes to the cooling curve

- Depresses the eutectic temperature
- Increases the undercooling for the nucleation of eutectic
- Increases the undercooling time

The depression in the eutectic growth temperature (T_e) during the modification treatment can be effectively used to estimate the modification level. Larger the magnitude of ΔT_e , higher will be the level of modification. The regression analysis and/or the artificial neural-network method are used to analyze the relationship between eutectic temperature and microstructure. But, the use of temperature alone as the criterion for prediction of modification has a limitation, as it cannot predict over modified structures. The undercooling increases with modification and then falls off as the structure becomes over modified. Hence a possible relationship between the eutectic temperature change and undercooling is needed for accurate prediction of the over modified structure. Chen et al. (2006) correlated the eutectic temperature difference (ΔT_e) with modification level and were of the opinion that the (ΔT_e) could be effectively used to evaluate the modification level of the Al-7Si alloys other than in the over modified conditions.

Djurdjevic et al. (2001) found a correlation between eutectic temperature depression, Sr treatment and modification level. The temperature increases and then remains constant with increasing Sr content as shown in the Figure 2.21. The level of modification achieved also tends to follow the same trend.

Unlike hypoeutectic Al-Si alloys, characterization of hypereutectic Al-Si alloys using thermal analysis is very rarely done. Robles Hernández and Sokolowski (2006) carried out a thermal investigation on hypereutectic alloys (390.1 and 393.2). Figure 2.22 shows the cooling and first derivative curves of hypereutectic alloy obtained using thermal analysis technique. The results were used to confirm the transformation of Si agglomerates into primary silicon and to detect the other phases involved.

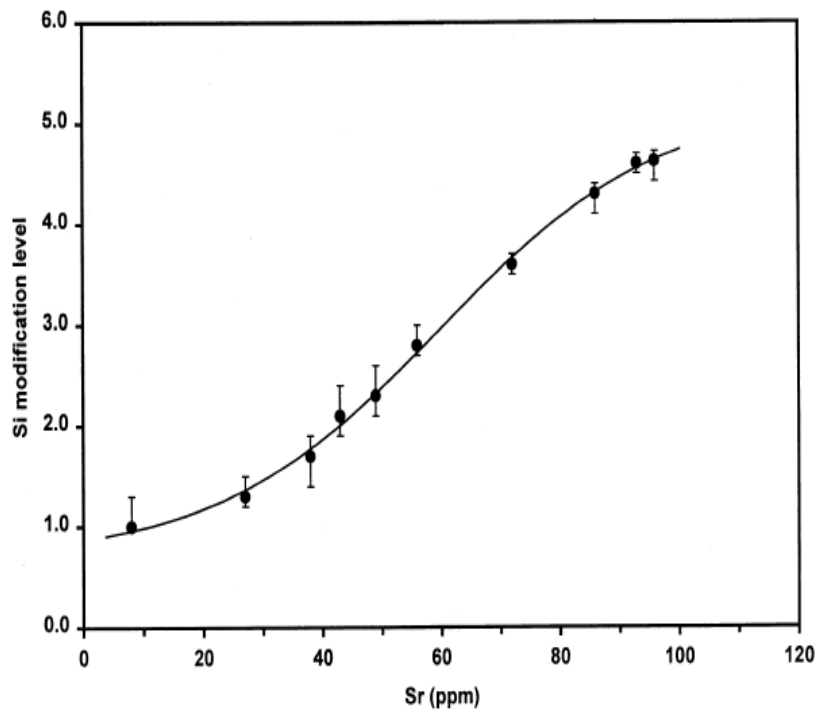
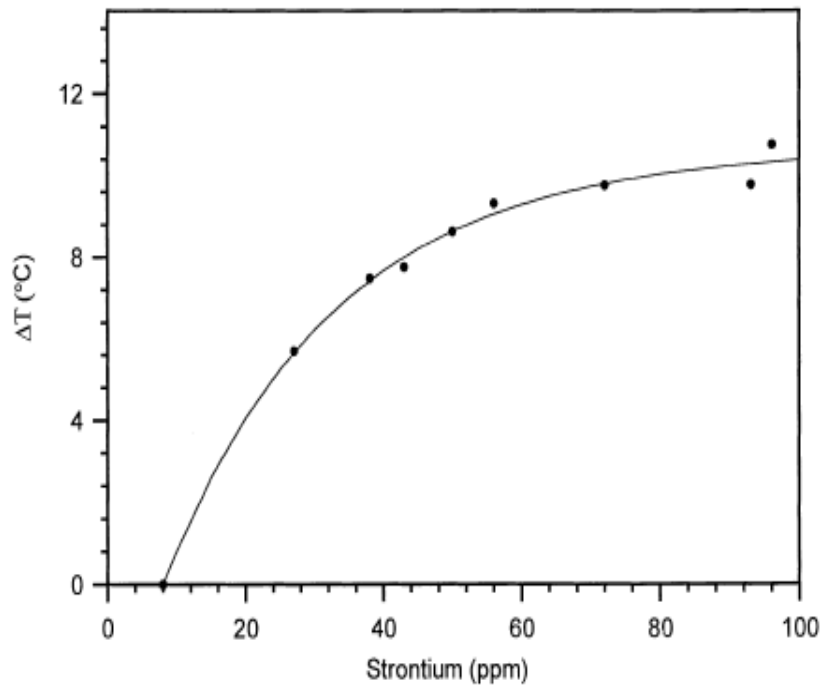


Figure 2.21 Relationship between modification level and temperature depression with Sr content (Djurdjevic et al. 2001)

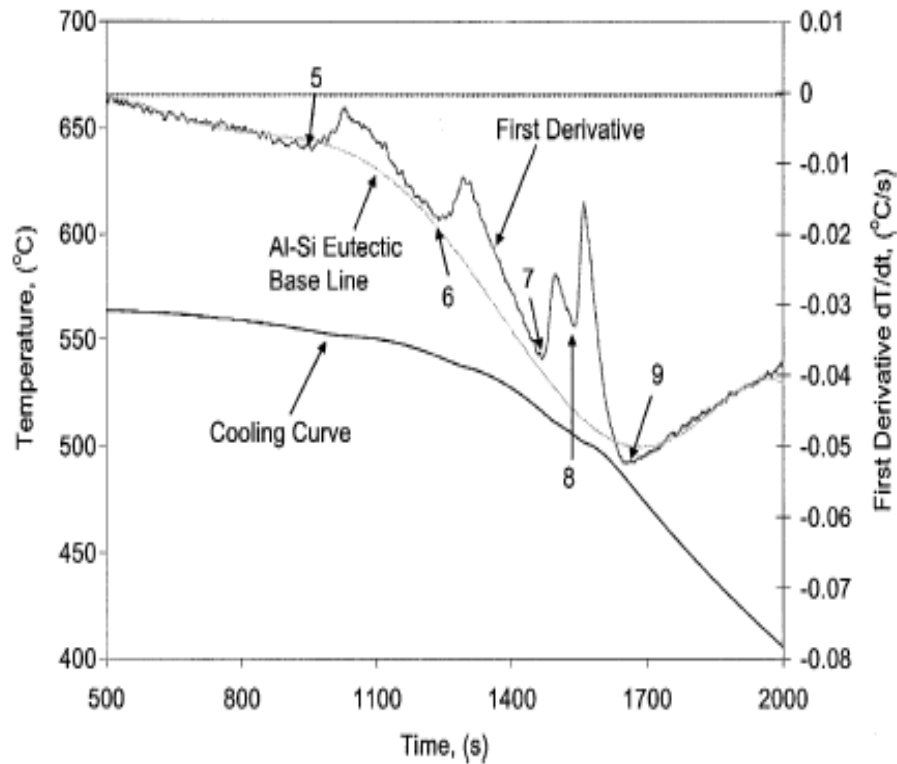


Figure 2.22 Cooling curve, derivative curve and eutectic base of hypereutectic Al-Si alloy [Robles Hernández and Sokolowski 2006]

Commercial hypereutectic Al-Si alloys contain additional elements like Mg, Ni, Cu and other trace elements. These elements are added deliberately to improve the properties of the alloy during casting or during post-casting operations. The amount of exothermic heat released during the solidification is proportional to the amount of precipitating phases, latent heat and enthalpy of transformation. Therefore, the prediction of ‘apparent fraction solid’ (af_s) for all phases involved and relating it to the mechanical properties of the alloy, the strengthening effect of the particular phases can be assessed [Robles Hernández and Sokolowski 2006].

The microstructure of hypereutectic Al-Si alloys is influenced by the factors such as the chemical composition and solidification conditions. Most importantly morphology of silicon is influenced by the cooling rate. Therefore thermal analysis technique can be used to monitor the cooling rate and predict the microstructure of hypereutectic

alloy. Cooling curve along with the derivative curve and apparent fraction solid curve can be utilized to predict the precipitating phases and response of the alloy towards heat treatment.

2.7 Heat transfer Studies

The simulation of casting solidification is useful for (i) determination of temperature distribution, fraction solid, location of defects like shrinkage porosity, hot tear (ii) prediction of the microstructure and mechanical properties. The accuracy and reliability of a simulation model mainly depends on the input parameters like thermo-physical properties of the mold/ casting and the boundary interfacial heat transfer coefficient [Kumar and Prabhu 1991] [Velasco et. al 1999]. The casting/chill interfacial heat transfer is dependent on factors like alloy, super heat, latent heat of fusion and chill variables like surface roughness, chill size and thermo physical properties of the chill [Gafur et al. 2003] [Suresha and Prabhu 2004]. However, the influence of melt treatment on interfacial heat transfer is yet to be fully understood.

The interfacial heat transfer is assessed by recording the temperature inside the chill and solving the heat conduction problem inversely. The heat transfer across the interface can also be calculated by measuring the gap formed between the casting and the chill surface [Prabhu et al. 2012]. The heat transfer rate across the casting/chill interface increases to peak value as the liquid metal comes in contact with chill surface and then drops to lower constant value as the solidification proceeds. This drop in interface heat transfer is mainly due to formation of the solid shell and contraction of that shell. As the melt comes in contact with chill surface, a thin solid shell is formed. During initial stages, the metallostatic pressure from the liquid pushes solid shell to the chill surface and increases the heat transfer rate. As the solidification proceeds, solid shell thickens and overcomes the metallostatic pressure and distorts away from the chill surface creating an air gap at the metal/chill interface. Eventually the heat transfer rate decreases due to the gap formed [Emadi et al. 1993]. The heat transfer rate in the initial stages depends mainly on the actual area of contact between the two surfaces. The surface profile of the contacting surfaces has a significant effect

on the interfacial heat transfer rate. Ho and Pelke (1985) explained that the initial heat transfer transients depend on the mould surface roughness on which liquid metal rest. At this stage heat transfer occurs by conduction through points of actual contact between mould and casting asperities. As the skin formed thickens and deforms, the heat transfer occurs by conduction through interfacial gas.

Prabhu and Ravishankar (2003) studied the effect of Na modification on Al-13%Si alloy and found that the modifying the melt improved the heat flux from the solidifying casting to the chill material as shown in the Figure 2.23. This was attributed to the increased ability of the liquid metal to wet the chill surface and decreased surface tension of liquid due to addition of sodium. In unmodified alloy, the heat conduction is hindered due to the presence of coarse silicon and poor thermal contact. The addition of modifiers decreases the surface tension of Al-Si alloy. This results in better thermal contact conditions at the metal/chill interface leading to the enhanced heat transfer rates from solidifying alloy to chill.

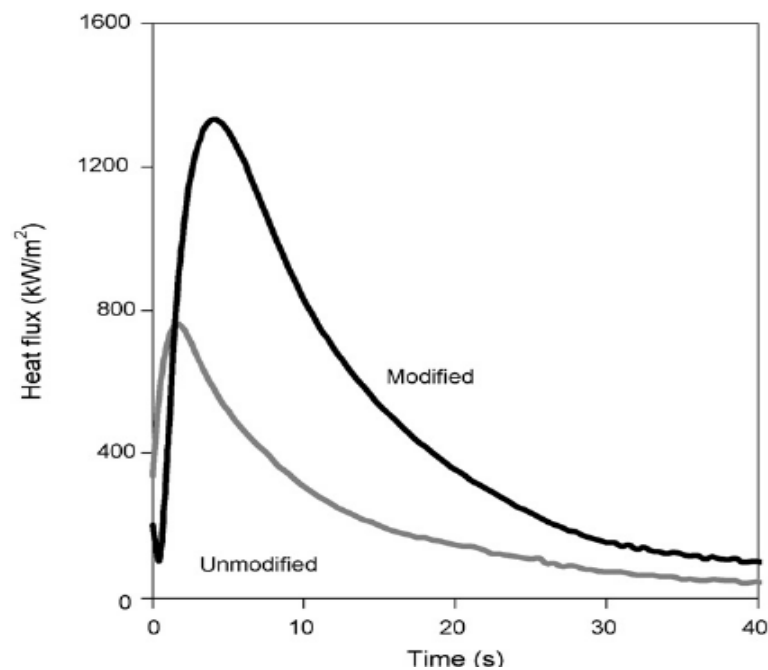


Figure 2.23 The effect of modification on heat flux transient (Kumar et al. 2007)

Modification and chilling have a synergistic effect in increasing the rate of heat transfer from the solidifying casting to the chill material. The modification melt treatment also improves the efficiency of the chilling ability of the mold. Kumar et al. (2007) studied the effect of modification on heat transfer characteristic of 356 alloys. The thermal analysis parameters were affected significantly by modification and chilling. Modification treatment resulted in the increase of cooling rate, heat evolved, heat flux and eutectic growth velocity. A significant depression in eutectic arrest temperature and arrest time was observed. A correlation between normalized values of peak heat flux and eutectic arrest time was derived.

Hegde et al. (2006) studied the effect eutectic modification and casting thickness on thermal analysis parameters. They concluded that the dimensionless heat flux (the fraction of heat in the mold relative to the heat contained in the casting) is high for small section thickness and increases with modification. The metal/mold interfacial heat transfer increases with increase in section thickness and modification melt treatment. The thermal analysis parameters of A357 alloy were affected significantly by the combined action of both modification and chilling power of the mold and section thickness.

2.8 Summary of Literature

Al-Si alloys are the best among the aluminum casting alloys due to their high fluidity, high resistance to corrosion, low shrinkage and low coefficient of thermal expansion. The mechanical properties of the Al-Si alloys are greatly improved by the grain refinement, modification and heat treatment process. The grain refinement in hypoeutectic alloys is achieved by melt treating the Al-Si alloy with boron rich Al-Ti-B master alloys, whereas, the silicon refinement in hypereutectic alloys are brought by addition of P containing master alloys. Sr is an effective eutectic silicon modifier in hypoeutectic and eutectic Al-Si alloys. However, the combined additions of B or P with Sr does not yield refined and modified structures.

The combined addition of refiners and modifiers would lead to mutual poisoning of

each other's effect. The addition of Ti- B and Sr lead to the formation SrB_6 and P and Sr results in the formation of strontium phosphide. The simultaneous modification and refinement of pro-eutectic phase and eutectic silicon in Al-Si alloys with rare earth, especially with Ce is an emerging and promising field. The existing literatures on Ce melt treatment of Al-Si alloys are scant, moreover, its effect on Al-Si alloys varies with melt treatment and solidification conditions.

Alternatively, rapid /chill solidification also leads to refined microstructure in Al-Si alloys. Hence further refinement in microstructure constituents achieved by chilling and addition of modifier/refiners. Various models have been developed to correlate cooling rate, microstructure and mechanical properties. But, the models lack to predict the influence of combined effect of cooling rates and refinement/modification on the properties. Moreover, the influence of Ce melt treatment on Al-Si alloys at various cooling rates is yet to be investigated.

Computer aided cooling curve analysis is an effective non destructive tool to measure and quantify the effect of cooling rate, refinement and modification of Al-Si alloys. The literature review clearly brings out the role of thermal analyses as a non destructive tool to control the melt quality. Since the liquidus temperature of the alloy is greatly influenced by the grain refiners, the prediction of grain refinement is done by analyzing the change in the liquidus parameters of the cooling curve. Thus the quality of the casting can be analyzed in advance before the start of solidification. The extent of eutectic silicon modification can also be predicted online using cooling curve analysis. Conventionally, the eutectic silicon modification level in Al-Si is evaluated by destructive sampling. The depression in the eutectic growth temperatures during the modification treatment can be used to estimate the modification level. The CACCA was also used for the calculation of change in latent heats of the alloy with grain refinement. There is a lack of data on the effect of Ce on thermal analysis parameter during solidification of Al-Si alloys.

Heat treatment of Al-Si alloys improves the mechanical properties by precipitation ageing and spheroidization. The role of role of silicon Si morphology after melt treatment on spheroidization during heat treatment largely remains an unexplored area.

CHAPTER 3

MATERIALS AND METHODS

3.1. Materials

Four alloys with varying silicon content were used for solidification experiments. The chemical compositions of the alloys are given in Table 3.1. The procured alloy ingots are cut into small pieces weighing about 350 ± 50 g.

Table 3.1 Composition of Alloys used for experiments

Elements wt. (%)	Si	Cu	Fe	Mg	Mn	Ni	Al
Hypo	8 ± 0.5	2 ± 0.2	0.3 ± 0.1	0.55 ± 0.5	0.02 ± 0.01	0.05	Rest
Eutectic	13 ± 0.2	0.5 ± 0.1	1.1 ± 0.1	0.04 ± 0.01	0.005 ± 0.01	0.001	Rest
Hyper	14 ± 0.5	0.4 ± 0.1	2.5 ± 0.1	0.7 ± 0.1	0.04 ± 0.02	0.02	Rest
Hyper	23 ± 1	0.4 ± 0.1	1.1 ± 0.1	0.03 ± 0.01	0.05 ± 0.01	0.003	Rest

3.2 Melting and Melt Treatment

About 350 ± 50 g of the alloy sample was melted in a clay-graphite crucible using an electrical resistance furnace. The alloy was treated with Cerium (Alfa Aesar, Cerium ingot, 99% pure (REO)) strontium (Al-10Sr master alloy) and phosphorus (Cu-8Pmaster alloy) in varying quantities at $750 \pm 10^\circ\text{C}$. Ce was added in the range of 0.5, 1.0, 1.5, 2.0 wt.%, Sr was added in the range of 0.02, 0.04, 0.06, 0.08 wt. % and P in the range 0.05, 0.1, 0.2 and 0.4 wt.%. The list of experiments carried out is given in Table 2. The required quantity of additions were wrapped in an aluminum foil and inserted into the melt. The temperature was carefully controlled in order to avoid any overheating and oxidation of the melt. The holding time was about 30 minutes at 750°C for each of the melt.

3.3 Casting and Cooling Curve Analysis

After holding for 30 minutes, the dross was skimmed and the molten alloy was quickly poured into a type 304 stainless tube with/without chill at the bottom. Figure 1 (a) shows the experiment set-up used for the study. A stainless steel tube of 50 mm outer diameter and 1 mm wall thickness was attached to the top of the chill. Stainless steel tube was selected as it has low thermal conductivity (16 W/mK). To maintain constant cooling conditions, the stainless tube was covered with insulation. Thermal analysis was carried out by inserting two K-type thermocouples, one at the center and other near the wall into the melt to record the cooling behavior of the alloy in the temperature range of 800-400°C during solidification, as shown in Fig 3.1(b). The set-up was positioned to ensure a constant thermocouple height of 10mm from bottom of the crucible. Thermocouples were connected to a high-speed data acquisition system (NI USB 9162) interfaced with a PC

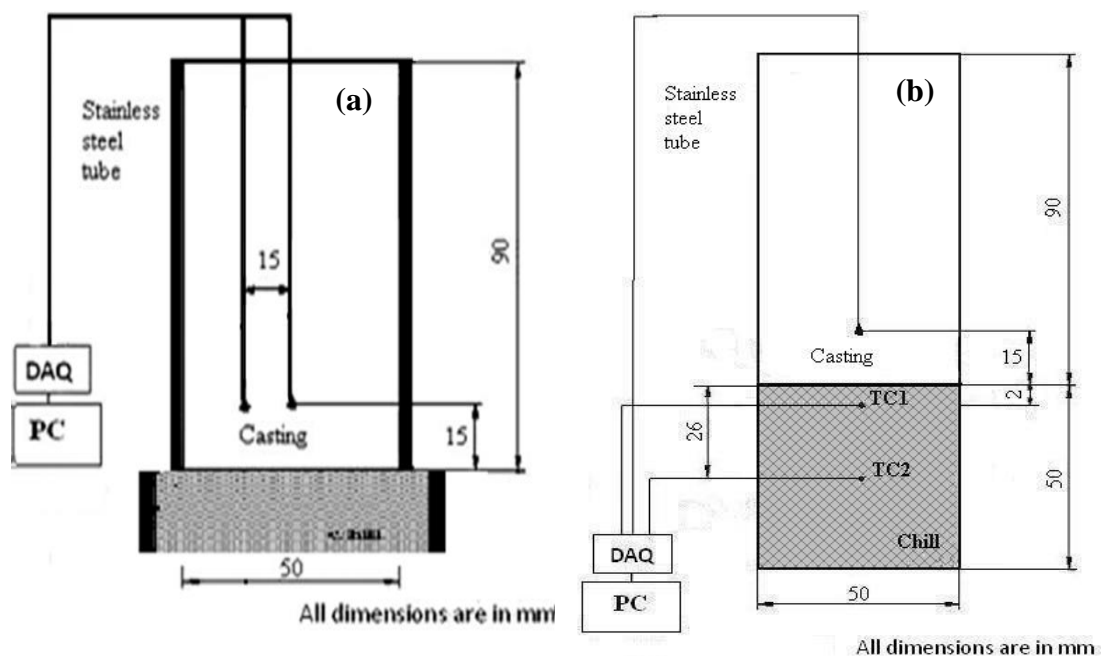


Figure 3.1 Schematic sketch of solidification setup (a) with chill (b) without chill

3.4 Heat Transfer Studies

Heat transfer studies were carried out by using copper, brass and cast iron chills. Chills having varying thermal conductivities were selected to obtain different cooling rates. Surface roughnesses of chills before and after casting were measured using a surface profilometer (Form Talysurf Series 50mm Intra). The chill roughness before experiment was set at $0.5\pm 0.05\mu\text{m}$. A schematic sketch of the experimental setup is shown in Figure 1 (b). A stainless steel tube of 50 mm outer diameter with a wall thickness of 1 mm was attached to the top of the chill. Two holes of 1 mm diameter and 25 mm depth were drilled on to the cylindrical surface of the chill at distances of 2 mm (TC1) and 26 mm (TC2) respectively. Two mineral insulated thermocouples (K-type) were inserted into the drilled holes and were connected to a PC through a data acquisition system (NI USB 9162). The measured temperatures at TC1 and TC2 were used as input to inverse heat conduction model TmmFE Inverse solver (Thermet solutions Private Ltd, Bangalore) to determine the heat flux across the casting/chill interface and the chill FEM domain models.

3.5 Microstructure Evaluation

For microstructure evaluation, samples of 15 mm in diameter, and 15 mm in height were cut from the center portion of the castings and polished using silicon carbide papers of varying grit sizes of 180, 220, 400, 800, and 1000- μm . The final polishing was done using a rotating disc polisher with $0.3\mu\text{m}$ de-agglomerated alumina solution. The microstructures of specimens were examined under JEOL JSM-6380LA scanning electron microscope. The silicon particle size and grain size were measured using Axio Vision image analysis software. The eutectic Si characteristics like area, length, width and perimeter were measured at different locations of samples.

3.6 Determination of Mechanical Properties

Tensile samples were cast in metallic molds. The mold material was the same as the material (copper, brass and stainless steel) used for solidification analysis. The bottom

gated mold had three cavities of diameter 15 mm and length of 210 mm. Tensile specimens were cut from the center of the cylindrical bars and were machined as per the ASTM Standard B-557M. Tensile tests were carried out using SHIMADZU universal testing machine (AGX-100KN) at room temperature of 22°C. The ultimate tensile strength/percentage of elongation was reported as average of three tests.

The fractured surfaces were observed and captured using a scanning electron microscope (JEOL JSM-6380LA) for failure analysis. Samples of 15 mm diameter and 15 mm height were cut from the cast cylindrical bars for the measurement of hardness. The Brinell hardness number (BHN) of the alloy was measured using a hardness tester (SHIMADZU HMV-G). A mean of five hardness readings was calculated for each sample.

3.7 Heat Treatment

T6 heat treatment of alloys was carried out by subjecting the alloys to solution treatment, quenching and ageing. The alloys were homogenized at a temperature of $480\pm 10^{\circ}\text{C}$ for 5h in an isothermal furnace and then quenched to room temperature using water. The selection of ageing time and temperature was based on the results of a series of ageing experiments for varying temperatures and time. Based on the results, the hypoeutectic and eutectic alloys were artificially aged for 12 h at 150°C and Al-22%Si alloys were aged at 200°C for 12h.

The list of experiments carried out in the present investigation is given in [Table 3.2](#).

Table 3.2 List of experiments carried out

Solidification condition/Melt treatment	Al-8% Si alloy									Solidification condition
	WA	0.5% Ce	1.0 %Ce	1.5 %Ce	2.0 %Ce	0.02 %Sr	0.04 %Sr	0.06 %Sr	0.08 %Sr	
Unchilled	✓	✓	✓	✓	✓	✓	✓	✓	✓	
Copper chill	✓	✓	✓	✓	✓	✓	✓	✓	✓	Copper mold
Brass chill	✓	✓	✓	✓	✓	✓	✓	✓	✓	Brass mold
SS chill	✓	✓	✓	✓	✓	✓	✓	✓	✓	SS mold
	Al-12% Si alloy									
	WA	0.5 %Ce	1.0 %Ce	1.5 %Ce	2.0 %Ce	0.02 %Sr	0.04 %Sr	0.06 %Sr	0.08 %Sr	
Unchilled	✓	✓	✓	✓	✓	✓	✓	✓	✓	
Copper chill	✓	✓	✓	✓	✓	✓	✓	✓	✓	Copper mold
Brass chill	✓	✓	✓	✓	✓	✓	✓	✓	✓	Brass mold
SS chill	✓	✓	✓	✓	✓	✓	✓	✓	✓	SS mold
	Al-14% Si alloy									
	WA	0.5 %Ce	1.0 %Ce	1.5 %Ce	2.0 %Ce	0.05 %P	0.1 %P	0.2 %P	0.4% P	
Unchilled	✓	✓	✓	✓	✓	✓	✓	✓	✓	
Copper chill	✓	✓	✓	✓	✓	✓	✓	✓	✓	Copper mold
Brass chill	✓	✓	✓	✓	✓	✓	✓	✓	✓	Brass mold
SS chill	✓	✓	✓	✓	✓	✓	✓	✓	✓	SS mold
	Al-22% Si alloy									
	WA	0.5 %Ce	1.0 %Ce	1.5 %Ce	2.0 %Ce	0.05 %P	0.1 %P	0.2 %P	0.4% P	
Unchilled	✓	✓	✓	✓	✓	✓	✓	✓	✓	
Copper chill	✓	✓	✓	✓	✓	✓	✓	✓	✓	Copper mold
Brass chill	✓	✓	✓	✓	✓	✓	✓	✓	✓	Brass mold
SS chill	✓	✓	✓	✓	✓	✓	✓	✓	✓	SS mold

CHAPTER 4

RESULTS

4.1 Computer Aided Cooling Curve Analysis

The effect of addition of various concentration of cerium on cooling curves of Al-8% Si alloy for different cooling conditions are shown in the Figures 4.1 and 4.2 (a and b). Similarly, Figure 4.3 shows the effect of Sr melt treatment on the cooling curves for different solidification conditions.

The effects of varying content of Ce and Sr addition on the cooling curve of Al-13% Si alloy are shown in Figures 4.4 and 4.5. Figure 4.5 and 4.7 shows the effect of Ce and P addition on the cooling curve of Al-14Si alloy. Similarly, Figure 4.8 and 4.9 shows the cooling curves of Al-22Si alloys with and without Ce and P.

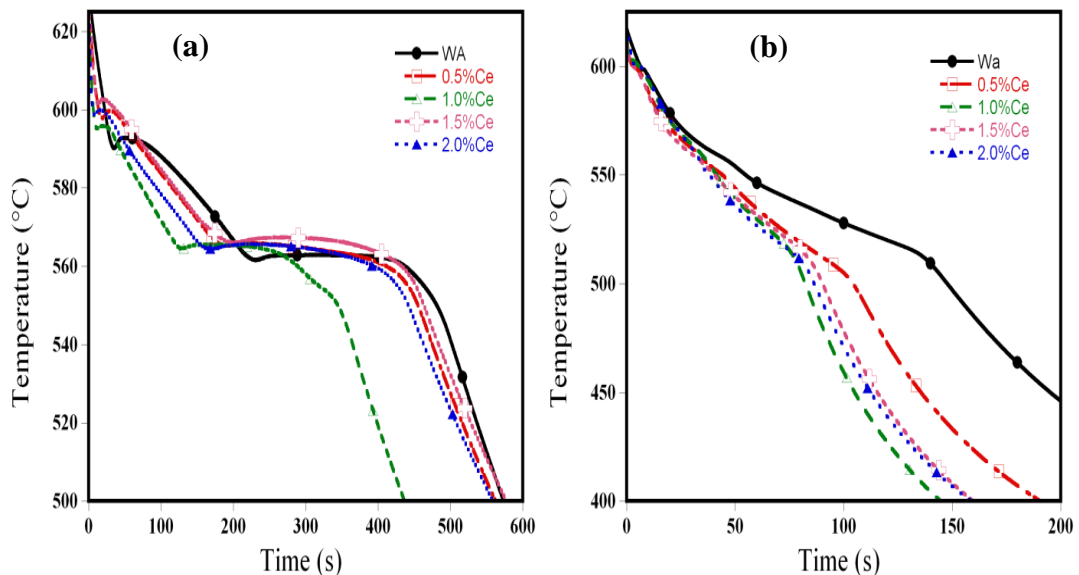


Figure 4.1 Cooling curves of Al-8%Si alloys with varying Ce content solidified on (a) unchilled (b) copper chilled alloys

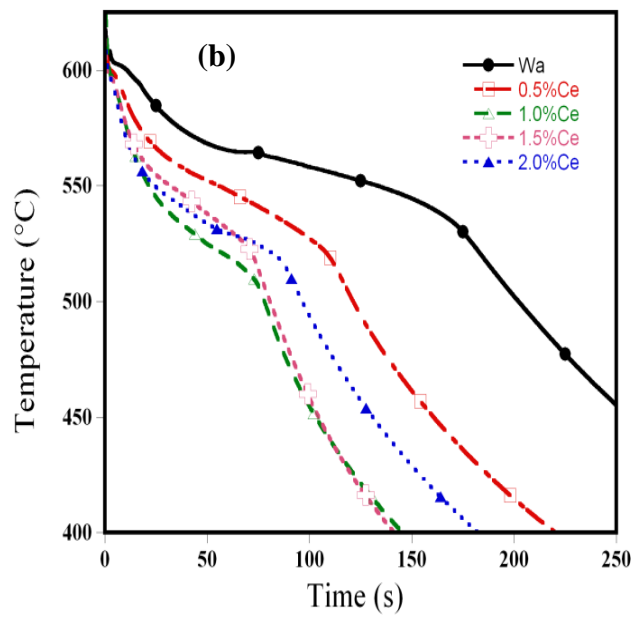
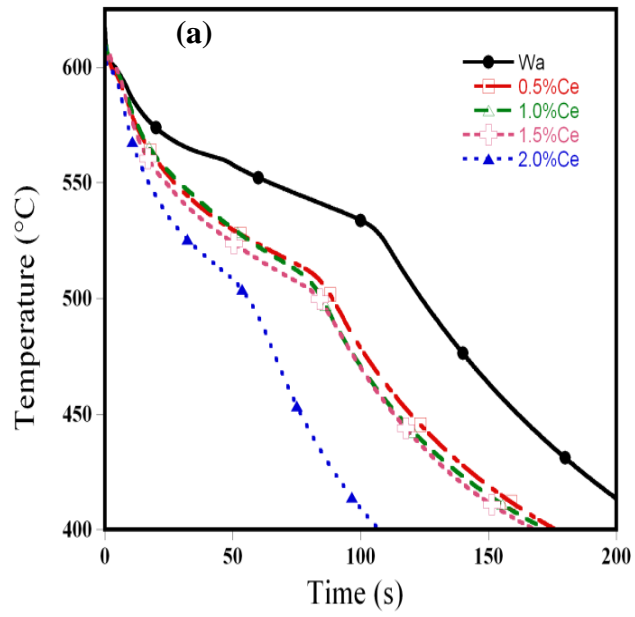


Figure 4.2 Cooling curves of Al-8%Si alloys with varying Ce content solidified on (a) brass and (b) stainless steel chills

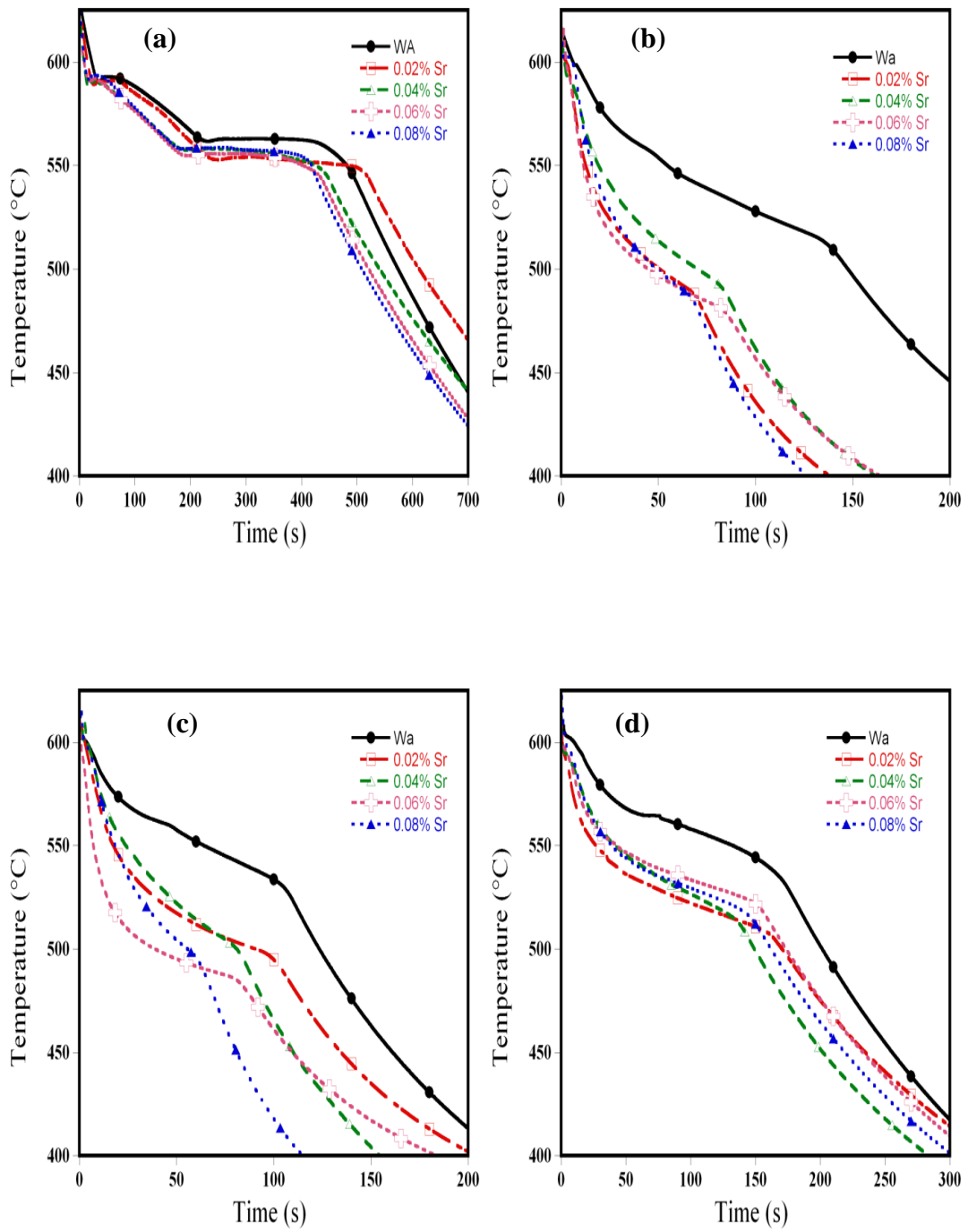


Figure 4.3 Cooling curves of Al-8%Si alloys with varying Sr content solidified on (a) unchilled (b) copper (c) brass and (d) stainless steel chills

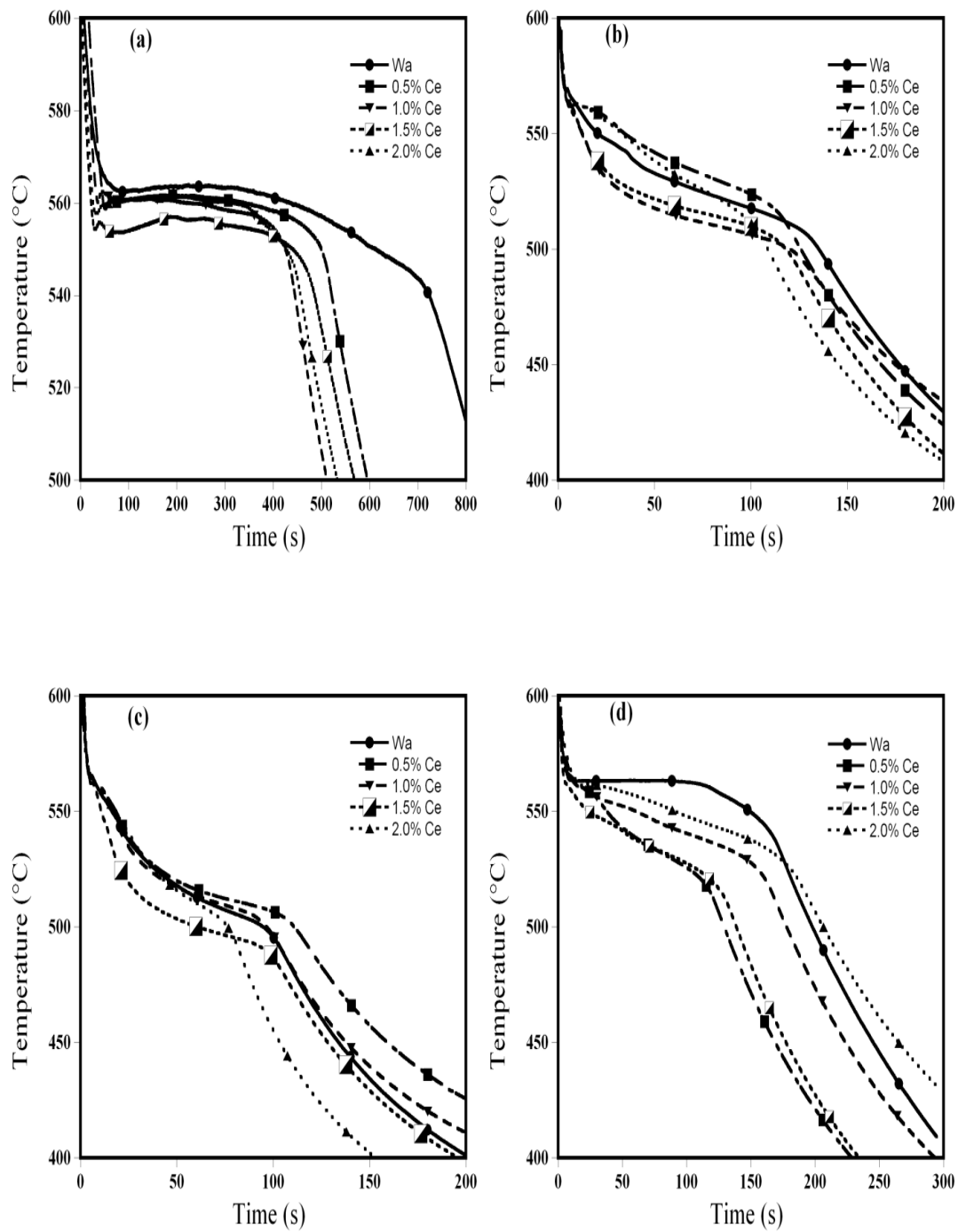


Figure 4.4 Cooling curves of Al-13%Si alloys with varying Ce content solidified on (a) unchilled (b) copper (c) brass and (d) stainless steel chills

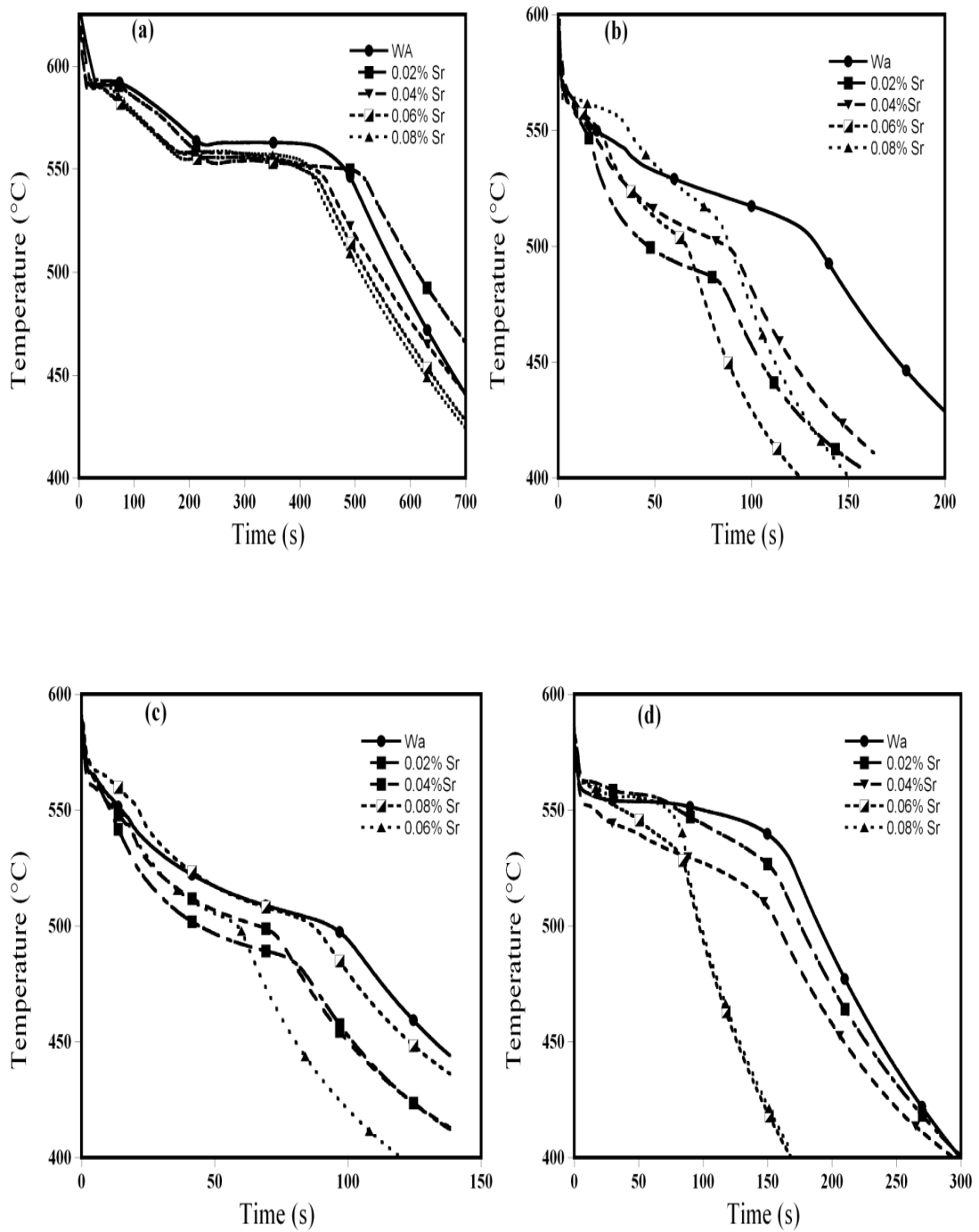


Figure 4.5 Cooling curves of Al-13%Si alloys with varying Sr content solidified on (a) unchilled (b) copper (c) brass and (d) stainless steel chills

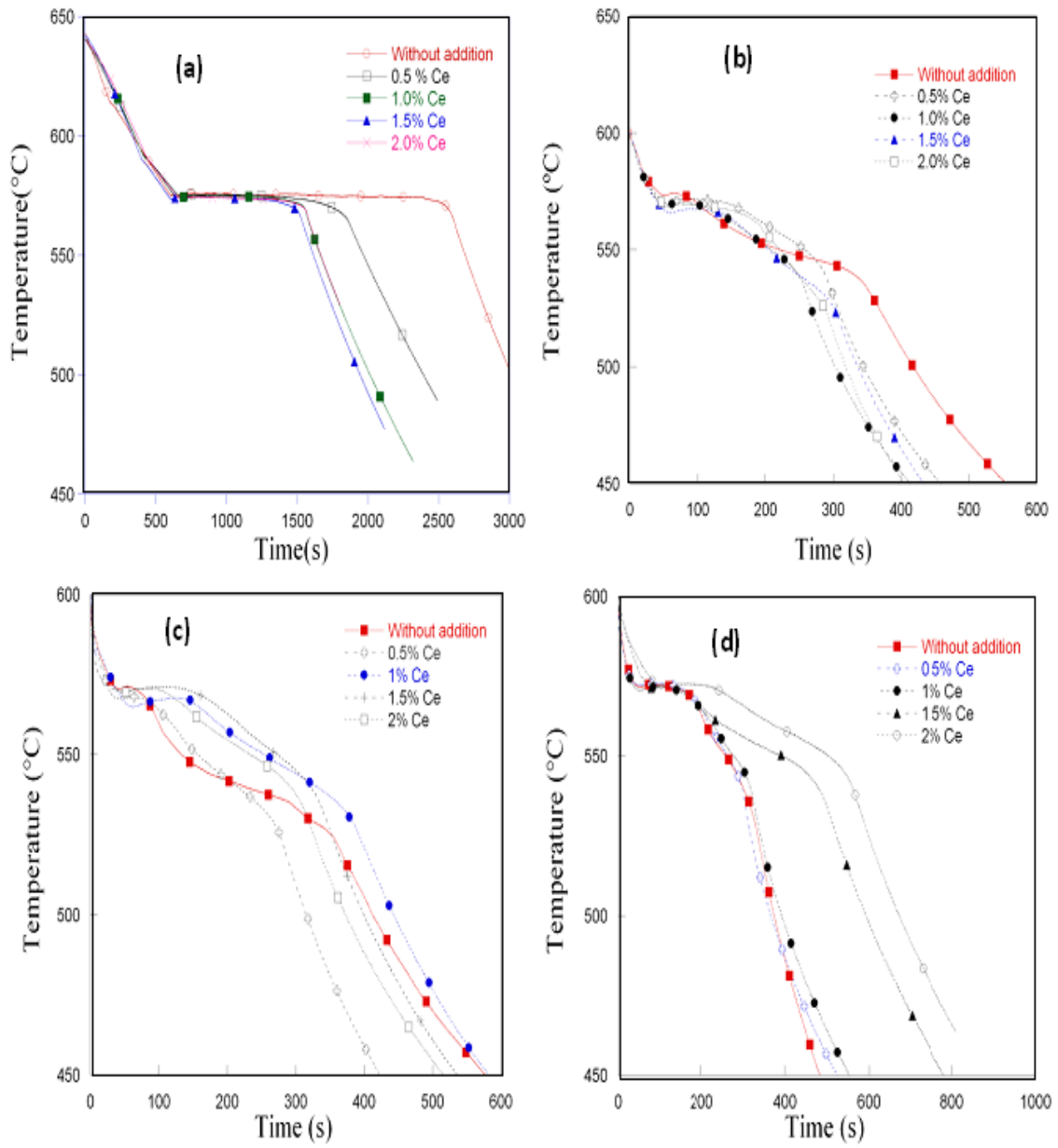


Figure 4.6 Cooling curves of Al-14%Si alloys with varying Ce content solidified on (a) unchilled (b) cast iron (c) brass (d) copper chills

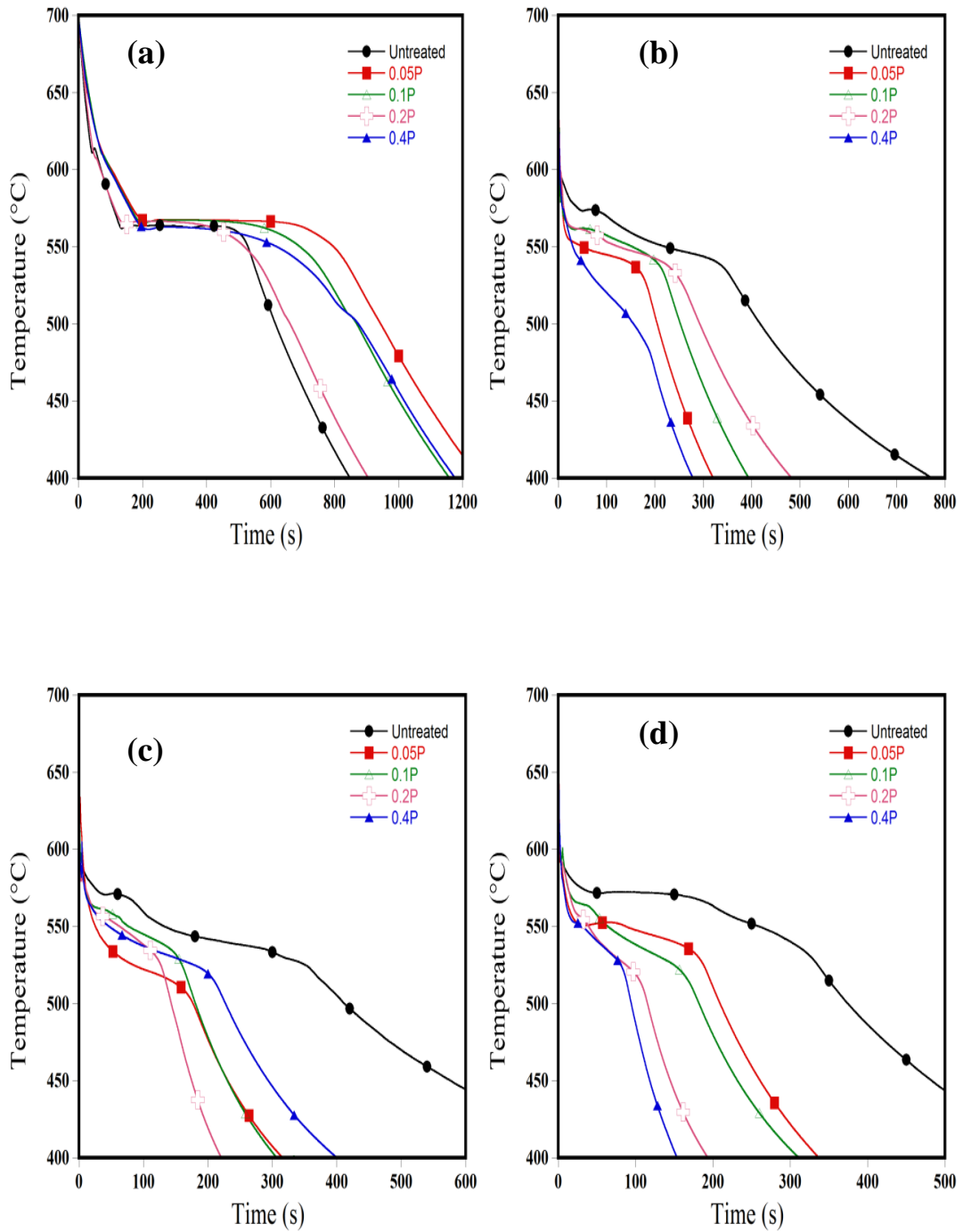


Figure 4.7 Cooling curves of Al-14%Si alloys with varying P content solidified on (a) unchilled (b) cast iron (c) brass (d) copper chills

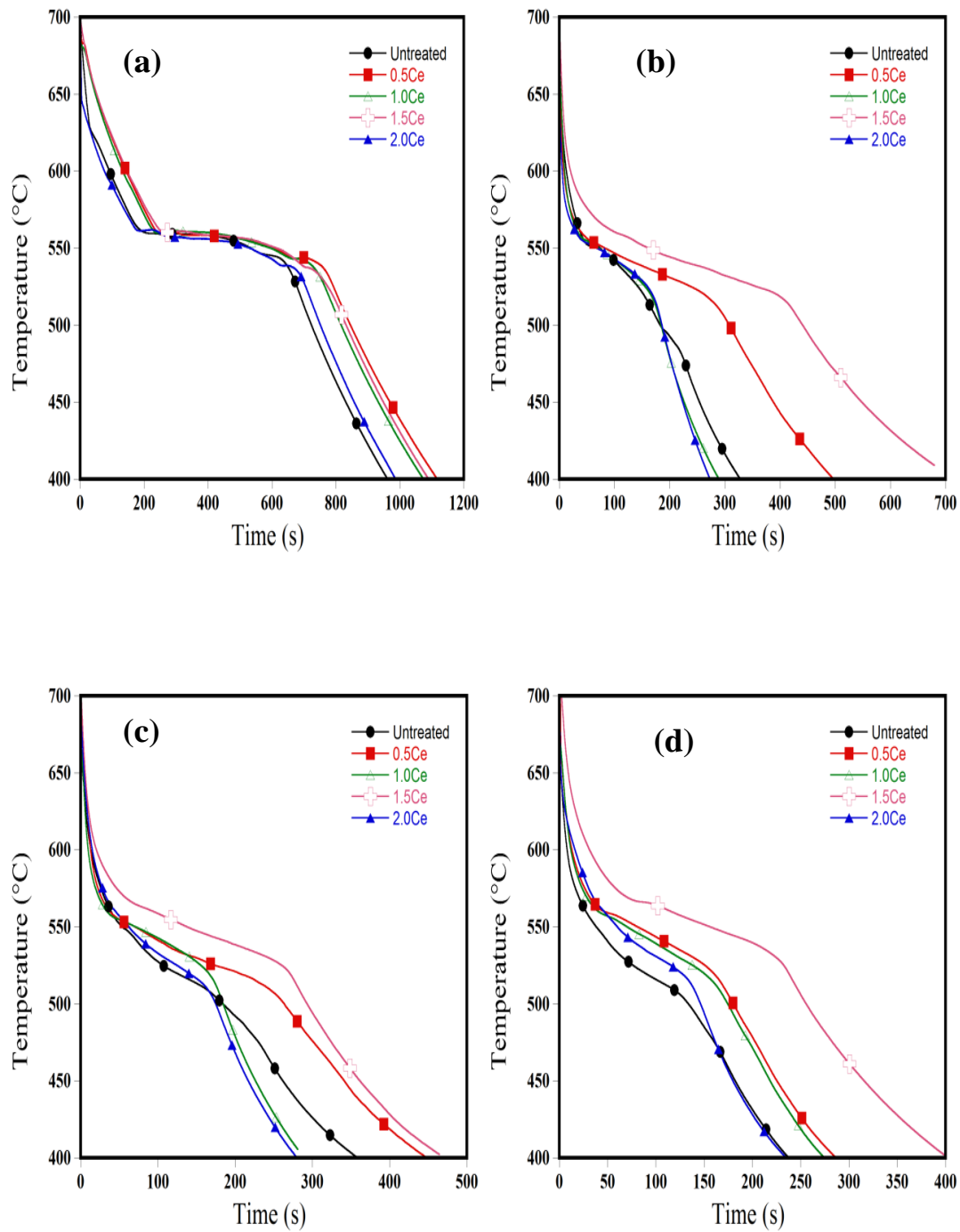


Figure 4.8 Cooling curves of Al-22%Si alloys with varying Ce content solidified on (a) unchilled (b) cast iron (c) brass (d) copper chills

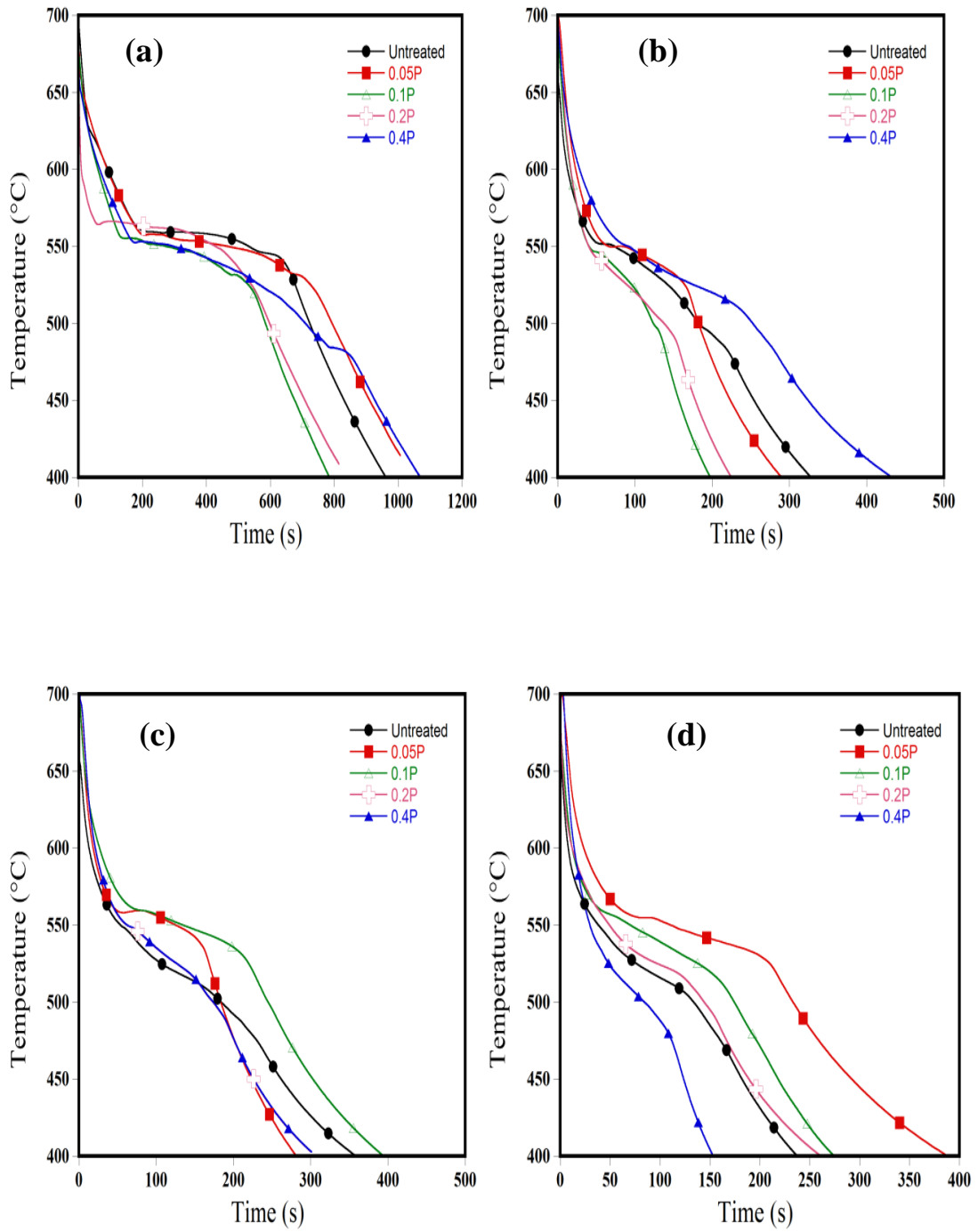


Figure 4.9 Cooling curves of Al-22%Si alloys with varying P content solidified on (a) crucible cooled (b) SS (c) brass (d) copper chills

4.2 Effect of Melt treatment on the Interfacial Heat Flux

Thermal history in the chill during solidification of Al-8%Si alloys against copper chill is shown in Figure 4.10. The temperature recorded at 2mm from the casting/chill interface (TC1) showed a maximum value of 207.5°C after a period of about 2-3s. The surface temperature estimated using the inverse solver showed a peak value of 220°C. Thermal history at TC1 and TC2 was recorded for brass and cast iron chills as well. Figure 4.11 shows the heat flux estimated across the interface for the copper chill. The heat flux increases rapidly as the melt comes in contact with the chill interface and reaches a peak value. Figure 4.12 shows the influence of the chill material on the estimated heat flux across the casting/chill interface. The peak heat flux increased with the increase in thermal conductivity of the chill. Copper being the material with high thermal conductivity (395 W/mK) showed a higher heat flux.

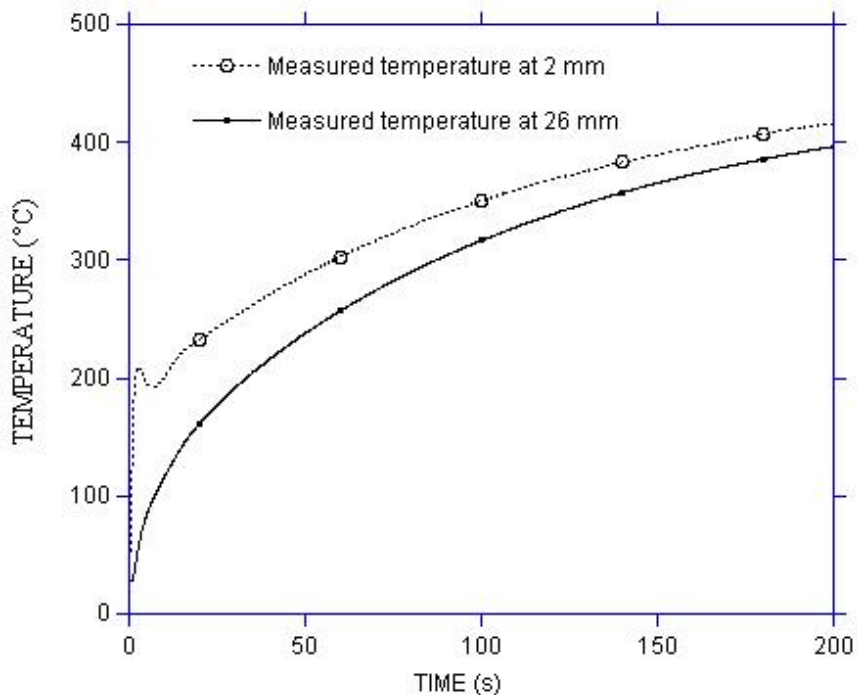


Figure 4.10 Temperature-time curves at different locations from interface in the copper chill

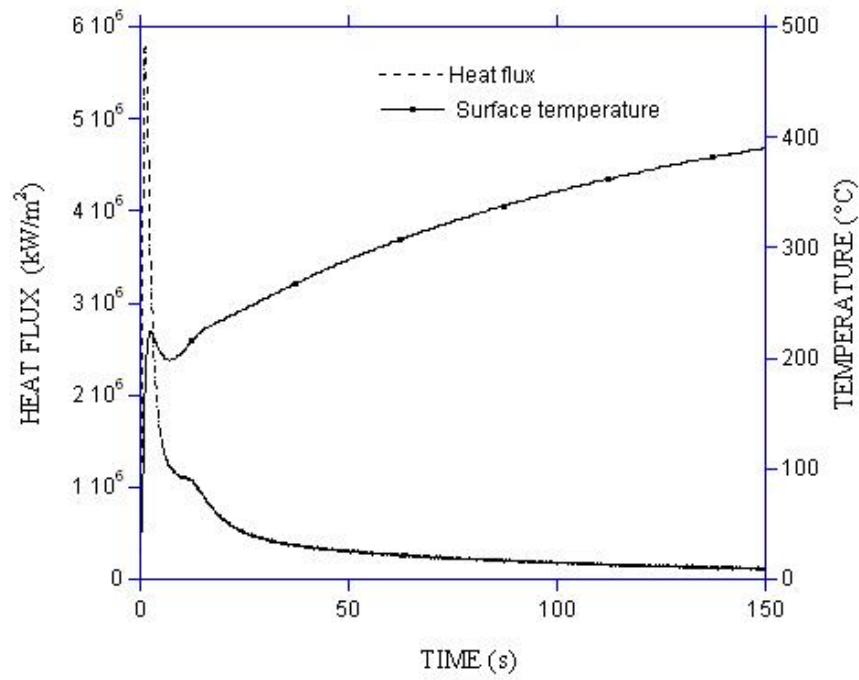


Figure 4.11 Variation of heat flux and chill surface temperature with time

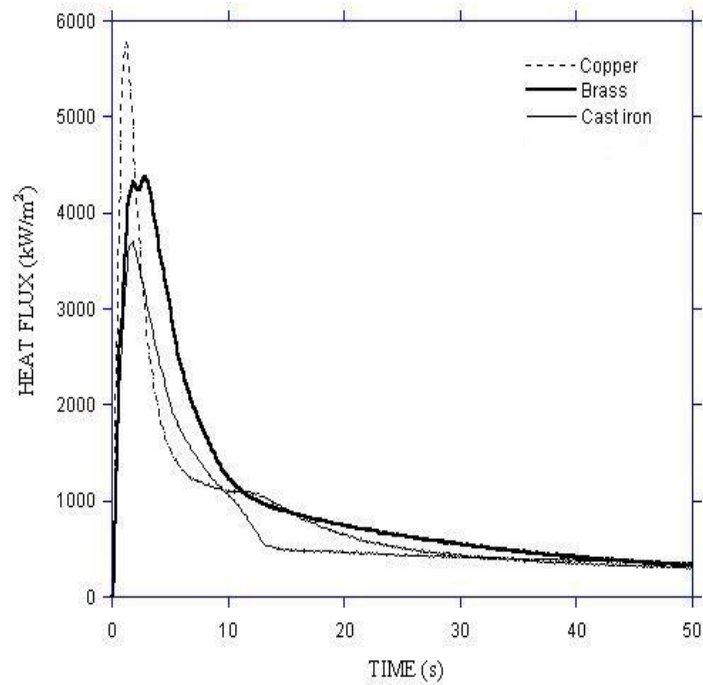


Figure 4.12 Effect of chill material on casting/chill interfacial heat flux transients

The variation of peak heat flux with the melt treatment of Ce and Sr for Al-8Si alloy is given in the Table 4.1. The heat flux increased for chilled alloys with the addition of Ce and Sr and reached a maximum at concentrations of 1.0 % Ce and 0.06 wt. % Sr respectively. Similarly, for brass and SS chills the peak fluxes were enhanced by the melt treatments.

Table 4.1 Effect of melt treatments on peak heat flux transients of Al-8Si alloy

Melt treatment	Peak heat flux (q_{max}) (kW/m ²)		
	Copper	Brass	Stainless steel
Untreated	8750±200	4320±70	2860±50
0.5 wt-%Ce	9900±60	7000±50	4420±30
1.0 wt-%Ce	12350±134	8100±60	4800±70
1.5 wt-% Ce	10100±20	7500±110	4300±80
2.0 wt-% Ce	10650±25	5500±90	4200±70
0.02 wt-% Sr	10800± 150	5200±90	4500±100
0.04 wt-%Sr	12670±130	4850±90	4600±80
0.06 wt-% Sr	13400±300	7320±50	4900±140
0.08 wt.% Sr	10250±50	6950±40	4500±70

The effect Ce and Sr addition on the peak heat flux of Al-13Si alloy are given in the Table 4.2. The peak heat flux increased with both the type of melt treatments, Sr modified alloys showed higher values of heat flux. For all conditions, the peak heat flux increased with additions reaching a peak at 0.5 wt. % Ce and 0.06 wt.% Sr respectively and then decreased at higher concentration of additions.

Table 4.2 Effect of melt treatment on heat flux transients of Al-13Si alloy

Melt treatment	Peak heat flux (q_{\max}) (kW/m ²)		
	Copper	Brass	Stainless steel
Untreated	10650±500	5660±500	3610±600
0.5 wt-%Ce	11200±800	10090±800	4800±400
1.0 wt-%Ce	10830±500	7900±800	4780±200
1.5 wt-% Ce	8920±600	7900±1000	5000±300
2.0 wt-% Ce	7760±1000	8800±500	5200±200
0.02 wt-% Sr	9400± 400	5000±500	4850±700
0.04 wt-%Sr	11600±600	6000±900	4670±800
0.06 wt-% Sr	12600±700	7000±1000	4000±900
0.08 wt.% Sr	10150±300	6350±400	4000±700

Table 4.3 shows the variation of peak heat flux with Ce and P additions for Al-14Si alloys. The addition of Ce to the alloy significantly increased the peak heat flux. The peak heat flux increased with Ce addition and showed a maximum value of 9541 kW/m² at a concentration of 1.5 % Ce. Similarly, on brass and stainless steel chills the peak fluxes were enhanced by 74% and 45% respectively with addition of 1.5% Ce.

Table 4.3 Effect of melt treatment on heat flux transients of Al-14Si alloy

Additions\Chill	Peak heat flux (q_{\max}) (kW/m ²)		
	Copper	Brass	Stainless steel
Untreated	6909±498	4790±232	3348±418
0.5 wt-%Ce	8354±481	6248±613	4162±675
1.0 wt-%Ce	9221±298	6828±971	4270±87
1.5 wt-% Ce	9541±458	6803±475	4821±360
2.0 wt-% Ce	8314±475	8212±512	5091±255
0.05 wt-% P	6700±200	4500±100	3700±260
0.1 wt-%P	6500±350	4600±300	3900±150
0.2 wt-% P	6250±200	4900±400	4150±200
0.4 wt.% P	6750±150	6240±800	4670±150

The peak heat flux of Al-22Si alloy for various melt treatment and solidification condition is given in the Table 4.4. Unlike other alloys, the peak flux decreased with the addition of varying content of Ce and P. The decrease was more significant in Ce added alloys. This was attributed to the increased nucleation of primary silicon affecting the conductivity of the alloy.

Table 4.4 Effect of melt treatment on heat flux transients of Al-22Si

Melt treatment	Peak heat flux (q_{\max}) (kW/m ²)		
	Copper	Brass	Stainless steel
Untreated	10400±500	9690±450	4200±100
0.5 wt-%Ce	3500±100	1800±200	4800±200
1.0 wt-%Ce	3700±200	2030±200	3000±150
1.5 wt-% Ce	4550±300	2600±300	4200±250
2.0 wt-% Ce	2500±150	2820±50	3500±100
0.05 wt-% P	9270±200	6250±600	3050±50
0.1 wt-%P	6320±150	6080±500	4050±100
0.2 wt-% P	5200±180	4230±200	4150±50
0.4 wt-% P	1900±100	4170±100	4200±75

4.3. Effect of Melt Treatment on the Microstructure of Alloys

Figure 4.13 (a and b) show micrographs of an untreated Al-8% Si alloy solidified without chill. The microstructure consists of long needle-like eutectic silicon in a matrix of pro-eutectic α -aluminium. The slowly cooled untreated hypoeutectic alloy consists of large columnar pro-eutectic α -aluminium along with acicular eutectic silicon. The alloy also contains several intermetallic phases depending on the concentration of Fe, Mg and Mn in the alloy. One of such phase, α -Fe intermetallic in the untreated alloy matrix is highlighted in the Figure 4.13 (b). Figure 4.14 and 4.15 shows the effect effect of cerium and strontium additions on the microstructure of the alloys solidified against different chills. Figure 4.16 shows the effect of melt treatment on the macrostructure of the alloy.

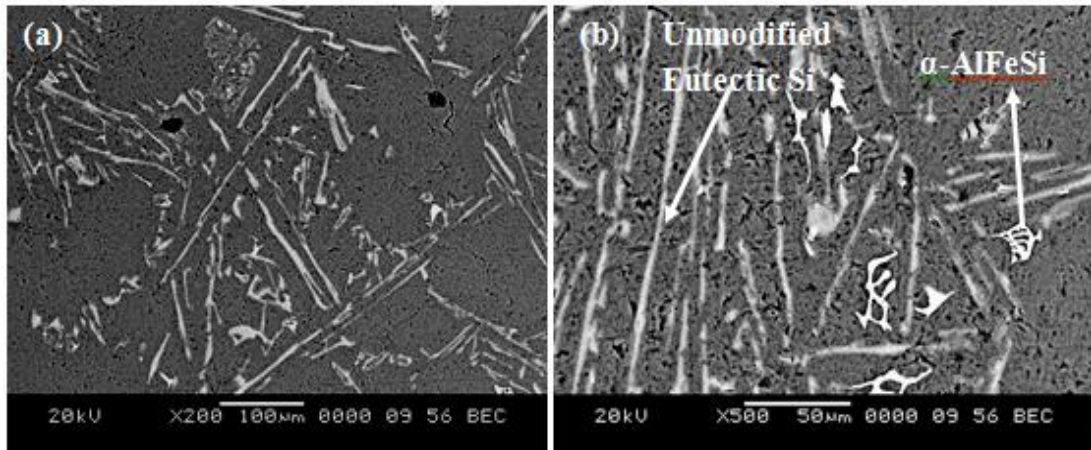


Figure 4.13 Microstructure of untreated and unchilled Al-8% alloy

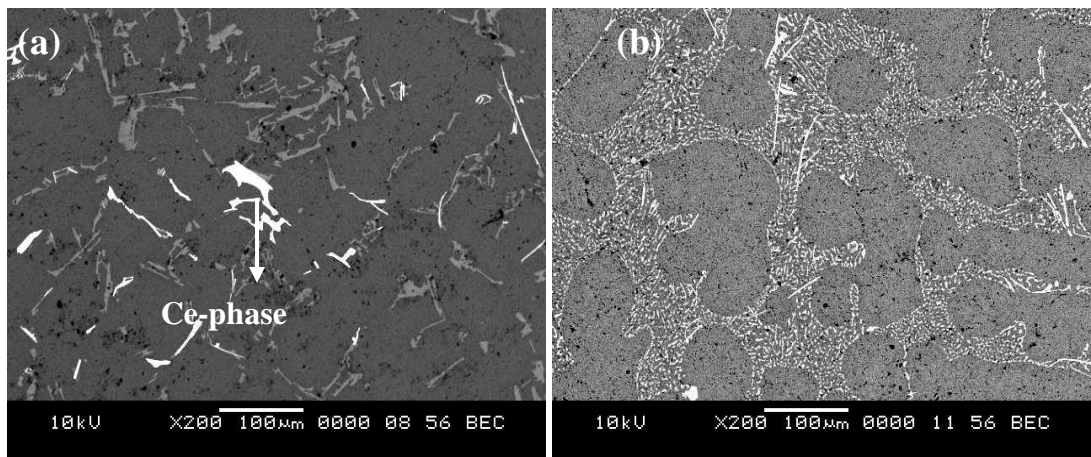


Figure 4.14 Microstructure of unchilled alloys treated with (a) 1.5% Ce (b) 0.04% Sr

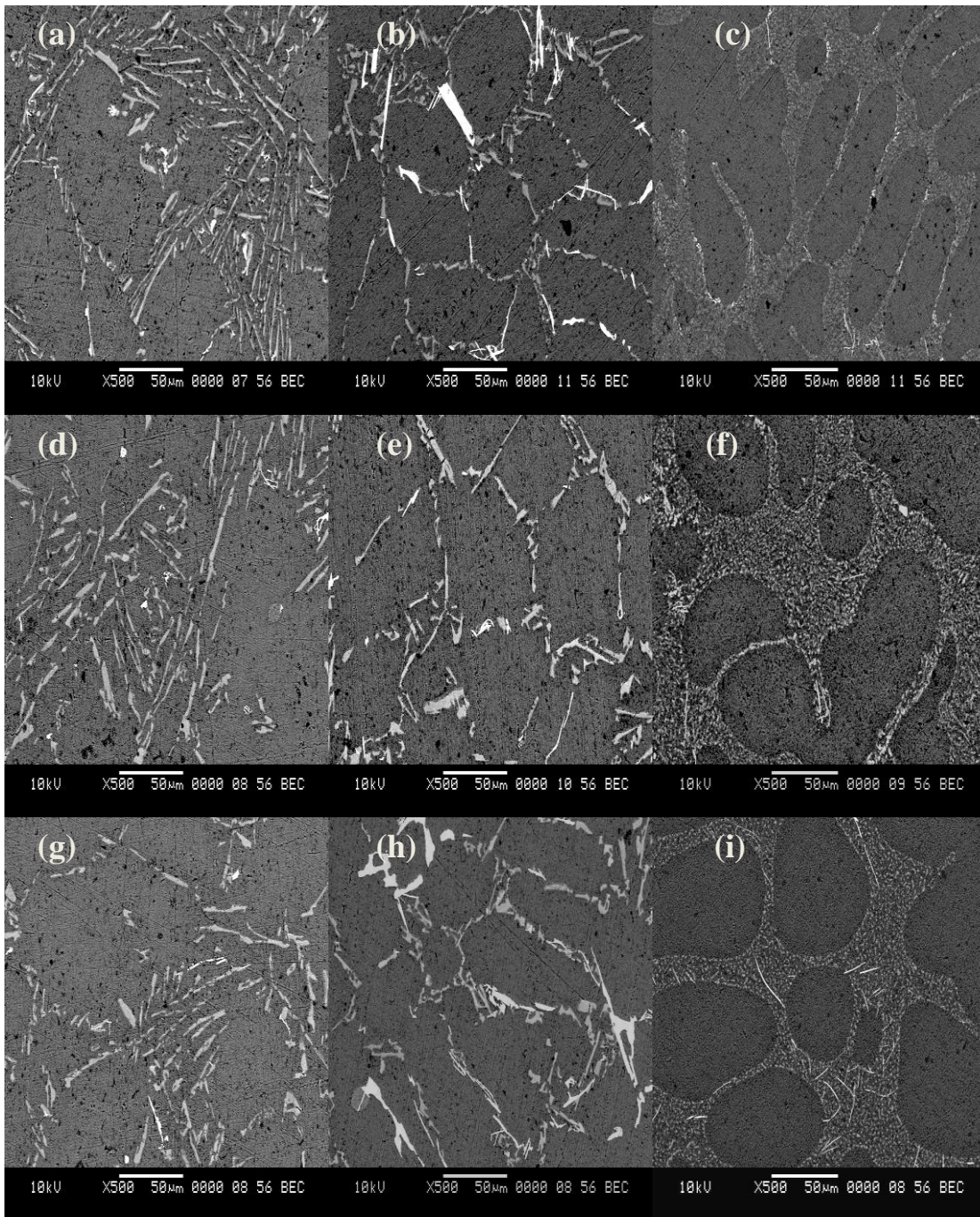


Figure 4.15 Micrographs of Al-8%Si alloy solidified on different chills (a) untreated - copper chill (b) 0.5 wt.% Ce- Cu chill (c) 0.04 wt.% Sr- copper chill (d)) untreated - brass chill (e) 1.0 wt.% Ce- brass chill (f) 0.04 wt.% Sr- brass chill (g) Untreated SS chill (h) 1.5 wt.% Ce- SS chill (i) 0.04 wt.% Sr- SS chill

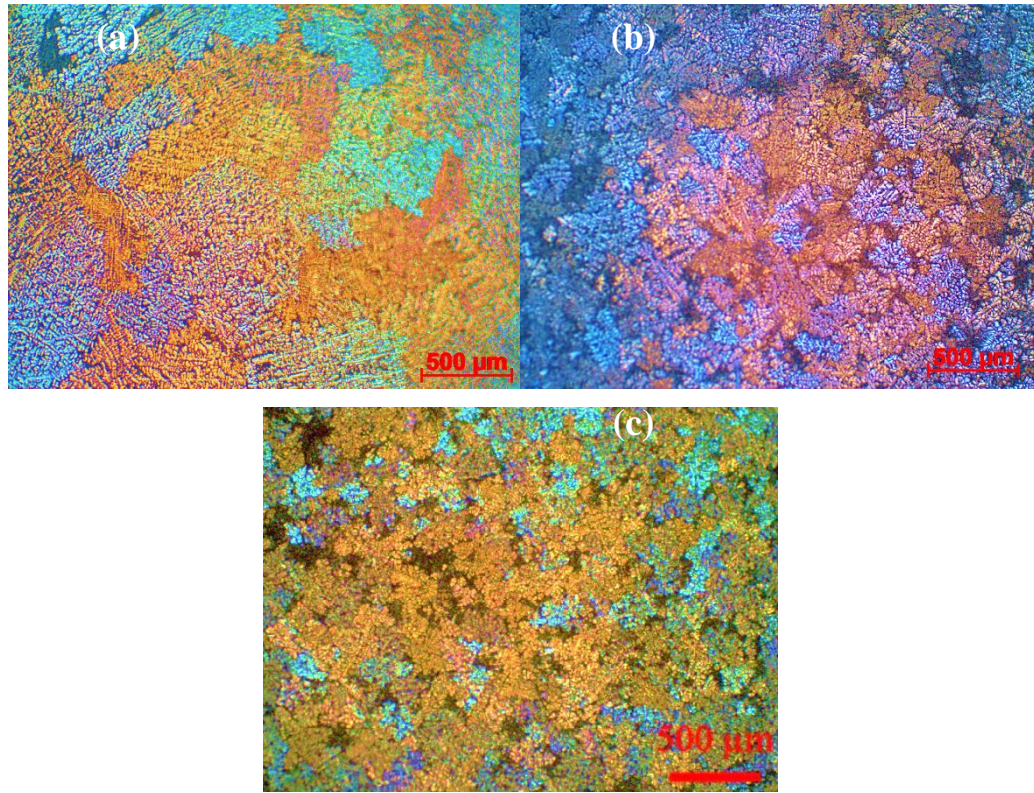


Figure 4.16 Macrostructures of Ce treated alloy (a) untreated (b) 0.04% Sr (c) 1.0% Ce

Figure 4.17 shows the microstructures of the Al-13% Si alloys treated with Ce and Sr. The untreated microstructure consists of long needle like (unmodified) eutectic silicon and β -Fe intermetallic with a platelet morphology. The addition of Ce had resulted in the transformation of eutectic Si into short rod-like particles and in the formation of rod shaped Ce based intermetallic compounds. Similarly, addition of strontium transformed the eutectic silicon from needle-like shape to fine fibrous form. In addition, the microstructure consisted of β - Fe intermetallic along the grain boundaries.

Figure 4.18 shows the effect of Ce and P melt treatment on the microstructures of Al-14%Si alloys solidified under different cooling conditions. The slowly cooled untreated microstructure consists of irregular shaped primary silicon and long needle-like eutectic silicon in a eutectic matrix. The addition of P to the alloy transformed the irregular primary silicon into polygon shaped primary silicon and the silicon particles were found to be well distributed all along the microstructure. The addition of P, however, did not show any effect on the eutectic silicon and the morphology of the eutectic silicon remained unchanged. On the other hand, addition of Ce to the hypereutectic Al-Si alloy resulted in the simultaneous refinement of primary silicon and modification of the eutectic silicon.

Figures 4.19 shows the microstructures of Al-22%Si alloy before and after Ce and P treatment respectively. The untreated hypereutectic alloy generally consists of segregated irregular shaped pro-eutectic primary silicon and unmodified eutectic silicon. The addition of P to the alloy transformed the irregular primary silicon into polygon shaped primary silicon and the silicon particles were found to be well distributed all along the microstructure. But, the addition of P did not show any effect on the eutectic silicon and the morphology of the eutectic silicon remained more or less same. On the other hand, the addition of Ce to the hypereutectic Al-Si alloy resulted in the simultaneous refinement of primary silicon and modification of the eutectic silicon.

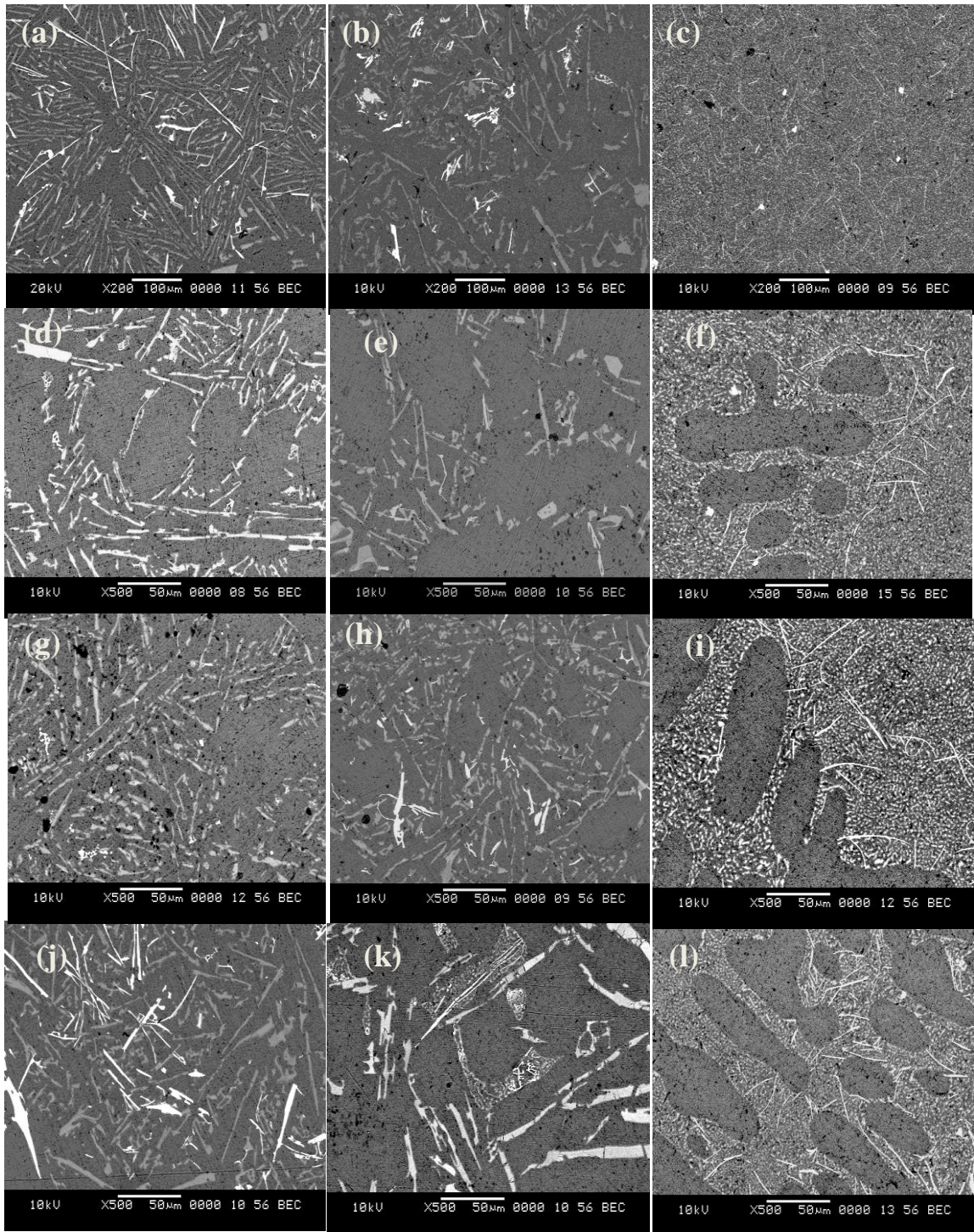


Figure 4.17 Micrographs of Al-13%Si alloy (a) unchilled-untreated (b) unchilled- Ce treated (c) unchilled-P treated (d) untreated -copper chill (e) copper chilled-Ce (f) copper chilled-P treated (g) brass chilled- untreated (h) Ce- brass chill (i) brass chilled-P treated (j) SS chilled-untreated (k) SS chilled-Ce treated (l)SS chilled- P

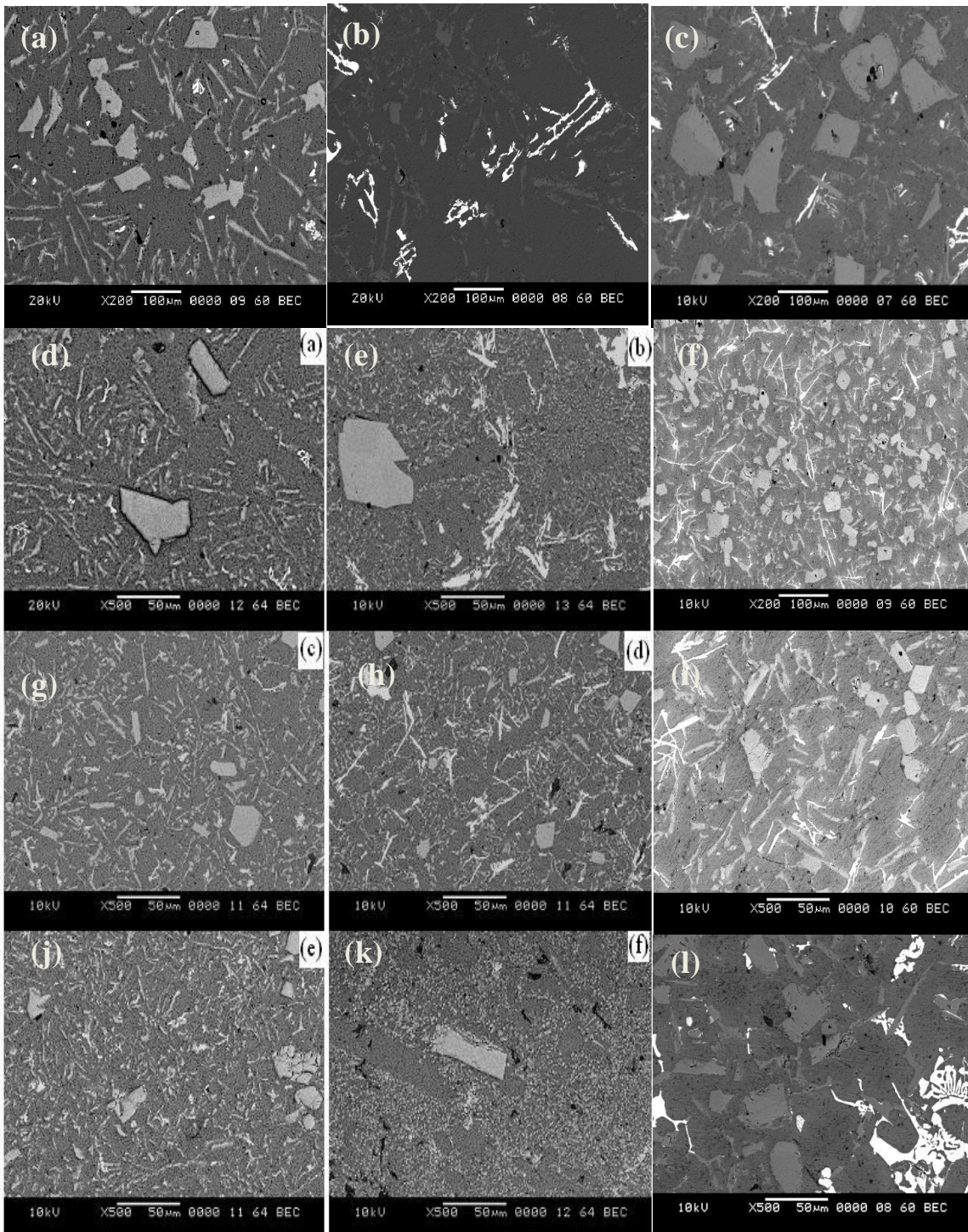


Figure 4.18 Micrographs of Al-14%Si alloy (a) unchilled-untreated (b) unchilled- Ce treated (c) unchilled-P treated (d) untreated -copper chill (e) copper chilled-Ce (f) copper chilled-P treated (g) brass chilled- untreated (h) Ce- brass chill (i) brass chilled-P treated(j) SS chilled-untreated (k) SS chilled-Ce treated (l)SS chilled- P treated

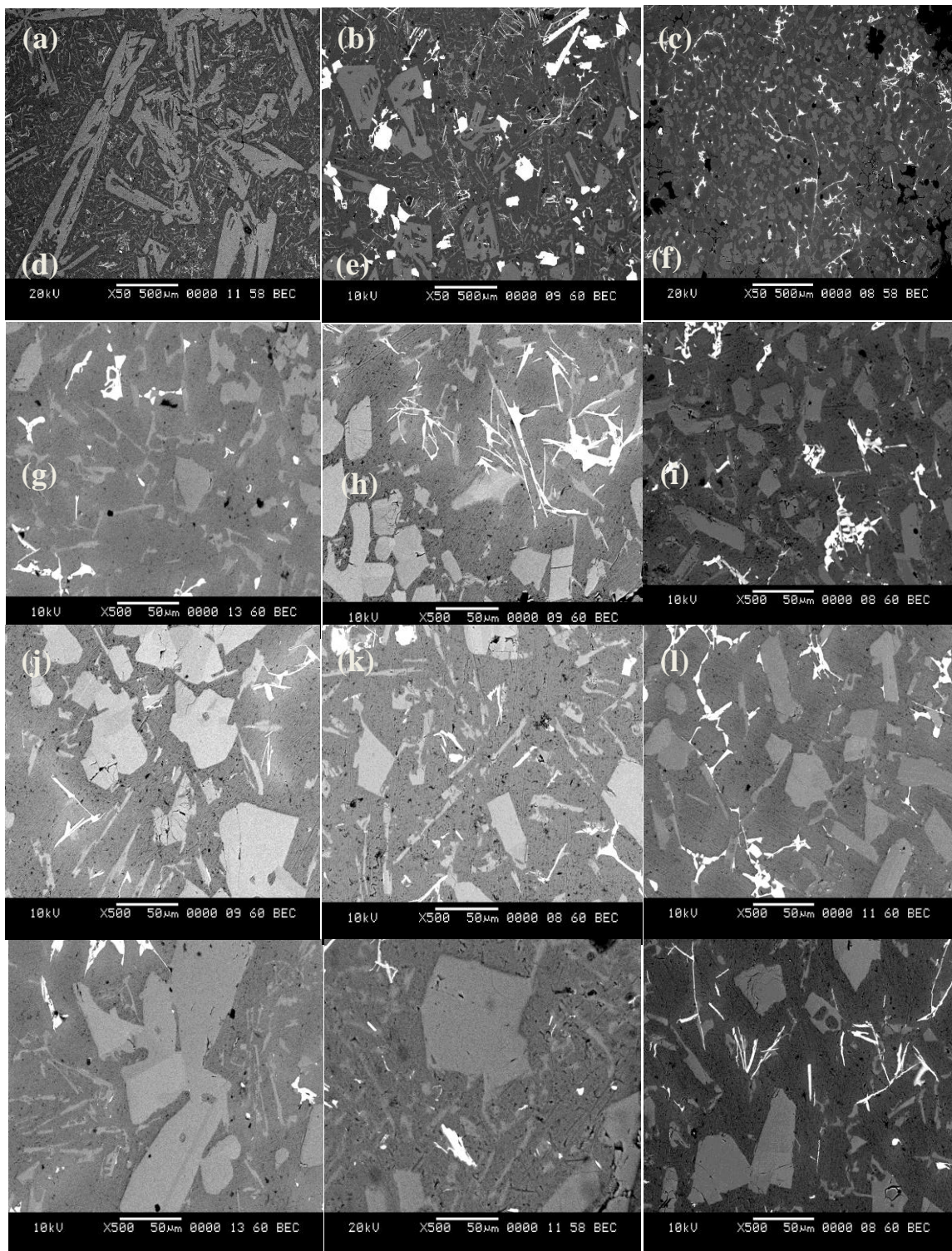


Figure 4.19 Micrographs of Al-22%Si alloy (a) unchilled-untreated (b) unchilled- Ce treated (c) unchilled-P treated (d) untreated -copper chill (e) copper chilled-Ce (f) copper chilled-P treated (g) brass chilled- untreated (h) Ce- brass chill (i) brass chilled-P treated(j) SS chilled-untreated (k) SS chilled-Ce treated (l)SS chilled- P treated

4.4 Effect of Melt Treatment on the Tensile Properties of Alloys

Figure 4.20 (a and b) shows the stress strain curve of slowly cooled Al-8Si alloy before and after Ce treatment. Similarly Fig 4.21 shows the stress strain curve of Al-8Si alloy solidified in copper mold. The maximum stress before the break point was taken as ultimate tensile strength and corresponding the percentage of elongation. Subsequently, the ultimate strength and percentage elongation for different solidification condition is given in Table 8.

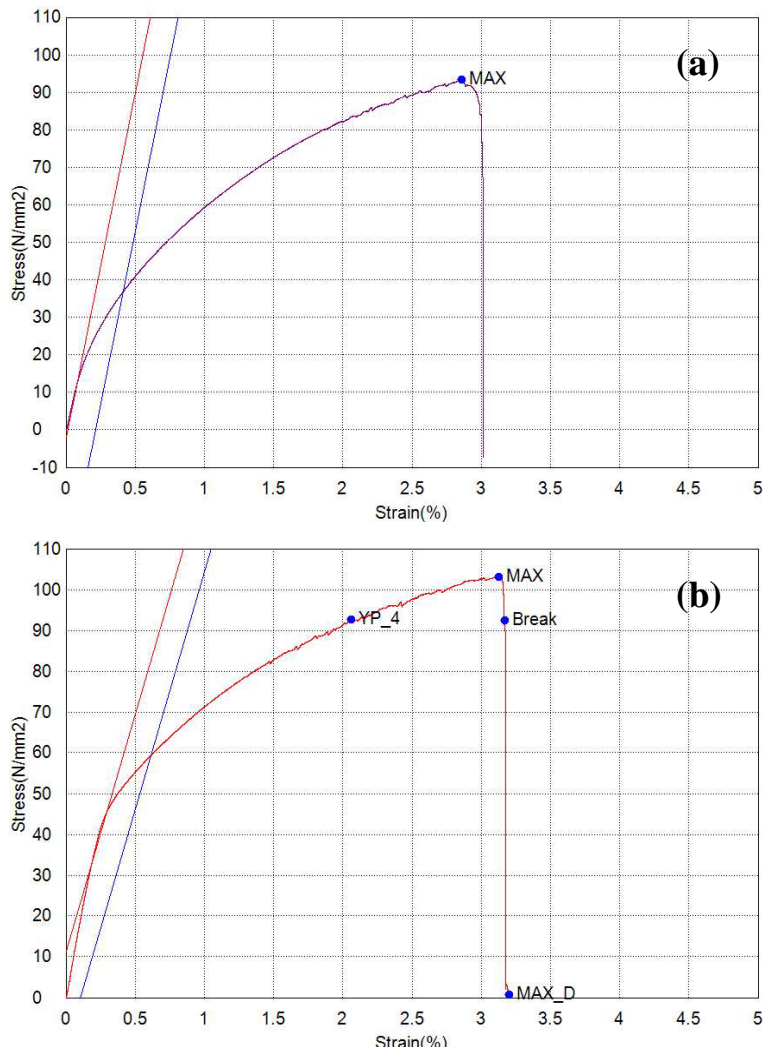


Figure 4.20 Stress-strain curve of Al-8Si alloy solidified against sand (a) untreated
(b) 2 wt.% Ce treated

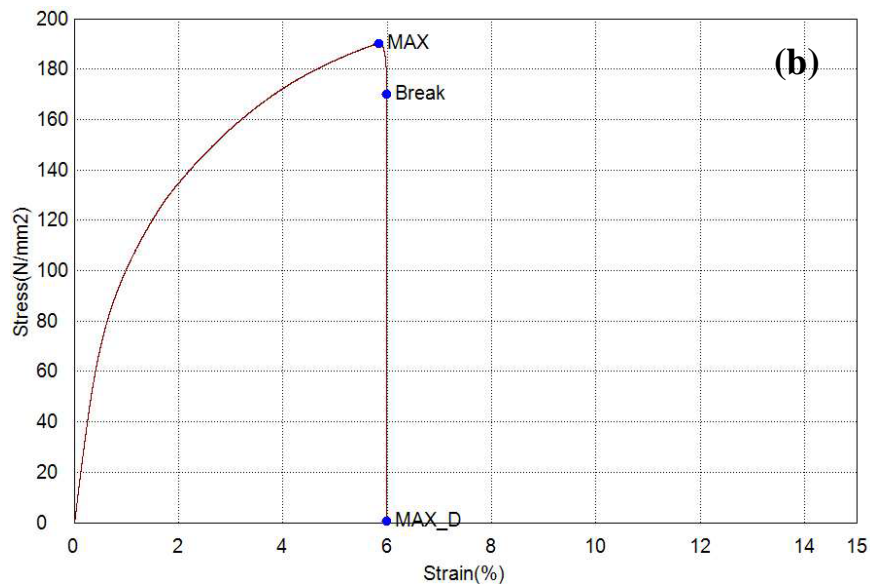
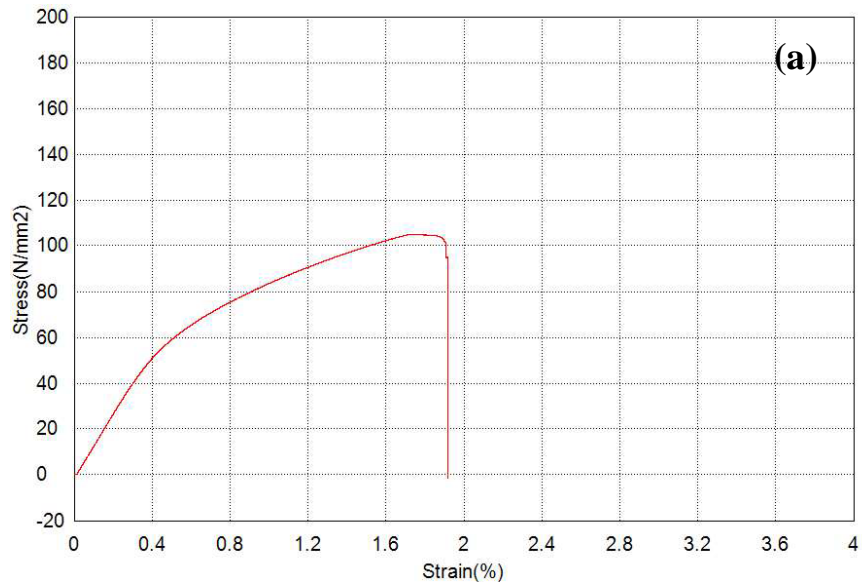


Figure 4.21 Stress-strain curve of Al-8Si alloy solidified on copper mold (a) untreated (b) 1.5 wt.% Ce treated

Similarly, the ultimate tensile strength and percentage of elongation of Al-8Si alloys, Al-13Si alloys, Al-14Si alloys and Al-22 Si alloys for different solidification condition and melt treatment are given in Tables 4.5, 4.6 4.7 and 4.8 respectively.

Table 4.5 The effect of melt treatment on tensile properties of Al-8Si alloy

Melt treatment	Ultimate tensile strength							
	Unchilled		Copper		Brass		Stainless steel	
	As-cast	HT	As-cast	HT	As-cast	HT	As-cast	HT
Untreated	94.7	112.5	107.7	147.0	105.0	156.0	105.0	161.5
0.5 wt-%Ce	102.3	100.3	143.5	114.0	156.0	122.0	175.0	109.5
1.0wt-%Ce	106.7	93.0	172.5	117.0	150.5	122.5	165.5	138.5
1.5 wt-% Ce	96.0	97.5	164.0	118.0	154.8	113.5	180.0	121.0
2.0 wt-% Ce	96.3	100.0	162.0	110.0	152.5	103.5	173.0	110.0
0.02wt-% Sr	85.0	86.0	145.0	117.0	155.0	118.0	172.5	115.0
0.04 wt-%Sr	100.5	92.0	152.0	116.5	164.0	115.0	180.5	119.0
0.06 wt-% Sr	113.0	92.0	159.0	113.0	159.0	99.0	182.5	119.0
0.08 wt.% Sr	114.3	88.0	165.0	112.5	157.5	95.0	170.0	109.5
Melt treatment	Percentage elongation (%)							
	Unchilled		Copper		Brass		Stainless steel	
	As-cast	HT	As-cast	HT	As-cast	HT	As-cast	HT
Untreated	3.2	4.8	1.7	5.3	1.4	13	1.4	21
0.5 wt-%Ce	3.5	3	2.9	5.2	5	6	3.6	3.3
1.0wt-%Ce	3.5	3.5	4.2	6.5	3.3	7.38	3.8	6.2
1.5 wt-% Ce	2.3	3.2	3.8	4.9	5.5	5.9	5.1	5.1
2.0 wt-% Ce	2.25	3.1	3.7	4.5	4.1	5.5	5	4±0.3
0.02wt-% Sr	2.2	3.5	3	5	3.7	3.5	5	2.9
0.04 wt-%Sr	3.9±	5.8	3.2	5.5	3.9	3.6	5.4	2.7
0.06 wt-% Sr	5.7	4.5	5.5	6	3.4	4	6	2.9
0.08 wt.% Sr	4.9	4.5	7	6.7	3.4	4.4	5.4	3.8

Table 4.6 The effect of melt treatment on tensile properties of Al-13Si alloy

Melt treatment	Ultimate tensile strength (MPa)							
	Unchilled		Copper		Brass		Stainless steel	
	As-cast	HT	As-cast	HT	As-cast	HT	As-cast	HT
Untreated	113.3	137.1	160.7	176.7	126.7	138.5	135.0	172.7
0.5 wt-%Ce	117.3	109.0	164.0	161.0	211.0	134.0	169.3	171.5
1.0wt-%Ce	102.4	111.9	178.0	154.0	219.3	137.0	152.1	149.0
1.5 wt-% Ce	65.3	93.0	173.0	138.5	246.5	135.0	200.5	156.3
2.0 wt-% Ce	57.9	85.0	173.8	118.5	217.5	152.0	182.5	137.5
0.02wt-% Sr	135.8	144.5	224.3	194.0	180.0	158.7	202.0	170.0
0.04 wt-%Sr	147.0	144.5	211.0	158.5	187.8	160.3	190.0	143.0
0.06 wt-% Sr	161.0	154.0	209.0	167.0	211.0	166.6	204.0	150.4
0.08 wt-% Sr	139.7	144.8	200.0	150.0	166.0	138.5	211.0	154.0
Melt treatment	Percentage elongation (%)							
	Unchilled		Copper		Brass		Stainless steel	
	As-cast	HT	As-cast	HT	As-cast	HT	As-cast	HT
Untreated	2.3	4.1	3.5	9.5	1.9	4.6	3.6	3.5
0.5 wt-%Ce	2.4	2.1	2.8	12.0	11.2	4.6	3.7	10.3
1.0wt-%Ce	1.8	2.2	2.8	7.5	10.9	4.0	2.2	4.5
1.5 wt-% Ce	2.4	1.45	3.1	5.8	11	4.9	3.5	7.9
2.0 wt-% Ce	1.8	2.7	2.6	2.3	8.7	6.5	3.0	4.4
0.02wt-% Sr	3.1	5.6	6	18.6	3	7.3	6.0	15.5
0.04 wt-%Sr	4.8	5.6	5.7	8.8	3.3	14.2	5.6	8.0
0.06 wt-% Sr	10	9.8	6.7	20	6.8	15.4	8	11.5
0.08 wt-% Sr	4.8	7.3	6.5	8.25	3.4	4.6	11	13.8

Table 4.7 The effect of melt treatment on tensile properties of Al-14Si alloy

Melt treatment	Ultimate tensile strength (MPa)							
	Unchilled		Copper		Brass		Stainless steel	
	As-cast	HT	As-cast	HT	As-cast	HT	As-cast	HT
Untreated	94.4	105.5	136.3	146.6	135.0	149.3	130.7	144.2
0.5 wt-%Ce	116.2	155.3	157.5	135.8	142.0	122.9	155.0	150.8
1.0wt-%Ce	112.0	96.5	189.0	123.4	145.0	121.7	159.5	125.0
1.5 wt-% Ce	113.0	107.0	160.0	129.7	178.5	118.3	158.0	139.2
2.0 wt-% Ce	94.5	103.5	163.5	120.9	165.8	103.4	145.0	136.0
0.05 wt-% P	125.0	133.0	159.0	121.1	150.5	107.2	169.0	163.2
0.1 wt-%P	122.0	145.5	147.4	117.0	150.5	135.8	167.0	142.7
0.2 wt-% P	123.0	148.0	89.6	81.7	161.5	172.0	173.0	158.0
0.4 wt.% P	136.0	194.5	78.1	105.2	90.5	181.0	164.0	178.7
Melt treatment	Percentage elongation (%)							
	Unchilled		Copper		Brass		Stainless steel	
	As-cast	HT	As-cast	HT	As-cast	HT	As-cast	HT
Untreated	1.3	2	2.5	4.2	1.6	7.6	1.6	3.9
0.5 wt-%Ce	1.6	1.7	2.2	2.8	1.8	3.5	2.5	4.8
1.0wt-%Ce	1.6	1.0	4.1	3.0	2.5	2.3	2.7	2.5
1.5 wt-% Ce	1.5	1.4	2.3	3.8	3.9	3.5	2.8	3.6
2.0 wt-% Ce	1.1	1.4	2.8	2.5	3.3	1.7	2.1	3.8
0.05 wt-% P	2	2.0	2.1	2.5	2.1	2	1.5	5.3
0.1 wt-%P	1.3	2.	2.1	2.1	1.9	2.6	0.9	4.0
0.2 wt-% P	1.6	2.1	0.6	0.9	2.2	3.6	1.9	5.2
0.4 wt.% P	1.6	2.5	0.5	2.2	0.8	2.1	1.5	1.8

Table 4.8 The effect of melt treatment on tensile properties Al-22Si alloy

Melt treatment	Ultimate tensile strength (MPa)							
	Unchilled		Copper		Brass		Stainless steel	
	As-cast	HT	As-cast	HT	As-cast	HT	As-cast	HT
Untreated	81.0	96.000	146.2	142.00	122.00	126.50	107.50	116.0
0.5 wt-%Ce	93.2	143.20	173.6	144.60	140.00	145.80	138.00	145.0
1.0wt-%Ce	97.5	113.00	140.9	133.40	175.00	137.30	137.30	135.0
1.5 wt-% Ce	98.4	116.00	176.0	123.30	174.00	124.00	171.00	125.0
2.0 wt-% Ce	95.0	112.50	172.0	114.50	165.00	120.00	168.00	125.0
0.05wt-% P	115.0	116.90	152.6	121.70	129.50	127.10	123.00	114.50
0.1 wt-%P	105.0	144.45	157.0	117.00	152.80	108.5	130.00	135.00
0.2 wt-% P	120.9	163.65	135.5	130.70	131.90	134.60	109.00	184.00
0.4 wt-% P	137.1	176.00	185.1	224.70	129.25	184.55	145.50	152.00
Melt treatment	Percentage elongation (%)							
	Unchilled		Copper		Brass		Stainless steel	
	As-cast	HT	As-cast	HT	As-cast	HT	As-cast	HT
Untreated	1.1	1.6	1	2.5	1.0	2	1.3	1.4
0.5 wt-%Ce	1.2	1.3	1.1	2.3	1.2	1.9	1.4	1.5
1.0wt-%Ce	1.0	1.5	1.2	2.5	1.3	1.3	1.3	1.1
1.5 wt-% Ce	1.2	2.0	1.0	2.8	1.6	2	1.9	0.8
2.0 wt-% Ce	1.1	2	1.4	1.4	1.8	2.4	1.7	0.8
0.05wt-%P	1.5	2.0	2.3	1.9	1.2	2.2	1.8	1.6
0.1 wt-%P	1.4	1.7	2.7	1.7	2.0	1.2	2	1.9
0.2wt-% P	1.8	1.9	2.2	4	1.5	1.2	1.02	2.5
0.4 wt-% P	1.8	2.3	4.4	6.3	1.6	1.6	1.3	1.4

CHAPTER 5

DISCUSSION

5.1 Thermal Analysis

5.1.1 Al-8Si alloys

Figure 5.1 shows the cooling and first derivative curves of unchilled and untreated Al-8 % Si alloy. The thermal analysis characteristic points are marked in the Figure. T_N (No. 1 in the figure) corresponds to the point where the nucleation of α -dendrites starts and is identified by deflection in the derivative curve occurred due to the liberation of heat. T_{min} (No.2) corresponds to a minimum temperature in the cooling curve and a point where derivative curve reaches zero. It also represents the temperature at which a stable nucleus is formed. T_G (No.3) is the point at which the dendrites start growing. Similarly, No. 4, 5 and 6 are corresponding thermal analysis characteristics of eutectic nucleation. T_s (7) correspond to the end of solidification.

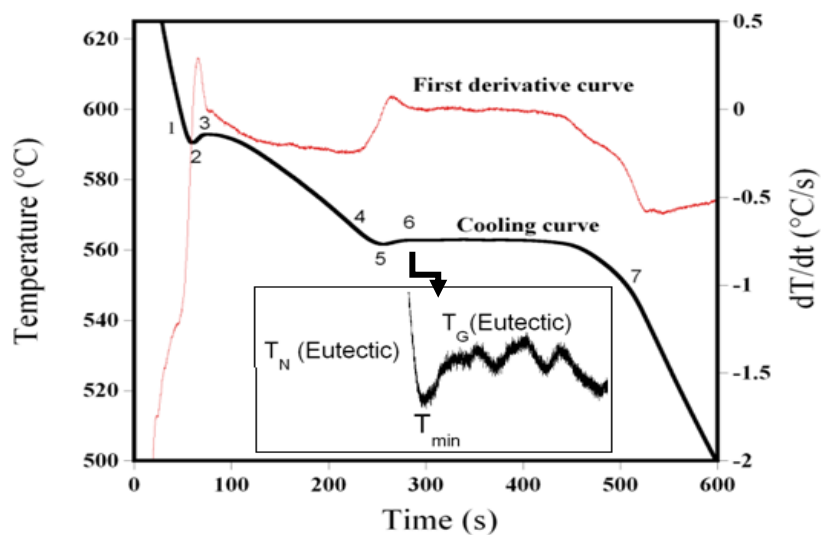


Figure 5.1 Cooling and first derivative curve for Al-8%Si alloy

NOMENCLATURE

1	$T_N(\alpha)$	α - Aluminum nucleation temperature
2	$T_{min}(\alpha)$	α - Aluminum minimum nucleation temperature
3	$T_G(\alpha)$	α - Aluminum growth temperature
4	$T_N(Eut)$	Eutectic nucleation temperature
5	$T_{min}(Eut)$	Eutectic minimum nucleation temperature
6	$T_G(Eut)$	Eutectic growth temperature
7	T_S	Solidus temperature

The temperature characteristics such as T_N , T_{min} , T_G , ΔT_G (growth temperature difference) and the degree of undercooling ($T_{under}=T_N-T_{min}$) were used to assess the effect of melt treatment on cooling curves.

The effect of Ce and Sr melt treatment on the nucleation temperatures of Al-8Si alloys are given in Table 5.1. The reported values are average of three trials with mean standard deviation of 0.6 °C. The alloy solidifies as pro-eutectic α -Al and eutectic phases. The temperature characteristics are separately tabulated for both pro-eutectic and eutectic phases in the table. The nucleation temperature of pro-eutectic aluminum and eutectic silicon of untreated alloy were found to be 602°C and 564°C respectively.

Figure 5.2 (a) shows the effect of Ce melt treatment on the α -Al nucleation temperature. The temperature corresponds to the beginning of the α -Al nucleation. The additions had varying effect on the α -Al nucleation temperature and the addition of Ce resulted in an increase in the nucleation temperature. Depending on the cooling rate, the temperature increased up to certain level of addition and decreased thereafter. For example, in unchilled alloys the α -Al nucleation temperature increased to 610.9 °C with an addition of 0.5 wt% Ce and then decreased with further addition, whereas, in brass chilled alloys, the temperature increased from 598.8 to a peak value of 603.6 °C with an addition of 1.5 wt.% Ce. The trend remained same for copper and SS chilled alloys as well. Backerud et al. (1990) [Mohanty and Gruzleski 1996] reported a similar kind of increase in liquidus temperature of pure aluminum with the addition of grain refiner.

Table 5.1 Cooling curve analysis of Al-8% Si alloy

	Ce/Sr wt-%	T _N (α) (°C)	T _{min} (α) (°C)	T _G (α) (°C)	Δ T _N (α) (°C)	T _N (Eut) (°C)	T _{min} (Eut) (°C)	T _G (Eut) (°C)	Δ T _N (Eut) (°C)	T _s (°C)
Unchilled	0	602.	590.2	592.4	12.7	564	562	563.2	2	540
	0.5Ce	610.	592.5	594	18.4	566.4	564.2	565.2	2.2	538
	1.0 Ce	607.	595.6	596.2	12.1	566.1	564.4	565.4	1.7	535
	1.5Ce	603.	601.9	602.6	1.3	568.2	566.4	567.4	1.8	536
	2.0 Ce	602.	598.4	600	4.2	566.3	564.5	565.6	1.8	536
	0.02Sr	600	589.1	590.6	10.9	554.7	552.2	553.3	2.5	525
	0.04Sr	601.	590.2	590.9	11.7	556.1	553.3	554.9	2.8	520
	0.06Sr	601.	589.2	590.2	12.2	557.1	553.3	554.1	3.8	518
	0.08Sr	601	590.7	591.9	10.3	554.9	552.2	553.1	2.7	520
Copper	0	598.	598.2	598.6	0.5	561	559.7	559.2	1.3	510
	0.5Ce	602.	601.8	602	0.5	562	559.6	556.2	2.4	508
	1.0 Ce	602.	602.2	602.1	0.2	561.8	559	556	2.8	502
	1.5Ce	602.	602.1	602.3	0.1	561.2	558.2	555.2	3	498
	2.0 Ce	600.	600	600.4	0.3	556.8	554	553.2	2.8	504
	0.02Sr	594.	594	594.6	0.6	554.6	552	551.7	2.6	484
	0.04Sr	594.	593.7	594.2	0.5	552.6	550.5	548.6	2.1	475
	0.06Sr	597.	597.3	597.5	0.6	550.5	548.6	547.1	1.9	472
	0.08Sr	598.	597.8	598.2	0.9	549.1	547.2	546.8	1.9	471
Brass	0	598.	598	598.7	0.8	562.7	561	561.2	1.7	514
	0.5Ce	598.	597.8	597.4	0.6	561.8	560	557.7	1.8	508
	1.0 Ce	601.	601.2	600.9	0.2	561.9	560	556.8	1.9	505
	1.5Ce	603.	603	602.5	0.6	561.2	559.2	556.5	2	498
	2.0 Ce	599.	599.2	598.5	0.6	559.5	558	556.2	1.5	498
	0.02Sr	595.	594.1	594.5	1.3	560.9	558.3	558	2.6	497.1
	0.04Sr	595.	594	594.8	1.4	554.7	552.1	552	2.6	490
	0.06Sr	595.	593.5	594.8	2.4	551.6	549.5	546.2	2.1	480
	0.08Sr	595.	593.2	594.5	2.1	548.8	547	545.3	1.8	475
Stainless steel	0	596.	594.5	595.1	1.6	562.8	561	561.9	1.8	527
	0.5Ce	596.	594.8	594.4	1.4	562.5	560.5	560.1	2	515
	1.0 Ce	601.	600.8	600.6	1.1	562.2	559.1	557.2	3.1	512
	1.5Ce	601.	600.2	599.9	1	559.5	556.2	555.1	3.3	511
	2.0 Ce	599.	598.4	598.3	1.2	559.1	557	555.3	2.1	510
	0.02Sr	595.	593.6	595	1.6	556.7	554.1	553.6	2.6	509
	0.04Sr	595.	594	594.9	1.6	555.9	553.1	552.4	2.8	508
	0.06Sr	599.	597.8	598.3	1.7	555	552.1	549.3	2.9	508
	0.08Sr	599.	598.1	598.2	1.8	552.6	548.6	545.9	4	506

Hence, the increase in liquidus temperature with Ce treatment is associated with the grain refinement as the additions have nucleating the aluminum grains at higher temperatures.

Figure 5.2 (b) shows the effect of Sr melt treatment on the α -Al nucleation temperature. Unlike Ce treated alloys, the Sr treated alloys showed a depression in the α -Al nucleation temperature and the depression increased with increase in cooling rate. Previous studies on hypoeutectic Al-Si alloys shows that the Sr addition to hypoeutectic alloy decreases the α -Al nucleation temperature and the magnitude of depression with cooling rate [Zhongwei and Ruijie 2010].

Figure 5.3 (a and b) shows the effect of melt treatment on the α -Al minimum nucleation temperature ($T_{\text{Min},\alpha\text{-Al}}$) and $T_{\text{Min},\alpha\text{-Al}}$, is the temperature at which stable nucleus is formed. T_{Min} temperature increased with the addition of Ce and decreased with Sr. The addition of Ce up to an certain concentration increased the minimum temperature, whereas, further addition decreased the temperature. Unlike Ce addition, the increasing concentration of Sr depresses the α -Al minimum nucleation temperatures at all solidifying conditions.

Figure 5.4 shows the variation of α -Al nucleation undercooling with varying contents of Ce and Sr melt treatment. The addition of Ce decreases the degree of undercooling which indicates that the energy required for nucleation decreased with addition. A similar kind of decrease in undercooling was observed with addition of Al-5Ti-B to 319 alloys and was associated with grain refinement [Shabestari and Malekan 2010]. However, the decrease in undercooling with grain refinement was only at slow cooling rate, it increased when addition was carried out at higher cooling rates.

The undercooling acts as an energy barrier for the nucleation of dendrites. In the absence of any heterogeneous nucleation agent, the nucleation of dendrites occur at higher degree of undercooling leading to the nucleation of less number of grains and coarse grained structure.

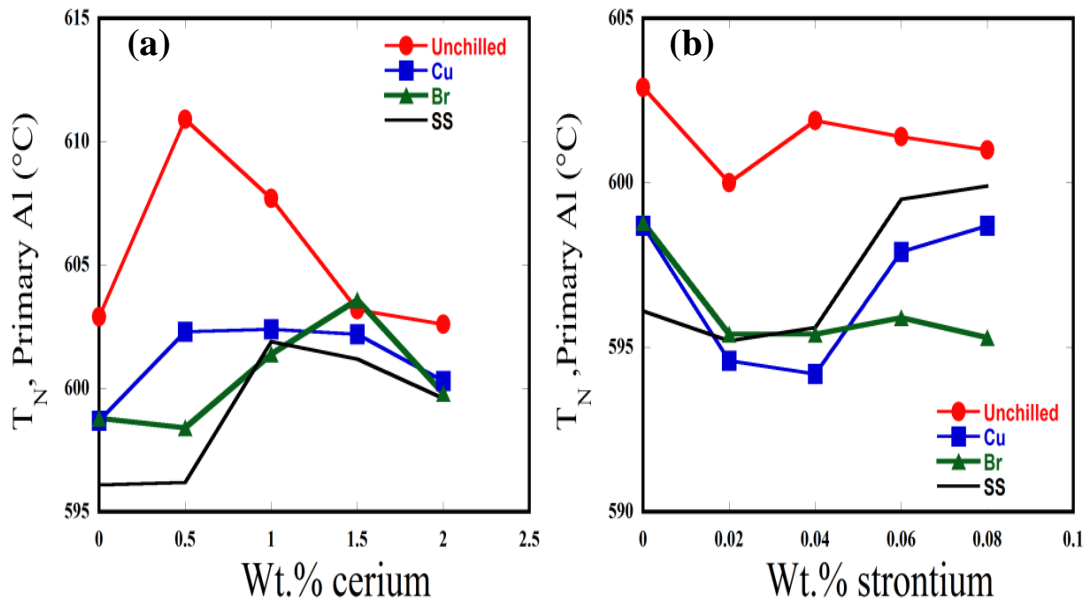


Figure 5.2 Variation of α -Al nucleation temperature with varying content of (a) Ce (b) Sr

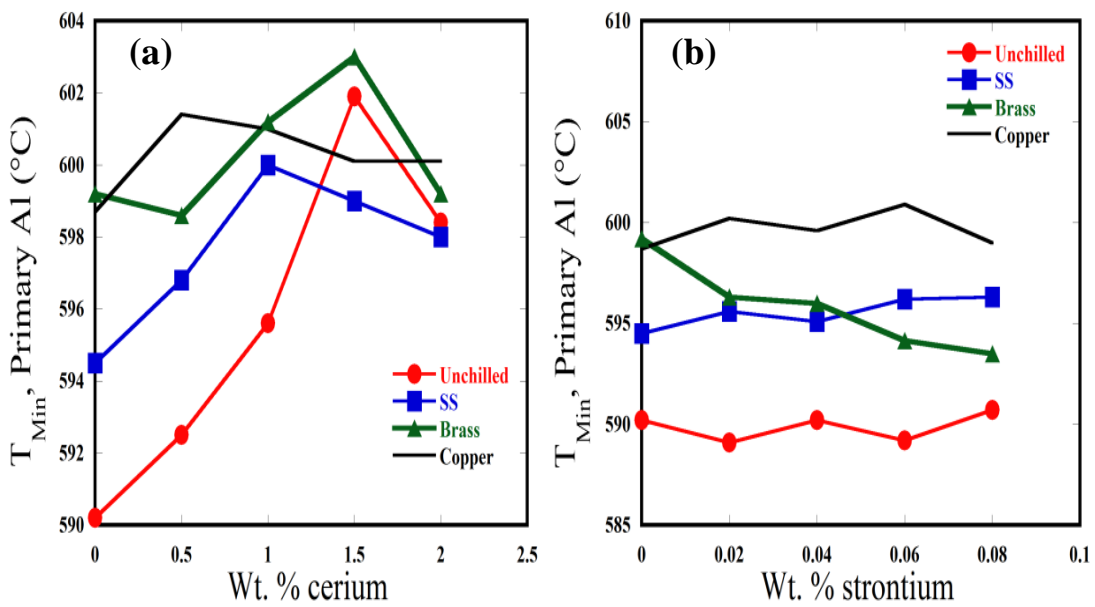


Figure 5.3 Variation of α -Al minimum nucleation temperature with varying content of (a) Ce (b) Sr

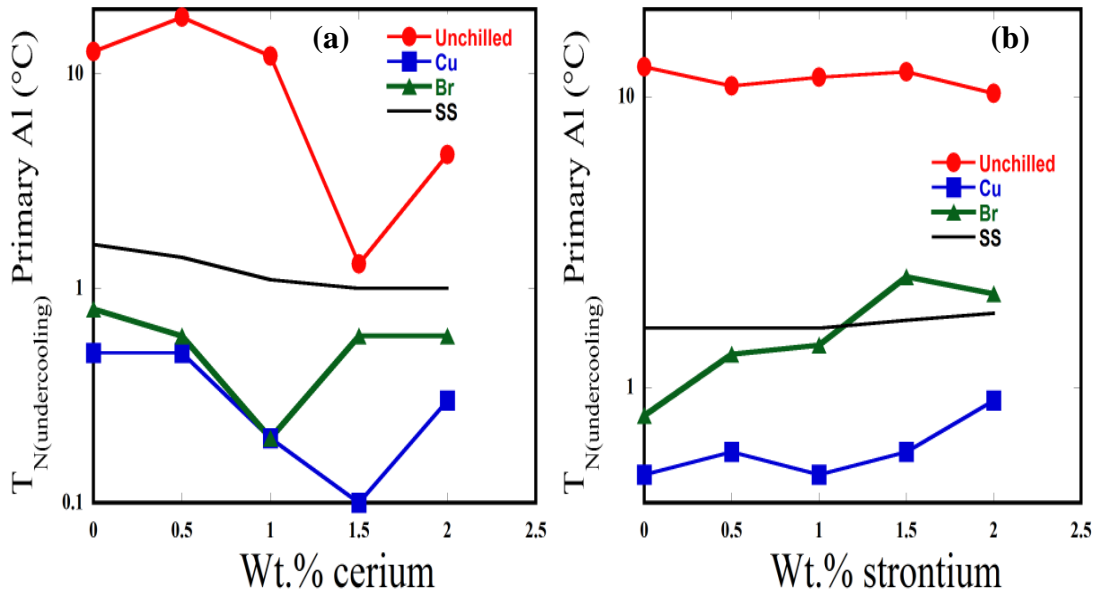


Figure 5.4 Variation in degree of undercooling of α -Al with varying content of (a) Ce (b) Sr

The presence of heterogeneous nucleants in the melt will decrease the energy required for the nucleation by providing nucleation sites and thereby decreasing the undercooling. The nucleation of large number grains from less undercooled melt results in fine grained structure [Mohanty and Gruzleski 1996] [Shabestari and Malekan 2010]. The addition of Sr had an opposite effect on primary aluminum undercooling. The degree of undercooling increased with the increase in Sr concentration and this would correspond to coarse grained structure. The thermal analysis results were in complete agreement with the microstructure study discussed in 5.4.1.

Figure 5.5 shows the effect of varying concentrations of Ce and Sr melt treatment on the eutectic nucleation temperature. Similar to the aluminum nucleation temperature, the addition of Ce also increased the eutectic nucleation temperature at slower cooling rates. When an addition of 0.5 wt% Ce increased the α -aluminum nucleation temperature by 8°C it increased the eutectic temperature by 2°C . However, the eutectic silicon nucleation temperature of chilled alloys decreased with Ce additions, even though there was an increase in α -Al nucleation temperature. The additions

depressed the minimum nucleation temperature as shown in Figure 5.6 (a and b). For example, the eutectic minimum temperature $T_{\min}(\text{Eut})$ of untreated alloys solidified on copper, brass and stainless steel were found to be 559.7, 561.4 and 561.5°C respectively, whereas, with 2 wt.%-Ce addition the $T_{\min}(\text{Eut})$ of the alloy decreased to 554, 558.2 and 557.3 °C respectively.

It was observed that the Sr additions did not show any significant effect on the α -Al nucleation temperature under any cooling conditions, but it significantly depressed the eutectic nucleation temperatures. A constant decrease in nucleation temperature with increase in Sr concentration was observed at all cooling rates. The lowest T_{\min} (Eutectic) temperatures was obtained with an addition of 0.08 % of Sr and were 552, 547, 547.2 and 546°C for alloys solidified against sand copper, brass and stainless steel chills respectively. The decrease in eutectic nucleation temperature was due to the adsorption of modifying atom on to the silicon-aluminum interface.

In the absence of any chemical modifiers, silicon nucleates on the β -Fe intermetallic (Al-Fe-Si) present in the alloy prior to the nucleation of aluminum and grow as acicular structured silicon. The addition of modifiers such as strontium suppresses the nucleation of eutectic silicon on Fe by poisoning the Fe intermetallic and as a result the nucleation of silicon is hindered, wherein Al nucleates before silicon. In the process, the silicon is forced to nucleate between the Al dendrites, aided with twinning to form fine fibrous structure [Shabestari and Ghodrat 2007] [Ludwig et al. 2013] [Shankar et al. 2004].

Figure 5.7 (a and b) shows the effect of melt treatment on the degree of eutectic undercooling. The addition of Ce and Sr had similar effect on the eutectic undercooling and it increased significantly with additions for all cooling conditions. A decrease in eutectic growth temperature was observed along with the increase in undercooling temperature. The presence of chemical modifiers such as strontium decreases the surface tension of the melt and alters the wetting characteristic between eutectic liquid and heterogeneous substrates like Fe intermetallics making it unavailable for eutectic nucleation [Aparicio et al. 2013].

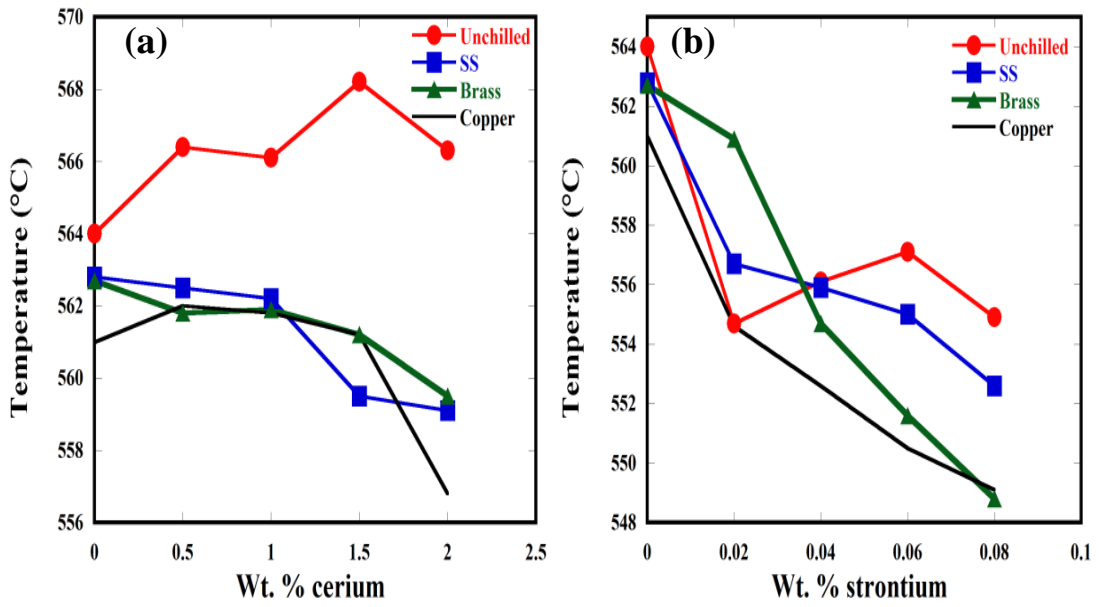


Figure 5.5 Variation of eutectic nucleation temperature with varying content of (a) Ce
(b) Sr

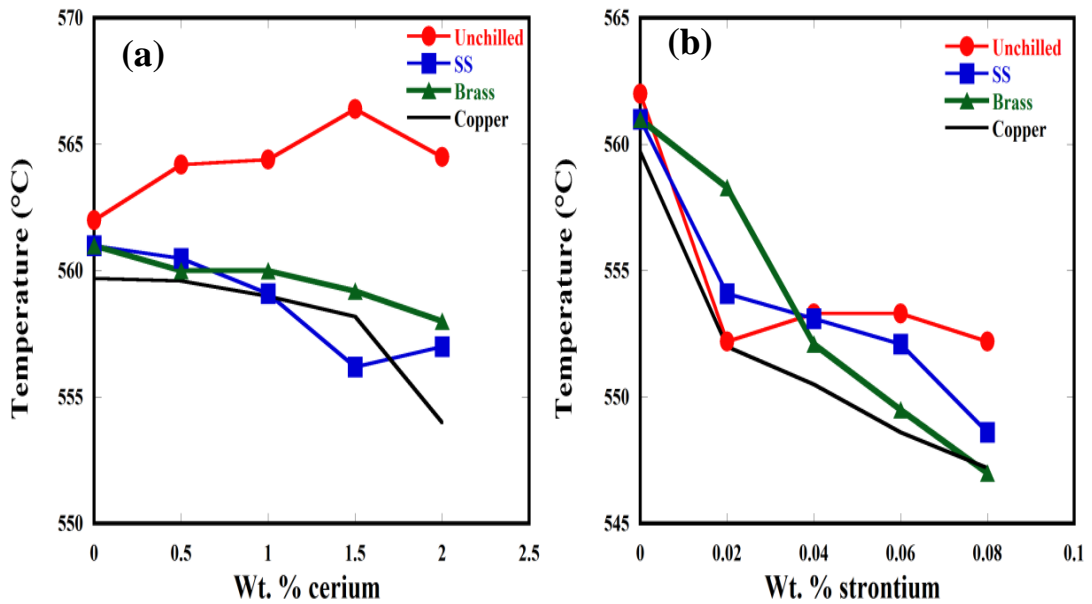


Figure 5.6 Variation of eutectic minimum nucleation temperature with varying content of (a) Ce (b) Sr

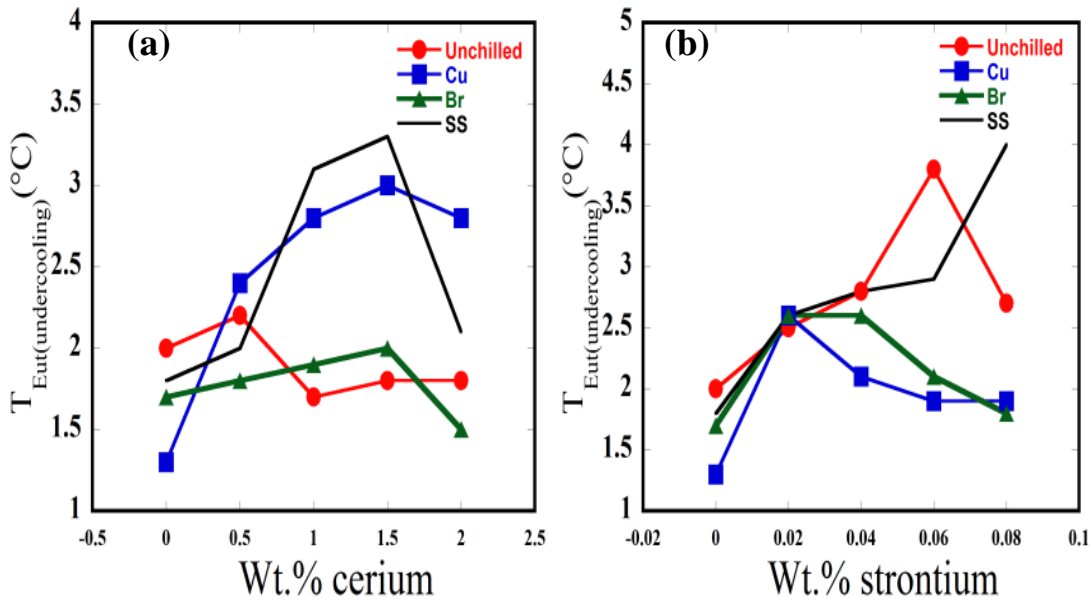


Figure 5.7 Variation in degree of undercooling of eutectic with varying content of (a) Ce (b) Sr

Hence it is more likely that the eutectic silicon do not nucleate on the substrates present and thereby forcing it to nucleate from highly undercooled melt. The increased undercooling will result in decreased silicon growth and increased twin density [Aparicio et al. 2013]. According to Djurdjevic et al. (2001), the modification of eutectic silicon is associated with the depression in eutectic temperature and an increase in eutectic undercooling. Larger the magnitude of eutectic temperature depression, higher will be the level of modification.

ΔT_G was used to quantify the effect of Ce addition on thermal analysis parameters for varying solidifying conditions. Figure 5.8 shows the variation of ΔT_G with cooling rate for different melt treatment. The cooling rate is calculated as $(T_N - T_S / t_N - t_S)$, where, T_N is the primary phase nucleation temperature and T_S is the solidus temperature, t_L and t_S are the solidification time at corresponding temperatures respectively. The ΔT_G was obtained by finding out the difference between treated alloys with untreated unchilled alloy. Since the cooling rate is calculated separately for each melt treatment, the Figure accounts the actual cooling rate occurred during melt treatment. The ΔT_G values increased with the addition of Ce and this indicates

that the growth temperature decreased with the addition. The chilled alloys showed significant decrease in growth temperatures compared to the slowly cooled alloys. The ΔT_G values were influenced by both cooling rate and melt treatment. The increase in ΔT_G with cooling rate and melt treatment indicates the modification of eutectic silicon. The Ce and Sr melt treatment significantly increased the ΔT_G values, and this can be directly correlated to the magnitude of modification. The Sr addition yielded higher ΔT_G values than the Ce treated alloys. The addition of Ce at lower cooling rates would yield negative ΔT_G , indicating the inefficiency of Ce in modifying eutectic silicon at lower cooling rates. However, at higher cooling rates the Ce melt treatment was as effective as Sr.

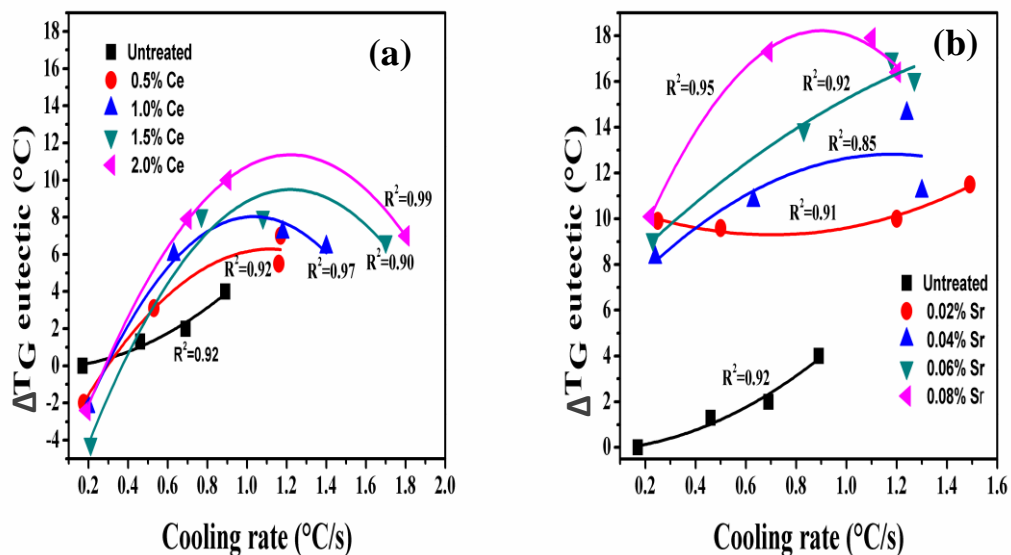


Figure 5.8 Eutectic growth temperature differences versus cooling rate for varying content of (a) Ce (b) Sr

5.1.1.1 Effect of melt treatment on the dendrite coherency point (DCP)

DCP is a point in cooling curve at which the growing dendrites in metal/alloys start to touch each other and would begin to form interconnected networks throughout the casting [Chavez-Zamarripa et al. 2007]. It is also a point at which the mass feeding of the liquid metal shifts to inter-dendrite feeding and casting defects, such as segregation, hot-tearing and shrinkage porosity are believed to be formed after this point during solidification. DCP is of great interest in solidification simulation as it influences the ability of the metal in filling complex shapes and in the formation of inter-metallic compounds.

The DCP can be determined either by rheological methods or by thermal analysis. The rheological method identifies DCP as the point where there is an abrupt change in the measured torque due to the change in the mechanical strength of the solidifying sample [Veldman et al. 2001]. In thermal analysis, DCP corresponds to the point where the thermal conductivity of the solidifying sample increases from a minimum value. It is based on the fact that the thermal conductivity of the solid is higher than the liquid. The method uses two thermocouples, one at center (T_c) and another near to the wall (T_w), to record temperature differences with respect to the solidification time. The minimum point in the temperature difference ($\Delta T = T_w - T_c$) versus curve corresponds to the DCP [Djurdjevic et al. 2012].

Figure 5.9 illustrates the two thermocouple method for determination DCP in Al-8% Si alloy. DCP is identified as the first minimum point in time versus ($T_w - T_c$) curve. The corresponding temperature in center thermocouple is the dendrite coherency temperature (DCT). Figure 5.10 (a) show the effect of addition of Ce and Sr on the DCT. The addition of Ce resulted in the increase and Sr in decrease of DCT temperature. The increased temperature indicates that the DCT occurred much earlier than the untreated alloys. Figure 5.10 (b) shows the variation of fraction solid at DCP with melt treatment. The fraction solid at DCP increased with Ce melt treatment and decreased with Sr treatment. A maximum of 10% increase in fraction was observed

with 1.5 wt% Ce addition, this indicates that the fraction of solid formed before the begin of inter-dendritic feeding increases with Ce melt treatment.

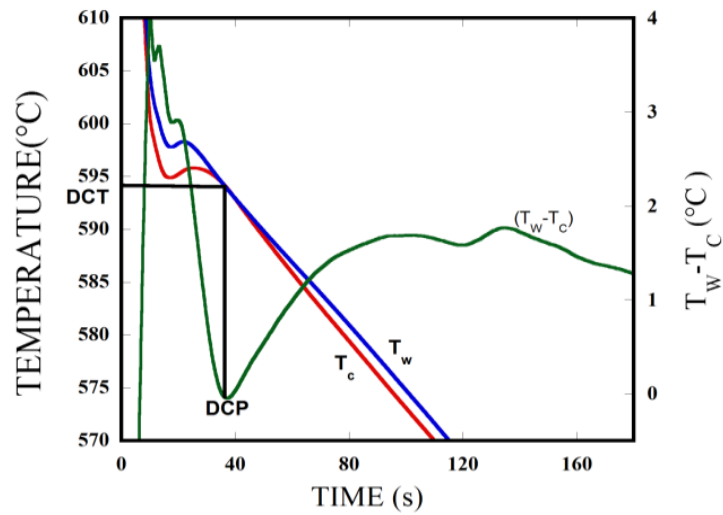


Figure 5.9 Illustration of dendrite coherency temperature (DCT) determined from cooling curves

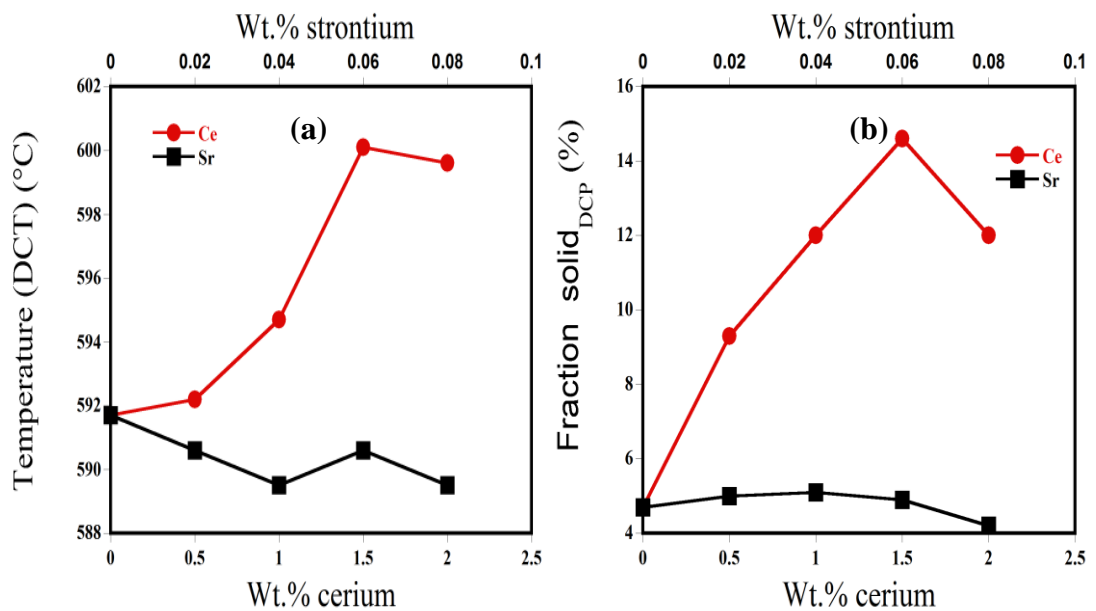


Figure 5.10 The Effect of melt treatment on (a) dendrite coherency temperature (b) fraction solid at DCP

5.1.2 Al-13Si alloys

The effect of varying content of Ce and Sr addition on the solidification temperature characteristics of Al-13% Si alloy are given in the Table 5.2. Figure 5.11 (a and b) shows the variation of eutectic nucleation temperature with varying content of Ce and Sr melt treatment. Both Ce and Sr additions had similar effect on the eutectic nucleation temperature and it decreased with increase in concentrations, however, the nucleation temperature of unchilled alloy increased with both kind of addition. The extent of decrease was greater in Sr treated alloys and the depression was mainly due to the combined effect of chilling and modification. Similarly, the minimum nucleation temperature also decreased on melt treatment as shown in the Figure 5.12. For example, in unchilled alloys, the eutectic minimum decreased from 562.5 to 557.8°C with an addition of 2 wt.% Ce and the addition of 0.06 wt.% Sr decreased the temperature to 557.1 °C. The addition of Ce and Sr to chilled alloys also showed similar kind of depression in eutectic minimum temperature. Figure 5.13 (a and b) shows the effect of Ce and Sr additions on the degree of eutectic undercooling. The increase in degree of undercooling with additions corresponds to the degree of eutectic modification.

Along with depression in the eutectic temperature, the melt treatment also resulted in the shift in the eutectic point towards the right. As a result, the alloy solidified as hypoeutectic alloy rather than a eutectic alloy and the nucleation of aluminum dendrites occurred prior to the nucleation of eutectic. It was reported that the nucleation of silicon in the untreated eutectic alloy occurs on the primary silicon particles formed prior to the eutectic phase [Liao et al. 2010]. The primary silicon particles are observed to be commonly present in the commercial near eutectic Al-Si alloys. The eutectic phase nucleates on such primary silicon with much less or no undercooling as acicular silicon and aluminum eutectic. The microstructure of the present alloy shown in the Figure 4.17, also shows the presence of primary silicon in it and which would be invariably present in the commercial eutectic alloys. Hence, based on the thermal analyses results and microstructure, it can be inferred that the nucleation of eutectic Si in the untreated alloys has occurred on the primary silicon.

Table 5.2 Cooling curve analysis of Al-13Si alloy

	Ce/Sr wt-%	T _N (α) (°C)	T _{min} (α) (°C)	T _G (α) (°C)	ΔT _N (α) (°C)	T _N (Eut) (°C)	T _{min} (Eut) (°C)	T _G (Eut) (°C)	ΔT _N (Eut) (°C)	T _s (°C)
Unchilled	0					565.1	562.5	563.8	2.6	545
	0.5Ce	591.2	589.7	589.7	1.5	573.5	561	563.4	12.5	539
	1.0 Ce	588.2	588	587.8	0.2	573	560.7	562.2	12.3	536
	1.5Ce	587.5	587	586.5	0.5	573.1	559.6	561.4	13.5	536
	2.0 Ce	586	585	584.3	1	573.4	557.8	559.8	15.6	536
	0.02Sr	596.8	589.2	589.2	7.6	566.5	560.5	562.4	6	529
	0.04Sr	588	585.2	585	2.8	566.4	559.5	562.2	6.9	527
	0.06Sr	585	572.8	572	12.2	566.2	557.1	560.3	9.1	525
	0.08Sr	587	580.6	580.2	6.4	565.9	560	561.4	5.9	526
Copper	0					566.7	566.2	566.4	0.5	520
	0.5Ce	565.9	564.7	564.5	1.2	562.4	561.7	561.5	0.7	505
	1.0 Ce	565.1	564.5	564	0.6	562.2	561.5	561.2	0.7	496
	1.5Ce	564.5	564.1	564	0.4	559.5	558.1	558	1.4	488
	2.0 Ce	565.3	564.5	564.2	0.8	564.1	562.9	563	1.2	494
	0.02Sr	573.4	572.6	570.4	0.8	562.5	561.5	561.5	1	489
	0.04Sr	569.5	568.4	568.3	1.1	561.5	560	560.1	1.5	486
	0.06Sr	567.9	566.4	566.4	1.5	560.2	558.5	558.9	1.7	488
	0.08Sr	565.2	563.8	563.9	1.4	561.8	560.6	560.5	1.2	490
Brass	0					565.7	565.1	565.4	0.6	525
	0.5Ce	567.2	565.5	565.5	1.7	561.8	560	560.2	1.8	495
	1.0 Ce	567.9	566.6	566.4	1.3	561.2	559.5	559.7	1.7	489
	1.5Ce	568.4	568.1	568	0.3	563.2	561.9	561.9	1.3	500
	2.0 Ce	566.1	565.4	565	0.7	563.5	561.9	561.7	1.6	502
	0.02Sr	570.1	569.5	569.2	0.6	565.7	564.8	565.8	0.9	490
	0.04Sr	567.7	567.1	567	0.6	563	561.1	560	1.9	488
	0.06Sr	566.8	566.3	566.5	0.5	562.8	560.9	560.2	1.9	489
	0.08Sr	565.9	564.8	565	1.1	563	561.1	560.1	1.9	492
Stainless steel	0					563.4	562	562.5	1.4	529
	0.5Ce	571.3	566.6	566	4.7	563.8	558.9	558.7	4.9	510
	1.0 Ce	569	565.4	564.5	3.6	568.2	560.7	560.2	7.5	507
	1.5Ce	567	564	563.5	3	564	560.3	560	3.7	504
	2.0 Ce	567	563.8	563	3.2	564	561	560.8	3	508
	0.02Sr	570	564	564.5	6	561.4	558.7	559	2.7	509
	0.04Sr	569.8	562.3	562.5	7.5	560	557.5	557.2	2.5	505
	0.06Sr	567.7	563	563.3	4.7	559	556	555.8	3	502
	0.08Sr	567.5	563.2	563	4.3	559.9	557.8	558	2.1	504

The addition of modifiers such as Sr or Na suppresses the nucleation of primary silicon by poisoning their nucleation sites and thereby suppresses the nucleation of eutectic silicon to lower temperatures. In addition to the temperature depression, the modification also shifts the eutectic point towards high silicon content and results in the transformation of eutectic alloy to a hypoeutectic alloy. The nucleation of α -aluminum occurs instead of primary silicon and the eutectic silicon nucleates between the aluminum dendrites from an highly undercooled melt as fine fibrous structure [Liao et al. 2010] [Lu and Hellawell 1995].

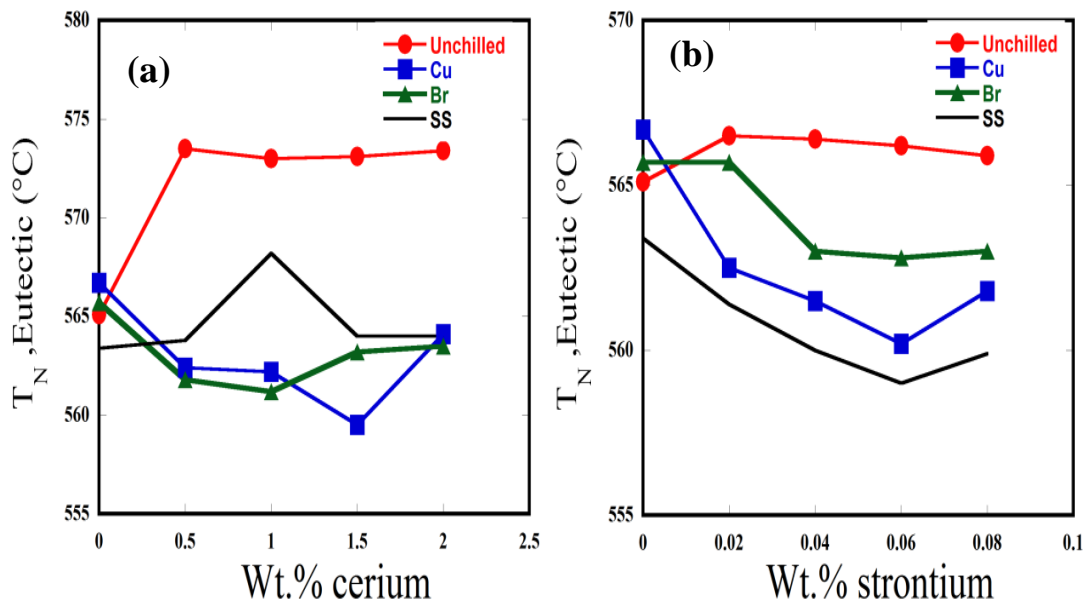


Figure 5.11 Variation of eutectic nucleation temperature of Al-13Si alloy with varying content of (a) Ce (b) Sr

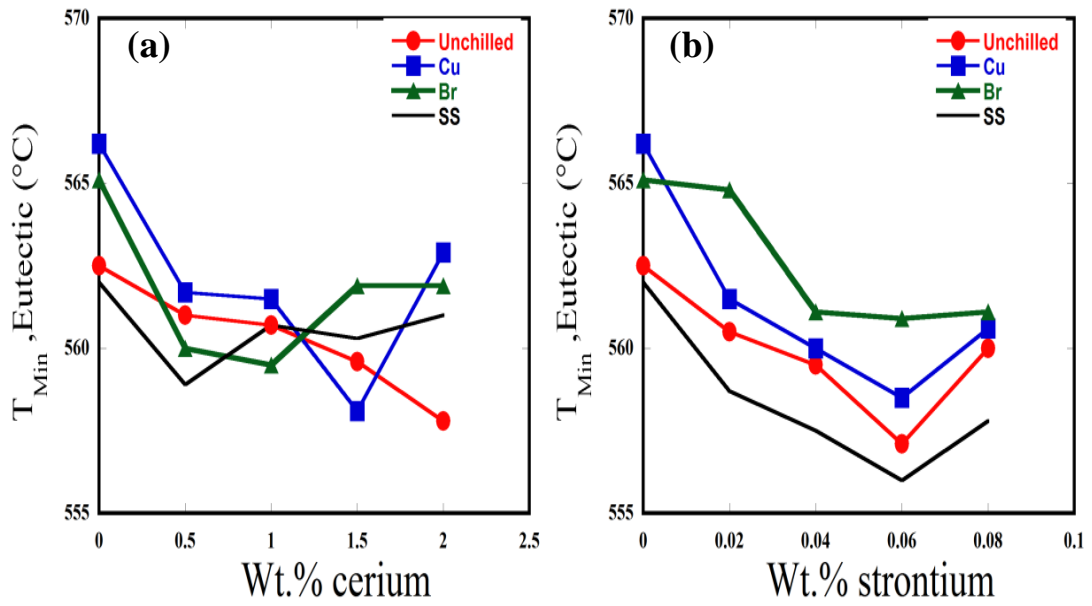


Figure 5.12 Variation of eutectic minimum temperature of Al-13Si alloy with varying content of (a) Ce (b) Sr

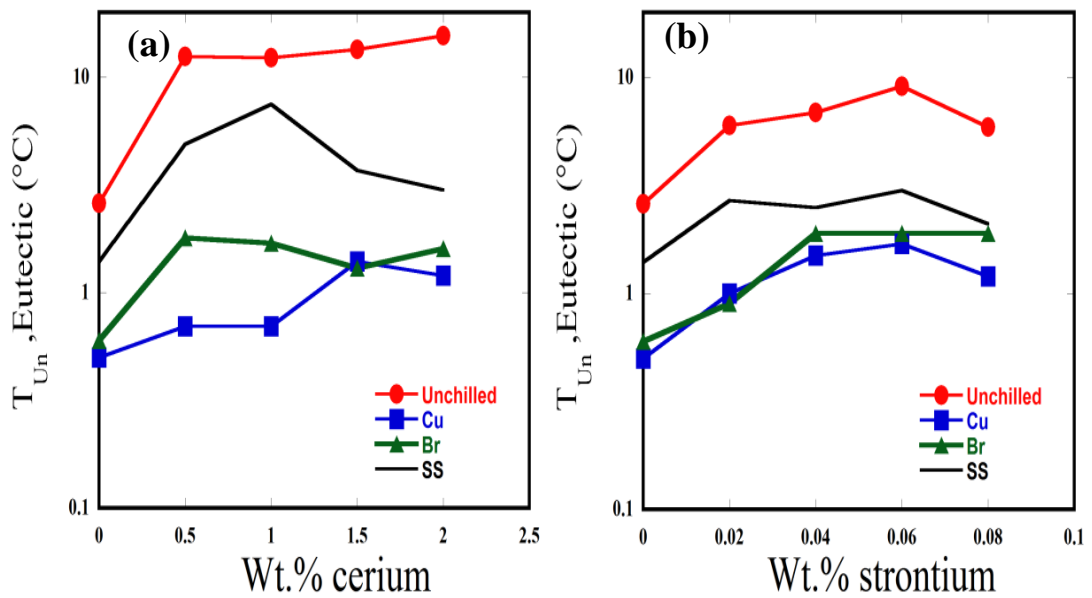


Figure 5.13 Variation of eutectic undercooling of Al-13Si alloy with the addition of varying content (a) Ce (b) Sr

Similarly, the increase in eutectic undercooling with addition of Sr and Ce is associated with the modification of eutectic silicon. The additions poison potential nucleation sites of silicon to hinder its nucleation. As a result, the silicon was forced to nucleate at lower temperature with high degree of undercooling. The depression in association with the shift in the eutectic point alters the nucleation pattern of the alloy.

The alloy behaves as a hypoeutectic alloy rather than the eutectic alloy to nucleate aluminum dendrites prior to the nucleation of eutectic silicon. The thermal characteristics of the primary aluminum formed due to the melt treatment for various cooling conditions are given in the Table 5.2. The eutectic silicon will be forced to nucleate and grow between dendritic arms with heavily twined fibrous structure. The increase in the degree of undercooling with melt treatment was associated with the difficulty in nucleation of silicon. The aluminum temperature characteristics decreased with increase in the concentration of Ce or Sr. The primary aluminum nucleation temperature increased with the cooling rate. The aluminum undercooling was decreased on addition of Ce and increased with addition of Sr.

Figure 5.14 shows the effect of cooling rate and melt treatment on the eutectic ΔT_G . The ΔT_G values increase with melt treatment and cooling rate. Figure shows a peak at 0.5°C/s and 1.5% Ce among Ce treated alloys and 0.7°C/s and 0.06% Sr among Sr treated alloys. The addition of Ce increases the ΔT_G up to 1.5 wt.% for cooling rates and then decrease on further increase in concentration. The reason for this would be the formation of blocky Ce intermetallics, discussed in chapter 5.4.2. The addition of Sr showed a consistent increase in ΔT_G with increase in concentration and cooling rate.

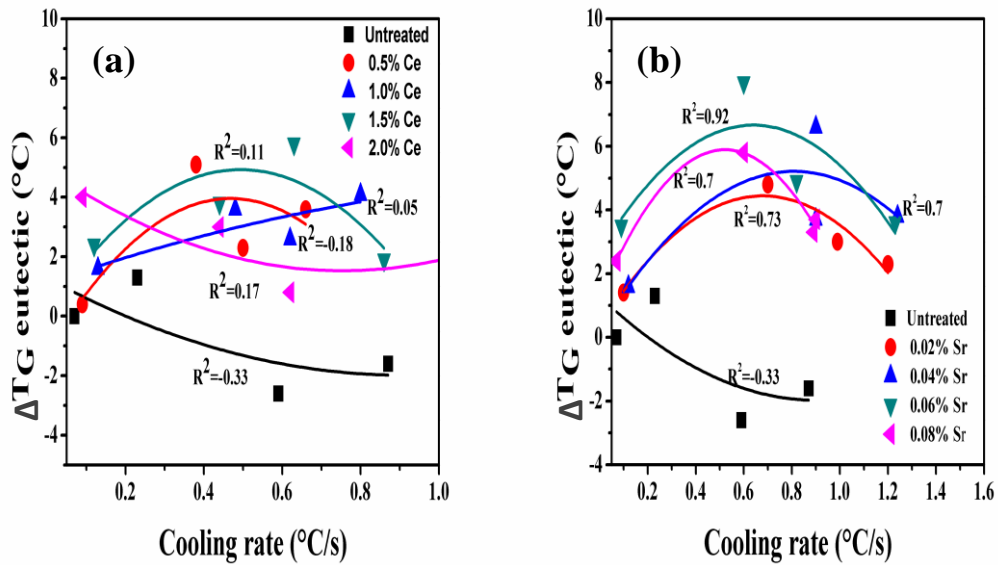


Figure 5.14 Eutectic growth temperature differences versus cooling rate for varying content of (a) Ce (b) Sr

5.1.3 Al-14Si alloys

In hypereutectic Al-Si alloys, the primary silicon solidifies prior to the nucleation of eutectic phase. The Si-Si atoms segregate to form clusters at temperatures as high as 1075°C with a different crystalline structure than that of solid silicon. The clusters would be beneficial for the formation of primary silicon, the morphology and size of primary silicon particles are directly dependent on the arrangement and size of these Si clusters [Xu and Jiang 2006] [Robles Hernandez and Sokolowski 2006].

The nucleation and growth of primary silicon particles from liquid into the surroundings causes rejection of aluminum solvent until the local concentration is sufficient to nucleate α -Al phase. The partitioned Al phase from the growing crystals accumulates around the Si particles and appears as halos and restricts the further growth of Si particles. The precipitation of α -Al phase results in an increasing Si content in the remaining liquid and eventually crystallizes as the coupled zone to form eutectic silicon [Lu and Hellawell 1995].

The effect of Ce and P additions on cooling curve parameters of the alloy at various solidifying conditions are shown in the Table 5.3. At untreated and unchilled condition, the primary silicon was found to nucleate at 622.8°C, with an undercooling of 13.5°C. The primary silicon nucleation temperature decreased with addition of Ce and P for all cooling conditions as shown in the Figure 5.15. Similarly, the minimum temperature also decreased due to the addition as shown in the Figure 5.16 (a and b). The magnitude of decrease in nucleation temperatures increased with cooling rate with copper chilled alloys showing the lowest temperatures. Among Ce treated alloys, due to the synergistic effect of copper chilling and 2% Ce addition the minimum nucleation temperature was decreased to 583.8 °C. A similar kind of decrease in nucleation temperature of primary silicon was reported by Kores et al. 2010. They studied the effect of Ce addition on cast iron mold solidified Al-17 % Si alloy and reported that, the primary silicon nucleation temperature decreased from 686°C to 591.9°C on 1% Ce addition to the melt. They reported that the decrease in primary silicon nucleation temperature with Ce addition was due to the adsorption of Ce atom to the interface of primary silicon.

The addition of P also resulted in the decrease in primary silicon nucleation temperature as of with Ce treatment, except with 0.05% P. At slow cooling conditions (SS chill and unchilled), the addition of 0.05 wt% P increased the primary silicon minimum nucleation temperature by 4°C. The copper chilled alloy showed a lowest primary silicon nucleation temperature of 581°C with an addition 0.4% P. The addition of P to hypereutectic Al-Si alloy is known to refine primary silicon by providing heterogeneous nucleation sites. The added phosphorus will react with Al to give a stable compound, 'AlP' with a melting point higher than 982°C. Both AlP and Si are cubic crystals with very similar lattice parameters (Si 5.42 Å, AlP 5.45 Å). Thus during solidification the primary silicon nucleates heterogeneously on the solid AlP particles at higher temperatures with a cube-cube orientation relationship and solidifies, promoting the refinement of primary silicon [Zhang Ying et al. 2007] [Zuo et al. 2009]

Table 5.3 Cooling curve analysis of Al-14% Si alloy

Chills	Ce/P wt-%	T _N (α) (°C)	T _{min} (α) (°C)	T _G (α) (°C)	Δ T _N (α) (°C)	T _N (Eut) (°C)	T _{min} (Eut) (°C)	T _G (Eut) (°C)	Δ T _N (Eut) (°C)	T _s (°C)
Unchilled	Untreated	618.8	611.3	613.7	13.5	580.4	573.2	574.8	7.2	543
	0.5Ce	620.4	607.3	603.6	13.1	578.5	572.6	574	5.9	534
	1Ce	610.2	602.3	600.9	7.9	577	572	573.6	5	528
	1.5Ce	609.3	599.9	597.2	9.4	575.5	571.6	571.2	3.9	528
	2Ce	617.3	606.7	605.2	10.6	575.7	571	572.6	4.7	530
	0.05P	650.7	649.3	648.2	1.4	576.6	575.8	577.1	0.8	545
	0.1P	616.9	609.5	608.2	7.4	576.4	573.9	575.9	2.5	524
	0.2P	615	608	604.2	7	575.5	573.5	577.1	2	520
	0.4P	617	610	608.2	7	574	572.5	577.4	1.5	519
Copper	Untreated	626.8	595	594.4	31.8	573.5	573	573.3	0.5	514
	0.5Ce	596.5	590	589	6.5	572.3	571.9	572.5	0.4	505
	1Ce	593	585.9	584	7.1	572.5	570.3	571	2.2	502
	1.5Ce	590	583.4	582	6.6	570.1	566.4	567.1	3.7	500
	2Ce	590.5	583.8	582.5	6.7	568	564.1	564.8	3.9	500
	0.05P	598.5	591	590	7.5	572.3	572	572.5	0.3	510
	0.1P	596	588	586.5	8	572	571	571.2	0.2	509
	0.2P	595	585	583	8.5	570.4	570	570.8	0.4	508
	0.4P	588.6	581	578.9	7.6	569.8	569	570	0.8	508
Brass	Untreated	625.8	598.1	597	27.7	573.4	572.8	573.3	0.6	522
	0.5Ce	594	590	589.1	4	573.3	571.7	571.7	1.6	515
	1Ce	595	587	586	8	573.3	569.3	570.5	4	514
	1.5Ce	592	585	583.5	7	573.4	567.8	569	5.6	510
	2Ce	593	586	584	7	572	565.6	566	6.4	508
	0.05P	598.3	590	589.4	8.3	573	571.2	572	1.8	520
	0.1P	595.2	587	586.4	8.2	572.8	571	572	1.8	518
	0.2P	593.9	586	585	7.9	572	570.3	571.5	1.7	518
	0.4P	590.1	584.8	584.1	5.3	572	570	571.2	2	517
Stainless steel	Untreated	624.2	608.5	607	15.7	575.7	574.6	575	1.1	526
	0.5Ce	606.1	598	602.1	8.1	573	572.2	573.2	0.8	518
	1Ce	600.5	592	591	8.5	573.1	568.3	569.5	4.8	515
	1.5Ce	593.5	587	585.8	6.5	573	567.3	568.9	5.7	513
	2Ce	595.2	589.2	588	6	571.2	566.2	567.5	5	507
	0.05P	616.4	612.5	605.3	3.9	574.5	574	574.5	0.5	524
	0.1P	608	600	599	8	574	572.5	573.2	1.5	522
	0.2P	603.2	596	593.4	7.2	575	573.2	574	1.8	520
	0.4P	602.5	594.1	591.9	8.4	575.4	573.4	574.2	2	520

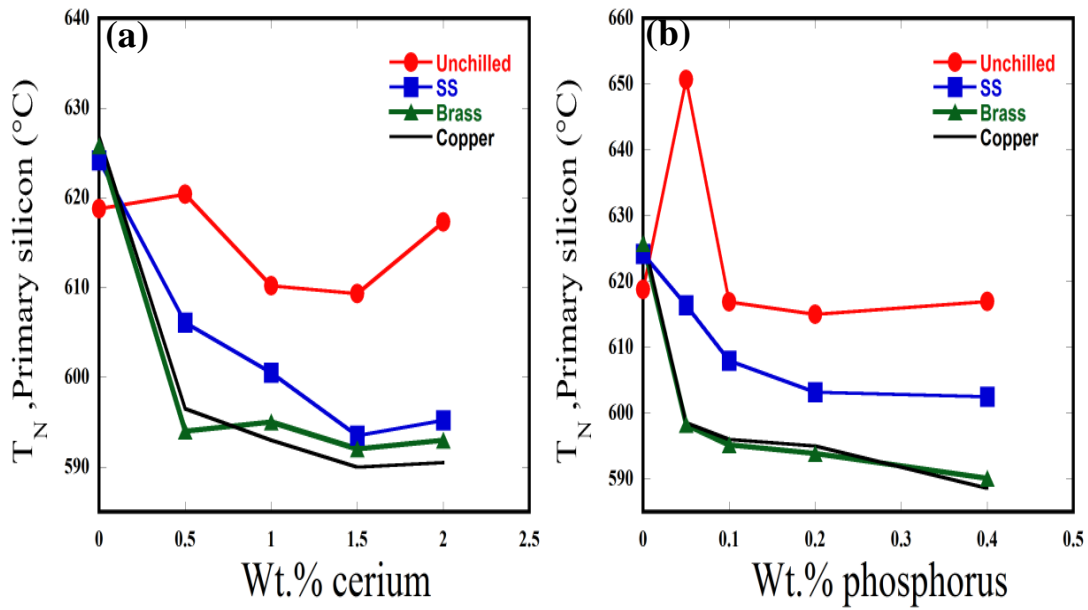


Figure 5.15 Variation of primary silicon nucleation temperature of Al-14Si with varying content of (a) Ce (b) P

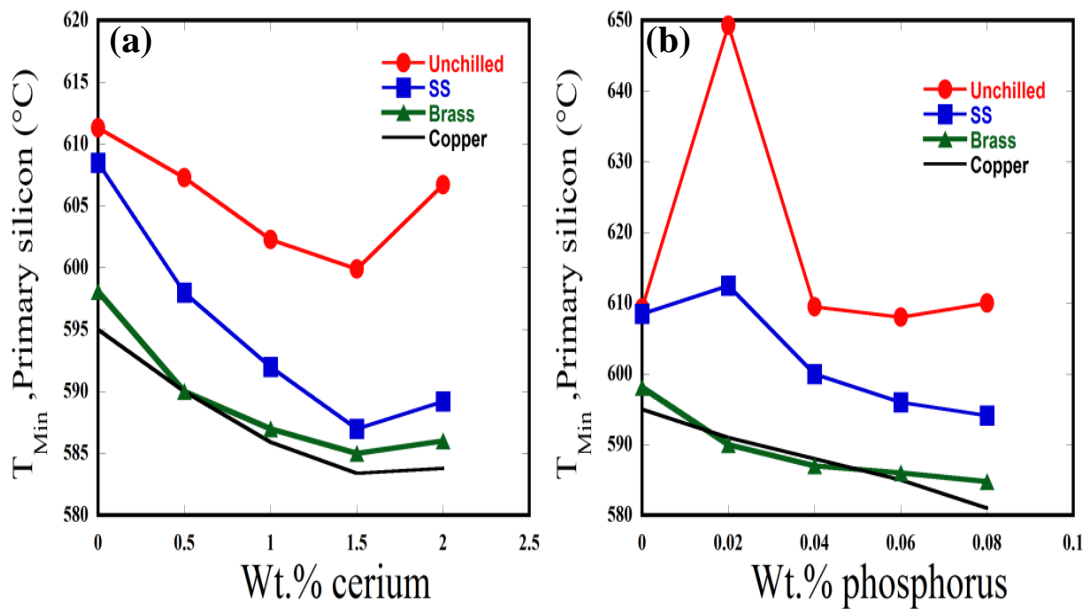


Figure 5.16 Variation of primary silicon minimum nucleation temperature of Al-14Si alloy with varying content of (a) Ce (b) P

In the present alloy, the addition of P did not show any increase in the primary silicon precipitation temperature except with 0.05wt. % P, and would be due to the addition of P above the optimum concentration for Al-14Si alloy. The present results are in good agreement with results of Colligan and Gunes (1973), they reported that the primary silicon crystallization temperature decreased with the addition of P. The reason for this would be in the limitation in the solubility of P in the alloy. Similarly, Nafisi et.al (2004) reported a 65°C decrease in primary silicon nucleation with the addition of P. In yet another study, Faraji et al. (2009) found that the primary silicon formation temperature decreased with the addition of P to Al-19Si alloy. The extent of decrease increased with the increase in cooling rate and is in good agreement with the results of the present study.

When AIP is added to the melt using a master alloy, the AIP dissociates into Al and P. Due to the potential difference in the P content of the melt, P dissolves into melt. This continues till the solubility limit of P in the melt is reached at that temperature. Later, during solidification, as the temperature decreases, the solubility of P decreases in Al-Si melt. The dissolution reaction is reversed by forming AIP from the precipitated P. The newly precipitated AIP is much smaller in size and will be distributed more evenly in the melt than the externally added P and satisfy the criteria for favorable nuclei. The precipitated AIP heterogeneously nucleates primary silicon with cube-cube orientation relationship. The pre-existing AIP particles form a random orientation relationship with the primary silicon [Lescuyer et al. 1998]. Thus, higher concentration of P would not influence the nucleation of primary silicon. Studies have shown that the optimum concentration of P for 390 alloys are between 0.1-0.2 wt% and for the present alloy it would be much lesser than that concentration [Zhang Ying et al. 2007].

Figure 5.17 (a and b) shows the effect of Ce and P additions on the primary silicon nucleation undercooling. The degree of undercooling decreased with additions

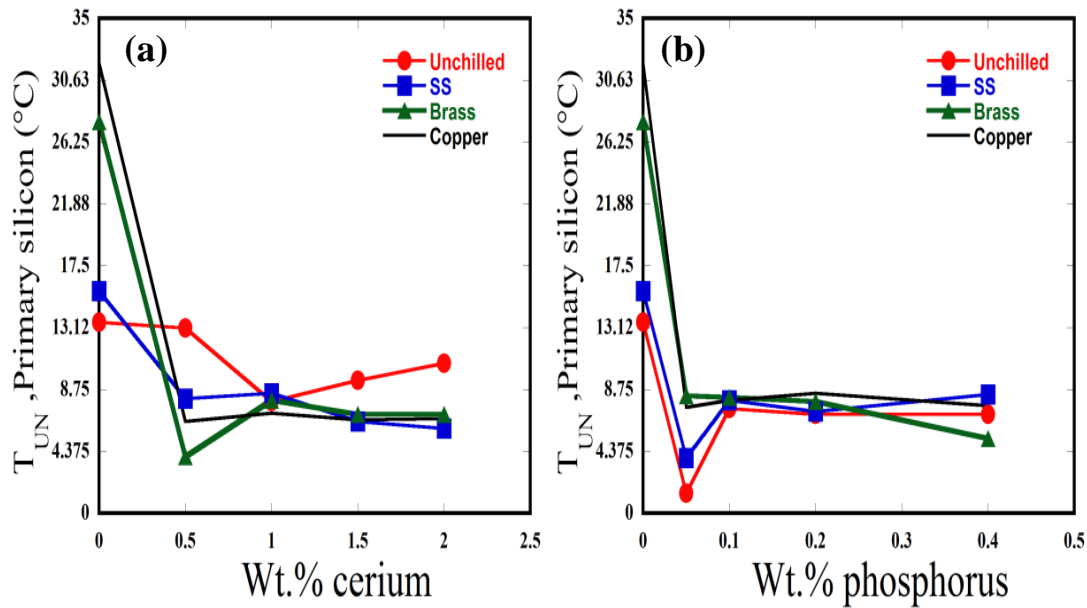


Figure 5.17 Variation of primary silicon undercooling of Al-14Si alloy with the addition of varying content (a) Ce (b) Sr

irrespective of the cooling condition. In both conditions (chilling and unchilled) the undercooling was about $8 \pm 1^\circ\text{C}$ for all additions. In the absence of any additions, the undercooling for the nucleation primary silicon increased with the increase in cooling rate, indicating the difficulty in the agglomeration of silicon clusters to form silicon crystals. The addition of P and formation of AlP decreases the energy barrier for the formation of primary silicon by providing heterogeneous nucleation sites and decreases the undercooling required for the nucleation. Similar kind of decrease in undercooling with P was reported in literature. Terai (1958) reported that the addition of P decreased the undercooling by increasing the primary silicon formation temperature. Yet in another study, Kyffin et al. (2001) found that the 50 K undercooling of primary silicon in Al-20%Si alloy was nullified by the addition of 100 ppm P.

The presence of Ce in the melt affects differently to decrease the primary silicon undercooling temperature. There is no reported literature on Ce forming any heterogeneous nucleation sites for primary silicon. Chang et al. (1998) investigated

the presence of Ce in and around primary silicon crystals and found that a maximum concentration of Ce was in the matrix between the silicon crystals rather than inside the crystals. A similar kind of presence of Ce atoms around primary silicon crystals were detected and reported by Kores et al. (2010). Hence it was presumed that the primary silicon was not nucleated on Ce or Ce containing phases.

The effect of Ce and P melt treatment on the eutectic phase formation temperatures are given in Table 5.3. Figure 5.18 shows the variation of eutectic nucleation temperature with additions of Ce and P at varying cooling conditions. Similarly, Figure 5.19 shows the effect of melt treatment on the minimum nucleation temperature. The nucleation of eutectic in the untreated and unchilled alloy occurred at 580.4°C and the minimum nucleation temperature and growth temperatures were 573.2 and 574.8°C respectively. The eutectic nucleation temperature of untreated alloy increased with chilling and with thermal conductivity of the chill.

The melt treatment had significant effect on the eutectic nucleation temperatures. The effect was more significant with minimum nucleation temperature. While both the additions decreased the eutectic formation temperatures, the decrease was more significant with Ce additions. However, the decrease was marginal for unchilled alloys. For example, T_{\min} decreased from 575.0 °C to 573.5 °C on addition of 2 wt.% Ce and the T_{\min} decreased to 564.2°C on addition of 2% Ce to copper chilled alloy. The P treatment had marginal effect on the eutectic silicon nucleation temperatures and it decreased with chilling. In hypereutectic alloys, the nucleation and growth of eutectic phase depends on the morphology of primary silicon. Since, the crystallization of primary silicon occurs prior to the precipitation of the eutectic silicon, it acts as a heterogeneous nucleation sites for the eutectic silicon depending on the condition. In P refined alloys, a large number of primary silicon are nucleated at higher temperatures from less undercooled melt and crystallizes as regular polyhedral crystals. The eutectic silicon, which solidifies at the later stages are nucleated on the refined primary silicon at higher temperatures and solidifies as faceted silicon [Wu et al. 2010]. The nucleation of eutectic silicon in untreated alloy does not occur on primary silicon, the difficulty in the nucleation results in high undercooling as shown

in the Figure 5.20. The P refined primary silicon offers very less energy barrier for the nucleation of eutectic silicon, hence, it is nucleated with low or no undercooling as shown in the Figure 5.20 (b). Unlike P treatment, the addition of Ce does not favor the nucleation of eutectic silicon. As a result, the eutectic silicon is forced to nucleate at lower temperature from highly undercooled melt. The increase in eutectic undercooling is similar to that observed with Sr modification [Liao et al. (2010)] The high undercooling was due to the poisoning effect of Sr on AlP, a heterogeneous nucleant of primary silicon, which in turn increased the energy required for the nucleation of eutectic.

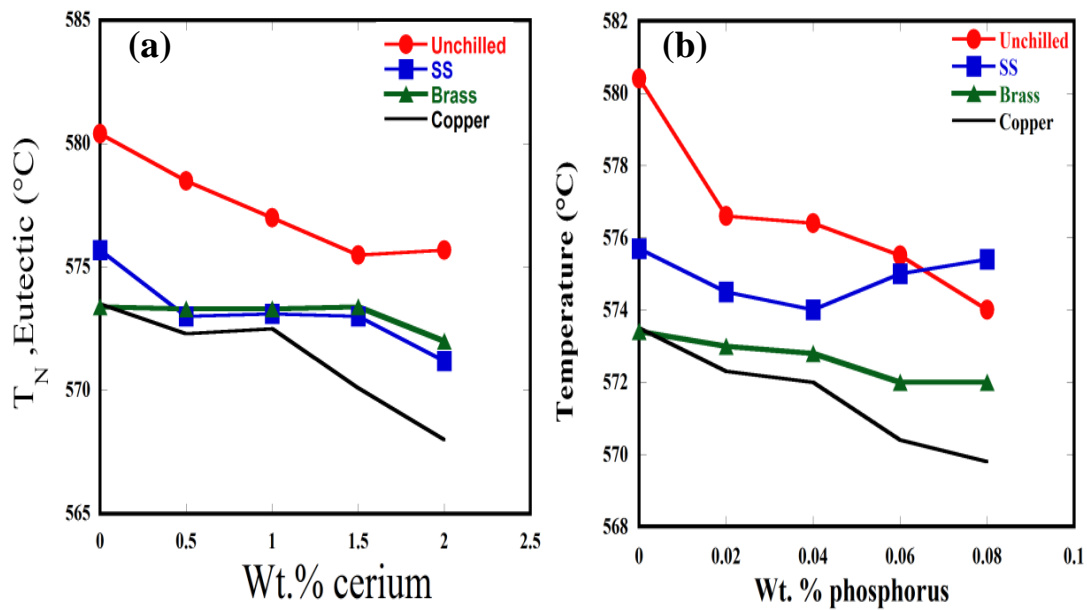


Figure 5.18 Variation of eutectic silicon nucleation temperature in Al-14Si alloy with varying content of (a) Ce (b) P

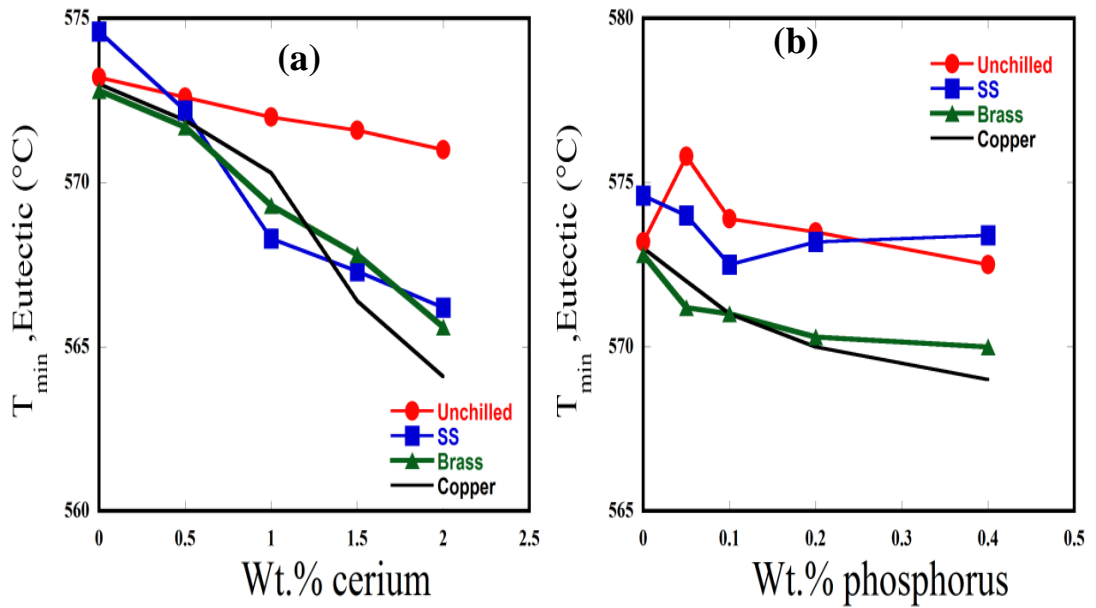


Figure 5.19 Variation of eutectic minimum nucleation temperature in Al-14Si alloy with varying content of (a) Ce (b) P

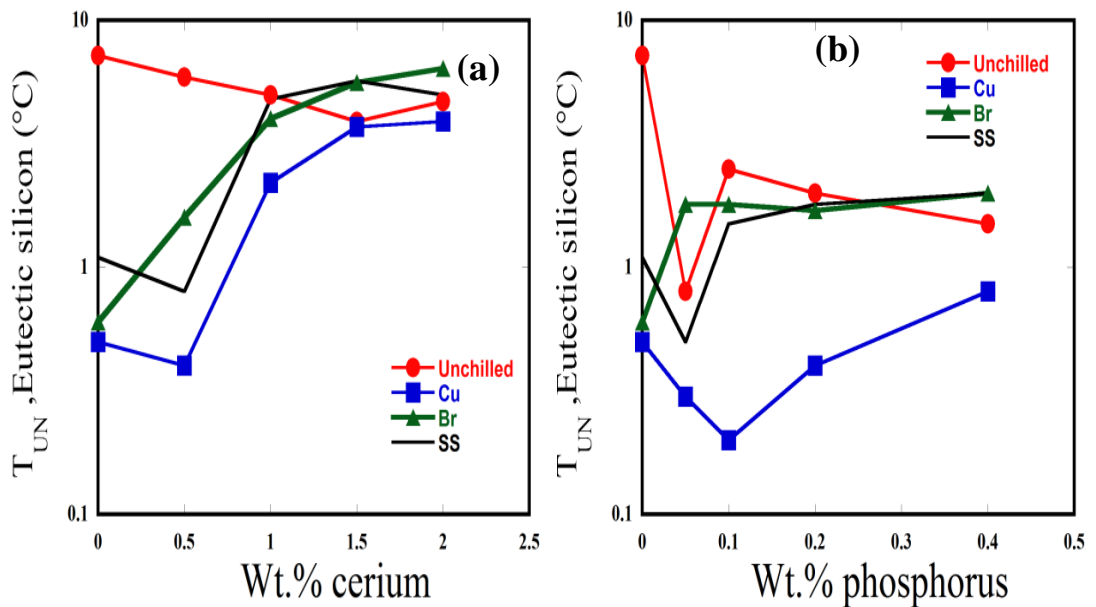


Figure 5.20 Variation of eutectic undercooling of Al-14Si alloy with varying content (a) Ce (b) P

Figure 5.21 shows the effect of cooling rate and melt treatment on the eutectic temperature difference (ΔT_G). The melt treatment had varying effect on the cooling rate and ΔT_G and the ΔT_G increased significantly with Ce melt treatment and decreased with P treatment. The addition of high concentration of P at higher cooling rates resulted in marginal increase in ΔT_G . The reason for this is the nucleation well faceted primary silicon and associated nucleation of eutectic silicon from the primary silicon. The addition of P favors the nucleation of primary silicon and it acts as nucleation sites for eutectic silicon to nucleate eutectic silicon at higher temperature. The Ce melt treatment hinders the nucleation of primary silicon and the nucleation of eutectic silicon and forces the eutectic silicon to nucleate at lower temperature from highly undercooled melt leading to the modification of eutectic silicon.

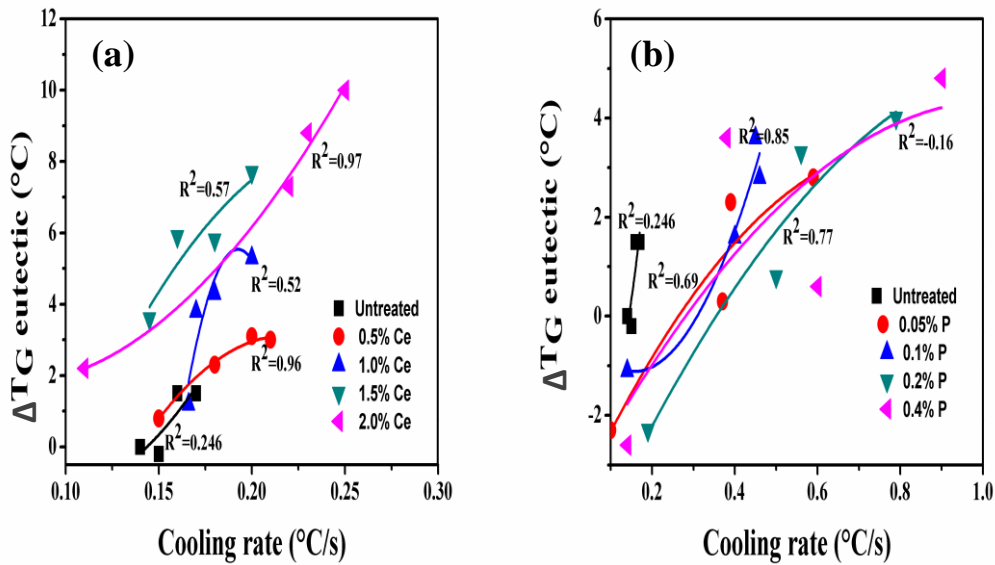


Figure 5.21 Eutectic growth temperature differences with cooling rate for varying content of (a) Ce (b) P

5.1.4 Al-22Si alloys

The nucleation temperatures of Al-22Si alloy before and after the addition of varying content of Ce and P are given in the Table 5.4. Figure 5.22 shows the effect of additions on the primary silicon nucleation temperature. Under slow solidifying condition, the primary silicon in untreated alloy was nucleated at 661.2°C and the nucleation temperature decreased with increase in the cooling rate. It was reported that in hypereutectic Al-Si alloys, the primary silicon nucleates on the Si clusters formed at higher temperatures [Robles Hernández and Sokolowski 2006]. At low cooling rate, the silicon clusters spontaneously arrange themselves into a tetrahedron cluster and agglomerates into five- fold twinning polyhedral. At higher temperatures it acts as a stable nucleant for primary silicon with low energy barrier for faceted growth of fivefold silicon crystals [Lijia et al. 2010]. Hence higher cooling rates suppress the agglomeration of Si clusters and formation of former stable nucleation sites. The primary silicon will be nucleated on the high energy sites as fine Si clusters from highly undercooled melt.

Ce and P melt treatment had varying effect on the primary silicon nucleation temperatures. Under slow solidifying condition, the addition of Ce decreases the primary silicon nucleation temperature, whereas, it increased with addition of P. At higher cooling conditions (chilled), both the melt treatment had similar effect on the nucleation temperatures. The primary silicon nucleation temperatures increased with the addition of Ce as well as with P. Among all, addition of 0.1wt.% P to brass chilled alloy resulted in a peak nucleation temperature of 750.7 °C.

The additions also had similar effect on the minimum formation temperature (T_{\min}) as shown in the Figure 5.23. A constant increase in formation temperatures was observed with addition of P for all cooling condition. The reason for this was the formation of AlP, which provides a stable and low energy nucleation sites for primary silicon. As a result, the primary silicon was nucleated at higher temperatures. Based on results, the minimum concentration of P required to attain peak formation temperature was in the range of 0.05-0.1wt.% P.

Table 5.4 Cooling curve analysis of Al-22% Si alloy

	Ce/P wt-%	Primary Silicon				Eutectic Silicon				T_s (°C)
		T_N (α) (°C)	T_{min} (α) (°C)	T_G (α) (°C)	ΔT_N (α) (°C)	T_N (Eut) (°C)	T_{min} (Eut) (°C)	T_G (Eut) (°C)	ΔT_N (Eut) (°C)	
Unchilled	Untreated	661.2	657.7	663.7	3.5	571.6	566.1	566.9	5.5	530
	0.5Ce	653.7	647.8	648.7	5.9	574	560.2	560.5	13.8	520
	1Ce	651.3	645.6	646.9	5.7	573.8	559.7	560.9	14.1	513
	1.5Ce	642.6	641.9	642.5	0.7	571.3	559.9	560.8	11.4	506
	2Ce	640.5	640	641.2	0.5	573.9	562.5	562.6	11.4	503
	0.05P	660.4	657.3	653.6	3.1	564	557.5	558.2	6.5	521
	0.1P	669.4	667.1	666.5	2.3	560.2	555.6	555.7	4.6	516
	0.2P	669.2	666.8	666.1	2.4	564.1	560.2	561	3.9	518
	0.4P	668.8	667	666	1.8	564	560	561.2	4	518
Copper	Untreated	656	647.8	647	8.2	566	558	557.9	3	520
	0.5Ce	671	669.1	664.7	1.9	570.8	568.3	565.9	2.5	508
	1Ce	687.2	685.5	680	1.7	576	572.1	571.4	3.9	510
	1.5Ce	729.5	727.8	725	1.7	578	575.1	574.8	2.9	512
	2Ce	698.9	697	696.5	1.9	574.7	572.1	578.6	2.6	513
	0.05P	702	698.6	698	3.4	568.1	567.8	567.1	0.3	515
	0.1P	672.2	669.1	668.1	3.1	568.2	566.8	566	1.4	508
	0.2P	667.9	665.3	664.4	2.6	568.6	566.5	566	2.1	504
	0.4P	662	660	659	2	568.1	566.2	564.1	1.9	500
Bras	Untreated	658.3	654	654	4.3	566	559	558.2	3.5	522
	0.5Ce	675	674.7	674	0.3	562.3	561.9	561.3	0.4	523
	1Ce	684.7	684.4	683.5	0.3	565.7	565.3	564.1	0.4	525
	1.5Ce	730.5	730.2	729.5	0.3	573.1	572.1	571.4	1	527
	2Ce	681.8	679	678.5	2.8	573.5	571.2	571	2.3	526
	0.05P	691.5	690.9	690.2	0.6	568.9	568.1	569.3	0.8	530
	0.1P	750.7	750.3	749.6	0.4	570.3	569.5	569.2	0.8	535
	0.2P	700	698.5	698.4	1.5	570.9	568.3	568	2.6	531
	0.4P	696.5	695	694	1.5	571	569	568.2	2	530
Stainless steel	Untreated	659.7	656	657.3	3.7	566	562	550.3	4	525
	0.5Ce	660	658	657	2	566.8	564.2	564	2.6	526
	1Ce	665.7	664	663.5	1.7	570.5	567.5	568.5	3	527
	1.5Ce	730	728	727.7	2	571.2	569.1	568.5	2.1	529
	2Ce	680	675	674	5	570.2	567.3	567.1	2.9	527
	0.05P	700.8	700	700.3	0.8	570.2	569.5	569	0.7	530
	0.1P	716.5	716	683.2	0.5	571.8	569.5	568.2	2.3	532
	0.2P	701	699.7	698.1	1.3	568.7	566.4	566.5	2.3	530
	0.4P	697.2	696.5	696	0.7	568	566	565	2	527

Unlike P, the addition of Ce had varying effect on the primary silicon formation temperatures depending on the cooling rate. This was due to the formation of different Ce bearing compounds. At slow solidifying condition, the Ce spontaneously forms a compound which suppresses the nucleation of primary silicon. Similar to the effect of Sr in the Al-Si alloy, which suppress the silicon nucleation and growth [Tenekedjiev et al. 1989]. At high cooling rate, the Ce atoms aided the nucleation of primary silicon by decreasing the energy for nucleation of primary silicon. Figure 5.24 shows the variation of undercooling with the melt treatment of Ce and P. The increase in undercooling with cooling rate indicates the difficulty in the nucleation of primary silicon.

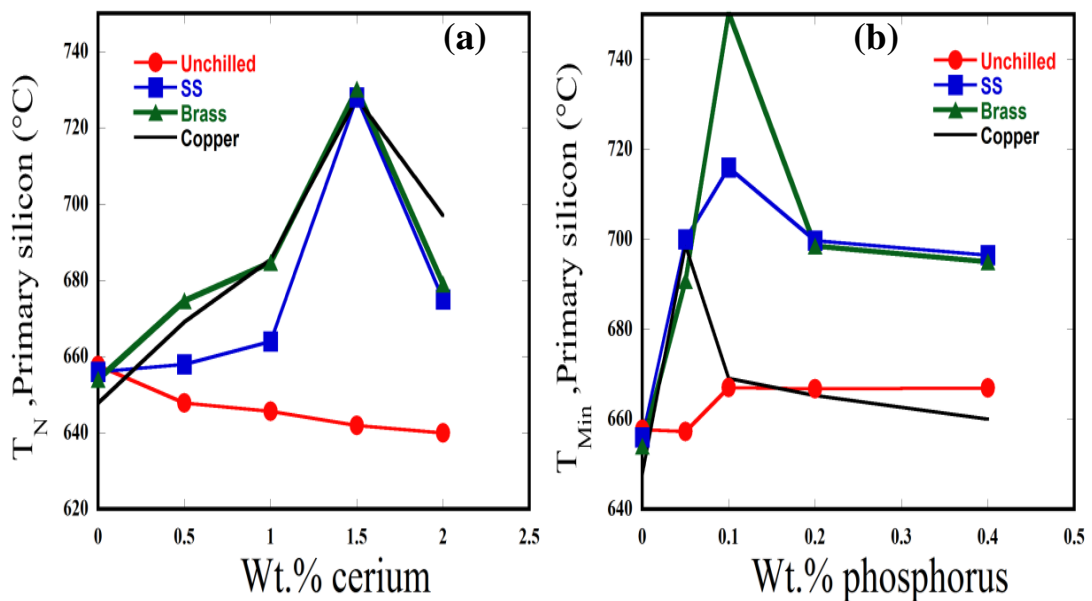


Figure 5.22 Variation of primary silicon nucleation temperature in Al-22Si alloy with varying content of (a) Ce (b) P

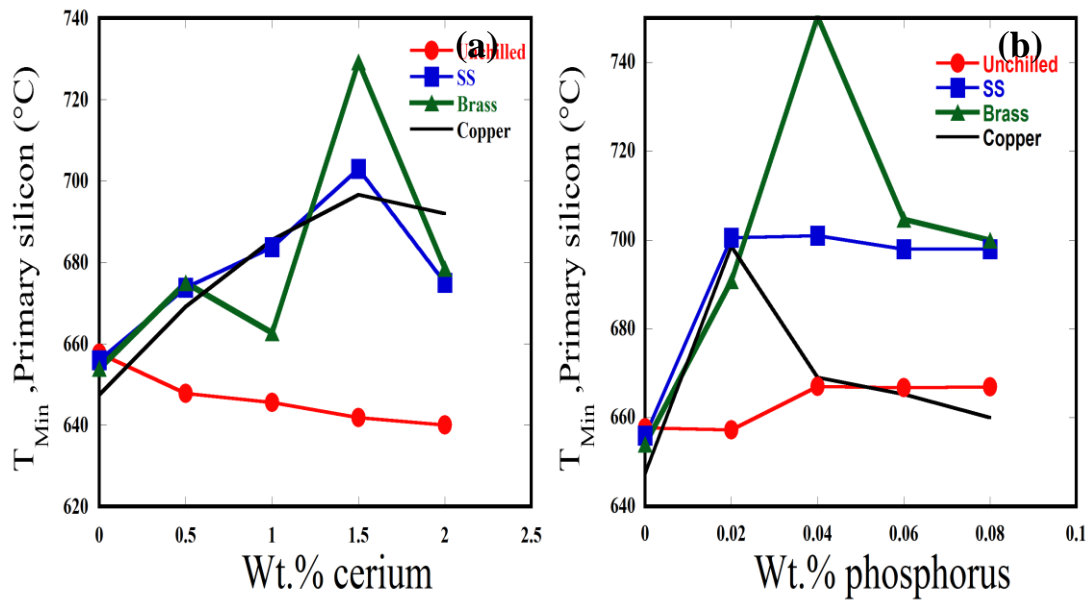


Figure 5.23 Variation of primary silicon minimum nucleation temperature in Al-22Si alloy with varying content of (a) Ce (b) P

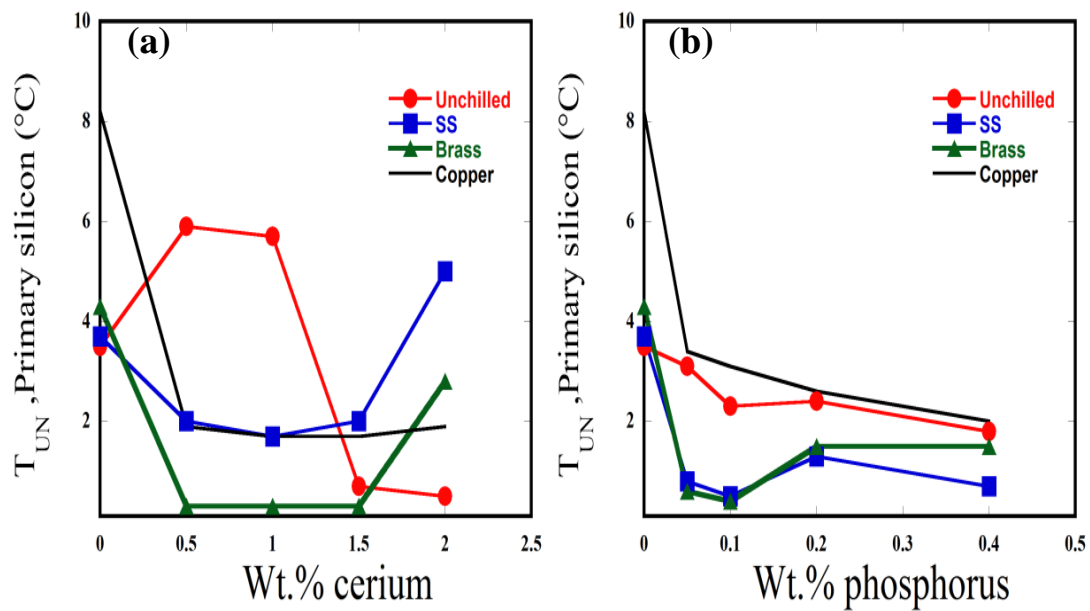


Figure 5.24 Variation of primary silicon undercooling of Al-22Si alloy with the addition of varying content (a) Ce (b) P

At slow cooling rates, the Si clusters get enough time to agglomerate into five- fold heterogeneous nucleation agent and primary silicon nucleate at these sites with very low undercooling. The increase in cooling rate hinders the growth of Si clusters and restricts the formation of five-fold nucleation sites. The primary silicon will be forced to nucleate at high undercooling and the decrease in undercooling with the addition of P is due to the formation of AIP, a favorable low energy nucleation site for silicon. The addition of Ce at low cooling rates will increase the primary silicon nucleation undercooling and poisons the primary silicon nucleants by adsorbing on to the growth sites of primary silicon [Kores et al. 2010]. The addition of Ce at high cooling rates decreased the undercooling required for nucleation of primary silicon.

Unlike the eutectic silicon in hypoeutectic alloys, the eutectic silicon in hypereutectic silicon is nucleated on the primary silicon. Hence, the energy barrier for the nucleation of eutectic is dependent on the nucleation of primary silicon. The variation of eutectic silicon thermal analysis parameters with Ce and P for various solidification conditions are given in Table 5.4. Figure 5.25 shows the effect of Ce and P melt treatment on the eutectic silicon nucleation temperature. The eutectic phase of the base alloy was found to nucleate at 571.6°C with a T_{\min} of 566°C. The nucleation temperatures were found to decrease with the increase in cooling rate. The increase in undercooling with cooling rate indicates the suppression in the nucleation of eutectic silicon. Under unchilled condition, the nucleation temperature was found to decrease with both kinds of addition, whereas, on chilling, the eutectic phase was precipitated at higher temperature on addition of Ce and P. Similar kind of trend was observed for T_{\min} as shown in the Figure 5.26.

Figure 5.27 (a and b) shows the effect of varying content of additions of Ce and P on the eutectic undercooling. Even though, the additions decreased the eutectic formation temperatures of unchilled alloys, the undercooling required for the nucleation of eutectic was decreased. This indicates that the eutectic silicon was heterogeneously nucleated by the addition. Wu et al. (2010) were of opinion that there is a certain relationship between the nucleation of primary silicon and eutectic silicon in hypereutectic alloys. They reported that the nucleation frequency of eutectic Si in P

treated alloy was higher than the untreated alloy. It was inferred that the refined primary silicon provided well-proportioned nucleation sites. The mechanism holds good in the present alloy as well. The addition of P forms AlP to nucleate large number of primary silicon at higher temperatures from less undercooled melt and grows as faceted primary silicon. During eutectic solidification, the eutectic silicon nucleates on the refined primary silicon at low undercooling. The primary silicon in the Ce added alloys do not nucleate the eutectic silicon. The decrease in nucleation temperature along with increased undercooling indicates that the addition of Ce suppressed the nucleation of eutectic Si.

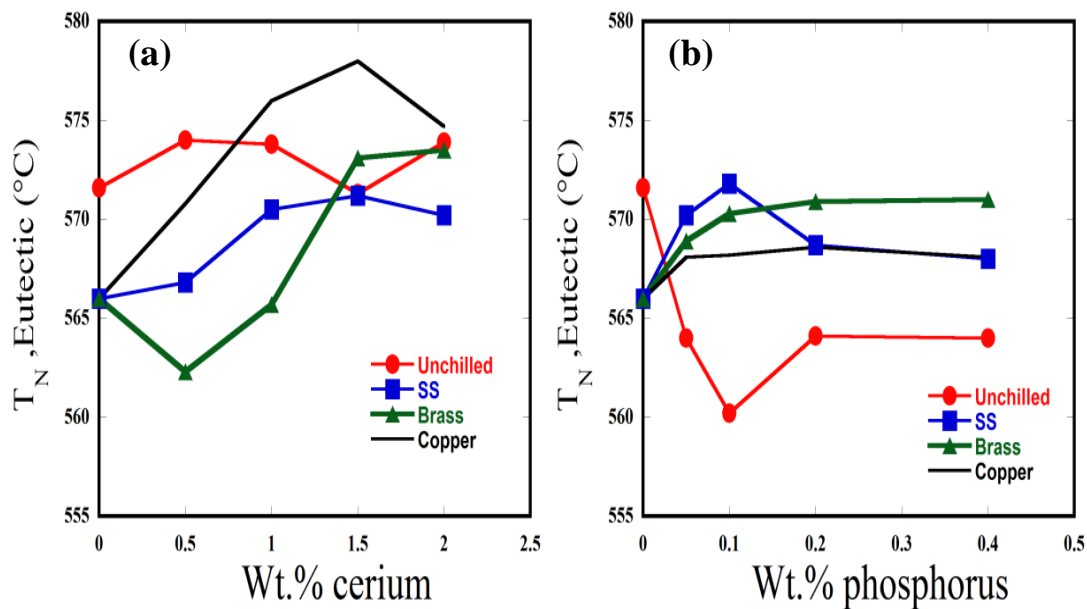


Figure 5.25 Variation of eutectic nucleation temperature in Al-22Si alloy with varying content of (a) Ce (b) P

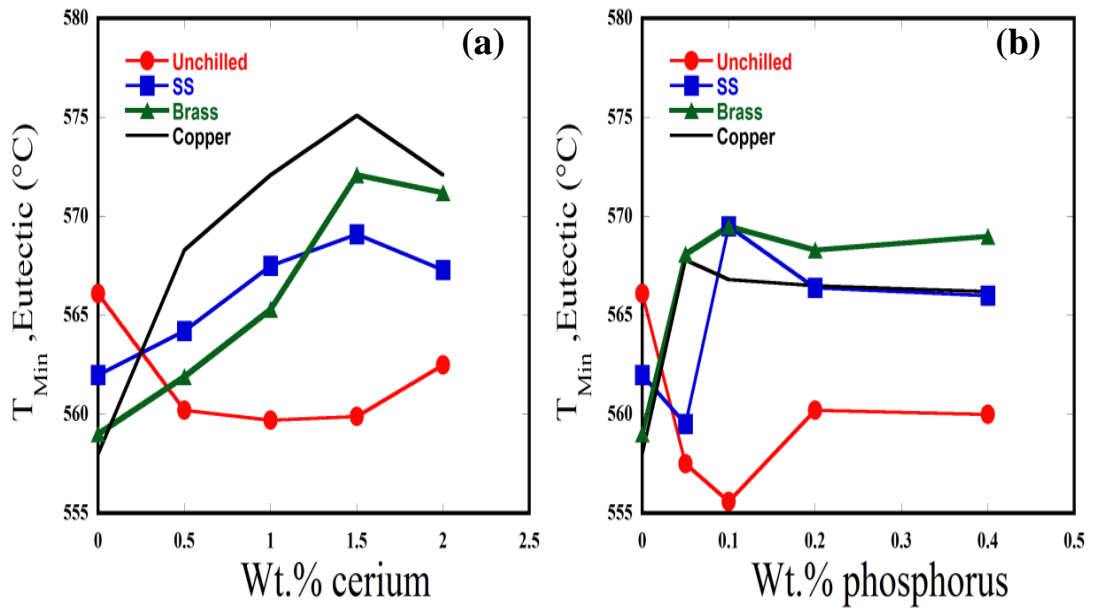


Figure 5.26 Variation of eutectic minimum nucleation temperature in Al-22Si alloy with varying content of (a) Ce (b) P

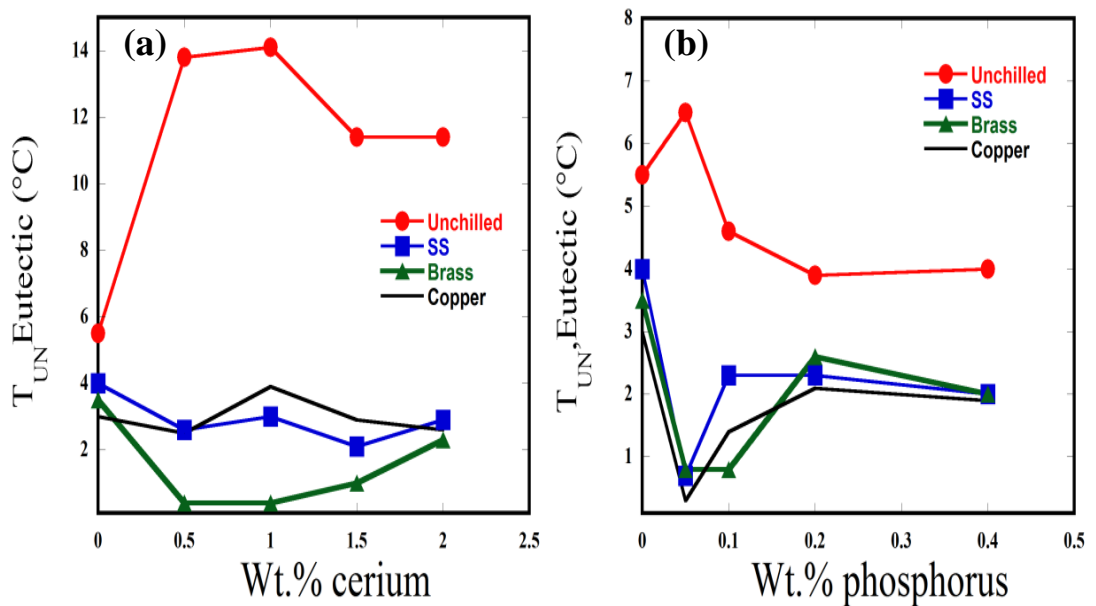


Figure 5.27 Variation of eutectic undercooling in Al-22Si alloy with varying content of (a) Ce (b) P

The increase in eutectic nucleation temperature and decrease in undercooling with increase in cooling rate indicates that the melt treatment favored the nucleation of eutectic silicon at high cooling rates. The eutectic Si nucleated on the refined primary silicon at higher temperatures with low undercooling will grow with acicular structure.

Figure 5.28 shows the effect of cooling rate and melt treatment on the ΔT_G values. Both kinds of melt treatment have similar effect on the ΔT_G . The ΔT_G decreased with increase in cooling rate and concentration of additions. The reason for this is the growth of eutectic silicon from the faceted primary silicon. The refinement of primary silicon by the addition of Ce and P led to the nucleation of eutectic silicon at higher temperature. The low undercooling values suggest that the additions favored the nucleation of eutectic silicon to decrease the ΔT_G and eutectic silicon modification.

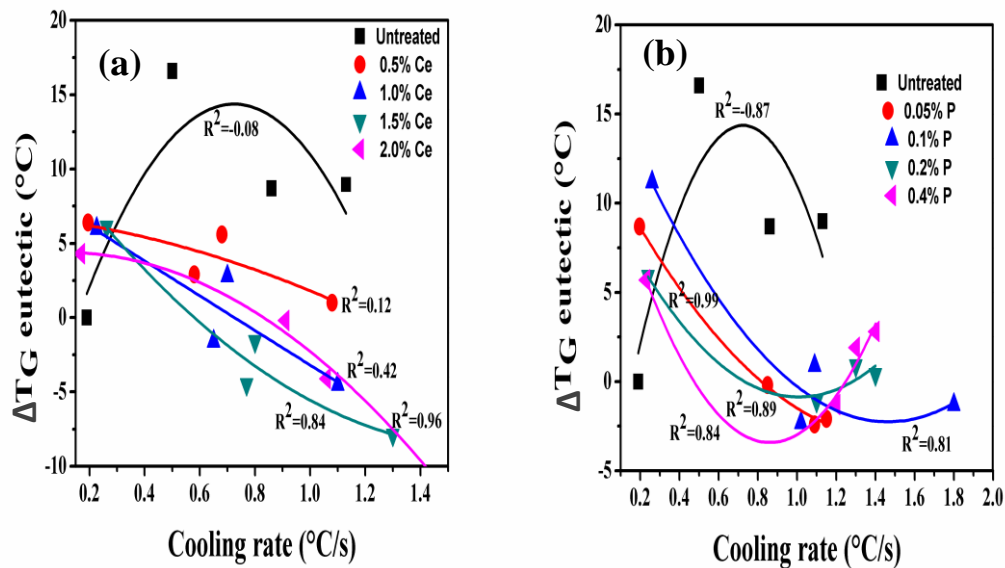


Figure 5.28 Eutectic growth temperature differences versus cooling rate for varying content of (a) Ce (b) P

5.2 Newtonian and Fourier Analyses for the Assessment of Latent Heat and Solid Fraction

Computer aided cooling curve analysis is an online prediction tool that can be used effectively to determine wide range of thermo-metallurgical information related to metals or alloys. The process involves measuring the temperature history of the sample with respect to time and determining the thermal characteristics, fraction solid and latent heat during melting or solidification. One of the key requirements in the determination of thermal analysis parameters is finding out the amount of heat liberated during metallurgical transformations. This is commonly done by fitting a data base line (DBL) to the first derivative curve (FDC) and then finding out the area between the curves. In other words, the DBL would be the path taken by the first derivative curve of the metal or alloy in the absence of any metallurgical reactions. There are two known techniques namely, Newtonian and Fourier analysis, using which a DBL is calculated and fitted to the derivative curve [Robles Hernández and Sokolowski 2006], [Marchwica et al. 2011] [Djurdjevic et al. 2012]

Theory

Newtonian analysis is based on the lumped heat capacitance method which assumes a negligible thermal gradient across the sample ($Bi < 0.1$). The heat transfer coefficient from the sample to the surrounding by convection, conduction and radiation can be a function of single unique temperature. The Newtonian analysis for solidification of an alloy is mathematically expressed as

$$\frac{dQ}{dt} - mC_P \frac{dT}{dt} = UA (T - T_0) \quad \text{Eq.1}$$

where, Q is the latent heat of solidification, C_P is the specific heat of the metal/alloy, T is the metal/alloy temperature, U is the overall heat transfer coefficient, A is the sample surface area and T_0 is the ambient temperature. In the absence of any metallurgical reaction ($\frac{dQ}{dt} = 0$) and equation 1 can be rewritten as

$$\frac{dT}{dt} = \frac{UA(T-T_o)}{mC_p} = \text{DBL} \quad \text{Eq.2}$$

Equation 2 corresponds to the data base line (DBL) for the Newtonian analysis. The DBL for Newtonian analysis is found out by fitting an appropriate polynomial of order greater than 2 to the portion of first derivative curve (FDC), corresponding to the mushy region ($T_{\text{liq}} < T < T_{\text{sol}}$). The area between the curves is calculated by subtracting DBL from first derivative curve. The total latent heat is calculated is determined in the form:

$$L = C_p \int_{t_s}^{t_e} (FDC - DBL) \quad \text{Eq.3}$$

where t_s and t_e are the times for start and end of solidification and the fraction solid between the duration can be obtained by finding out the cumulative area as the fraction of total area between the curves.

Fourier analysis assumes that heat transfer takes place by conduction only and considers the effect of thermal gradient during solidification. The analysis uses the temperature gradient across the sample to determine the base line. The Fourier equation with heat source can be written as:

$$\frac{\partial T}{\partial t} = \alpha \nabla^2 T + \frac{1}{C_p} \frac{\partial Q}{\partial t} \quad \text{Eq.4}$$

where, α is the thermal diffusivity, C_p is the specific heat and Q is the latent heat of solidification. The equation 4 is rearranged as

$$\frac{\partial Q}{\partial t} = C_p \left(\frac{\partial T}{\partial t} - \alpha \nabla^2 T \right); \text{ where, } \alpha \nabla^2 T = \text{DBL (Fourier)} \quad \text{Eq.5}$$

Considering a cylindrical mould with known temperature at radii R_1 and R_2 along the test sample, the temperature distribution $\nabla^2 T$ is calculated as:

$$\nabla^2 T = 4(T_2 - T_1) / (R_2^2 - R_1^2) \quad \text{Eq.6}$$

where, T_1 and T_2 are temperatures at radii R_1 and R_2 respectively. The thermal diffusivity in single phase regions is calculated by determining the diffusivity before and after solidification from the experiment data as

$$\alpha = \frac{\frac{\partial T}{\partial t}}{\nabla^2 T} \quad \text{Eq.7}$$

The thermal diffusivity in the two phase region during solidification is calculated as the function of time using the equation

$$\alpha(t) = \alpha_{\text{Liq}}[1 - f_s(t)] + \alpha_{\text{sol}} f_s(t) \quad \text{Eq.8}$$

The fraction solid is determined as

$$f_s = t - t_s / (t_e - t_s) \quad \text{Eq.9}$$

where, t_s and t_e are the time of start and end of solidification respectively.

The latent heat evolved is calculated from the equation

$$L = \int_{t_s}^{t_e} \frac{\partial Q}{\partial t} \quad \text{Eq.10}$$

The recorded thermal analyses data was used to plot cooling and first derivative curves of the alloy. For accurate identification of inflection points and base line calculation, the first derivative curve was smoothed before plotting.

5.2.1 Al-8Si alloys

Fitting DBL

The DBL is of immense importance for the calculation of latent heat and fraction solid using computer aided cooling curve analysis. In Newtonian analysis the linear fitting of DBL to the first derivative curve is done. In this technique a few data points, before and after solidification are used to fit a linear curve. Figure 5.29 (a) shows the first derivative curve merged with the linear curve, which form a DBL to the first derivative curve. Fourier analysis technique uses temperature gradient across the sample for base line determination. The difference in temperature between center (T_c) and near wall (T_w) was used for calculation of the base line. The thermal diffusivity of the alloy at the single phase region was calculated using equation 7. The thermal diffusivity in the two phase region was calculated using equation 8. The DBL (Fourier) is calculated using equations 5 to 9 and is fitted to the derivative curve as shown in the Figure 5.29 (b)

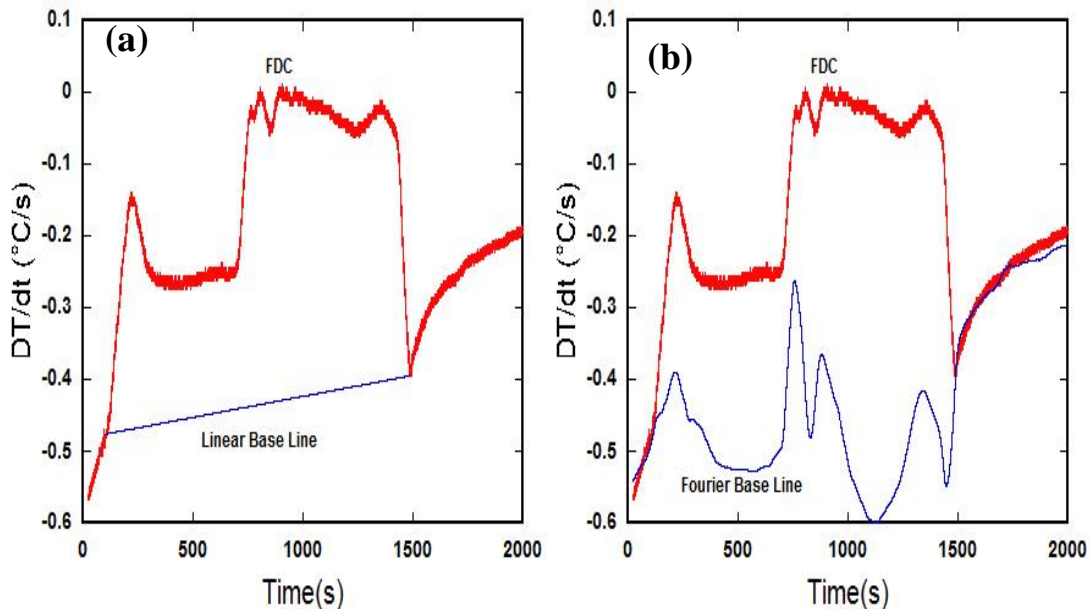


Figure 5.29 First derivative curve fitted with (a) linear data base line (b) Fourier base line

Calculation of fraction solid

The fraction solid in both the techniques was calculated by finding out the net area between the FDC and DBL curves. The fraction solid is expressed as

$$f_s = \frac{\int_{T_s}^T (\text{FDC} - \text{DBL})}{\int_{T_s}^{T_s} (\text{FDC} - \text{DBL})} \quad \text{Eq.11}$$

Calculation of latent heat

Both the techniques use Eq. 3 to calculate latent heat of the alloy. An average C_P value of 1.3 J/g-K was used for calculation. A comparison of solidified volume fractions predicted by Newtonian and Fourier methods with JMatPro result is shown in Figure 5.30. The figure shows a significant difference in fraction solid calculated in the temperature range between liquidus and eutectic point, below which the curves almost follows the same path.

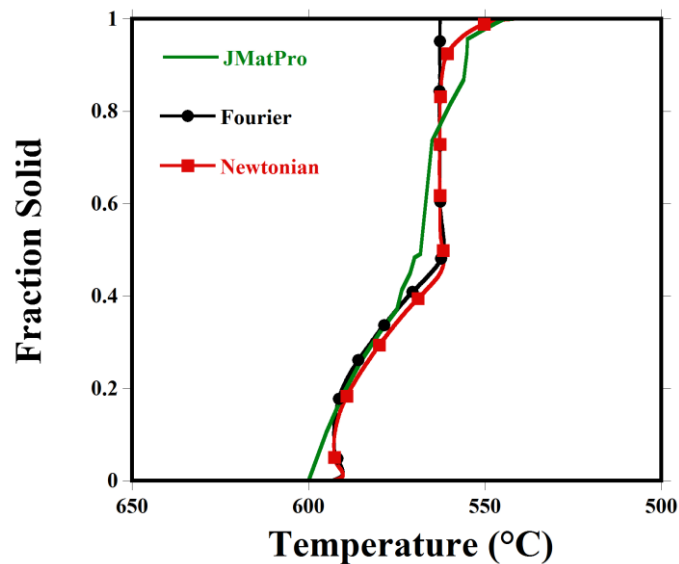


Figure 5.30 Comparison of fraction solid calculated using Newtonian and Fourier analysis for Al-8Si alloy

The accuracy of the fraction solid curves depends on the fitting of an appropriate DBL to the first derivative curve in Newtonian method and in finding out the accurate temperature difference profile across the solidifying sample in Fourier analysis. The calculated values of latent heat are compared with JMatPro results and are shown in Table 5.5. The results indicate that the latent heat calculated using the Fourier technique is more close to the result obtained from the JMatPro. This is due to the fact that the Fourier analysis fitted DBL was based on the actual temperature gradient across the sample measured using two thermocouples.

Table 5.5 Comparison of latent heat calculated using different methods

Alloy	Latent heat (J/g)		
	Newtonian	Fourier	JMatPro
Al-8Si	373	408	443

The fraction solid calculated using Fourier analysis can be reused in Eq. 8 to estimate the temperature dependent diffusivity and specific heat of the solidifying sample. The earlier equation used linearly increasing fraction solid values to compute the diffusivity. Figure 5.31 shows the computed diffusivity and the specific heat (C_p) with respect to temperature for Al-8Si alloy. The specific heat is calculated using the equation

$$C_p = \frac{k}{\rho\alpha} \quad \text{Eq.12}$$

where, k is the thermal conductivity, ρ is the density and α is the thermal diffusivity of the alloy. The k and ρ values used were calculated using JMatPro simulation software as a function of temperature. The specific heat for the alloy increased with temperature. The computed specific heat is used to estimate the enthalpy change as a function of fraction solid formed and is shown in Figure 5.32.

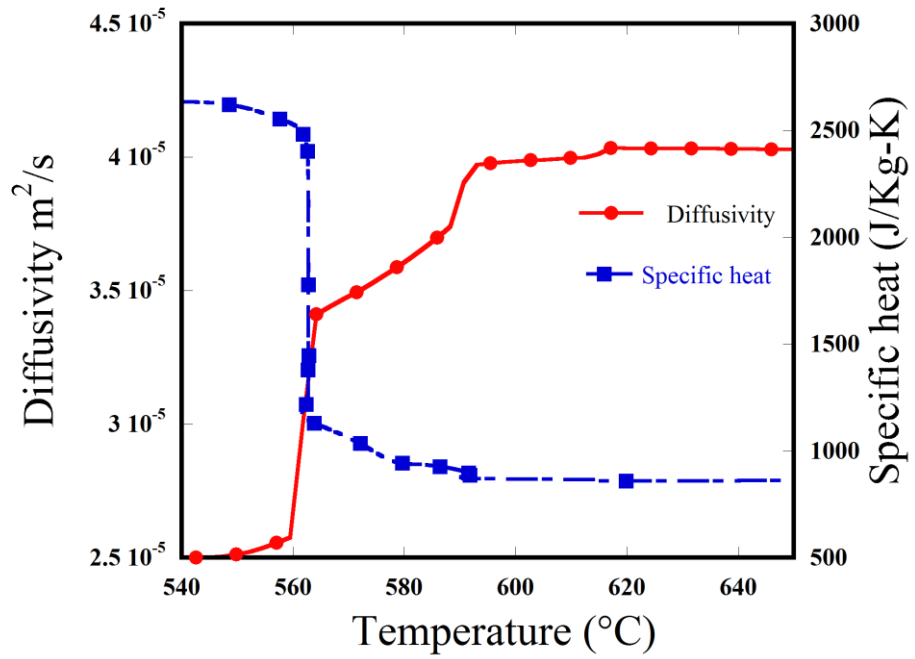


Figure 5.31 Diffusivity and specific heat of the alloy as a function of temperature

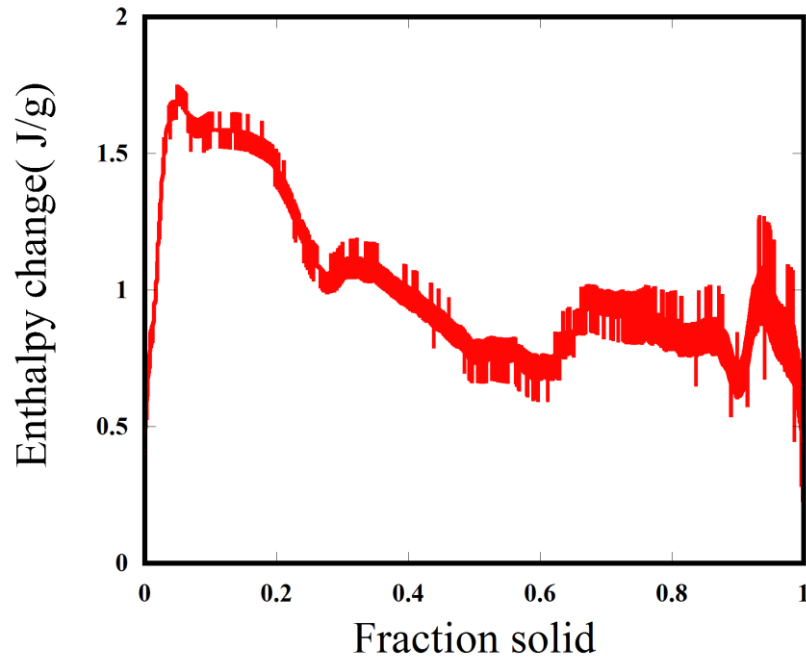


Figure 5.32 Enthalpy as a function of fraction solid

Figure 5.33 (a and b) shows the effect of Ce and Sr melt treatment on the fraction of solid formed during solidification. The fraction of solid formed increased with addition of Ce and decreased with Sr melt treatment, indicating that the Ce favors the formation of aluminum and Sr suppresses its nucleation. Figure 5.34 (a and b) shows the variation of the diffusivity of the alloy with melt treatment. The diffusivity of the untreated Al-8Si alloy decreases from $4.5 \times 10^{-5} \text{ m}^2/\text{s}$ to $2.5 \times 10^{-5} \text{ m}^2/\text{s}$ as the alloy solidifies from 650°C to 540°C respectively. The diffusivity of the alloy increased with both kinds of melt treatment. However, the increase in diffusivity was significant with Ce treatment. For example, with 0.04 wt.% Sr treatment, the diffusivity of the melt increased to $5.0 \times 10^{-5} \text{ m}^2/\text{s}$, whereas, with 2.0 wt.% Ce the diffusivity increased marginally to $4.7 \times 10^{-5} \text{ m}^2/\text{s}$.

Similarly, Figure 5.35 (a and b) shows the effect of melt treatment on the specific heat of the alloy. The specific heat of the untreated alloy increased from 900 J/kg-K to 2600 J/kg-K as the alloy solidifies from 650°C to 500°C . The specific heat of the alloy was significantly decreased with Sr and Ce melt treatment. For example, the addition of 0.04 wt.% Sr, the specific heat of the liquid alloy decreased from 900 to 700 J/kg-K and it remained unchanged with Ce treatment. Figure 5.36 (a and b) shows the latent heat evolved during solidification of Al-8Si alloys. A latent heat of 407 J/g was found to evolve during the solidification of untreated alloy and was decreased significantly with addition of Ce. However, the latent heat evolved remained unchanged with Sr melt treatment. The decrease in latent heat with Ce treatment was due to the formation of Ce intermetallics, which increased as the concentration of Ce increased in the alloy. Table 5.6 compares the latent heat calculated using Newtonian and Fourier techniques for various additions. The Fourier values are more accurate as it considers the change in diffusivity and specific heat with melt treatment.

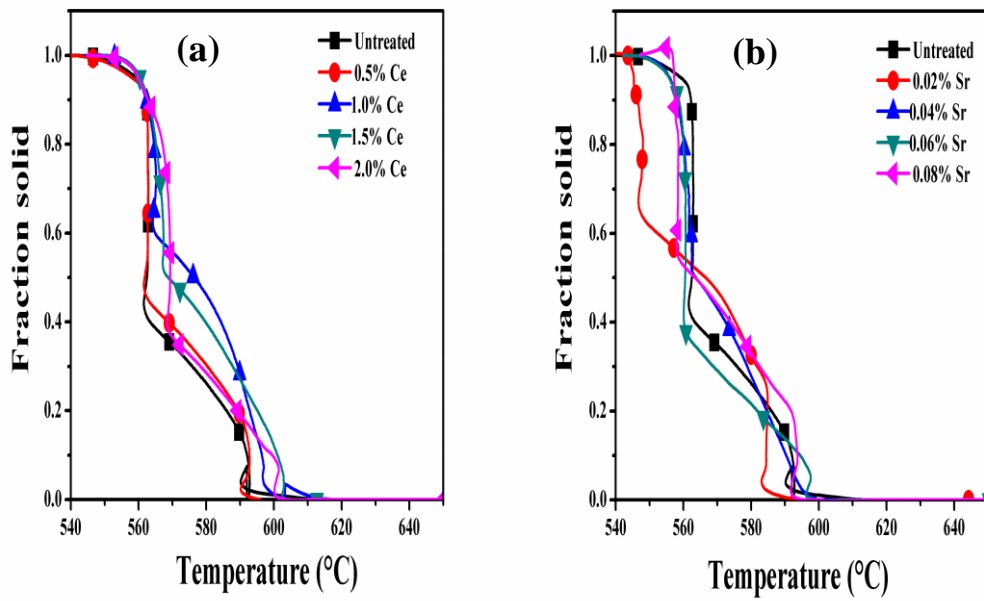


Figure 5.33 Variation in solid fraction formed during solidification of Al-8Si alloy with varying content of (a) Ce (b) Sr

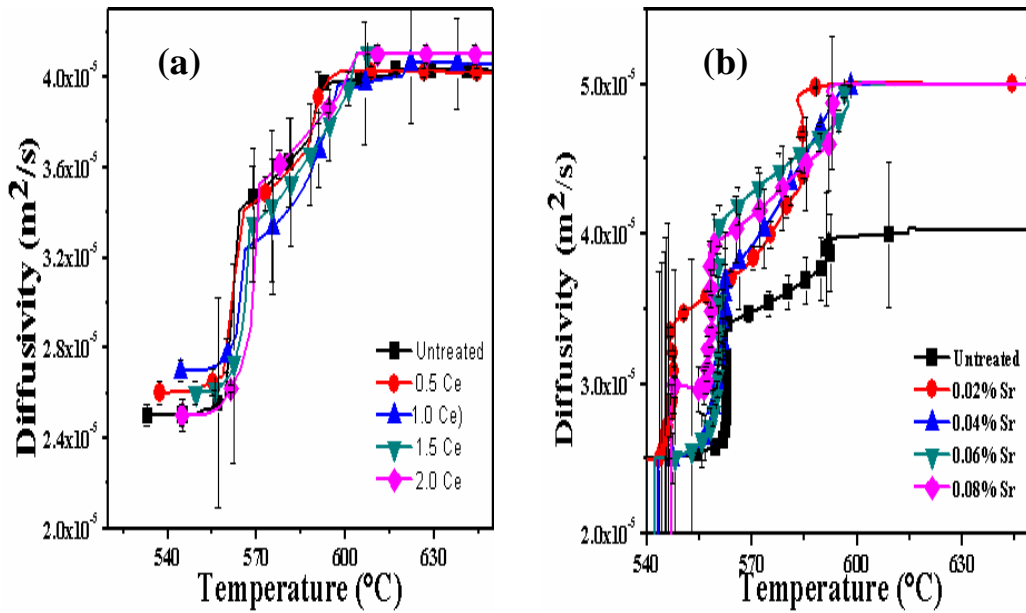


Figure 5.34 Variation in diffusivity of Al-8Si alloy with varying content of (a) Ce (b) Sr

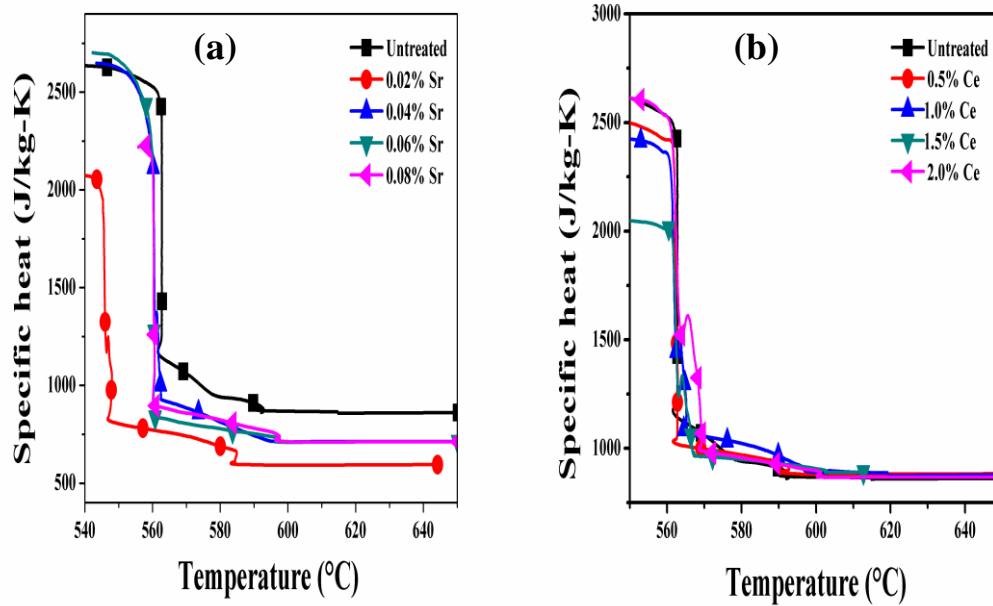


Figure 5.35 Variation in specific heat of Al-8Si alloy with varying content of (a) Ce
(b) Sr

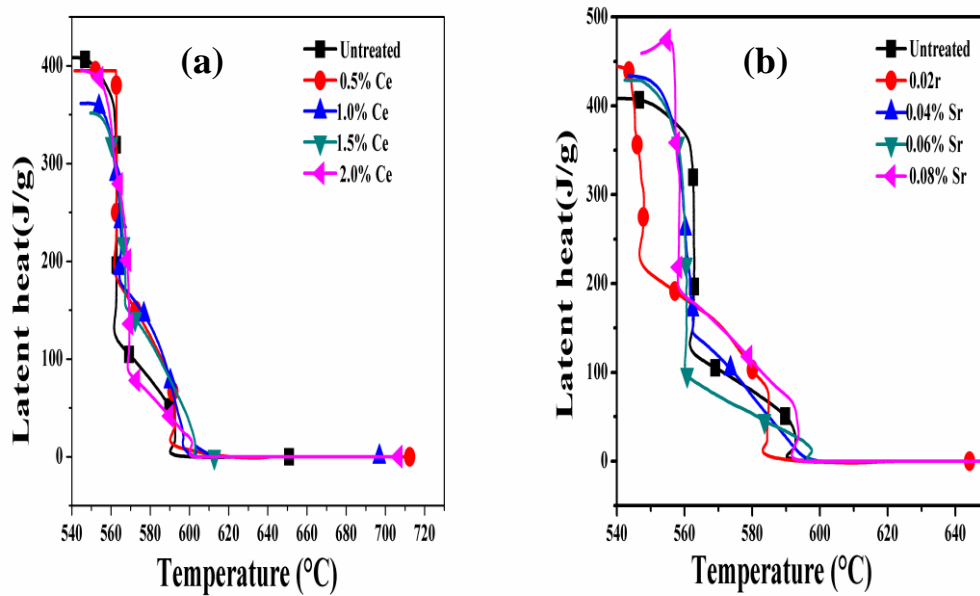


Figure 5.36 Variation in latent heat evolved during the solidification of Al-8Si alloy
with varying content of (a) Ce (b) Sr

Table 5.6 Effect of various melt treatment on the latent heat of Al-8Si alloy

Al-8Si	Latent heat (J/g)	
	Newtonian	Fourier
Untreated	373	408
0.5 wt.% Ce	367	394
1.0 wt.% Ce	338	360
1.5wt.% Ce	221	351
2.0 wt.% Ce	286	392
0.02 wt.% Sr	440	426
0.04 wt.% Sr	423	429
0.06 wt.% Sr	413	443
0.08wt.% Sr	473	460

5.2.1 Al-13 Si alloys

Figure 5.37 (a and b) shows the effect of Ce and Sr melt treatment on the solid fraction of Al-13Si alloys. Compared to the untreated alloy, both kinds of additions had similar influences on the solid fraction of the alloy. The increase in the solid fraction with melt treatment in the early stages of the solidification was due to shift in the eutectic point and due to the nucleation of α - aluminum. Figure 5.38 (a and b) shows the effect of Ce and Sr additions on the diffusivity of the alloy and Figure 5.39 (a and b) shows the effect melt treatment on the specific heat of the alloy. As the temperature decreased from 600 to 500°C, the diffusivity of the untreated alloy decreased from 4.5 to $3.5 \times 10^{-5} \text{ m}^2/\text{s}$ and specific heat increased from 700 to 1600 J/kg-K respectively. The melt treatment of the alloy decreased the diffusivity of the alloy to lower values and which was equal to that of untreated Al-8Si alloy. This indicates that the addition had transformed the Al-13Si alloy into a hypoeutectic alloy and resulted in the nucleation of α - aluminum. The latent heat evolved during solidification decreased with melt treatment is shown in the Figure 5.40 (a and b) and Table 5.7.

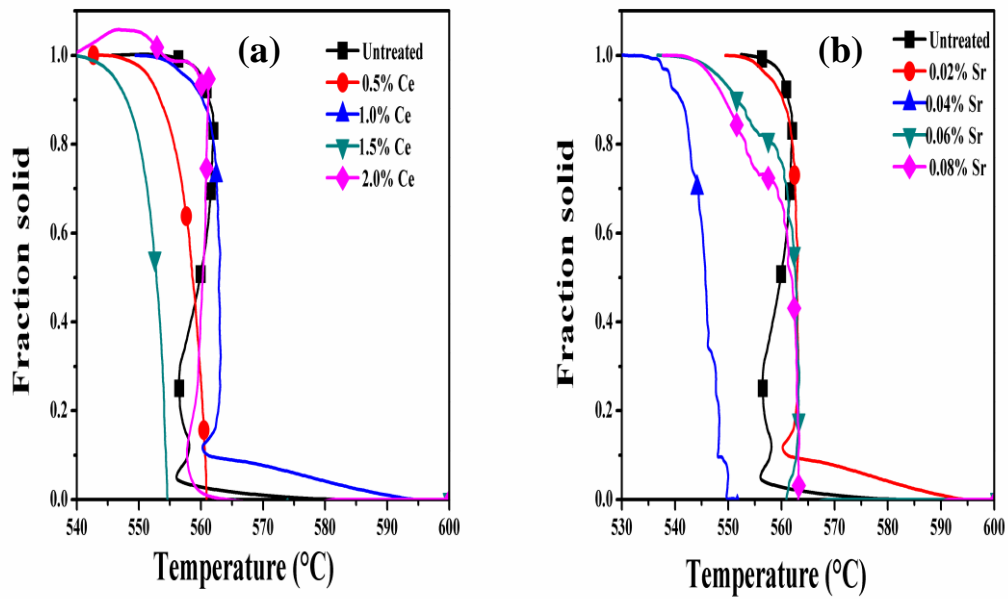


Figure 5.37 Variation in solid fraction formed during solidification of Al-13Si alloy with varying content of (a) Ce (b) Sr

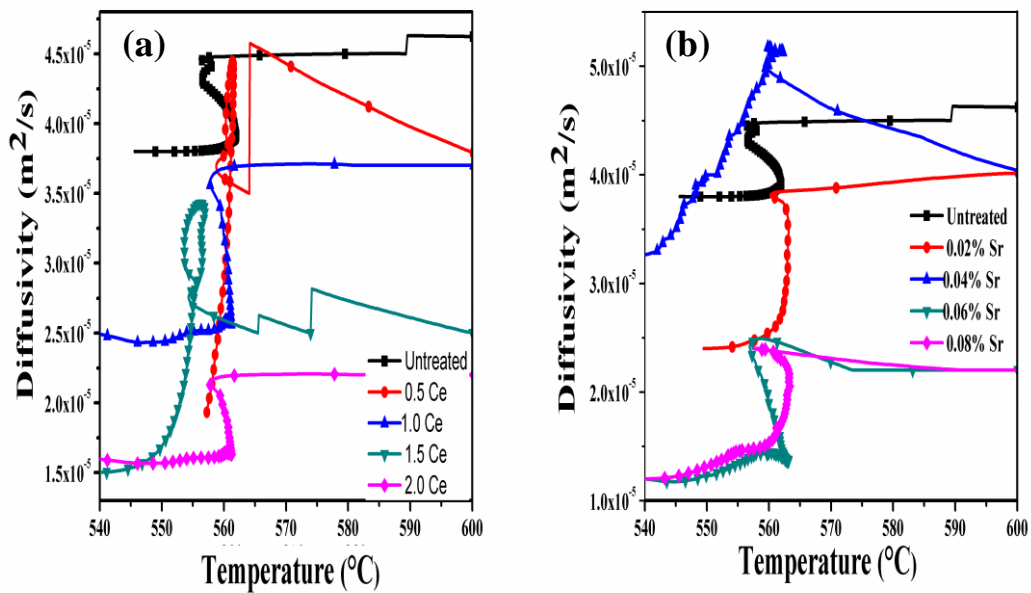


Figure 5.38 Variation in diffusivity of Al-13Si alloy with varying content of (a) Ce (b) Sr

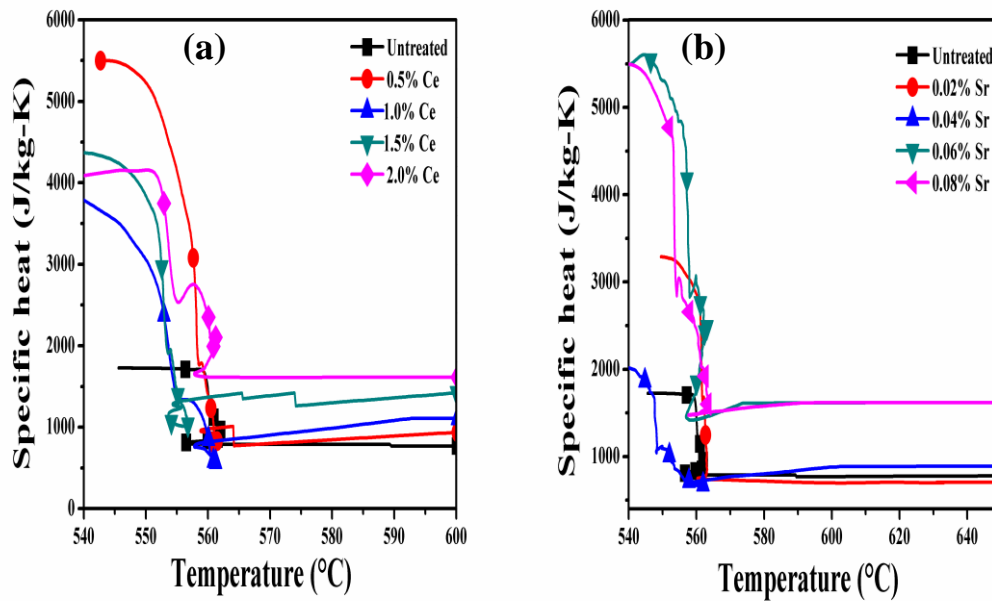


Figure 5.39 Variation in specific heat of Al-13Si alloy with varying content of (a) Ce
(b) Sr

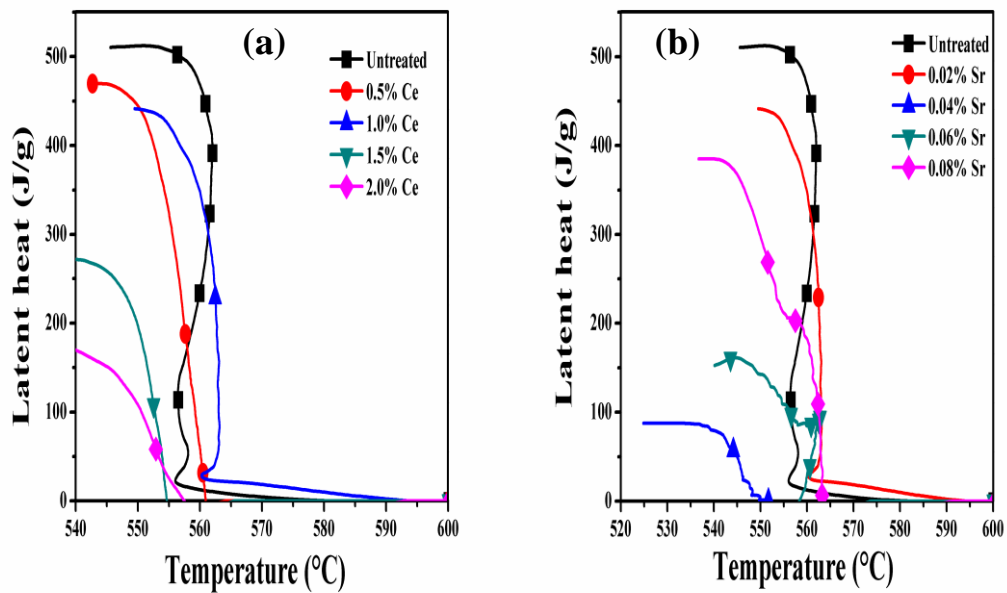


Figure 5.40 Variation in latent heat evolved during the solidification of Al-13Si alloy
with varying content of (a) Ce (b) Sr

Table 5.7 Effect of various melt treatment on the latent heat of Al-13Si alloy

Al-13Si	Latent heat (J/g)	
	Newtonian	Fourier
Untreated	384	510
0.5 wt.% Ce	428	470
1.0 wt.% Ce	688	439
1.5wt.% Ce	768	270
0.02 wt.% Sr	370	440
0.06 wt.% Sr	382	370
0.08wt.% Sr	510	383

5.2.3 Al-14Si alloys

Figure 5.41 shows the effect of Ce and P treatment on the fraction solid formed during solidification of Al-14Si alloys. Compared with untreated alloy, the percentage of the solid formed decreased with melt treatment indicating that the additions hinders the growth of primary and eutectic phase. In the presence of Ce, the eutectic phase was nucleated at lower temperature, resulting in higher eutectic modification. Similarly, Figure 5.42 (a and b) shows the effect of Ce and P treatment on the diffusivity of the alloy and Figure 5.43 (a and b) shows the variation of specific heat of the alloy with melt treatment. The diffusivity of the alloy increased with both Ce and P additions, whereas, the specific heat decreased with melt treatment. Among all, 0.05 wt.% P addition resulted in highest diffusivity and lowest specific heat. Figure 5.45 shows the variation in latent heat with melt treatment. A marginal increase in the latent heat was observed with 0.05 wt.% P addition due to the increase in primary silicon nucleation temperature. The latent heat of Ce treated alloys decreased with increase in Ce concentration due to the formation of Ce intermetallics. Table 5.8 compares the latent heat calculated with two techniques.

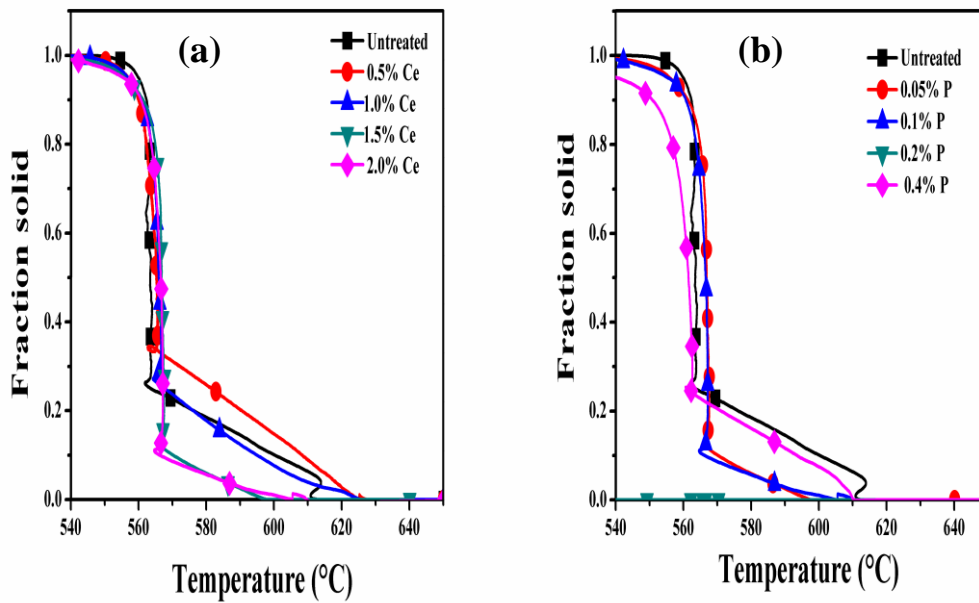


Figure 5.41 Variation in solid fraction formed during solidification of Al-14Si alloy with varying content of (a) Ce (b) P

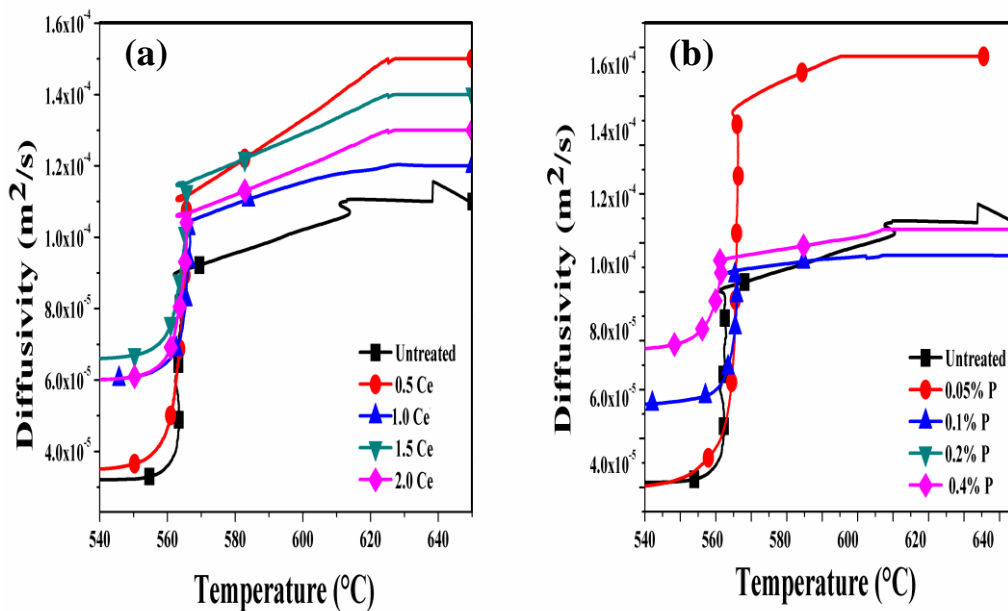


Figure 5.42 Variation in diffusivity of Al-14Si alloy with varying content of (a) Ce (b) P

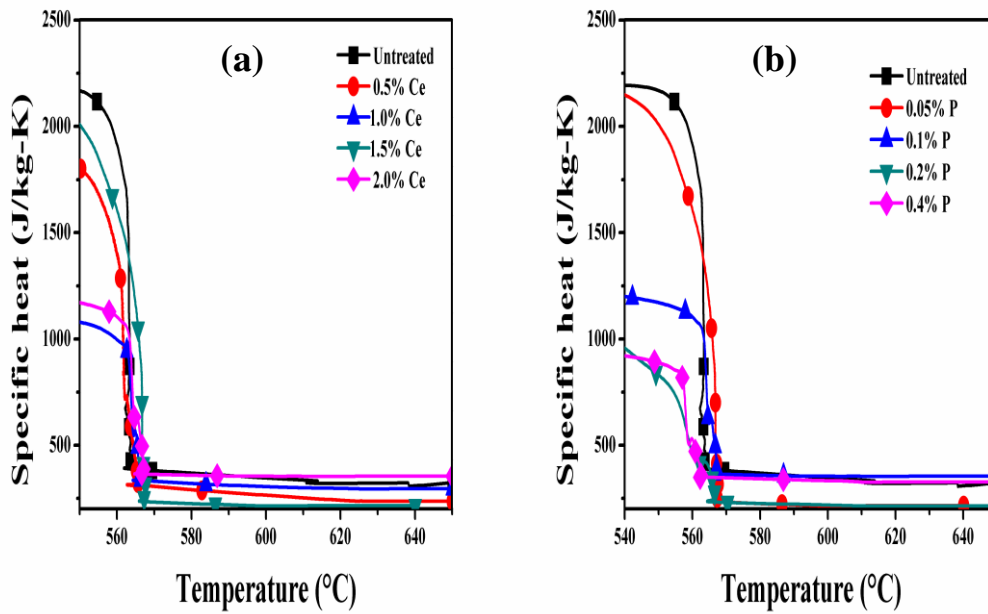


Figure 5.43 Variation in specific heat of Al-8Si alloy with varying content of (a) Ce
(b) P

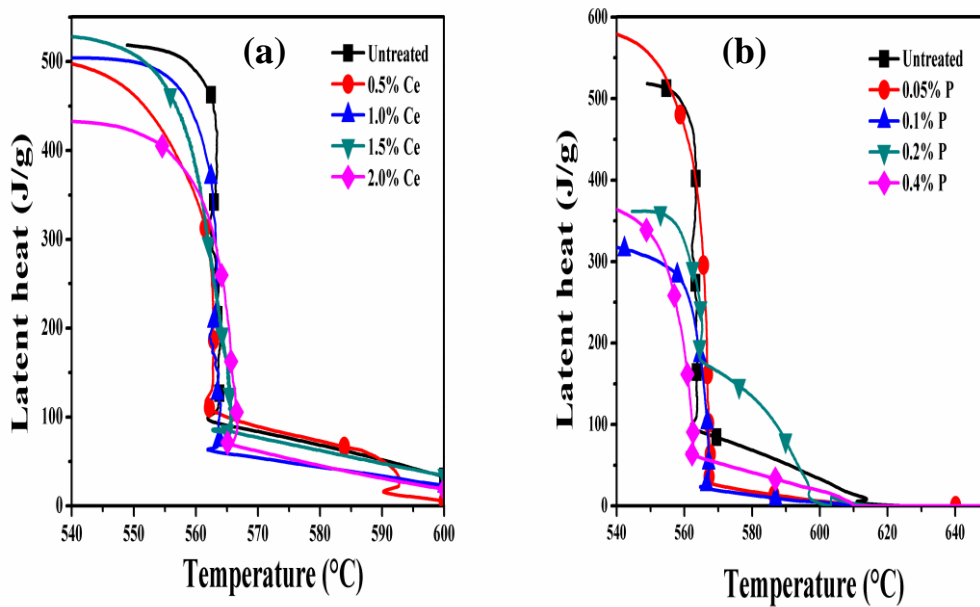


Figure 5.44 Variation in latent heat evolved during the solidification of Al-14Si alloy
with varying content of (a) Ce (b) P

Table 5.8 Effect of various melt treatment on the latent heat of Al-14Si alloy

Al-14Si	Latent heat (J/g)	
	Newtonian	Fourier
Untreated	579	517
0.5 wt.% Ce	646	520
1.0 wt.% Ce	677	502
1.5wt.% Ce	657	493
2.0 wt.% Ce	689	431
0.05 wt.% P	595	576
0.1 wt.% P	547	313
0.2 wt.% P	526	357
0.4wt.% P	521	360

5.2.4 Al-22Si alloys

Figure 5.45 (a and b) shows the effect of Ce and P additions on the solid fraction formed during the solidification of Al-22Si alloys. It was observed that the additions increased the fraction solid formed and indicates that the additions favored the formation of primary silicon. For example, at 640°C (after nucleation of primary silicon), the addition of 1.0% Ce and 0.05% P resulted in a solid fraction of 6% and 4% respectively, whereas, the solid fraction of the untreated alloy was observed to be 0.01, indicates that the fraction solid increased with melt treatment. Similarly, the additions favored the nucleation and growth of eutectic as well.

Figure 5.46 (a and b) shows the effect of additions on the diffusivity of the alloy. The diffusivity of the untreated Al-22Si alloy ranged from $4 \times 10^{-5} \text{ m}^2/\text{s}$ to $2.3 \times 10^{-5} \text{ m}^2/\text{s}$ as the alloy was solidified from 750°C to 500°C respectively. The diffusivity decreased to lower values with additions of Ce and P and decrease was found to be more significant with P treatment, however, the diffusivity increased with addition of

higher concentration. The decrease in diffusivity with addition of P would be associated with agglomeration and formation of silicon crystals. The thermal diffusivity of pure silicon at 750°C is about $2.5 \times 10^{-5} \text{ m}^2/\text{s}$ [Nishi T et al. (2003)] and is very near to the calculated diffusivity of the present alloy. The present alloy contains other elements that would affect the actual diffusivity. The decrease in the diffusivity is an indication that the addition favored the nucleation of primary silicon. Similarly, Figure 5.47 (a and b) shows the variation in specific heat of the alloy with melt treatment and it increased with addition of P and decreased with Ce. Figure 5.48 (a and b) and Table 5.9 shows the effect of melt treatment on the latent heat evolved. The untreated alloy resulted in an evolution of 607 J/g of heat and it decreased with Ce additions and increased with P additions. The decrease in latent heat was due to the formation of Ce intermetallics, which increased with the concentration of Ce added and the increase in latent heat is associated with the formation of primary silicon.

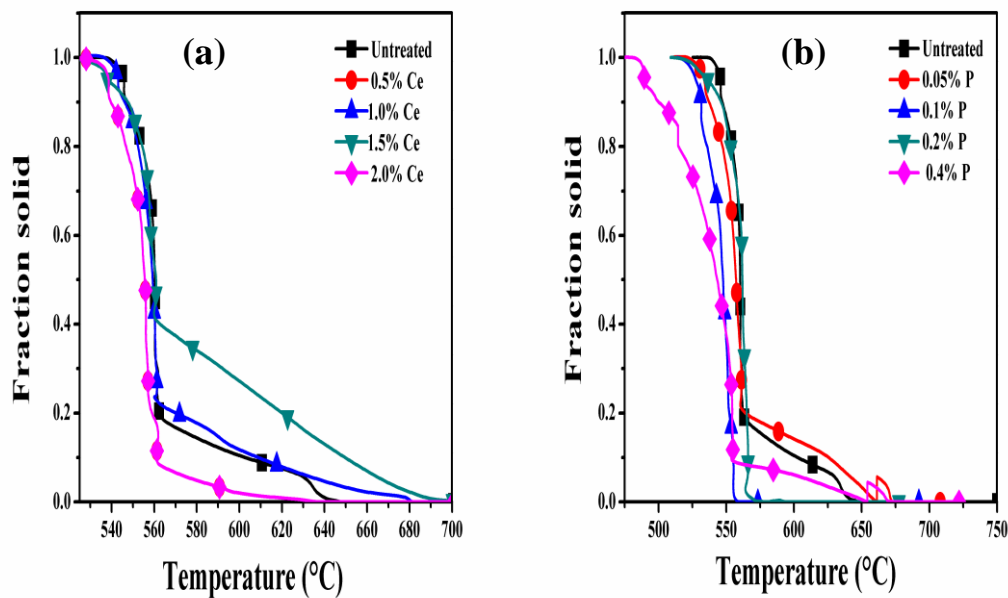


Figure 5.45 Variation in solid fraction formed during solidification of Al-22Si alloy with varying content of (a) Ce (b) P

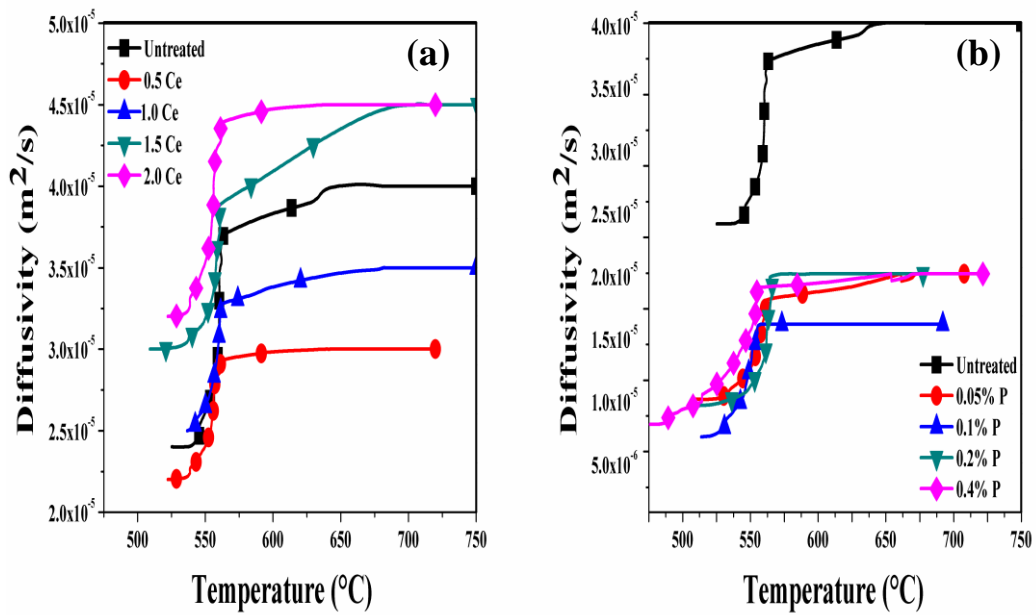


Figure 5.46 Variation in diffusivity of Al-22Si alloy with varying content of (a) Ce
(b) P

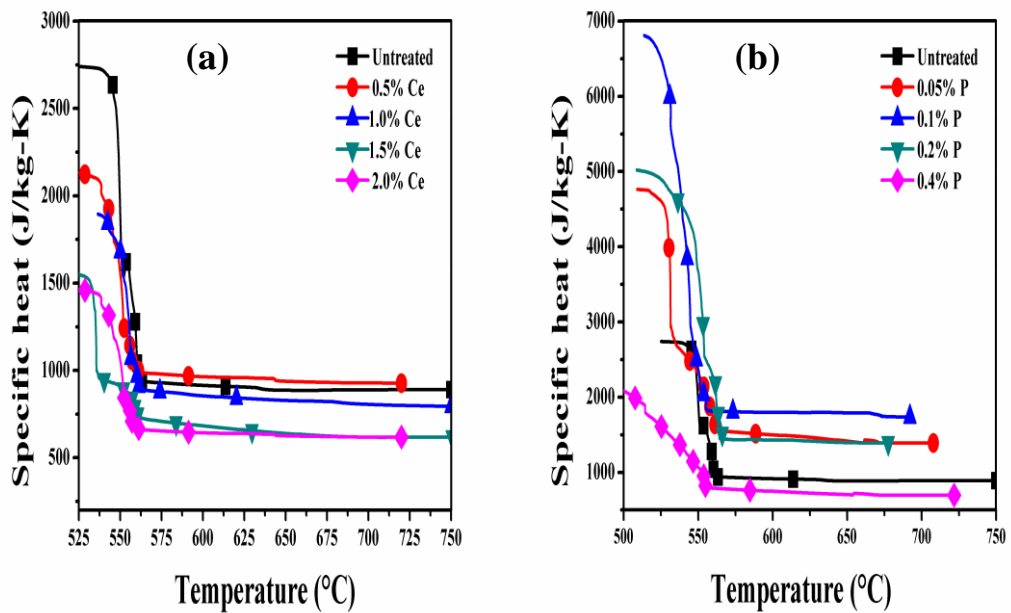


Figure 5.47 Variation in specific heat of Al-22Si alloy with varying content of (a) Ce
(b) P

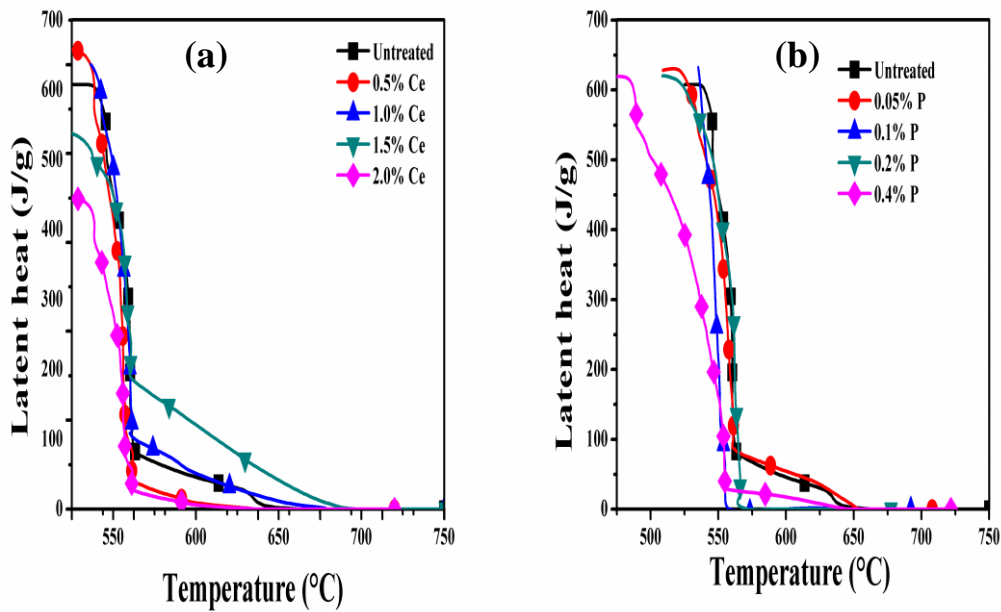


Figure 5.48 Variation in latent heat evolved during the solidification of Al-22Si alloy with varying content of (a) Ce (b) P

Table 5.9 Effect of various melt treatment on the latent heat of Al-22Si alloy

Al-22Si	Latent heat (J/g)	
	Newtonian	Fourier
Untreated	646	607
0.5 wt.% Ce	1264	658
1.0 wt.% Ce	1300	633
1.5wt.% Ce	1430	538
2.0 wt.% Ce	900	443
0.05 wt.% P	1293	630
0.1 wt.% P	1300	635
0.2 wt.% P	1462	620
0.4wt.% P	1264	615

5.3 The Effect of Melt Treatment of Al-Si Alloys on Interfacial Heat Flux Transients

The thermal history in the mold was used for calculating the interfacial heat flux transients using inverse analysis. The variation of heat flux with respect to time for the Al-8Si alloy in copper mold for untreated alloy is presented in the Figure 5.49. The heat flux increases rapidly as the melt comes in contact with the chill interface and reaches a peak value. This rapid increase in the heat flux was due to the formation of solid shell near the casting/chill interface during upward solidification. During initial stages of the formation of solid shell, the metallostatic pressure from liquid metal pushes the solid shell towards the chill surface. As the solidification proceeds, the solid shell thickens and pulls away from the chill surface resulting in a gas gap. The decrease in the heat flux after attaining maximum indicates the formation of gap between the casting and chill surfaces. The gaseous medium in the gap offers resistance to the heat flow across the surfaces. The contraction of the solid normal to the surface during cooling is a major factor in the formation of gap.

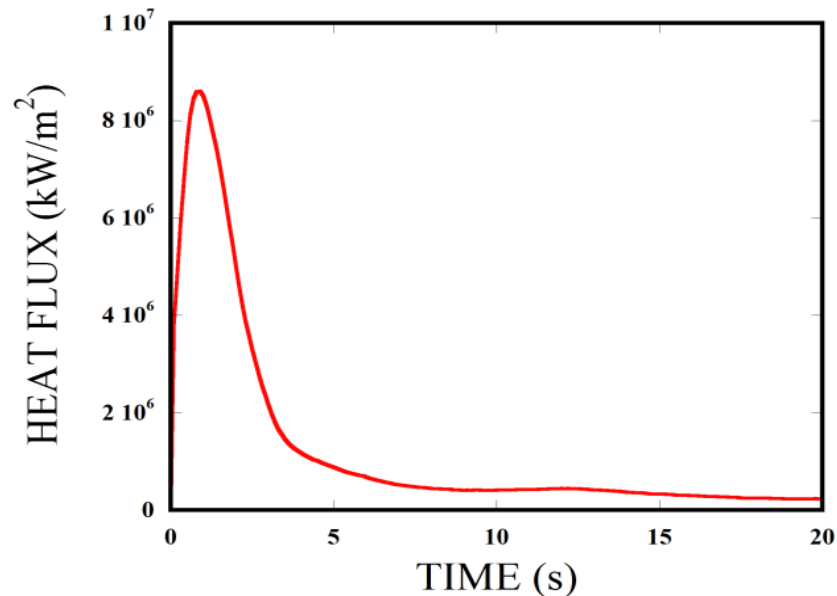


Figure 5.49 Variation in heat flux with time for copper chilled Al-8Si alloy

In the present study effect of melt treatment on peak heat flux is characterized. Figure 5.50 (a and b) shows the effect of Ce and Sr melt treatment of Al-8Si alloy on the peak heat flux during solidification against different chills. The peak heat fluxes of the treated alloys are considerably higher than the untreated alloys. For example, the heat flux attained in the untreated alloy casting solidified in copper mold was about 8750 kW/m² and with 1wt.% Ce and 0.06 wt.% Sr it treatment was about 12350 and 13400 kW/m². The additions had same effect on the heat flux for other chilling condition as well. The peak heat flux increased with the increase in thermal conductivity of the chill. Copper being the material with high thermal conductivity (395 W/mK) showed a higher heat flux than brass and SS chills.

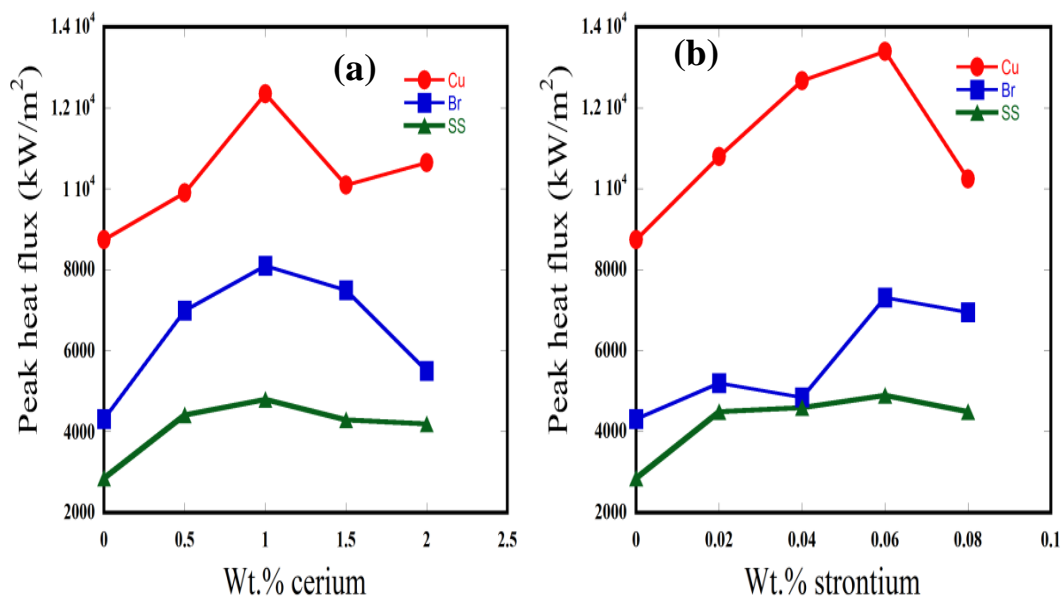


Figure 5.50 Variation of peak heat flux with varying content of addition (a) Ce (b) Sr

Similarly, Figure 5.51 shows the effect of varying content of Ce and Sr additions on the peak heat flux of Al-13Si alloy. The additions increased the heat flux similar to that in previous alloy. Even though heat flux increased with both the type of melt treatments, Sr modification resulted in higher heat flux. Figure 5.52 shows the variation of peak heat flux with Ce and P additions to Al-4Si alloy. The addition of Ce to the alloy significantly increased the peak heat flux. The peak heat

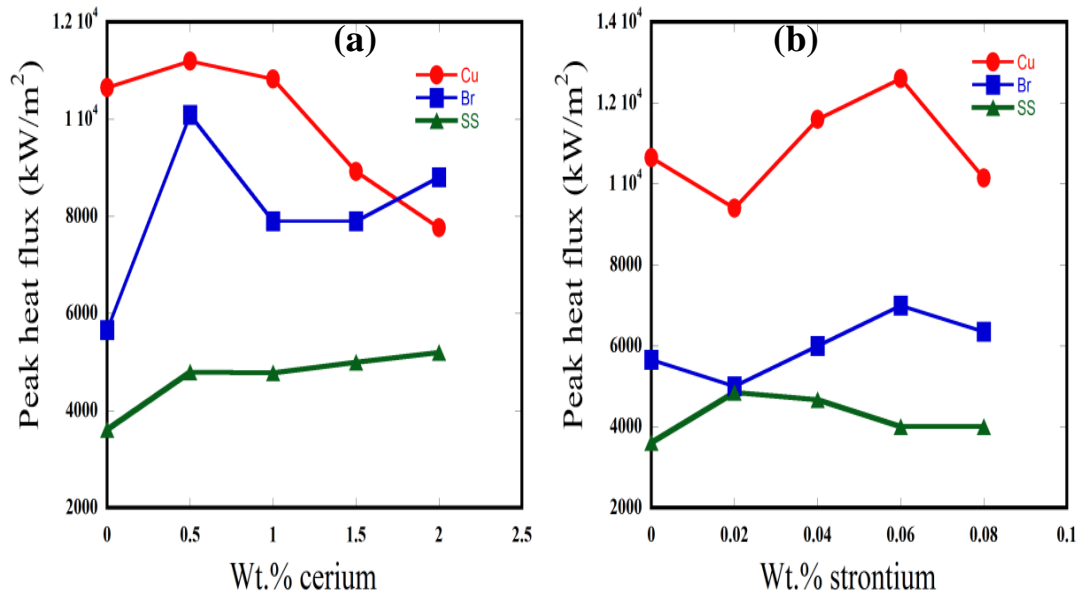


Figure 5.51 Variation of peak flux of Al-13Si alloy with varying content of (a) Ce (b) Sr

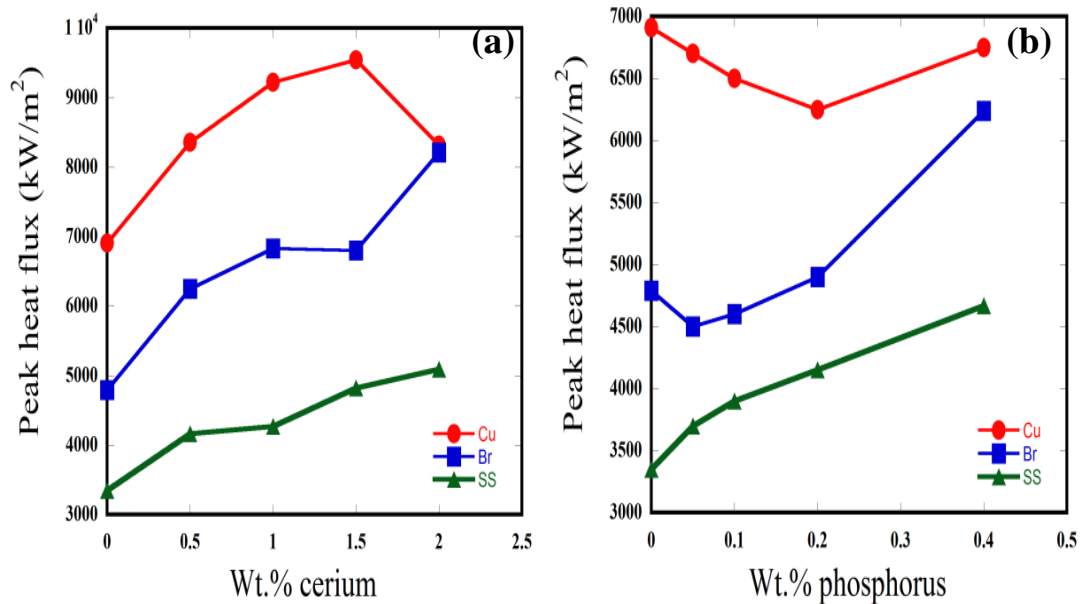


Figure 5.52 Variation of peak heat flux of Al-14Si alloy with varying content of (a) Ce (b) P

flux increased with Ce addition and reached a maximum value of 9541 kW/m² at a concentration of 1.5 % Ce addition. Similarly, on brass and stainless steel chills the peak fluxes were enhanced by 74% and 45% respectively with addition of 1.5% Ce. The improvement in heat transfer due to addition was mainly due to three factors: (i) change in liquid structure on melt treatment (ii) improved contact between the melt and the chill surfaces due to lower surface tension of the melt (iii) higher thermal conductance of the solid shell formed due to the transformation of silicon morphology from acicular to fibrous [Prabhu and Ravishankar 2003]. In untreated alloys, the acicular morphology of silicon prevents efficient contact between chill and solidifying casting. The fine fibrous morphology of the silicon of the initial solidified shell in the modified alloy increases the heat removal rate from the casting by increasing the electronic conduction leading to increase in the cooling rate.

On the other hand, the addition of P showed a decrease in heat flux and this was due to the inability of P in modifying the eutectic silicon. Similarly, the peak heat flux of Al-22Si alloy for various melt treatment and solidification condition is shown in Figure 5.53

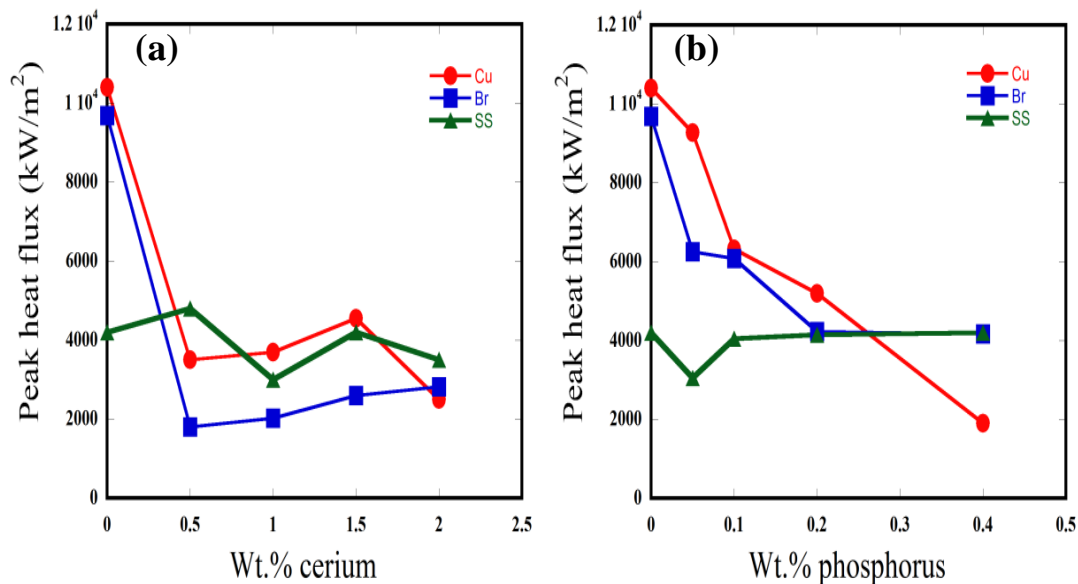


Figure 5.53 Variation of peak heat flux of Al-22Si alloy with varying content of (a) Ce (b) P

Unlike other alloys, the peak flux decreased with the addition of varying content of Ce and P. The decrease was more significant in Ce added alloys. The reason for this would be the nucleation of refined primary silicon and associated acicular eutectic silicon. The refined primary silicon would act as a well -proportioned nucleation sites for faceted (acicular) eutectic silicon. As the result the conductivity of the alloy decreases with the addition.

5.4 Microstructural characterization

5.4.1 Effect of Ce and Sr melt treatment on microstructure characteristics of Al-8Si alloy

The effect of varying content of Ce and Sr addition on the aluminium grain size is shown in the Figure 5.54. The aluminium grain size decreased with the addition of Ce and increased with Sr addition. The grain size was also decreased with increase in cooling rate.

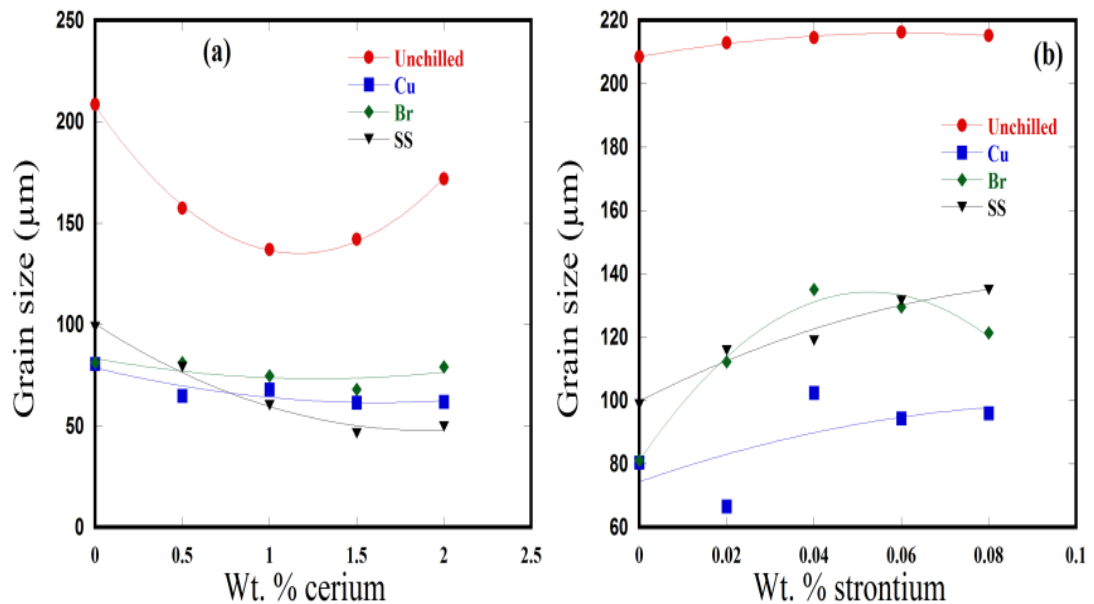


Figure 5.54 Variation of grain size in Al-8Si alloys with (a) Ce (b) Sr

The synergistic effect of chilling and Ce addition yielded finer aluminium grains than the untreated alloys, however, the grain size increased significantly with increase in Sr content and cooling rate. The addition of Ce transformed columnar aluminium grains into equiaxed grains, whereas, Sr treatment, increased the size of the columnar proeutectic α -aluminium.

The refinement in hypoeutectic can either occur directly on substrate by epitaxial growth of aluminum or by some phase reaction involving α -Al, the fine aluminum is precipitated as the result of reaction [Mohanty and Gruzleski 1996]. In the present study, observations of the microstructure did not reveal any such evidence of heterogeneous nucleation sites for aluminum formed due to the addition of Ce or Sr. Besides, the microstructures of Ce treated alloys showed the presence of Ce-phase intermetallic compounds along the grain boundaries. The presence of Ce in the compound was confirmed using SEM and EDS analysis and presented in the Figure 5.55. The EDS results show that the added Ce combines with Al, Si, Fe and trace amounts of Ag in the melt to form a Ce based intermetallic.

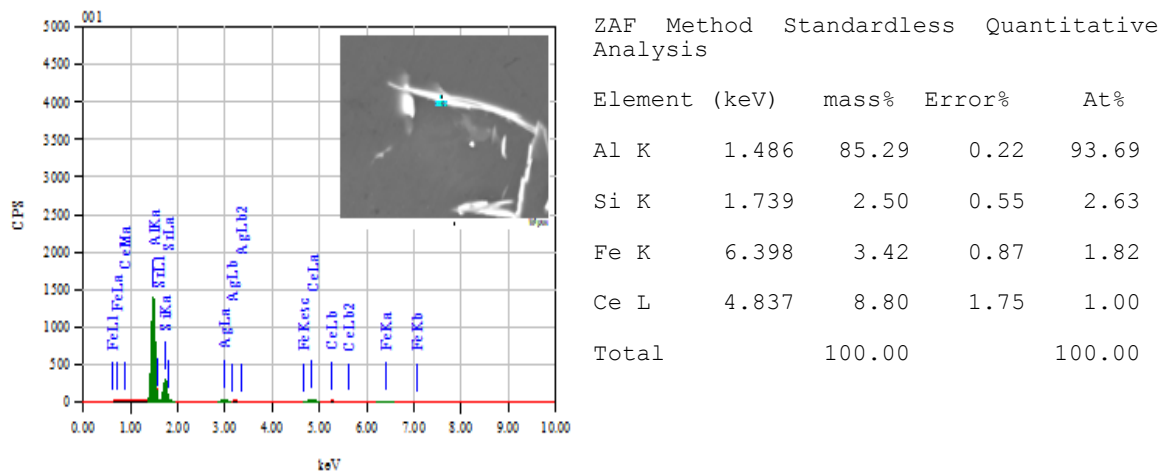


Figure 5.55 EDS analysis results of Ce intermetallic formed due to the addition of Ce

In the present study, the morphology of Ce phase changes from needle shaped to blocky crystals as the concentrations of Ce increases in the melt. This implies that the formation of the Ce based intermetallic has direct impact on the size and shape of the

microstructure constituents. Previous studies on Al-Ce-Si system reveal that at low concentrations of Ce only of two phases of Ce are stable (Γ_1 or Γ_2) [Grobner et al. 2004]. Hence for heterogeneous nucleation, a near perfect epitaxy between the nucleant and substrate should exist. In the case of α -Al (0.405 nm) and Γ_1 or Γ_2 no such match was observed in the lattice parameters and it can be indicates that the Ce phases do not heterogeneously nucleate α -Al. The presence of Ce based particle along the grain boundaries is the proof for not nucleating aluminum. Hence it is obvious that the refinement would be due to the precipitation of fine aluminum grains as the result of reaction involving Ce and aluminum. The DSC studies on Al-Si-Ce system by Grobner et al. (2004) supports this theory. Their studies revealed that the Γ_1 phase which is formed at 750 °C reacts with liquid metal to precipitate α -Al and Γ_2 at a temperature of 621°C. Similarly, in the present study the Γ_1 formed at higher temperature would have reacted to precipitate out fine equiaxed α -Al. The liquidus temperature of untreated Al-8% Si alloy is 599°C and the addition of Ce increased the nucleation temperature of α -Al. The increase in nucleation temperature was due to the formation of aluminum as a reaction product and this process would yield a fine and equiaxed grains compared to the untreated alloy. Unlike ternary Al-Si-Ce system, the present alloy contains other impurities which directly influences the reaction temperature and composition of intermetallic formed.

The addition of Sr was found to increase the size of aluminium grains. In the absence of any heterogeneous nucleation sites, very few aluminium grains will nucleate homogeneously at larger undercooling and grow as coarse grains [Kashyap and Chandrashekar 2001]. It is also equally probable that the commercial Al-Si alloys invariably contains some amount of Ti or B, which would act as an nucleation sites for aluminium dendrites. On addition of Sr, the Sr will interact with Ti or B to poison the nucleation sites present in the alloy and thereby increasing the undercooling required for nucleation [Liao and Sun 2003] [Lu and Dahle 2006]. Thus, the suppression of the nucleation of aluminium to lower temperature by Sr, would result in the nucleation of lesser number of grains. This was evident in the thermal analyses results as well, the undercooling required for the nucleation of primary aluminium increased with the addition of Sr for all solidifying conditions and hence coarser

grains were formed with Sr addition, whereas, the addition of Ce resulted in lesser undercooling and finer grains.

The effect of melt treatment on silicon modification was assessed by quantitatively measuring and analysing the eutectic Si particle characteristics, the results are given in Table 5.10. The spherical nature of the eutectic Si particle was assessed by the roundness factor and the aspect ratio. A roundness factor and aspect ratio of 1 indicates that the particle is perfect sphere. The results indicate that the untreated alloy displayed largest particle size (length, area and perimeter) and roundness value. The characteristic length of Si particles in untreated-unchilled alloy was found to be $65\pm 30\mu\text{m}$. The size of the silicon particles was significantly decreased with addition of Sr and Ce. An addition 0.08 % Sr resulted in the lowest particle size of $3.8\ \mu\text{m}$. Among cerium treated alloys, 2% Ce addition yielded the lowest particle size of $28\pm 18\ \mu\text{m}$. On the other hand, the untreated alloys solidified against chills showed a significant decrease in the particle characteristics compared to slowly cooled alloys. The characteristic length of the silicon particles decreased with increase in the thermal conductivity of the chill. The length of eutectic Si in copper, brass and stainless steel chills were found to be 16.6, 20.5 and $26.5\ \mu\text{m}$ respectively. Subsequently, the roundness factor was decreased to 5.6 with chilling and this indicates that the acicular nature of the eutectic silicon was least affected by chilling although it was refined. Figure 5.36 shows the effect of Ce and Sr addition on the eutectic silicon particle characteristics. The addition of Ce to chilled alloy significantly decreased the Si particle characteristics compared to unchilled alloys. The addition of 2 wt.% Ce to chilled alloys yielded lowest silicon characteristic length of 8.4, 7.9 and $8.5\mu\text{m}$ for copper, brass and stainless steel chills respectively. The addition of Sr yielded fine and fibrous eutectic silicon structure irrespective of the cooling conditions. The addition of Sr to chilled alloys resulted in an average the silicon characteristic length of $2.2\pm 0.4\ \mu\text{m}$, irrespective of the chilling conditions. The particle length of Sr treated alloys significantly decreased for all solidifying conditions, whereas, characteristic length of Ce treated alloys showed substantial decrease only in chilled conditions.

Table 5.10 Eutectic Si particle characteristics of Al-8 Si alloys

Chill	Ce/Sr wt-%	Length (μm)	Aspect ratio	Area (μm)²	Perimeter (μm)	Roundness factor
Unchilled	0.0	65.0±30	12.5	225.0±150	138.0±92	6.7
	0.5	50.0±15	9.4	206.0±98	130.0±33	6.5
	1.0	47.5±20	9.0	241.0±120	121.0±38	4.8
	1.5	29.5±18	6.6	112.0±65	76.0±30	4.1
	2.0	28.0±18	6.4	92.0±50	70.0±25	4.2
	0.02	4.3±1.6	2.4	8.5±4	14.0±4.5	1.8
	0.04	4.3±1.5	2.4	9.0±5	14.0±4	1.7
	0.06	4.2±1.6	2.3	9.2±4.5	14.0±5	1.7
	0.08	4.1±1.5	2.2	9.1±4.8	14.1±5.7	1.7
Copper	0.0	16.7±6.8	8.8	19.5±10	37.014	5.6
	0.5Ce	15.3±3.5	4.5	24.0±7	28.0±6	2.6
	1.0 Ce	10.8±6	3.4	19.0±9	25.0±10	2.6
	1.5Ce	11.6±3.6	3.4	17.7±8	21.0±6	2.0
	2.0 Ce	8.4±4	2.9	13.2±5	16.7±4	1.7
	0.02Sr	2.6±0.8	1.7	2.7±0.9	6.8±1.2	1.4
	0.04Sr	2.5±0.6	1.9	2.3±0.9	6.0±1.0	1.2
	0.06Sr	1.9±0.5	1.6	1.9±0.9	5.5±1.1	1.3
	0.08Sr	1.7±0.5	1.7	1.6±0.8	5.2±0.8	1.3
Brass	0.0	20.5±3.5	8.9	29.0±9	45.0±10	5.6
	0.5Ce	17.2±10	5.7	22.0±10	30.0±15	3.3
	1.0 Ce	10.1±4	3.3	18.0±9	26.0±10	3.0
	1.5Ce	10.0±4	3.0	19.5±8	22.8±11	2.1
	2.0 Ce	7.9±5	2.2	17.0±10	21.4±9	2.1
	0.02Sr	2.6±0.5	1.6	2.7±1.0	7±1.8	1.4
	0.04Sr	2.5±0.5	1.8	2.5±0.9	6.5±1.5	1.3
	0.06Sr	2.3±0.4	1.6	2.0±0.8	5.8±1.2	1.3
	0.08Sr	1.8±0.5	1.6	1.6±0.6	5.1±1.3	1.3
Stainless steel	0.0	26.5±12	9.1	43.0±19	55.0±19	5.6
	0.5Ce	18.3±6	6.1	32.0±12	38.0±14	3.6
	1.0 Ce	13.8±6	5.1	28.0±17	32.0±25	2.9
	1.5Ce	9.9±4	3.8	16.6±14	22.3±9	2.4
	2.0 Ce	8.5±4	3.1	15.0±10	19.5±8	2.0
	0.02Sr	2.7±0.9	1.8	2.5±0.9	7±1.5	1.4
	0.04Sr	2.5±0.8	1.9	2.2±0.8	6.7±1.3	1.4
	0.06Sr	2.4±0.6	1.8	2.3±0.9	6.6±1.2	1.3
	0.08Sr	1.9±0.7	1.7	1.5±0.5	5.5±0.9	1.3

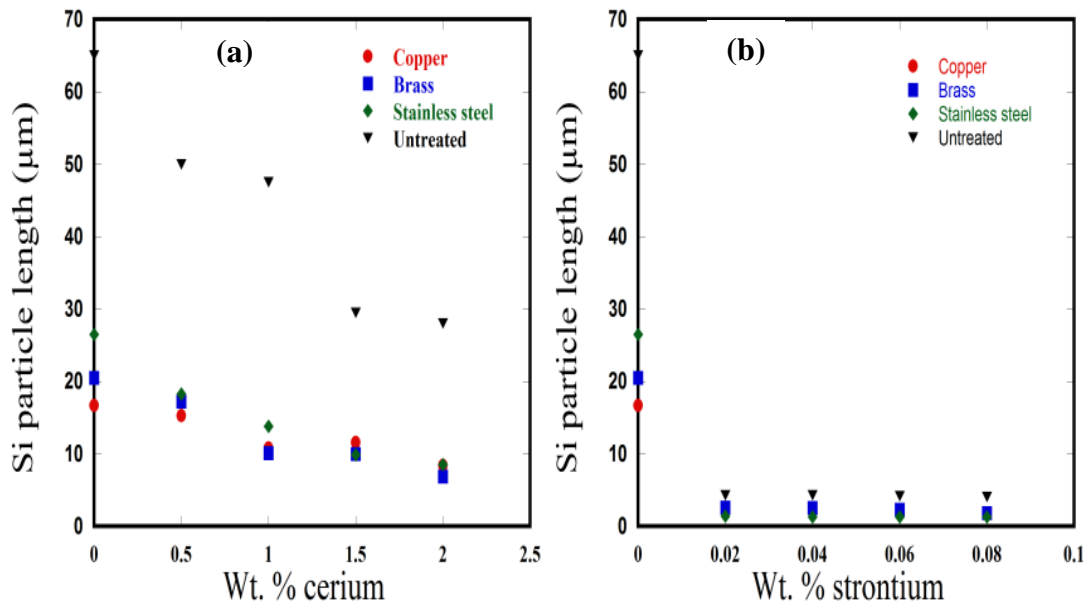


Figure 5.56 Variation of particle characteristic with varying content of (a) Ce (b) Sr

According to Dahle et al. (2005), the nucleation of eutectic silicon in hypoeutectic Al-Si alloys can happen in three ways. (a) Heterogeneous nucleation of silicon on or adjacent to aluminum dendrites or on Fe intermetallic present in the melt (b) nucleation of silicon between the aluminum dendrites, and (c) growth of eutectic solidification front opposite to thermal gradient. Subsequently, it was also reported that the nucleation of acicular silicon occur on the Fe intermetallic present in the melt and of modified silicon occur from highly undercooled melt between the aluminum dendrites [Shabestari et al. 2009] [Hegde and Prabhu 2008]. Based on the thermal analyses results and silicon particles characteristics results, both the addition resulted in higher undercooling and fine fibrous silicon. Hence, it can be concluded that the nucleation of silicon in the base alloy would have occurred on Fe intermetallic or on AIP from less undercooled melt, which are invariably present in the commercial alloys. The heterogeneous nucleation of Si would result in its nucleation before eutectic aluminum and would grow ahead of the aluminum front as faceted acicular silicon. The increased solidification rates would refine the eutectic silicon by suppressing the nucleation temperature and by increasing the undercooling.

The addition of modifiers to the melt is known to suppress the nucleation of silicon by

poisoning the nucleation sites of Si [Lu and Hellawell 1987]. As a result, the Si will be nucleated from lower temperature and highly undercooled melt. The addition of Sr and Ce also showed similar kind of decrease in eutectic temperature and increase in undercooling. This implies that the nucleation of silicon did not occur either from Fe intermetallic or on AlP. It was reported that the addition of eutectic modifiers such as Sr alters the surface tension of the melt as it is a surface active element [Closset and Gruzleski 1982]. This change in surface energy would have altered the heterogeneous nucleation of Si. The presence of Sr in the melt hinders the growth of the silicon by adsorbing on to growth sites and induces twinning offering growth in all direction.

In the case of Ce treated alloys, it was evident from the Figure 5.55 that the added Ce combined with Fe to form intermetallic, making Fe unavailable for the nucleation of Si. Moreover, Ce is also a surface active element and would adsorb on to the growth sites to hinder the growth of silicon. The addition of Ce simultaneously refined and modified aluminum and eutectic silicon, whereas, the addition of Sr resulted only in the modification of eutectic silicon. The extent of refinement and modification improved with increase in the cerium addition.

Figure 5.57 shows the correlation between eutectic microstructure characteristic, roundness factor and dimensionless thermal analysis parameter ($\Delta T_G/\Delta T_N$). A good correlation was obtained between roundness factor and dimensionless parameter. Even though, the roundness factor showed a correlation with eutectic growth temperature difference (ΔT_G), it was not considered as a better fit was observed with ($\Delta T_G/\Delta T_N$). The castings with high $\Delta T_G/\Delta T_N$ values yielded modified eutectic structure and with low values yielded unmodified eutectic structure. The roundness factor decreases with increase in $\Delta T_G/\Delta T_N$. A $\Delta T_G/\Delta T_N$ value of zero corresponds to unmodified structure having roundness value above 3.5 and $\Delta T_G/\Delta T_N$ value greater than 3 corresponds to modified eutectic silicon with roundness value closer to 1 as shown in Figure 5.57. The plot can be used to assess the eutectic silicon characteristics of chilled and melt treated Al-8Si alloy.

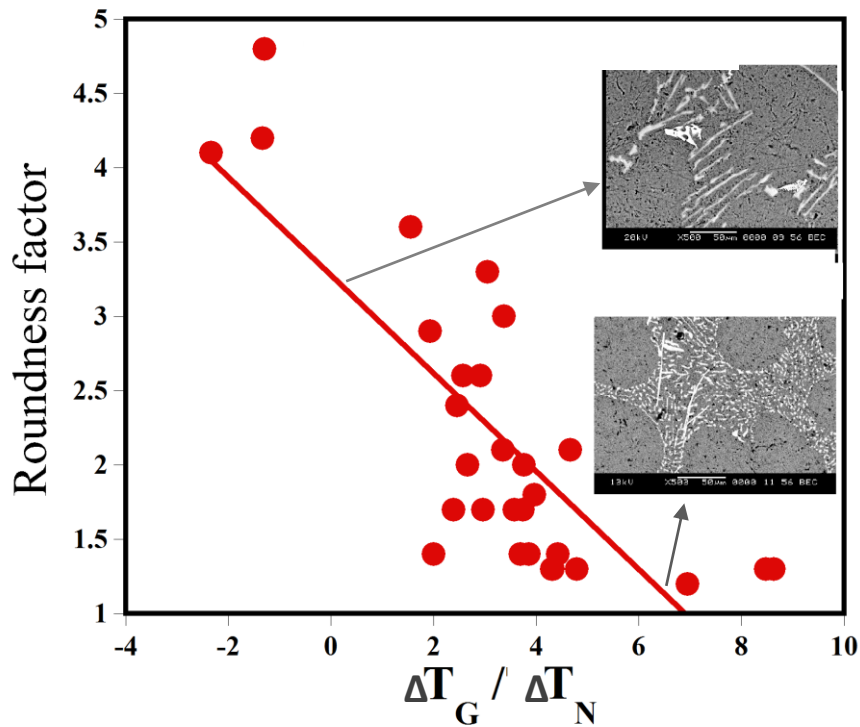


Figure 5.57 Correlation between dimensionless thermal analysis parameter and roundness factor of eutectic Si in Al-8Si alloy

5.4.2 Effect of Ce and Sr melt treatment on microstructure characteristics of Al-13Si alloy

The eutectic Si particle characteristic of the Al-13Si alloy for different cooling conditions and varying content of Sr and Ce additions are given in Table 5.11. The untreated alloy displayed largest particle size (length, area and perimeter) and a roundness value. The length of Si particles in untreated, unchilled alloy was found to be $85 \pm 25 \mu\text{m}$ and showed a roundness factor well over 6, indicating the acicular nature of the Si particles formed. The untreated alloys solidified against chills showed a significant decrease in the particle characteristics compared to slowly cooled alloys, but the acicular nature of the eutectic Si was marginally affected. The length of the silicon particles decreased with increase in the thermal conductivity of the chill. The length of eutectic Si in copper, brass and stainless steel chills were found to be 24, 25 and $65 \mu\text{m}$ respectively. The roundness factor of 5.6 was achieved due to chilling and

indicates that the acicular nature of the particle was least affected by chilling although it was refined.

Figure 5.58 (a and b) shows the effect of Ce and Sr treatment on the eutectic silicon particle characteristic of the Al-13Si alloy. The characteristic length of the eutectic silicon decreased with increase in Ce concentration of the melt. The 2% Ce addition to unchilled alloy yielded the lowest silicon particle length and was about 35 μm . The roundness ratio of the particle also decreased with Ce melt treatment. This indicates that the acicular Si particles are transformed to fibrous form with the addition of Ce. For example, the addition of 2% Ce decreased the roundness factor to 2.5, indicating that the addition of cerium results in more globular eutectic Si. The decrease in size was more significant with chilling. For example, the combination of copper chilling and 1.5 wt.% Ce yielded a characteristic length of 11.3 μm and roundness factor of 1.9 indicates that the addition of Ce is more effective at higher cooling rates.

The addition of Sr had decreased the silicon particle size further down irrespective of the chilling condition. The minimum silicon sizes were obtained on 0.06 wt%-Sr addition, about 1.9 μm for copper chilled alloy. Further addition of Sr resulted in marginal increase in silicon characteristics and was mainly due to the over-modification affect. The roundness factor was approached unity with Sr modification and indicates the extent of modification achieved with Sr melt treatment.

The role of Ce and Sr atoms in the modification of eutectic silicon is very much similar to that of in hypoeutectic alloys. Both the additions are found to suppress the nucleation of eutectic silicon forcing it nucleate at higher undercooling. Moreover, the shift in the eutectic point had caused the aluminum dendrites to nucleate prior to the eutectic silicon. The eutectic silicon in the base alloys are known to nucleate on the primary silicon or on some favorable heterogeneous substrate like (AlP, Fe intermetallic) at low undercooling and to grow as acicular silicon [McDonald et al. 2004].

Table 5.11 Eutectic silicon particle characteristics of Al-13Si alloys

	Ce/wt-%	Length (µm)	Aspect ratio	Area (µm) ²	Perimeter (µm)	Roundness ratio
Unchilled	0.0	85±35	8.6	160.0±95	110.0±70	6.0
	0.5	49.0±13	7.1	149.0±65	94.0±35	4.7
	1.0	48.8±16	6.3	140.0±46	73.0±16	3.0
	1.5	37.5±24	5.7	112.0±48	64.0±20	2.9
	2.0	35.0±20	5.8	100.0±40	58.0±18	2.7
	0.02	5.1±1.8	2.0	9.9±4	13.5±3	1.5
	0.04	4.2±1.5	2.0	7.7±4	11.8±3	1.4
	0.06	3.5±1.6	1.9	5.3±2.9	9.7±3.3	1.4
	0.08	3.6±1.2	1.6	4.5±2.4	8.8±2.5	1.4
Copper	Wa	24.0±7	10.9	26.0±13	32.0±16	3.1
	0.5Ce	12.0±8	3.6	27.7±11	27.7±11	2.2
	1.0 Ce	11.3±8	3.5	20.2±9	23.6±10	2.0
	1.5Ce	20.2±7	7.8	18.0±8	21.0±11	1.9
	2.0 Ce	15.0±9	4.8	16.0±6	19.3±6	1.9
	0.02Sr	3.4±1	1.5	5.2±2.2	9.9±2.6	1.5
	0.04Sr	2.3±0.8	1.6	2.2±1.0	6.4±1.5	1.5
	0.06Sr	1.9±0.6	1.6	1.9±0.6	5.7±1.3	1.4
	0.08Sr	2.2±0.5	1.5	2.1±0.4	5.8±0.9	1.3
Brass	Wa	25.3±4	11.0	20.6±7	29.4±7	3.3
	0.5Ce	17.3±9	5.8	33.6±20	30.9±14	2.3
	1.0 Ce	14.2±7	5.5	20.0±13	23.0±11	2.1
	1.5Ce	9.0±5	3.3	15.6±6	21.0±8	2.2
	2.0 Ce	9.9±3	3.3	7.6±3	14.5±5	2.2
	0.02Sr	3.0±1.2	2.0	2.0±1.1	6.3±3	1.6
	0.04Sr	1.4±0.2	1.3	2.0±1.1	6.0±3	1.4
	0.06Sr	2.4±1	1.8	1.9±1	5.6±2.0	1.3
	0.08Sr	2.4±1	1.8	2.3±0.8	6.2±1.2	1.3
Stainless steel	Wa	65.1±20	12.8	88.6±15	74.5±7	5.0
	0.5Ce	18.3±10	7.3	19.8±10	29.4±10	3.5
	1.0 Ce	17.4±10	6.7	18.9±10	22.4±10	2.1
	1.5Ce	14.8±10	6.4	14.2±10	20.0±15	2.2
	2.0 Ce	15.2±11	3.5	16.0±9	21.5±14	2.3
	0.02Sr	3.1±1.6	1.5	3.7±1.7	8.1±2	1.4
	0.04Sr	2.2±0.7	1.3	2.6±0.9	6.7±1.6	1.4
	0.06Sr	1.9±0.4	1.7	2.5±0.6	6.5±1.5	1.3
	0.08Sr	2.6±0.9	1.7	2.8±1.0	6.9±1.6	1.4

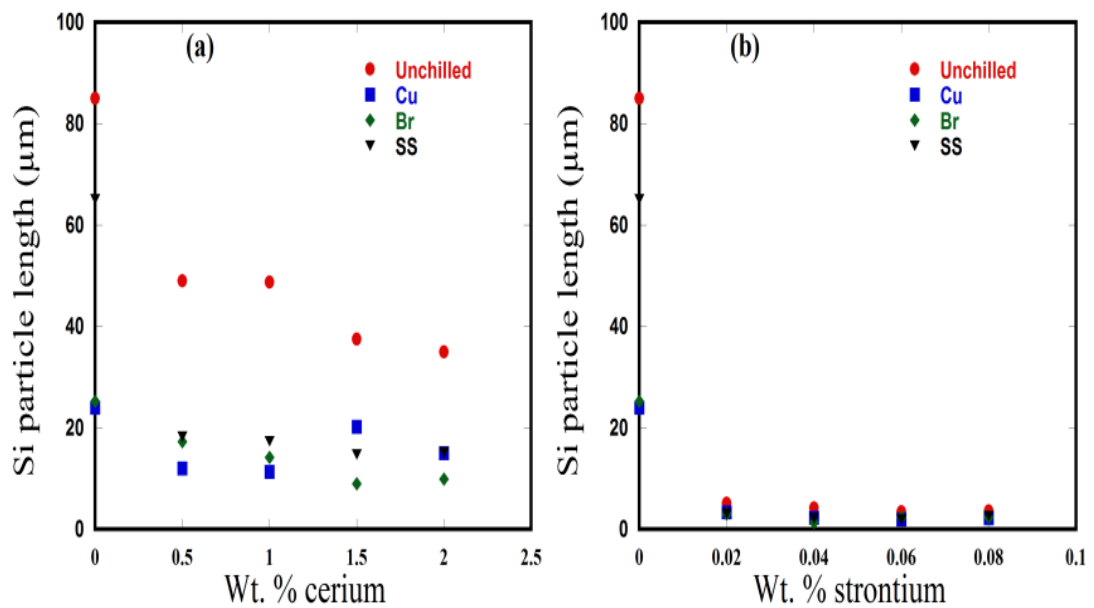


Figure 5.58 Variation of silicon particle characteristic with (a) Ce (b) Sr

The thermal analyses and microstructure analysis revealed that the nucleation pattern of the alloy had been altered on modification. Since the aluminum dendrites are nucleated prior to the silicon due to the poisoning of the silicon nucleation sites by the modification treatment. The eutectic silicon is forced to nucleate on aluminum and will be forced to grow between the dendritic arms. Moreover, the addition of modifiers hinders the growth of silicon by adsorbing on to the growth sites, increasing the twinning density of the silicon. The presence of modified silicon between the dendrite arm spacing shown in the Figure 5.59 is an evidence for the mentioned theory. The microstructure also shows the presence of intermetallic between the dendrites, Ce intermetallic in Ce modified alloys and Fe intermetallic in Sr modified alloys. This indicates that the modified eutectic Si did not nucleate on the Fe based intermetallic. The addition of Ce resulted in the formation of Ce based intermetallic involving Fe and Al and Si, restricting the formation of Fe intermetallic and making it unavailable for the nucleation of silicon. During eutectic solidification, the presence of Ce based intermetallics hinders the growth of the eutectic silicon to modify it.

Figure 5.60 shows the correlation between dimensionless parameter $\Delta T_G/\Delta T_N$ and eutectic roundness factor. The roundness factor decreases to 1 with increase in $\Delta T_G/\Delta T_N$ indicating the extent of eutectic modification.

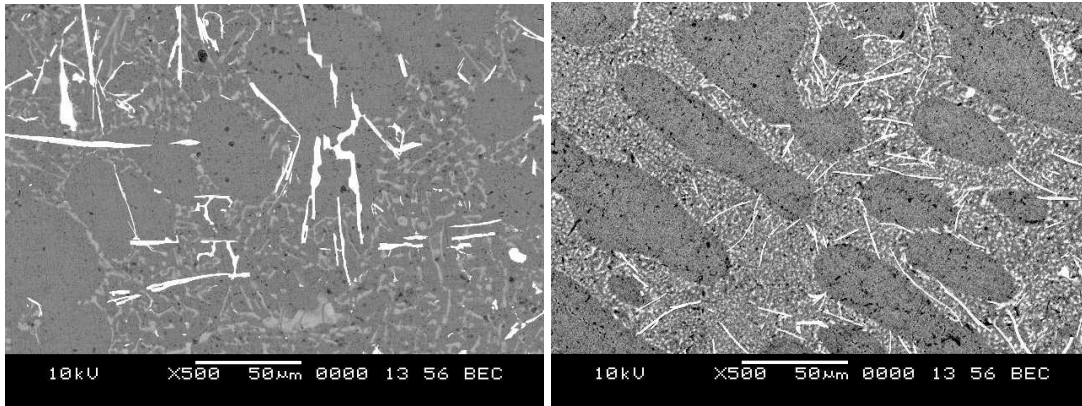


Figure 5.59 Microstructures of Al-13Si alloy after melt treatment (a) Ce modified (b) Sr modified

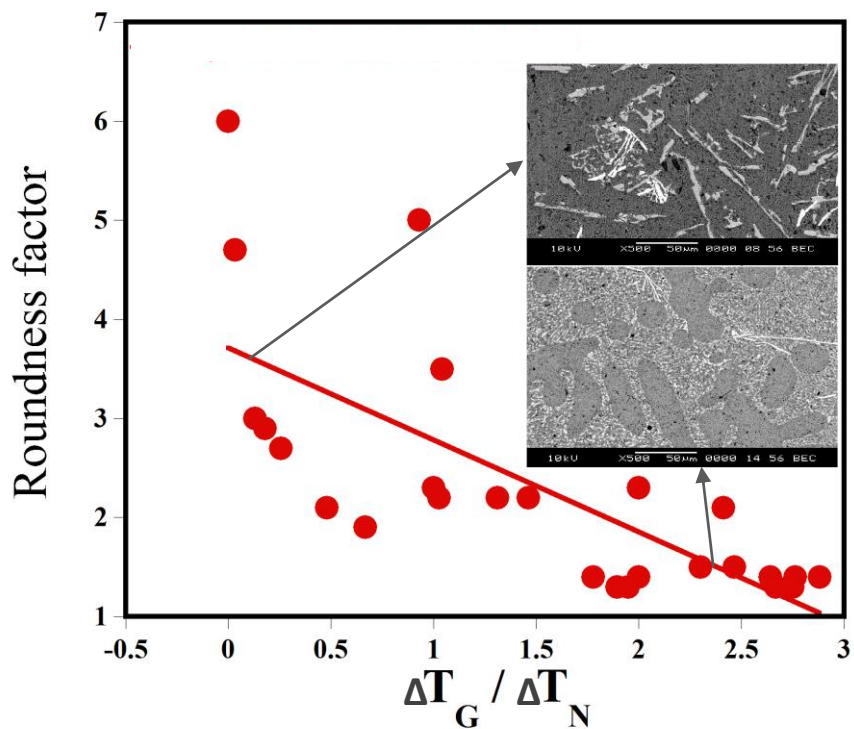


Figure 5.60 Correlation between thermal analysis parameter, $\Delta T_G/T_N$ and roundness factor of eutectic Si in Al-13Si alloy

5.4.3 Effect of Ce and P melt treatment on the microstructure characteristics of Al-14Si alloy

The microstructure of untreated and unchilled Al-14Si alloy consists of irregular shaped primary silicon in a eutectic matrix consisting of long needle-like eutectic silicon. During solidification, the silicon particles can grow into a wide variety of shapes depending on the cooling rate and undercooling of the melt. Unlike aluminum, which does not have a preferred growth direction, the growth of Si is carried out in an ordered manner. Silicon has a diamond cubic crystal structure and hence silicon has a strong tendency to facet in $\{111\}$ planes. The mechanism by which silicon grows in faceted manner is known as Twin Plane Reentrant Edge (TPRE) mechanism. According to this, a stable groove will be maintained at the surface of a twinned crystal and facilitates rapid growth in specific direction with a $\{111\}$ twin plane [Closset and Gruzleski 1982] [Lu and Hellawell 1995]. The primary silicon morphologies observed in cast microstructures of hypereutectic Al–Si alloy systems are quite diverse and vary significantly with growth velocity and thermal gradient. Depending on the solidification conditions such as cooling rate, presence of impurities and ease of nucleation, the silicon particles grow into different sizes and shapes. The coarser primary silicon in hypereutectic alloy is believed to form from highly undercooled melt, when there is prime shortage of external nucleation agent like AIP. As the melt cools, and under high undercooling conditions, the Si atoms clusters agglomerate to coarse primary silicon nucleus to form coarser primary silicon.

Figure 5.61 (b and c) shows the effect of Ce and P additions on the primary silicon size for various cooling conditions. The primary silicon size was measured from the microstructure as an equivalent diameter using an image analyzer. Both the additions decreased the primary silicon size for all cooling conditions. The additions also resulted in the transformation of primary silicon from irregular shapes into polygon shape and were distributed homogeneously along the microstructure.

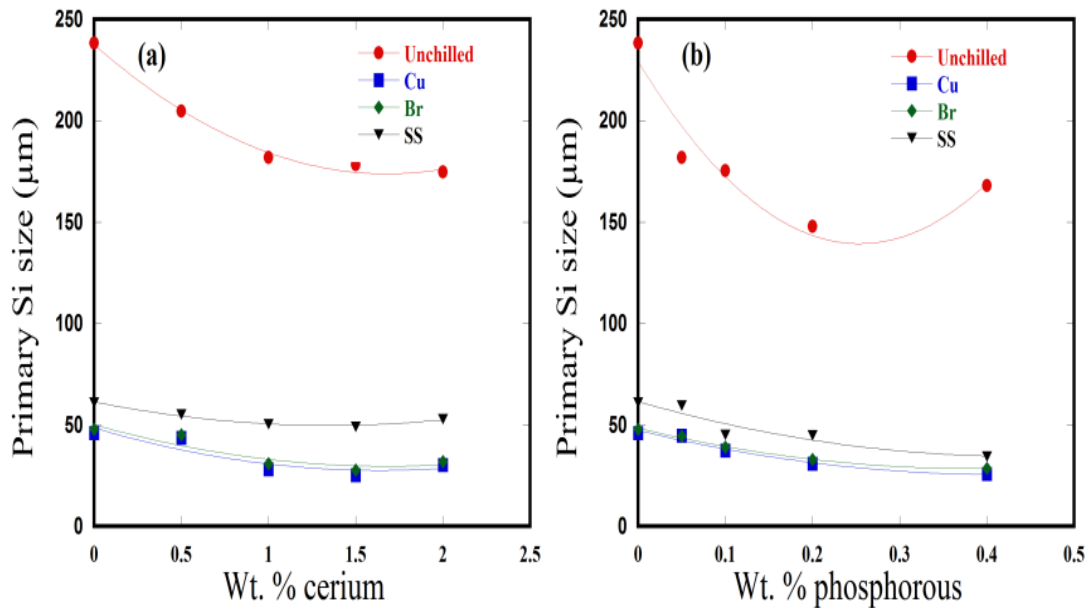


Figure 5.61 Variation of primary silicon characteristic with varying content of (a) Ce
(b) P

Studies show that the polyhedral types of morphologies of primary silicon are mainly found in hypereutectic alloys inoculated with phosphorous. Liang et al. (1995) studied the nucleation and growth of primary silicon and correlated the change in morphology of primary silicon in Al-18 %Si as a function of growth velocities, temperature gradient and cooling rates. For a cooling rate of 2.0 K/s and above, the shape of primary silicon was transformed to polyhedral shape.

The heterogeneous nucleation of polyhedral primary silicon on a substrate is dependent on the contact angle between each other and is a function of cooling rate. A contact angle of $30 \pm 4^\circ$ was found to be effective for heterogeneous nucleation of polyhedral primary silicon particles. Studies show that phosphorus satisfies the above criterion of contact angle at all slow solidification rates. An AIP particle in the melt greatly reduces the nucleation energy for the formation of primary silicon and enhances the growth in more regular shape with a uniform distribution. Xu and Jiang (2006) studied the effect of melt overheating temperature on morphology and reported that the primary silicon formed from a pouring temperature of 1,050 °C exhibited a

polygonal shape when compared to the irregular shape obtained at a pouring temperature of 850 °C. This change in morphology with temperature is due to the size of the Si–Si cluster formed as the nuclei of primary silicon. It is inferred that the “Si–Si cluster of larger size should be beneficial for the formation of star-like and other irregular morphologies and Si–Si cluster with smaller size should be beneficial for the formation of the nuclei of octahedral primary silicon”[Xu et al. 2006].

The addition of Ce was not found to form any nucleation sites for primary silicon instead it formed Ce intermetallic in the eutectic matrix between the primary silicon. Kores et al. (2010) and Zhang et al. (2006) found that the presence of cerium in the eutectic matrix. In the present alloy, based on the decrease in undercooling, size refinement achieved due to the addition of Ce and presence of Ce-based intermetallic in the microstructure, it can be deduced that the finer primary silicon are formed as the result of some invariant reaction between Si and Ce.

The effect of melt treatment of Al-14Si alloy by Ce and P on the eutectic silicon particle was assessed by the roundness factor. Table 5.12 shows the variation of silicon particle characteristics for various solidification condition and additions. The untreated alloy displayed largest particle characteristics (length, area and perimeter) and a roundness value of 7, indicates that the silicon particle is coarse and acicular nature. The addition of Ce to unchilled alloy did not show much effect on the acicular nature of the silicon particle, although the characteristic length was decreased by 38%. The untreated alloy solidified against chills showed a significant decrease in particle characteristics compared to unchilled alloys, but the acicular nature of the eutectic Si was least affected as the roundness factor more or less same.

Figure 5.62 (a and b) shows the effect of Ce and P additions on the eutectic Si particle characteristics. Even though both the additions (Ce and P) had similar effect on the primary silicon, but had varying effect on the eutectic silicon. While the addition of Ce significantly decreased the eutectic silicon characteristics to yield fine fibrous structure, the addition of P marginally decreased eutectic silicon characteristic.

Table 5.12 Eutectic silicon characteristics of Al-14Si alloys

	Wt.% Ce/P	Length (μm)	Aspect ratio	Area (μm^2)	Perimeter (μm)	Roundness factor
Unchilled	0	129 \pm 40	22	827 \pm 350	270 \pm 83	7
	0.5	92 \pm 50	13	490 \pm 180	200 \pm 100	6.5
	1	80 \pm 15	15	301 \pm 65	170 \pm 35	8
	1.5	86 \pm 18	16	319 \pm 90	182 \pm 42	8.3
	2	95 \pm 25	16	406 \pm 100	210 \pm 50	9
	0.05	110 \pm 40	20	750 \pm 280	255 \pm 120	6.9
	0.1	108 \pm 35	20	700 \pm 250	240 \pm 100	6.5
	0.2	105 \pm 23	18	680 \pm 200	250 \pm 100	7.3
	0.4	100 \pm 20	17	670 \pm 200	250 \pm 150	7.4
SS	0	19 \pm 7	7	52 \pm 18	44 \pm 16	5
	0.5	11 \pm 6	6	23 \pm 10	26 \pm 13	2.4
	1	5 \pm 2	3	9 \pm 3	13 \pm 5	1.75
	1.5	3 \pm 1	2	5.3 \pm 2.5	9 \pm 3	1.4
	2	2 \pm 1	1.2	3 \pm 0.5	8.6 \pm 2.5	1.8
	0.05	22 \pm 3	7.9	50 \pm 10	50 \pm 15	3.9
	0.1	20 \pm 2	7.4	40 \pm 8	46 \pm 10	4.2
	0.2	18 \pm 2	7.2	38 \pm 8	46 \pm 13	4.4
	0.4	15 \pm 3	6.5	36 \pm 10	45 \pm 15	4.4
Brass	0	10 \pm 2	7	12 \pm 3	23 \pm 6	3.5
	0.5	3.2 \pm 1.5	2.6	3.2 \pm 1	9 \pm 3.5	2
	1	2.3 \pm 0.5	1.5	3 \pm 1	8 \pm 2	1.7
	1.5	2.2 \pm 0.5	1.3	2.5 \pm 1	8 \pm 2	1.7
	2	1.8 \pm 0.2	1.1	1.9 \pm 0.3	6.7 \pm 1	1.8
	0.05	8 \pm 1	5.3	10 \pm 2	20 \pm 5	3.18
	0.1	6 \pm 1	4.3	6.4 \pm 2	18 \pm 4	4.03
	0.2	5 \pm 1	3.8	6 \pm 2	16 \pm 3	3.39
	0.4	5 \pm 1.5	3.8	5 \pm 2	16 \pm 3	4.07
Copper	0	7.5 \pm 2.5	5.6	7 \pm 2	18 \pm 6	4
	0.5	2 \pm 0.5	1.2	3.2 \pm 1.0	7.5 \pm 1	1.36
	1	1.5 \pm 0.3	1.1	1.8 \pm 0.4	5.8 \pm 0.7	1.45
	1.5	1.3 \pm 0.2	1	1.4 \pm 0.3	5.2 \pm 0.7	1.47
	2	1.6 \pm 0.2	1.1	2 \pm 0.8	6.2 \pm 2	1.5
	0.05	6 \pm 1	3.0	6.4 \pm 2	16 \pm 3	3.1
	0.1	5 \pm 1	2.4	4 \pm 1	12 \pm 3	2.8
	0.2	4.5 \pm 1	2.5	3.8 \pm 1	12 \pm 2	3
	0.4	4 \pm 1	2.2	3.7 \pm	14 \pm 3	4.2

The addition of Ce to chilled alloys resulted in further decrease in particle characteristics. The characteristic length decreased to $2\mu\text{m}$ from $19\mu\text{m}$ with addition of 1.5% Ce to SS chilled alloys. This was true for the alloys solidified in copper and brass chills as well. Subsequently, the roundness factor of the particle also decreased due to the additions, yielding fine fibrous structure of eutectic Si.

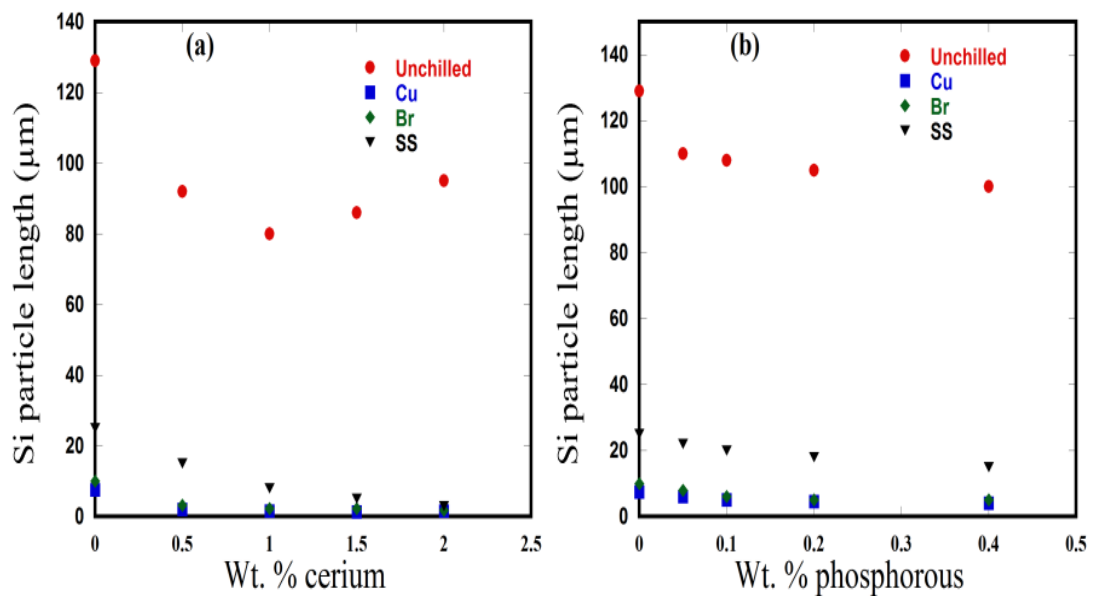


Figure 5.62 Variation of eutectic silicon characteristic with varying content of (a) Ce
(b) P

The roundness factor approached unity with varying content of Ce depending on the thermal conductivity of the chill. For example, addition of 1.5% Ce to the alloy solidified against SS chill resulted in a reduction of the roundness factor from 4.3 to 1.4. This indicates that the eutectic Si particle has become more spherical with addition of Ce compared to Si in the untreated alloy. The addition of P did not show any significant effect on the morphology of the eutectic silicon. The roundness factor remained more or less the same, indicating that the acicular nature of eutectic Si is least affected by the addition of P.

The nucleation mechanism of eutectic silicon in hypereutectic alloys is very much different than in the hypoeutectic alloys. In hypereutectic alloys, since the primary silicon is precipitated prior to the eutectic silicon, it is thought that the eutectic Si is

nucleated from the primary silicon. The addition of P will form AlP and refine the primary silicon and the refined primary silicon will form a well-proportioned nucleation sites for eutectic silicon [Wu et al. 2010]. In the presence of favorable nucleation sites, the eutectic silicon nucleate easily from less undercooled melt and grow as coarser silicon. This is also evident in the present alloy, the nucleation of the eutectic phase in the base alloy occurred from the less undercooled melt to precipitate coarser acicular Si. The decrease in undercooling with addition of P shown in Table 5.3 indicates the ease with which eutectic silicon nucleated and grown as faceted Si. For example, with addition of 0.1P to untreated alloy decreased the undercooling from 7.2 to 2.5°C.

On the other hand, the addition of Ce resulted in simultaneously refinement and modification of primary and eutectic silicon. Unlike P, the addition of cerium did not favor the nucleation of the eutectic silicon, instead it suppressed the nucleation of eutectic Si. The decrease in the eutectic nucleation temperature and increase in undercooling with Ce addition was due to this non favorable condition. In the presence of Ce the eutectic silicon are not nucleated on the primary silicon, instead it was nucleated homogenously from a highly undercooled melt. According to Lu and Hellawell (1995), the best modification effect is achieved when the ratio of atomic radius of the modifying agent and atomic radius of Si is closer to 1.65. The radii ratio (R_{Ce}/R_{Si}) for cerium and silicon is 1.56 and is near to 1.65. Hence, the presence of Ce in the melt would hinder the growth of the silicon to yield fine fibrous structure.

Figure 5.63 shows the relation between dimensionless parameter and roundness factor of Al-14 Si alloy. The $\Delta T_G/\Delta T_N$ increased with increase in Ce concentration and cooling rate, decreasing the roundness factor roundness factor. The microstructure of Ce melt treated alloy with lowest roundness factor is shown in the Figure. The roundness factor of P treated alloys was more or less same as that of untreated alloys.

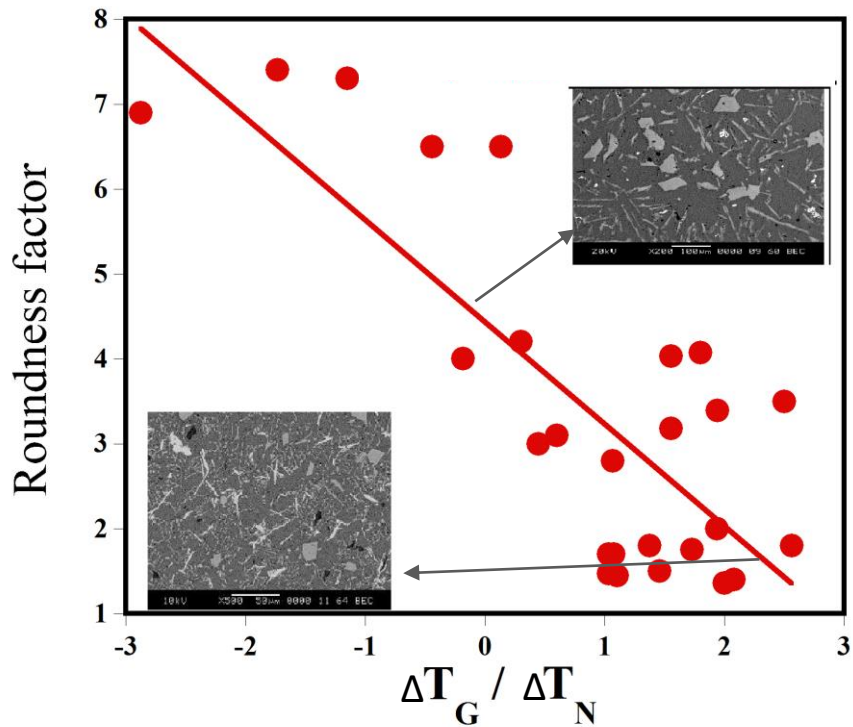


Figure 5.63 Correlation between thermal analysis parameter $\Delta T_G / \Delta T_N$ and roundness factor of eutectic Si in Al-14Si alloy

5.4.4 Effect of Ce and P melt treatment on microstructure characteristics of Al-22 Si alloy

The microstructure of untreated Al-22Si alloy consists of star shaped primary silicon and coarser eutectic Si. Studies reveal that the five-fold branched crystals grow from the decahedral nucleus, which consists of five silicon tetrahedrons in a twin orientation and share a common $\langle 110 \rangle$ axis. The growth of the crystal through branches can be well explained by TPPE mechanism, where a stable groove of 141° is maintained between the twinned planes and the nucleation occurs through the groove. An ideal decahedral nucleus offers four coordinated sites for nucleation with one twin plane at the center of each branch forming a 141° single groove at the branch tip. At ideal conditions the branch formed so will exhibit a re-entrant groove and continue to grow until the grooves are filled up. The nucleation and growth of star-like primary silicon mainly depends on the under cooling achieved and solidification rates [Pei and Hosson 2001]. Pei and Hosson (2000) found that the primary silicon

particles nucleated and grew within in the undercooled melt ahead of the solidification interface and continued to grow as long as the imposed undercooling was maintained. [Kang et al. 2005] characterized the primary silicon morphologies for increasing undercooling and concluded that the star-like primary silicon was obtained at lower undercooling. The formation star-like primary silicon increased with increase in Si and as the undercooling increases beyond a critical value star-like silicon transforms to massive silicon crystals.

The effect of Ce and P melt treatment on the primary silicon particle size is shown in the Figure 5.64. The particle size is measured as an equivalent diameter using image analysis software. The primary silicon size was found to decrease with both kinds of additions for all cooling conditions. The additions had transformed the coarser star shaped primary silicon into fine polyhedral shaped crystals. The refinement was more significant with the additions to chilled alloys. Thermal analyses results and microstructure characterization shows that the transformation of primary silicon from star shaped crystals to polyhedral crystals occur at lower undercooling, which contradicts the conclusion of [Kang et al. 2005]. Certainly, their studies did not consider the nucleation of primary silicon from heterogeneous nucleation sites at low undercooling. In the present alloy, both additions yielded polyhedral primary silicon from less undercooled melt. Hence it can be inferred that the additions had led to the heterogeneous nucleation of primary silicon. The addition of P will form AlP in the melt, a favorable nucleation site for silicon, whereas, there is no reported literature on Ce nucleating silicon.

The effect of Ce and P melt treatment on eutectic Si was assessed by quantifying the silicon particle characteristics. The silicon particle characteristics for varying concentrations of Ce and P and for different solidifying condition are given in Table 5.13. Figure 5.65 (a and b) shows the variation of eutectic silicon particle size with varying content of Ce and P. The addition of Ce to unchilled alloy resulted in significant decrease in eutectic silicon size compared to chilled alloys and the roundness factor also decreased attributing to the modification of eutectic silicon.

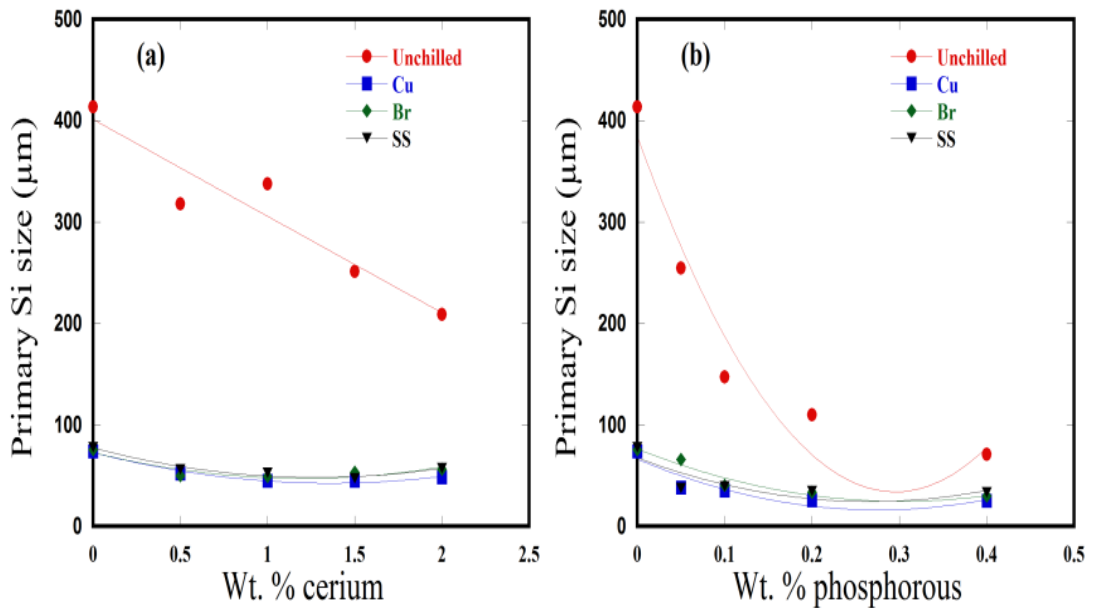


Figure 5.64 Variation of primary silicon size with varying content of (a) Ce (b) P

The addition of Ce and P to chilled alloys did not affect significantly the eutectic silicon. The reason for this is the refinement of primary silicon and subsequent nucleation of eutectic silicon from refined primary silicon. The decrease in the eutectic undercooling with addition of Ce and P to chilled alloys is an evidence for this theory. A similar kind of relation between the nucleation of primary silicon and eutectic silicon was reported by Wu et al. (2010). They reported that the acicular morphology of the silicon particle increased as the refinement of primary silicon increased.

Unlike other alloys, the dimensionless parameter did not show any relation with eutectic roundness factor in Al-22Si alloy, as both the additions did not modify the eutectic silicon. Since both the melt treatment had influenced the primary silicon nucleation temperature and primary silicon size, a correlation was obtained between ΔT_G and primary silicon characteristic parameter as shown in the Figure 5.66. The primary silicon characteristic parameter was defined as the ratio of equivalent diameter of the refined primary silicon to the equivalent diameter of the unrefined primary silicon. The characteristic parameter could be used to assess the extent of refinement of primary silicon.

Table 5.13 Eutectic silicon characteristics of Al-22Si alloy

	Wt.% Ce/P	Length (μm)	Aspect ratio	Area (μm^2)	Perimeter (μm)	Roundness factor
Unchilled	0	80 \pm 30	13.3 \pm 2	250 \pm 50	150 \pm 30	7.16
	0.5	70 \pm 10	10.0 \pm 1	220 \pm 20	130 \pm 10	6.11
	1	65 \pm 5	8.1 \pm 1	200 \pm 20	124 \pm 5	6.12
	1.5	65 \pm 5	7.2 \pm 1	190 \pm 10	120 \pm 4	6.03
	2	68 \pm 8	7.6 \pm 1	198 \pm 10	123 \pm 5	6.08
	0.05	75 \pm 10	13.6 \pm 1	230 \pm 10	145 \pm 6	7.27
	0.1	70 \pm 8	14.0 \pm 1.2	225 \pm 15	148 \pm 5	7.74
	0.2	70 \pm 5	14.0 \pm 1	225 \pm 10	150 \pm 4	7.96
SS	0	40 \pm 15	8.0 \pm 1.8	120 \pm 20	90 \pm 15	5.37
	0.5	38 \pm 10	6.3 \pm 0.6	115 \pm 10	90 \pm 8	5.60
	1	35 \pm 5	6.4 \pm 0.5	110 \pm 8	88 \pm 5	5.60
	1.5	30 \pm 5	6.3 \pm 0.4	110 \pm 10	90 \pm 4	5.86
	2	30 \pm 5	6.7 \pm 0.2	108 \pm 12	92 \pm 3	6.23
	0.05	38 \pm 6	8.4 \pm 0.6	120 \pm 10	100 \pm 10	6.63
	0.1	37 \pm 4	8.6 \pm 0.8	115 \pm 8	98 \pm 10	6.64
	0.2	35 \pm 3	8.3 \pm 0.4	115 \pm 5	100 \pm 10	6.92
Brass	0	20 \pm 10	6.7 \pm 1.5	50 \pm 10	50 \pm 10	3.98
	0.5	19 \pm 5	6.6 \pm 0.6	45 \pm 5	52 \pm 5	4.78
	1	18 \pm 4	6.4 \pm 0.4	40 \pm 6	50 \pm 2	4.97
	1.5	18 \pm 4	6.4 \pm 0.5	38 \pm 4	50 \pm 3	5.23
	2	19 \pm 3	6.6 \pm 0.5	36 \pm 2	49 \pm 2	5.31
	0.05	20 \pm 5	7.1 \pm 1.2	48 \pm 3	50 \pm 5	4.14
	0.1	18 \pm 6	7.2 \pm 1	47 \pm 2	52 \pm 3	4.58
	0.2	17 \pm 5	7.1 \pm 0.8	45 \pm 2	55 \pm 4	5.35
Copper	0	16 \pm 5	5.3 \pm 1	20 \pm 5	30 \pm 8	3.58
	0.5	14 \pm 3	6.4 \pm 0.8	18 \pm 2	30 \pm 2	3.98
	1	14 \pm 2	6.7 \pm 0.8	16 \pm 1	30 \pm 1	4.47
	1.5	12 \pm 3	6.7 \pm 1.5	15 \pm 0.5	30 \pm 1	4.77
	2	12 \pm 3	7.1 \pm 0.4	15 \pm 1	30 \pm 1.5	4.77
	0.05	15 \pm 4	6.8 \pm 0.6	18 \pm 1	31 \pm 2	4.25
	0.1	14 \pm 3	7.0 \pm 0.5	17 \pm 1.5	32 \pm 1.5	4.79
	0.2	14 \pm 2	7.4 \pm 0.8	16 \pm 2	33 \pm 1.5	5.41
	0.4	14 \pm 2	7.4 \pm 0.6	16 \pm 1	33 \pm 1	5.41

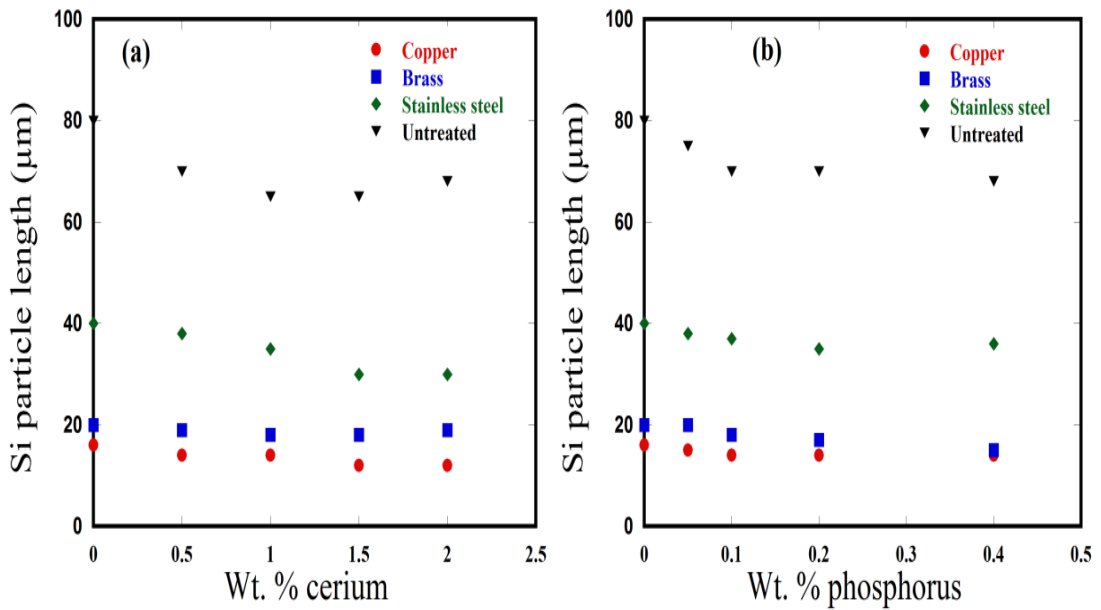


Figure 5.65 Variation of eutectic silicon characteristic with varying content of (a) Ce
(b) P

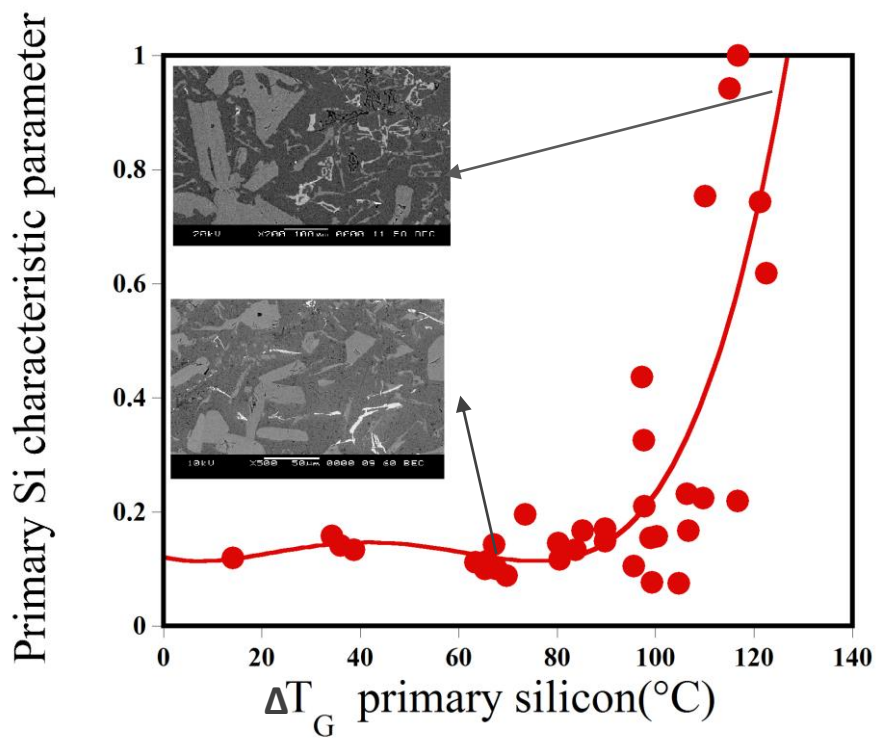


Figure 5.66 Correlation between thermal analysis parameter, ΔT_G and the primary silicon characteristic parameter in Al-22 Si alloy

5.5 Effect of Ce and Sr/P on the Mechanical Properties of Al-Si Alloys

5.5.1 Al-8Si alloy

Figures 5.67 and 5.68 shows the effect of Ce and P melt treatment on ultimate tensile strength and percentage of elongation of Al-8Si alloys. Among all, the untreated and slowly solidified alloy showed the lowest tensile strength, however a marginal increase in strength was observed with increase in cooling rate. The untreated Al-8% Si alloy solidified on copper mold showed a tensile strength and percentage elongation of 106 ± 6 MPa and 1.73 ± 0.2 respectively. The low strength of alloys is due to the unrefined and unmodified microstructure. The presence of large concentrations of Fe will also degrade the mechanical properties of the alloy due to formation of Fe based intermetallic, which act as stress raisers when exposed to tensile load.

The addition of Ce and Sr significantly improved the tensile strength as well as the percentage elongation of the alloy. The addition of 1 wt% Ce to copper mold yielded an ultimate strength and percentage elongation of 173 ± 3 MPa and 4.2 ± 0.1 respectively. Further increment in the cerium content showed a decrement in the strength and elongation. The addition of 1.5wt% Ce and 0.06 wt.% Sr to SS mold yielded maximum tensile strength of 180 ± 4 and 182 ± 2 MPa respectively. Even though there was a significant improvement in percentage of elongation with Ce addition, a considerable improvement was observed only at higher cooling rates, whereas, a constant increase in elongation was observed with Sr additions irrespective of the cooling conditions.

The mechanical properties of the Al-Si are affected by many factors which are related to microstructure constituents. Suarez-Pena and Asensio-Lozano (2006) reviewed few possible factors which have direct influence on the strengthening mechanisms and the mechanical properties. The hypoeutectic Al-Si alloys invariably consists of aluminum and eutectic phase, the α -Al forms the part of eutectic as well. The hard Si particles in the eutectic grow with acicular nature and confer the ductility of the alloy.

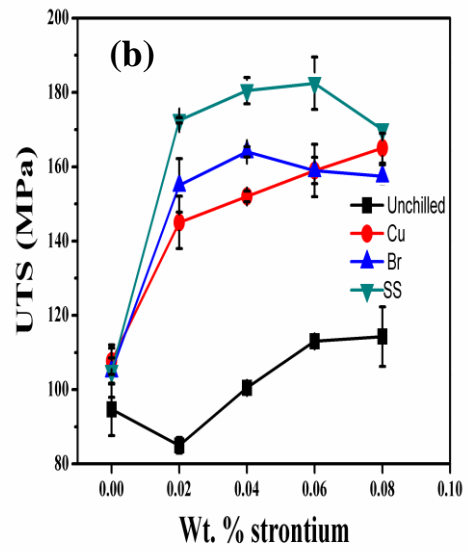
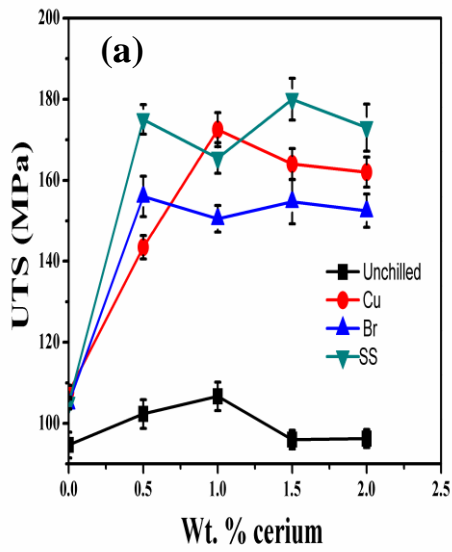


Figure 5.67 Variation of ultimate tensile strength with melt treatment (a) with Ce (b) with Sr

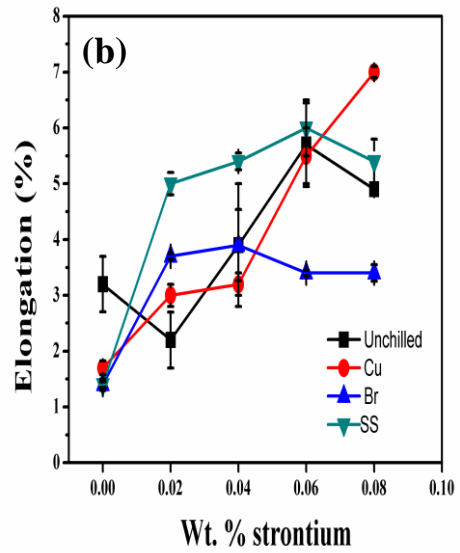
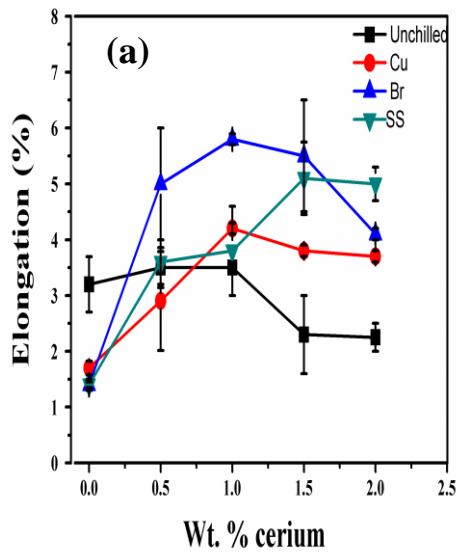


Figure 5.68 Variation of percentage of elongation with melt treatment (a) Ce (b) Sr

The presence of softer aluminum and harder silicon particle in the microstructure causes anisotropic distribution of the applied stress. This leads to a rapid strengthening of the alloy as α -Al/Si interfaces obstructs the easy movement of dislocation and promotes dislocations pile up. As a result, cleavage micro-cracks are observed on the fracture surfaces. The acicular morphology acts as the stress raisers at the edge of the softer phase promoting brittle fracture. In addition, the low interfacial bonding between α -Al and Si favors the growth of the crack, which proceeds easily through the soft aluminum phase. The modification of eutectic Si leads to the formation of globular Si particles, which considerably enhances the mechanical properties by evenly distributing the stress around the Si particle. This geometry change also leads to the disappearance of stress raisers. Subsequently, leads to the isotropic distribution of the stress along the soft aluminum and hard silicon phases.

Figure 5.69 shows the SEM micrographs of fractured surface before and after the melt treatment. It is clear from the Figure 8 (a) that the untreated alloy showed bright cleavages, a characteristic feature of brittle failure. The addition of Ce or Sr had transformed the failure mode into ductile with dimples on the fracture surface as seen in the Figure 5.69 (b and c). The addition of Ce resulted in a clear ductile fracture with dimples on the fractured surface.

Figure 5.70 shows the variation of hardness with addition of varying content of Ce and Sr. Both the additions were found to improve the hardness of the alloy. The addition of 1 wt. % Ce showed a maximum improvement in the hardness when compared with untreated alloy. The hardness of the Al-Si alloys is influenced by the distribution and morphology of the eutectic silicon in the alloy. Studies show that the improvement attained due to the addition of Sr was because of the fine fibrous silicon structure achieved due to modification [Fatahalla et al. 1999]. Similarly, the improvement in Ce melt treatment alloys would be due to the modified silicon and also due to the refinement of α -Al.

The improvement in properties with Ce treated alloys was because of the combined effect of grain refinement, modification and presence of Ce based intermetallic in the

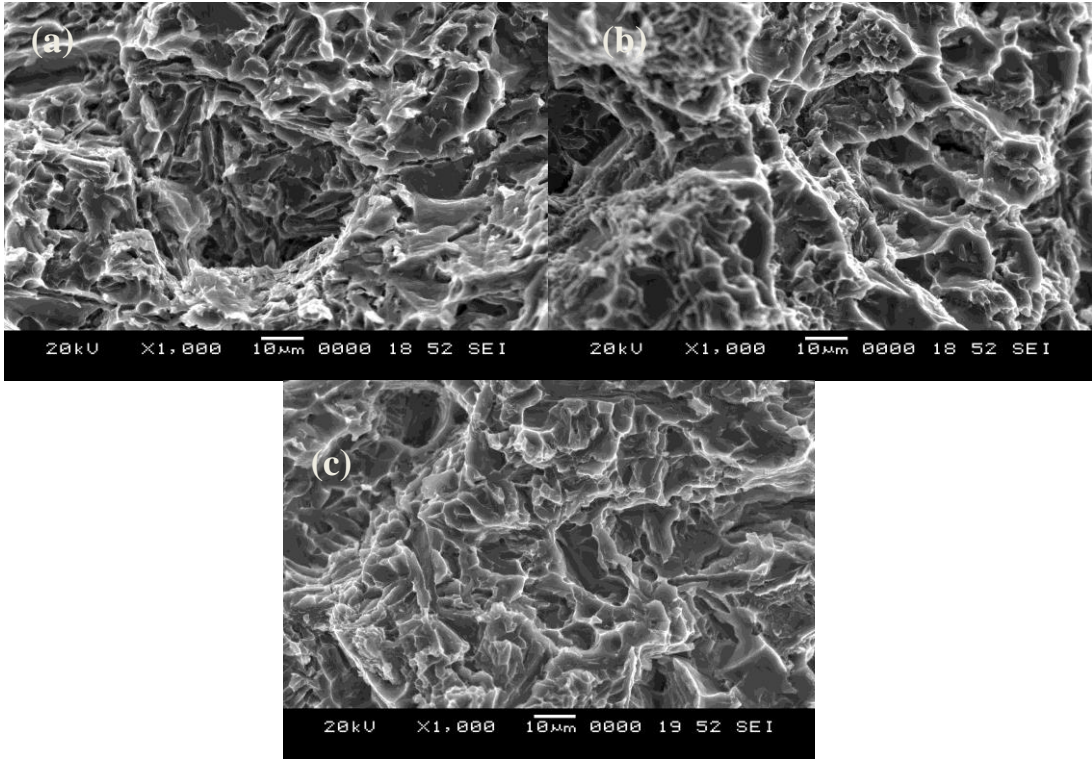


Figure 5.69 SEM micrographs of fractured surface (a) untrated (b) Ce treated (c) Sr treated

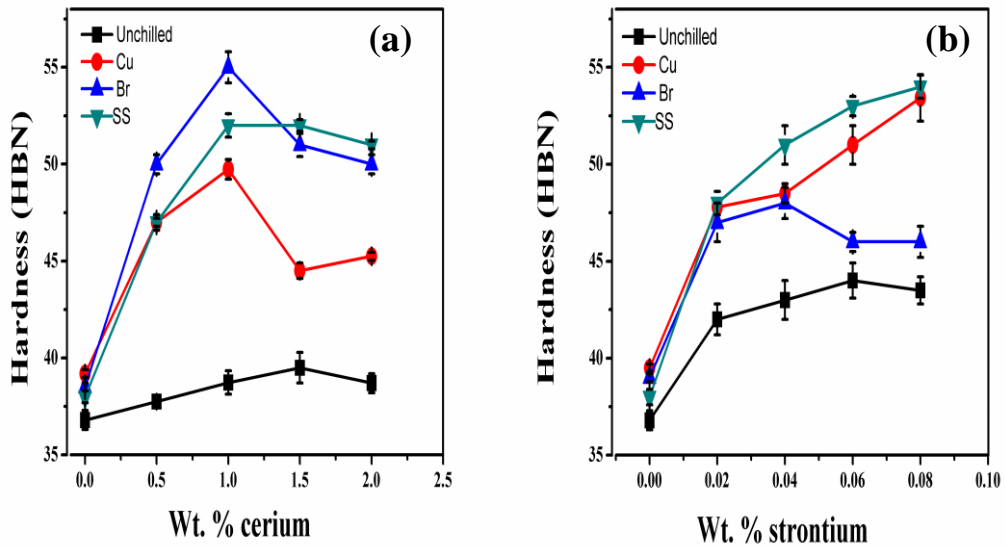


Figure 5.70 Effect of varying content of addition on the hardness of the alloy (a) Ce (b) Sr

microstructure. In the present study, the two processes, refinement and modification occur simultaneously to improve the properties. Moreover, the added Ce combines with Fe, Al and Si to form an intermetallic and it is believed to consume all the Fe present in the alloy, as no separate Fe phase was visible in the microstructure. Hence, it can be inferred that the formation of Ce based intermetallic has nullified the deleterious effect of Fe intermetallic. The decrease in mechanical properties with higher concentration of Ce would be due to the coarsening of the intermetallic formed. On the other hand, the improvement with Sr addition is solely because of modification.

5.5.2 Al-13Si alloy

Figure 5.71 (a and b) shows the effect of Ce and Sr melt treatment on the ultimate tensile strength of the Al-13Si alloy. The percentage of elongation is shown in Figure 5.72 (a and b). The both additions significantly enhanced the tensile properties when solidified against metal molds. The improvement was mainly due to the high degree of eutectic modification achieved at higher cooling rate. The lesser influence of the high concentration Ce on tensile properties of slowly cooled alloys was mainly due to the inefficiency of the Ce in modifying eutectic silicon and the formation of blocky shaped Ce intermetallic as shown in the Figure 5.73. The Ce treatment was found to be more effective when solidified against brass mold. The influence of Ce was highly influenced by the cooling rates, at slower cooling rates the Ce forms coarser intermetallic particles and at higher cooling rates very few intermetallic was formed as the diffusion of Ce was hindered by fast moving solidification front. At moderate cooling condition, right amount of intermetallic forms with needle-like morphology and would result in the modification of the eutectic silicon. The effectiveness of the Sr modification was less dependent on the cooling rates. The tensile properties were enhanced by Sr modification even under slow solidifying condition. This was due to the direct interaction of Sr atoms with silicon growth sites [Closset and Gruzleski 1982]. Unlike Ce modification (where the modification dependent on the intermetallic formed), the Sr atoms modifies the eutectic silicon by hindering the growth of the silicon. It is solely

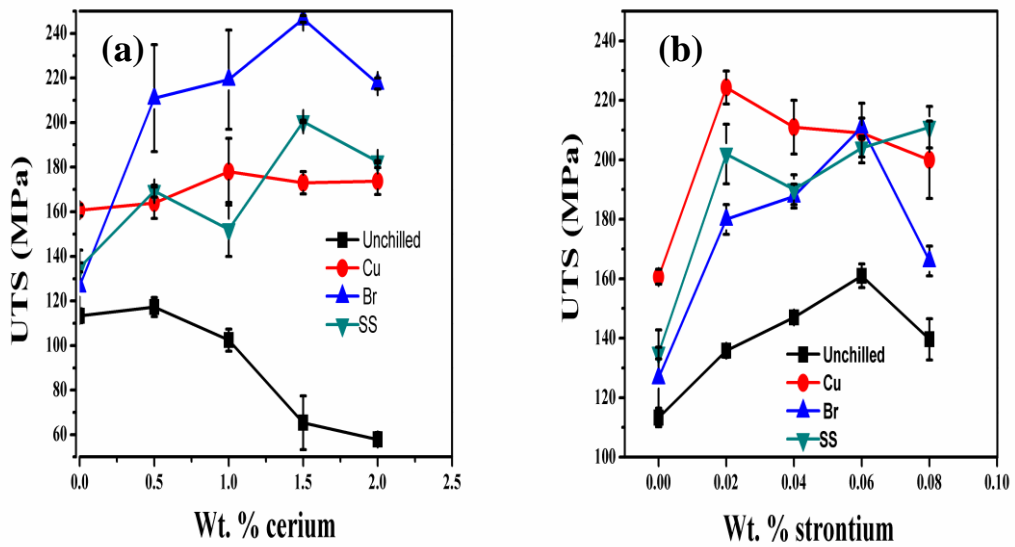


Figure 5.71 Variation of ultimate tensile strength with melt treatment (a) with Ce (b) with Sr

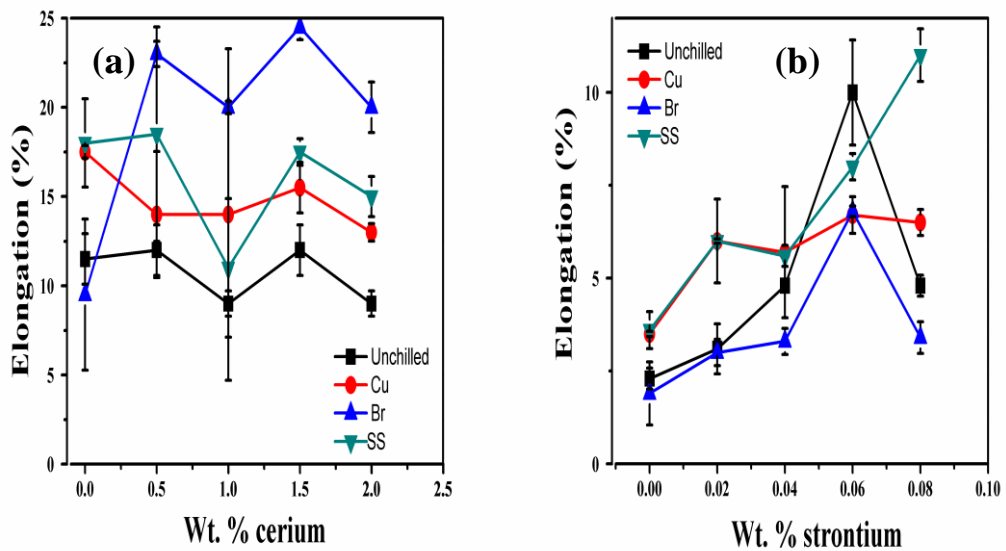


Figure 5.72 Variation of percentage of elongation with melt treatment (a) with Ce (b) with Sr

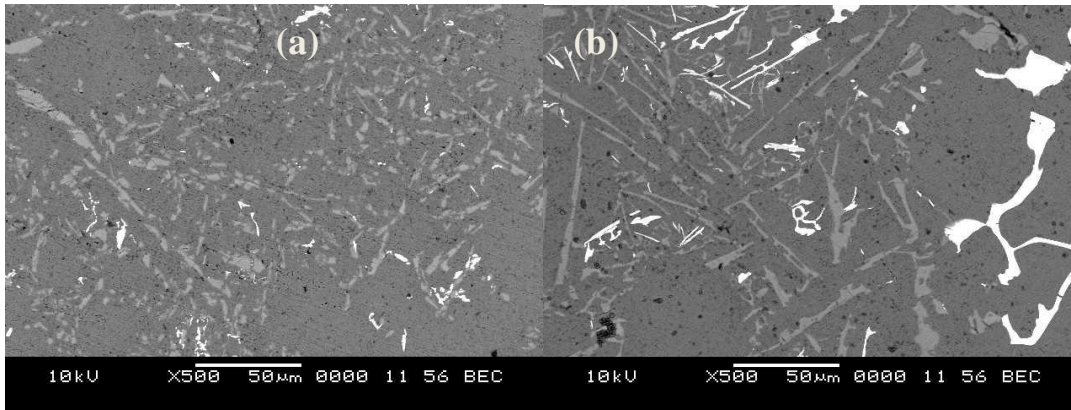


Fig. 5.73 Variation in Ce intermetallic morphology with cooling rate (a) copper chilled (b) SS chilled

dependent on the presence of optimum concentration of Sr atoms in the melt and not on the cooling rate. A similar trend was observed with hardness of the alloy as displayed in the Figure 5.74. The hardness increased substantially with both the additions due to the modification. The hardness values of Ce treated varied with cooling rate, whereas, hardness values Sr treated alloys was less affected by the cooling rates.

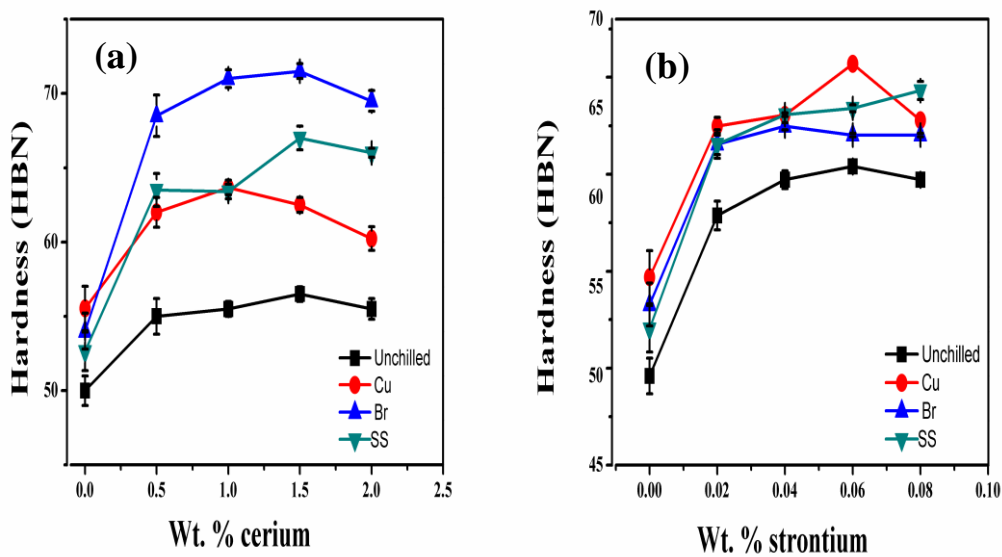


Figure 5.74 Effect of varying content of addition on the hardness of the alloy (a) Ce (b) Sr

5.5.3 Al-14Si alloy

Figure 5.75 (a and b) shows the influence of Ce and P melt treatment on the ultimate tensile strength of the Al-14Si alloy. Subsequently, Figure 5.76 shows the effect of melt treatment on the percentage of elongation and Figure 5.77 shows the effect of Ce and P treatments on the hardness of the alloy.

The mechanical properties of the hypereutectic Al-Si alloys are mainly dependent on the size and shape of primary silicon and eutectic silicon. It is reported that the fracture mechanism of Al-Si alloys depends on three factors [Zhou and Duszczkyk 1990]. (1) Size and distribution of Si particles in the matrix (2) bonding strength between the hard silicon particles and soft aluminum (3) ease with silicon crystals crack [Li et al. 2013]. The stress concentration and cracking of the silicon crystals are dependent on the morphology of the crystals. Larger and irregular crystals causes stress concentration at the Al/Si interface during tension.

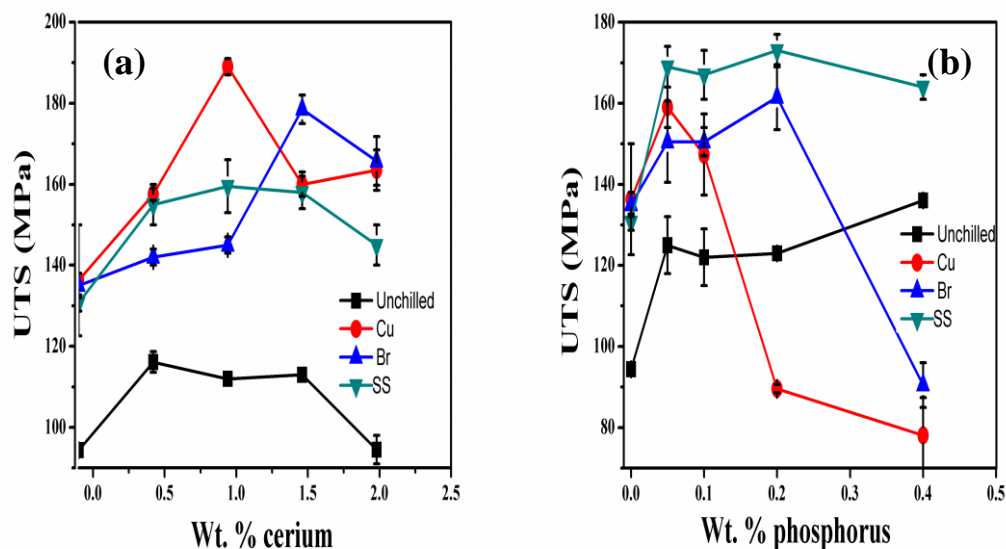


Figure 5.75 Variation of ultimate tensile strength with melt treatment (a) with Ce (b) with P

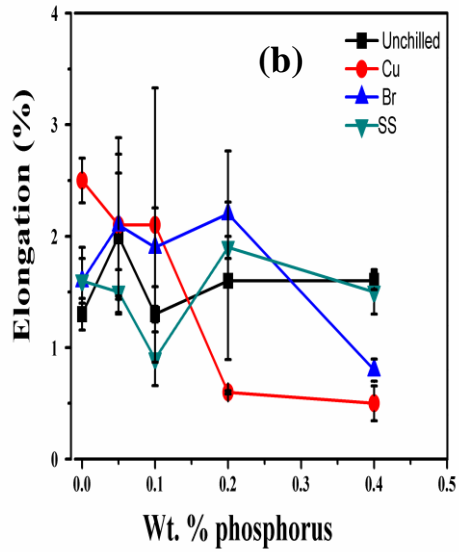
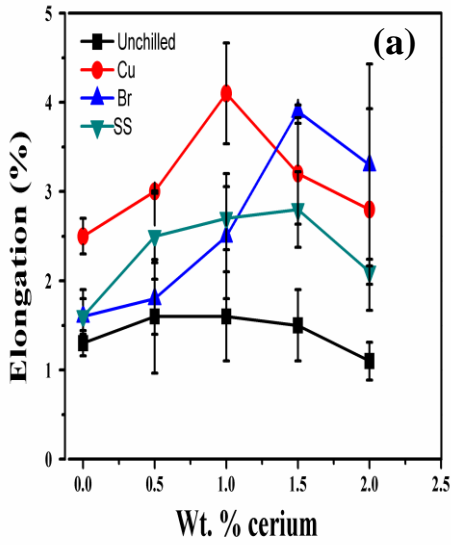


Figure 5.76 Variation of percentage of elongation with melt treatment (a) with Ce (b) with P

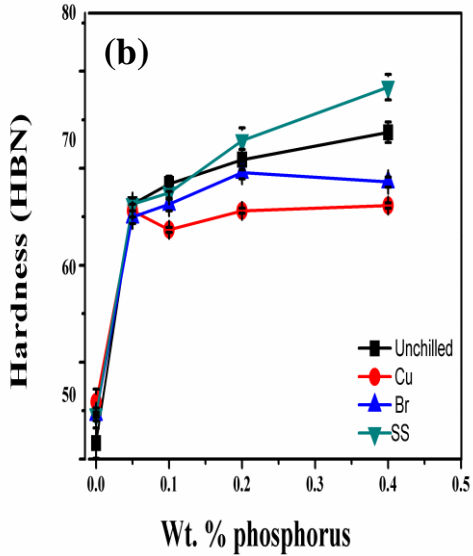
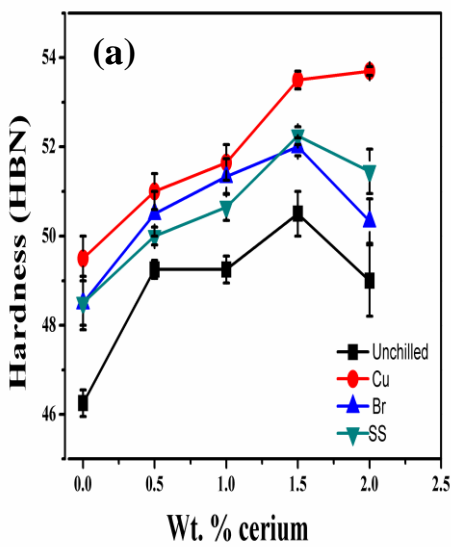


Figure 5.77 The effect of varying content of addition on the hardness of the alloy (a) Ce (b) P

As a result, the cracks are easily initiated within the crystals causing the debonding of the Si particles from the matrix. Subsequently, during deformation the cracks propagate through the grain boundaries and lead to a brittle fracture [He et al. 2010]. The refinement of primary silicon can improve the mechanical properties by decreasing the stress around the silicon crystal. The refinement process will lead to the formation of smaller and regular shaped crystal, which improves bonding of silicon with matrix. The mechanism is same with eutectic Si as well, acicular Si will act as the stress concentrators and initiators of the crack, on modification the stress will be evenly distributed around the particle. In addition, when the particles are finer, the cracks pass around the primary or eutectic silicon. The cracks pass through the particles when they are larger. Therefore, a significant improvement in the tensile properties can be obtained by controlling the size of the microstructure constituents

In the present study, both the additions had resulted in the refinement of primary silicon and improvement in the tensile strength. The refinement of the primary silicon improved with the increase in cooling rate. A lower tensile strength was observed with P treated alloys at higher concentration of P. The reason for this would be the over addition of P, higher than the optimum concentration. High concentration of P had negative effect on the ductility as well, as the acicular nature of the eutectic silicon will be increased with P. The addition of Ce increased the strength as well and the ductility of the alloy. The improved tensile properties were mainly due to the ability of Ce in achieving simultaneous refinement and modification. It was evident from the microstructure analysis that the addition of Ce to Al-14Si alloy yielded finer primary silicon and modified eutectic silicon.

The P treated alloys showed higher hardness values than the Ce treated alloys. The number of the primary silicon increases with P treatment resulting in finer and evenly distributed silicon cuboids along the microstructure [Ghomashchi 2004]. Similarly, P treatment of the present alloy also increased the number of Si particles along with refinement, and thereby increasing the hardness of the alloy. The hardness of the Ce treated alloy was majorly contributed by eutectic modification, which increased with cooling rate.

5.5.4 Al-22Si alloy

The mechanical properties of the high silicon content hypereutectic Al-Si alloys are determined by the size and shapes of the primary silicon. The refined octahedral shaped primary silicon would yield better mechanical properties than the segregated star shaped or irregular silicon primary silicon crystals [Dwivedi et al. 2005]. In the present study, the presence of star shaped crystals in the slowly cooled alloys had resulted in lower tensile properties of the alloy as shown in Figures 5.78 and 5.79. Subsequently, Figure 5.80 shows the variation of hardness of the alloy with melt treatment. The improvement in mechanical properties with melt treatment was due to the transformation of the primary silicon to polyhedral silicon crystals.

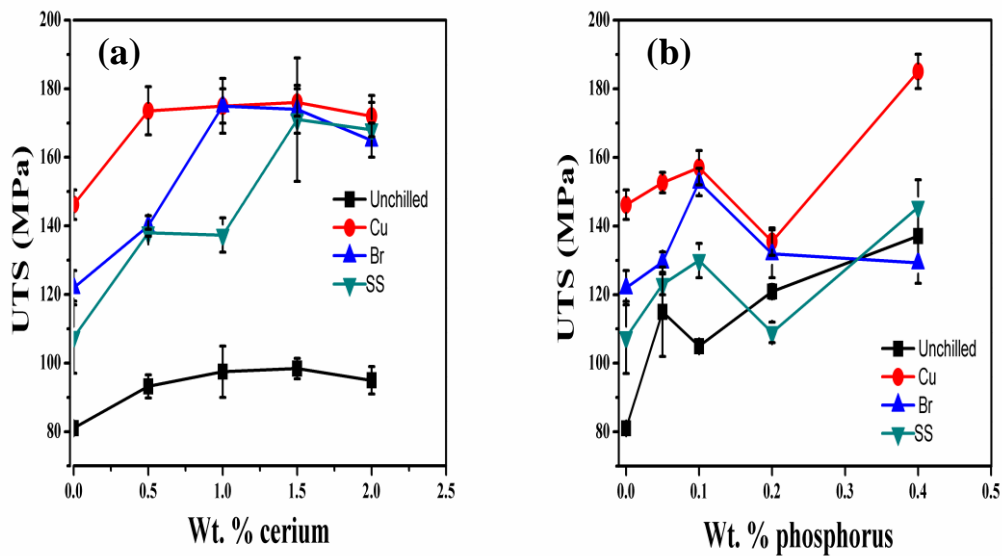


Figure 5.78 Variation of ultimate tensile strength with melt treatment (a) with Ce (b) with P

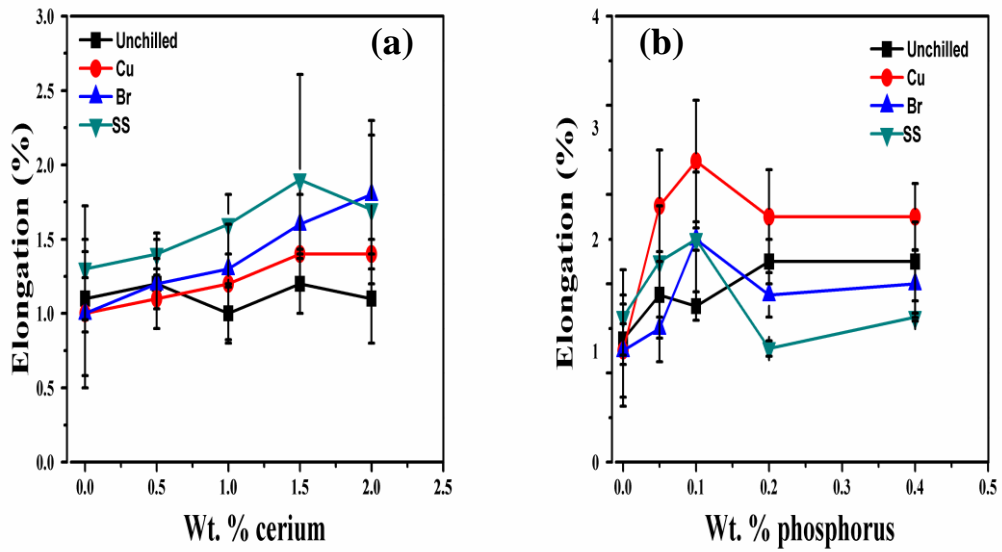


Figure 5.79 Variation of ultimate tensile strength with melt treatment (a) with Ce (b) with P

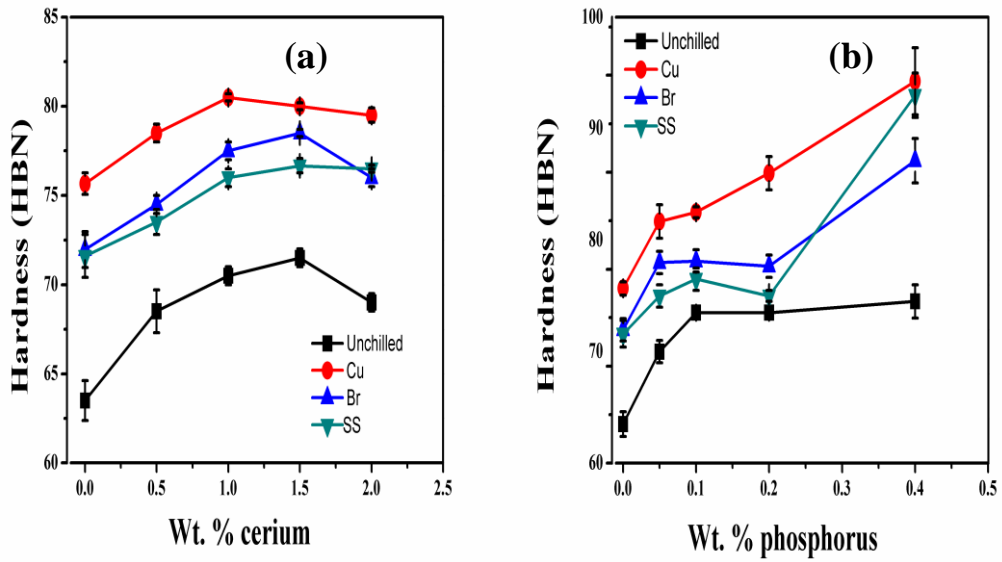


Figure 5.80 Effect of varying content of addition on the hardness of the alloy (a) Ce (b) Sr

The effectiveness of the Ce treatment improved with increase in cooling rate, whereas, addition of P was effective at all cooling rates. The Ce treatment resulted in better tensile properties and P treatment resulted in higher hardness values. The only differences observed with the microstructures are with sizes of the eutectic silicon. The addition of Ce yielded refined eutectic silicon along with the refined primary silicon, whereas, P treatment aided the growth of acicular silicon. The difference was evident in thermal analyses results as well, the eutectic undercooling increases with Ce treatment and decreases with P treatment.

The results indicate that the Ce favors the eutectic modification and P favors the growth of acicular silicon. The cooling rate had direct influence on the mechanical properties of the alloy as it was found to increase with cooling rate.

5.6 Effect of T6 Heat Treatment on the Mechanical Properties of Melt Treated Al-Si alloys

Figure 5.81 shows the effect of T6 heat treatment on the ultimate tensile strength of the Al-8Si alloys. Similarly, Figures 5.82 and 5.83 shows the effect of heat treatment and melt treatment on the percentage of elongation and hardness of the alloys respectively. The mechanical properties of untreated alloys were significantly improved with T6 heat treatment, whereas, the mechanical properties of melt treated alloys deteriorated when subjected to heat treatment.

The improvement in mechanical properties of untreated alloys on heat treatment was attributed to the homogeneous precipitation of Mg_2Si and Al_2Cu phases. In addition to dissolution and homogenization, the heat treatment of Al-Si alloys also result in spheroidization of eutectic silicon. Figure 5.84 shows the microstructures of Al-8Si alloys before and after the heat treatment process. The microstructure indicates that the size of the eutectic silicon was significantly reduced due to the spheroidization process. During solution treatment, the Si particles break and separate into small segments retaining the acicular morphology. Later, the fragmented segments spheroidize into fine globular Si [Sjölander and Seifeddine 2010].

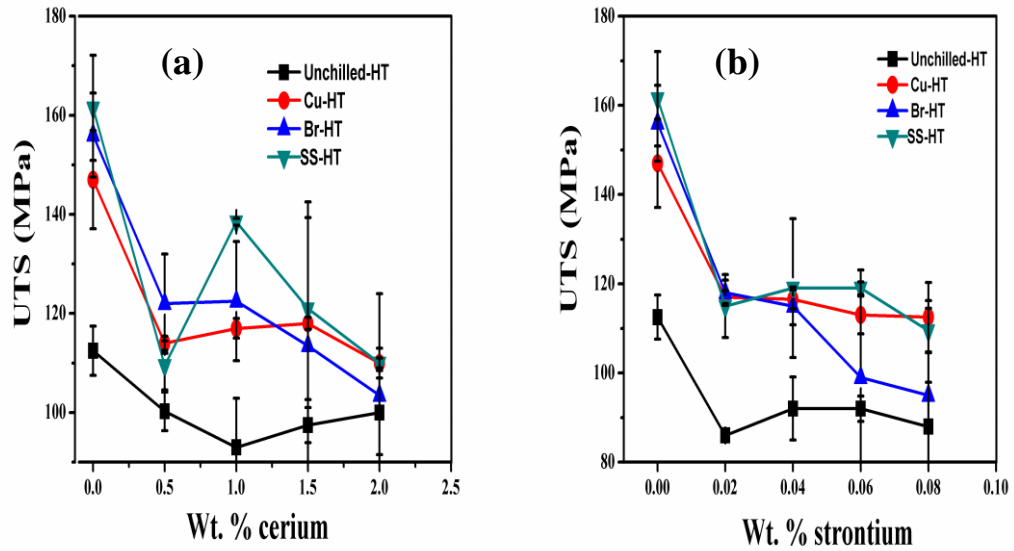


Figure 5.81 Effect of T6 heat treatment on the UTS of treated Al-8Si alloys (a) Ce treated (b) Sr treated

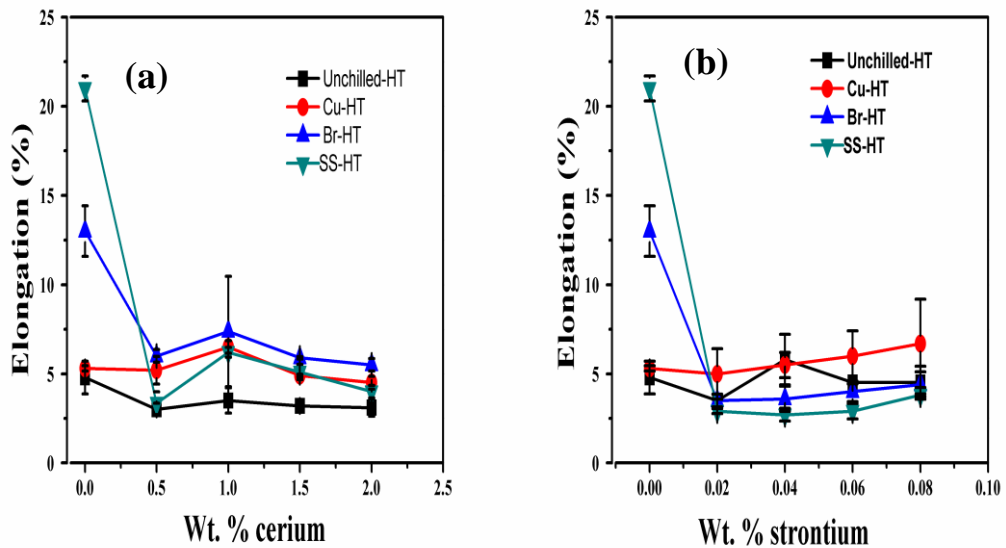


Figure 5.82 Effect of T6 heat treatment on the ductility of treated Al-8Si alloys (a) Ce treated (b) Sr treated

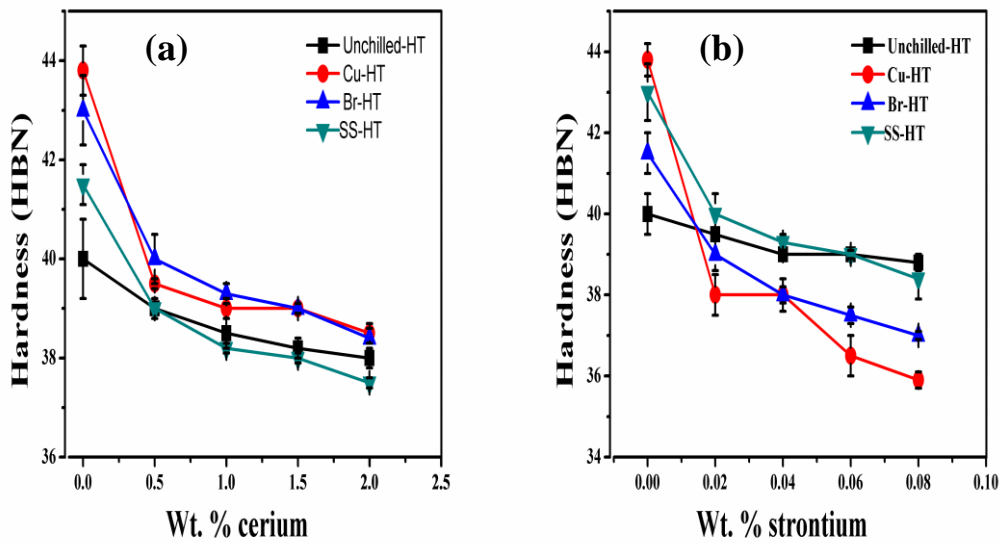


Figure 5.83 Effect of T6 heat treatment on the hardness of melt treated Al-8Si alloys

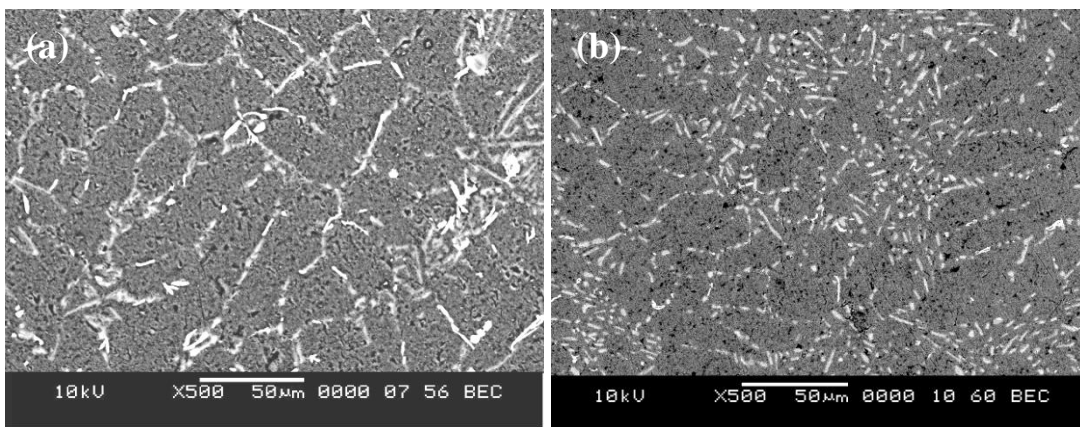


Figure 5.84 Microstructure of Al-8Si alloy (a) before and (b) after T6 heat treatment

The addition of elements like Sr and Ce transforms the eutectic silicon into fine globular Si by modification process to improve its mechanical properties and heat treatment improve the properties by silicon spheroidization and by precipitation hardening. Hence, the combination of two processes should yield an improved mechanical property, but, the mechanical properties of the present alloy decreased with conjunction of two treatments (eutectic modification and heat treatment). The

tensile strength of the alloys decreased drastically with increase in the concentration of additions. The results obtained are in agreement with few literatures. Samuel (1998) and Osorio et al. (2007) reported a similar kind of decrease in tensile strength due to the conjunction of modification and heat treatment. It was reported that the Sr modification of eutectic Si increased the spheroidization rate and decreased the coarsening rate of Si. But, heat treatment had negative impact on the mechanical properties of the modified alloy, however, the exact reason for the deterioration was not reported.

Figure 5.85 shows the fracture surfaces of the heat treated alloys and large number of pores were observed on the fracture surfaces of melt treated alloys. The fracture surface of the untreated alloy was found with no such pores and at higher magnification it shows the presence of dimples, a characteristic feature of ductile fracture. The possible reason for the presence of large number of porosity and the decrease in mechanical properties is the porosity associated with modification. The modification alters the porosity from macro to micro porosity. The addition of modifiers such as Sr has high affinity towards the oxygen to form oxides and these oxides play an important role in the formation of porosity [Liu et al. 2003] [Miresmaeili et al. 2005]. Similarly, Ce is also reacts with atmospheric oxygen to form cerium oxide [Chang et al. 1998]. Based on the fracture surfaces of the present alloys it can be inferred that during the heat treatment of the modified alloys the micro porosity in the modified alloys will add up to form large pores. As a result, the mechanical properties of the melt treated alloys decreased on heat treatment.

Figures 5.86 and 5.87 show the effect of T6 heat treatment on the tensile properties of Al-14Si alloys and Figure 5.88 shows the effect of heat treatment on the hardness of the alloys. The heat treatment had a positive impact on the mechanical properties of the untreated alloys compared to the melt treated alloys. The mechanical properties of the untreated alloys increased significantly with heat treatment, whereas, it decreased for melt treated alloys. The untreated alloys solidified at high cooling rate showed better response to heat treatment yielding higher tensile properties compared to slowly cooled alloys.

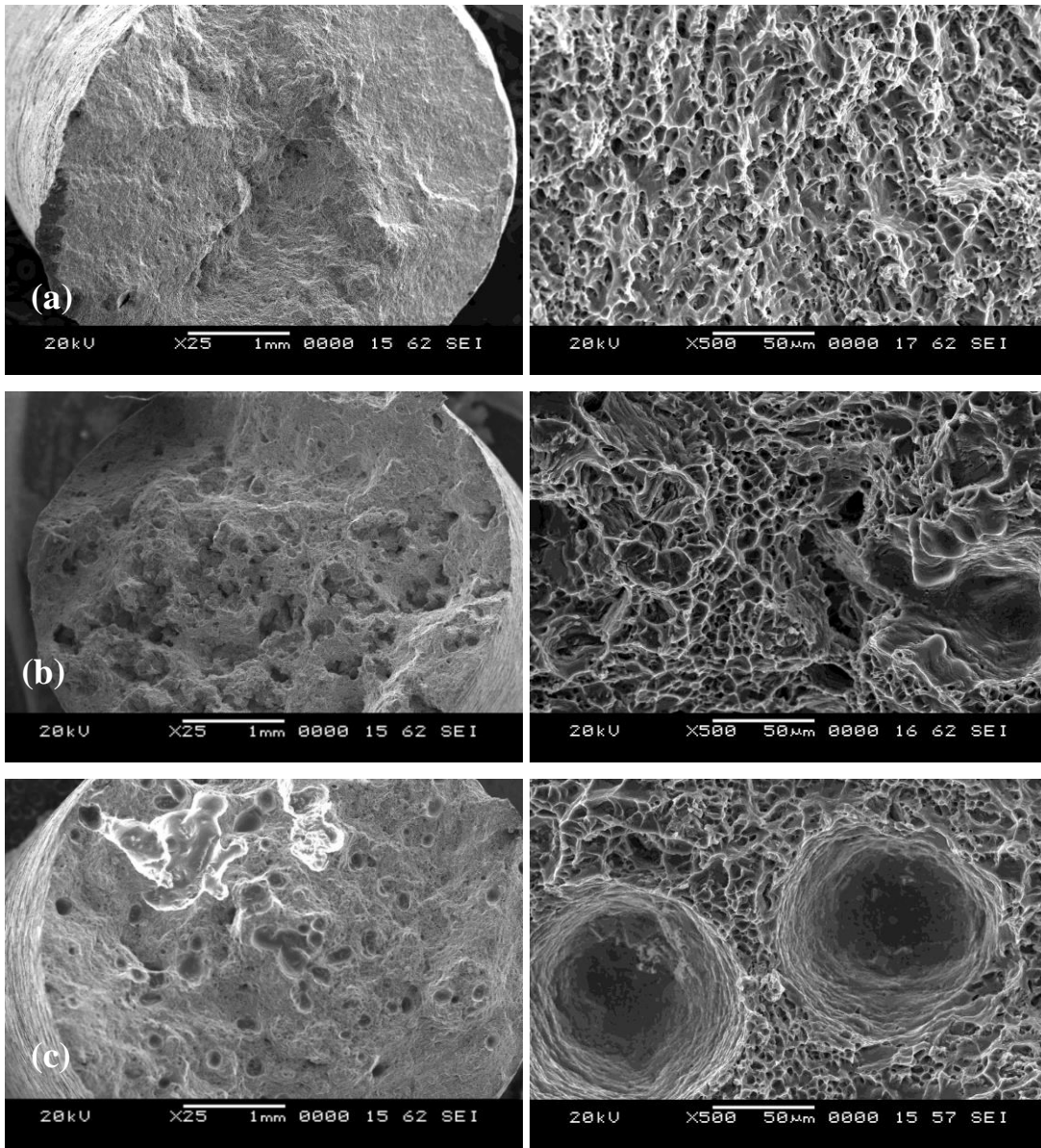


Figure 5.85 Micrographs of tensile fracture surfaces of heat treated Al-8Si alloys (a) untreated (b) Ce treated (c) Sr treated

Figure 5.89 shows the effect of heat treatment on the microstructure of the untreated alloy and it observed that the heat treatment had resulted in complete spheroidization of the eutectic silicon. The heat treatment had varying effect on the mechanical properties of melt treated alloys, where, the tensile strength decreased with Ce treatment and increased with P treatment. Similarly, the hardness of the alloy also decreased with Ce treatment and increased with P treatment. However, the percentage of elongation of decreased with heat treatment for both kinds of additions This variation in the properties with melt treatment is associated with eutectic silicon modification.

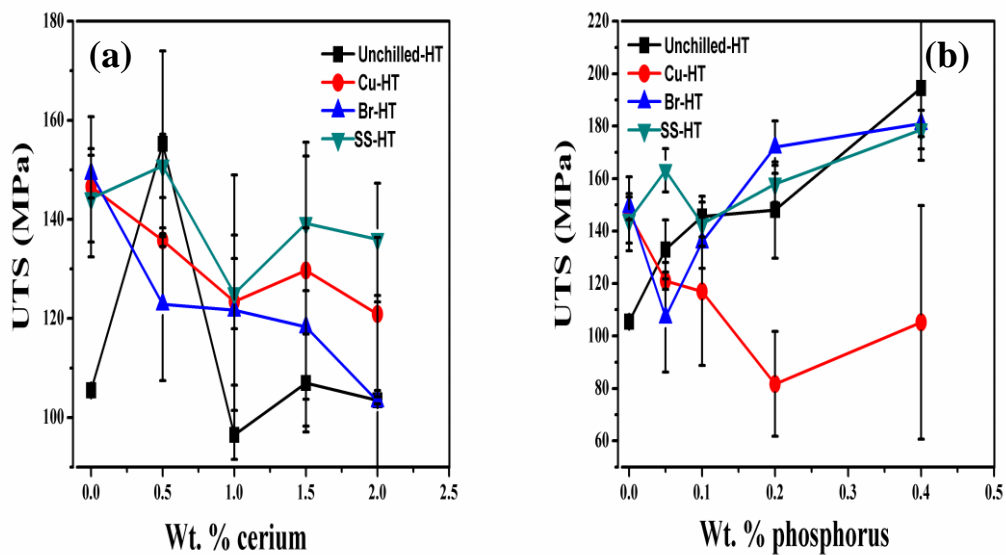


Figure 5.86 Effect of T6 heat treatment on the UTS of treated Al-14Si alloys (a) Ce treated (b) P treated

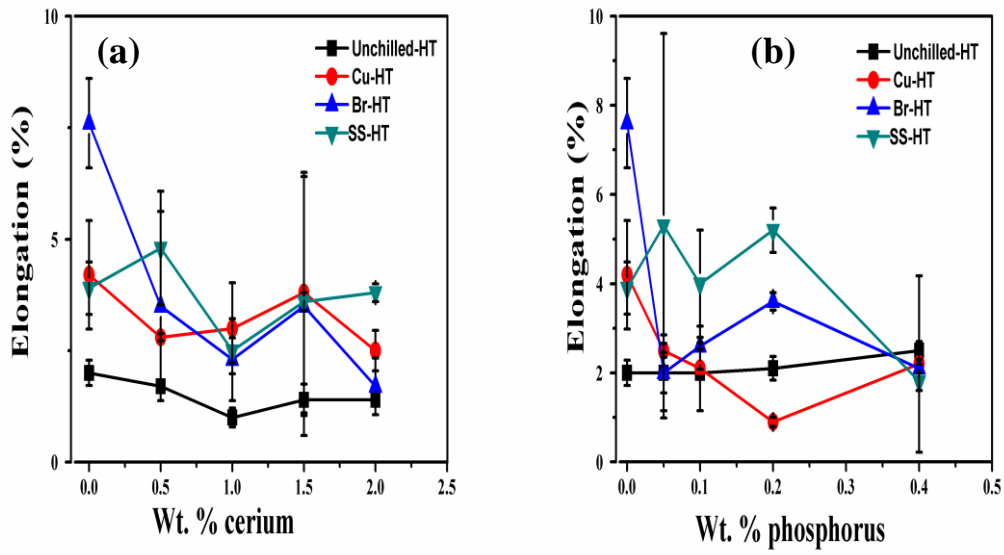


Figure 5.87 Effect of T6 heat treatment on the ductility of treated Al-8Si alloys (a) Ce treated (b) P treated

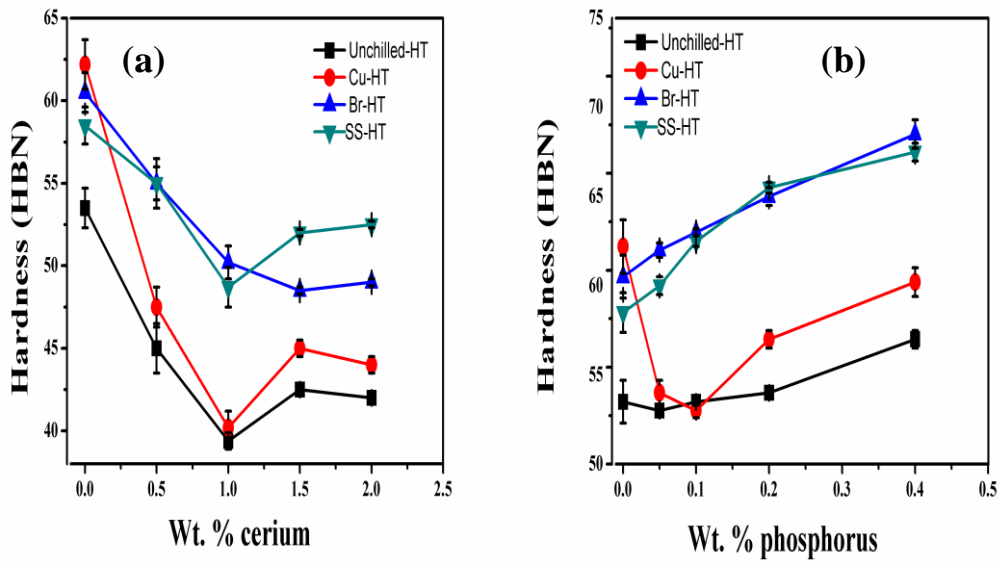


Figure 5.88 Effect of T6 heat treatment on the hardness of melt treated Al-14Si alloys

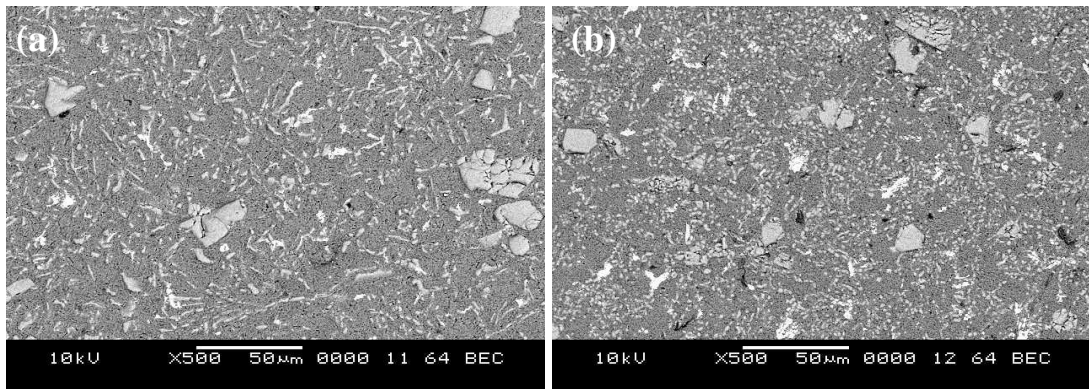


Figure 5.89 Microstructure of Al-14Si alloy (a) before and (b) after T6 heat treatment

Figure 5.90 shows the micrographs of the fracture surfaces of variously melt treated alloys after heat treatment. The large pores in the fracture surfaces of Ce treated alloys are formed from the micro porosity associated with eutectic modification. The decrease in mechanical property is mainly due to the growth of the micro porosity into large pores during heat treatment. Since the formation of large pores are associated with eutectic modification and heat treatment, it is absent in the P treated alloys. The addition of P favors the nucleation and formation of acicular eutectic silicon rather than modifying it. The eutectic silicon in the P treated alloys is very much similar to the eutectic silicon in the untreated alloys and hence the tensile strength increases during heat treatment due to the spheroidization processes. The addition of Cu along with P also adds to the improvement in mechanical properties after heat treatment.

Figures 5.91 and 5.92 shows the effect of heat treatment on the tensile properties of Ce and P melt treated Al-22Si alloys and Figure 5.93 shows the effect of heat treatment on the hardness of the alloys. The mechanical properties of the untreated alloy improved significantly with the heat treatment for all cooling conditions. This was mainly because of the spheroidization of the eutectic silicon as seen in the microstructure shown in the Figure 5.94.

Unlike melt treated Al-8Si alloys and Al-14Si alloys, the heat treatment had a positive impact on the mechanical properties of the melt treated Al-22Si alloys. The mechanical properties improved with both Ce and P melt treatments, however, the

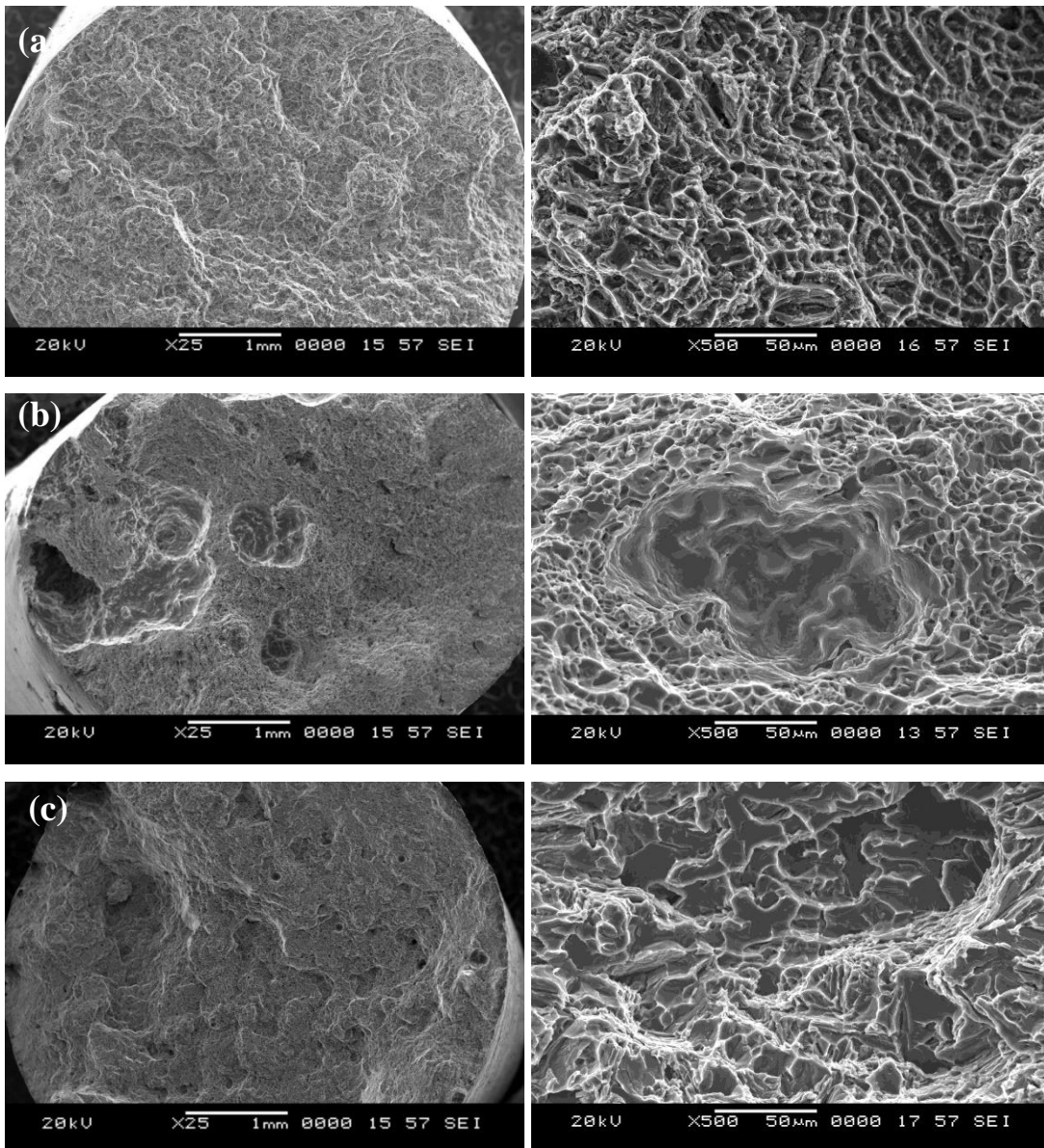


Figure 5.90 Micrographs of tensile fracture surfaces of heat treated Al-14Si alloys (a) untreated (b) Ce treated (c) P treated

tensile strength marginally decreased at high concentrations of Ce. Among all, the highest tensile strength of 220 MPa was obtained with heat treatment of 0.4%P addition. A similar trend was observed with percentage of elongation as well. The reason for the increase in mechanical properties with melt treatment is the nucleation of eutectic silicon from the primary silicon. The melt treatment of the Al-22 Si alloy with Ce and P lead to the nucleation of polyhedral primary silicon and which became a well-proportioned nucleation site for eutectic silicon. This leads to the nucleation and growth of acicular eutectic silicon as shown in the Figure 4.19. During heat treatment the eutectic silicon will spheroidize into fine form to enhance the mechanical properties. Moreover, the addition of P as Cu-8P master alloy will induce some amount of Cu to go into the alloy. The concentration of Cu increases with increase in weight percent of the added master alloy. Figure 5.95 shows the fracture surfaces of heat treated Al-22Si alloys with and without additions. It is worth noticing that the combination of melt treatment and heat treatment did not produce large cavities as in the fracture surfaces of Al-8Si alloys.

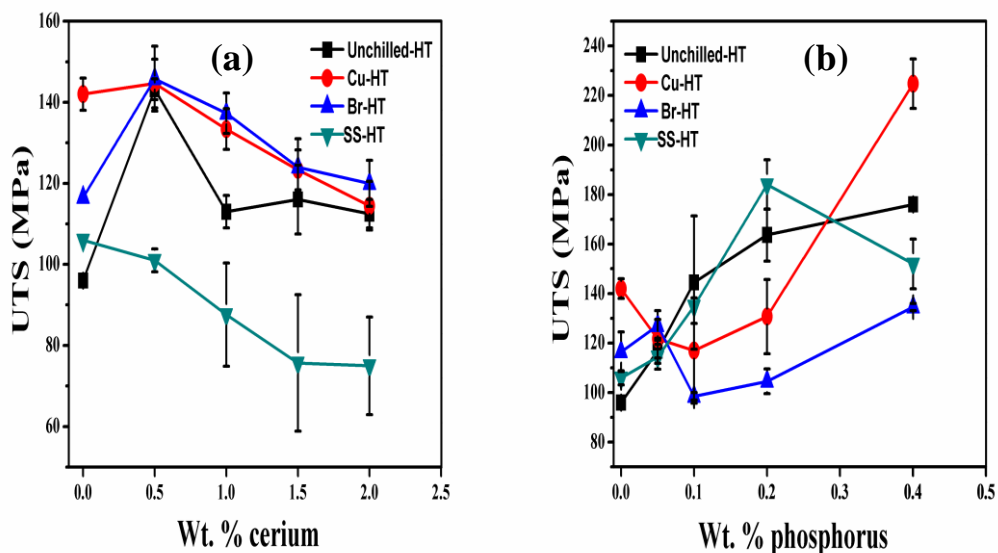


Figure 5.91 Effect of T6 heat treatment on the UTS of treated Al-22Si alloys (a) Ce treated (b) P treated

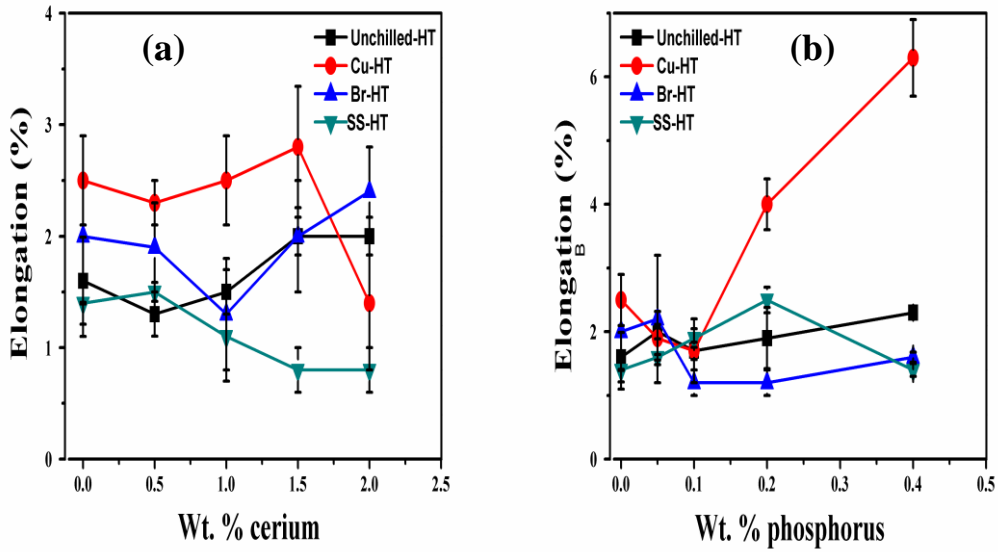


Figure 5.92 The effect of T6 heat treatment on the ductility of treated Al-22Si alloys
(a) Ce treated (b) P treated

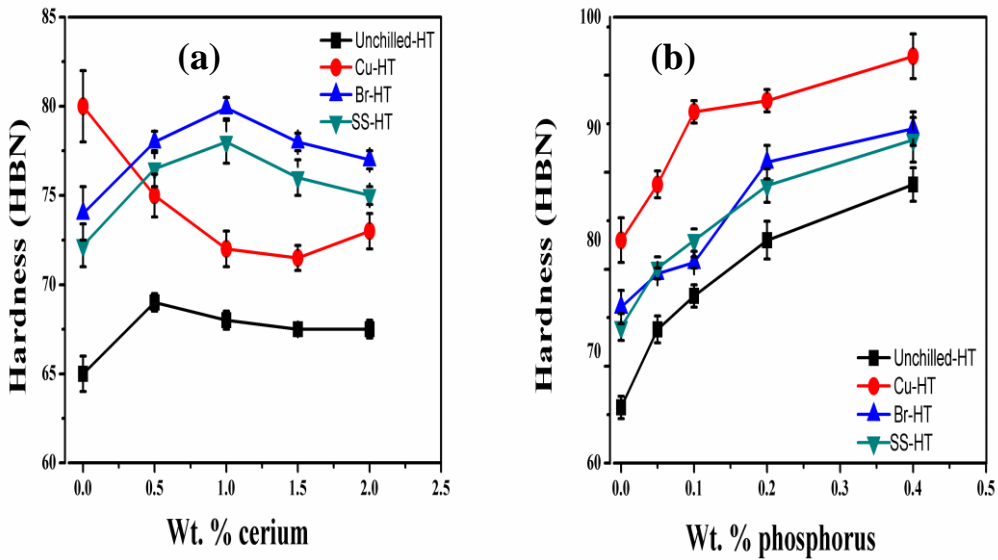


Figure 5.93 The effect of T6 heat treatment on the hardness of melt treated Al-22Si alloys

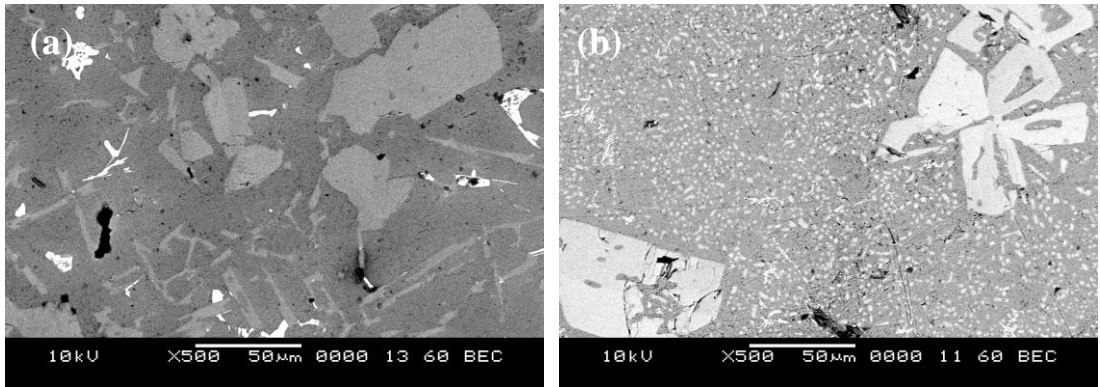


Figure 5.94 Microstructure of Al-22Si alloy (a) before and (b) after T6 heat treatment

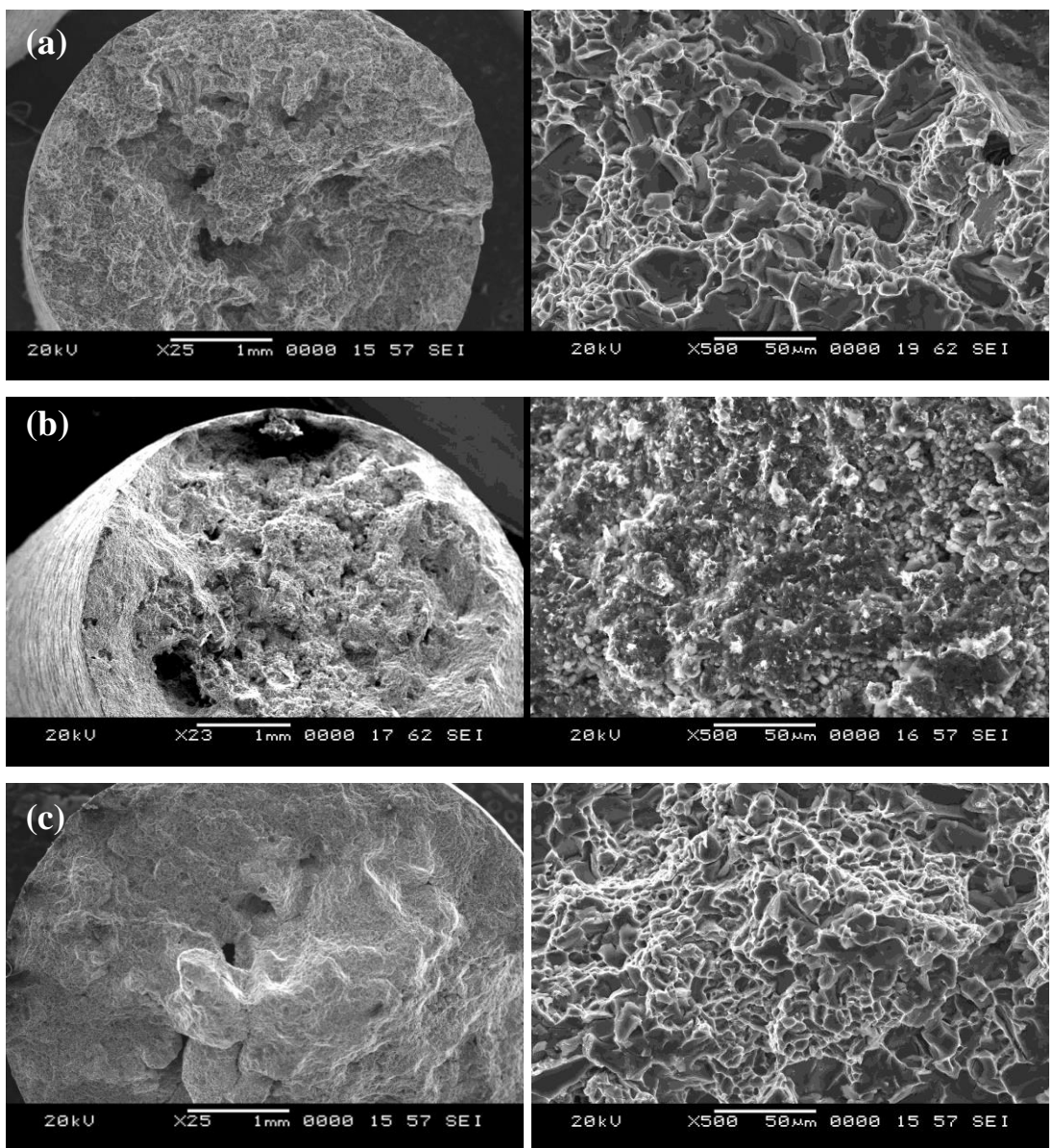


Figure 5.95 Micrographs of tensile fracture surfaces of heat treated Al-22Si alloys (a) untreated (b) Ce treated (c) P treated

5.7 Effect of Combined Additions on Thermal Analysis Parameters, Microstructure and Tensile Properties of Al-Si Alloys

The Ce in Al-8Si alloys, refined the aluminum grains by increasing the α -aluminum nucleation temperature and by decreasing the undercooling required for nucleation. On the other hand, Sr modified the eutectic silicon by depressing the eutectic nucleation temperature and by increasing the eutectic undercooling. The Ce melt treatment was found to modify eutectic silicon together with aluminum refinement, whereas, Sr treatment resulted in aluminum grain growth. The addition of Ce and Sr to Al-13Si alloy depressed the eutectic temperature and modified the eutectic silicon. Similarly, Ce improved the mechanical properties of the hypereutectic alloys by simultaneously refining and modifying primary and eutectic silicon respectively. The improvement observed with P treatment was solely due to refinement of primary silicon. Ce and P enhanced the nucleation temperature and decreased the nucleation undercooling thereby refining primary silicon. The melt treatment (Ce or Sr/P) significantly improved the mechanical properties, but had varying effect on the microstructure constituents of the alloy. Hence, a combination of Ce and Sr/P levels were selected and added. The concentrations of the additions were selected based on the effect of individual additions on the thermal analysis parameter, microstructure and mechanical properties.

The solidification characteristics of different alloys after combined additions are given in Table 5.14. The combined additions of Ce and Sr/P had influenced both primary and eutectic phases. The combined addition increased the α -aluminum/primary silicon nucleation temperatures and decreased the eutectic nucleation temperature, which is an ideal condition for simultaneous refinement and modification of the Al-Si alloys. The decrease in undercooling of primary phases (aluminum and primary silicon) is the evidence for heterogeneous nucleation of the phases, accrediting the refinement of primary aluminum in hypoeutectic alloy and primary silicon in hypereutectic alloy. Subsequently, the increase in eutectic undercooling accredits the modification of eutectic silicon. Based on the thermal

Table 5.14 Effect of combined additions on the solidification parameters of slowly cooled Al-Si alloys

Ce/Sr wt-%	T _N (α) (°C)	T _{min} (α) (°C)	T _G (α) (°C)	ΔT_N (α) (°C)	T _N (Eut) (°C)	T _{min} (Eut) (°C)	T _G (Eut) (°C)	ΔT_N (Eut) (°C)	T _s (°C)
Al-8Si (0.04Sr+1.5Ce)	598.1	596.5	598.5	1.6	558.5	556.8	556.9	1.7	540
Al-13Si (0.06Sr+1.5Ce)	567.0	564.5	566.5	2.5	560.7	556.3	556.6	4.4	534.4
Al-14Si (0.05P+1%Ce)	655.8	654.3	653.8	1.6	575.6	570.8	570.1	4.8	530.5
Al-22Si (0.1P+1%Ce)	743.9	742.7	742.6	1.2	564.9	560.3	561.3	4.6	525.6

analysis data of individual additions and combined additions, it can be inferred that the combined additions did not poison each other's effect. The Ce affected both the primary and eutectic phases, resulting in simultaneous refinement and modification. The addition of Sr and P had a better effect on the modification of eutectic silicon and refinement of primary silicon.

Figure 5.96 shows the effect of combined additions on the microstructures of the Al-Si alloys. It is evident from the microstructures that the combined addition resulted in simultaneous refinement and modification of the alloys. The microstructure of untreated Al-8Si alloy consisted of columnar α -Al grains and long acicular eutectic silicon. The individual addition of Ce transformed the columnar aluminum grains into equiaxed grains and refined the eutectic silicon. On the other hand, the addition of Sr resulted in the complete modification of eutectic silicon, but, increased the aluminum grain size. The combined addition of Ce and Sr transformed both α -Al grains as well as the eutectic silicon as shown in the Figure 5.96 (a). As observed, a refined aluminum grains and modified eutectic silicon was obtained by the combined addition of Ce and Sr. Similarly, a refined and modified microstructure is observed with

addition of Ce and Sr to Al-13Si alloy as shown in the Figure 5.96 (b). The nucleation of primary aluminum was observed in Al-13Si alloy as a result of shift in eutectic point. The addition of Ce and P to hypereutectic Al-Si alloys resulted in simultaneous refinement and modification of primary and eutectic silicon as shown in Figures 5.96 (c) and (d).

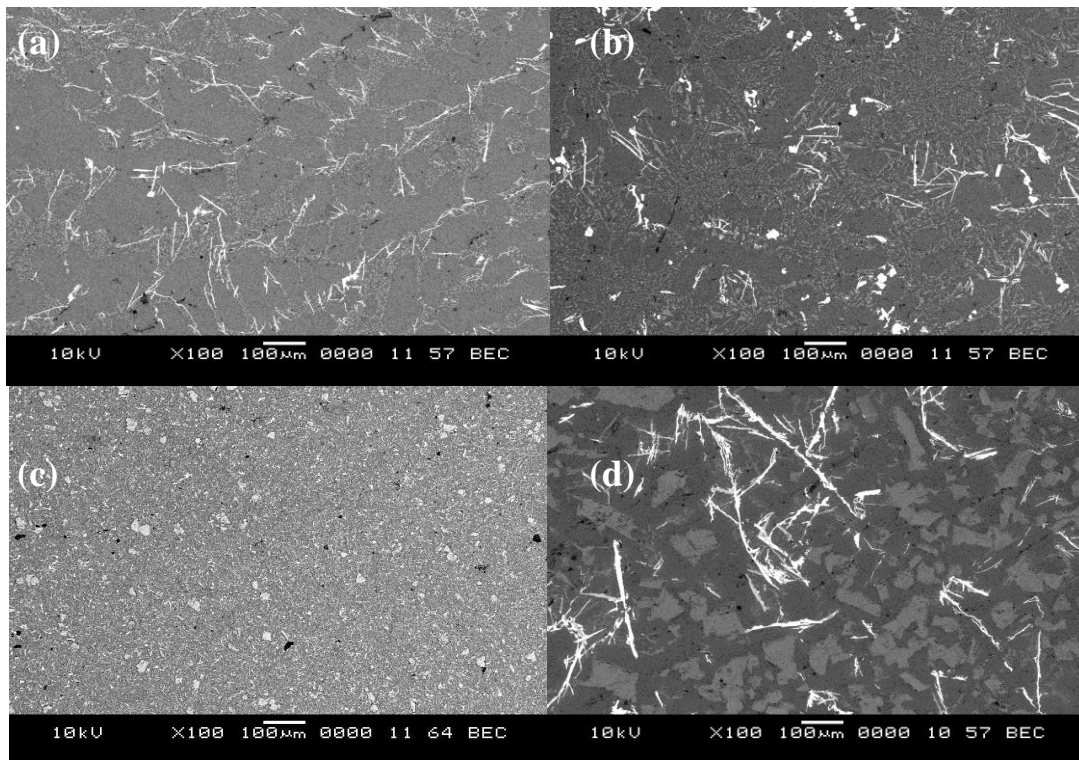


Figure 5.96 Effect of combined additions on the microstructures of (a) Al-8Si alloy (b) Al-13Si alloy (c) Al-14Si alloy (d) Al-22Si alloy

The benefits of the simultaneous refinement and modification are reflected in the tensile properties given in Table 5.15. All the additions resulted in significant improvement in the mechanical properties. The Sr and Ce melt treatment increased the tensile strength of the Al-8Si alloy by 40 and 52% respectively, the combined addition of Ce and Sr resulted in increase of tensile strength by 83%. Similarly, on combined addition the tensile strength of Al-13 Si, Al-14Si and Al-22Si alloy were increased 54%, 41% and 11% respectively.

Table 5.15 Ultimate tensile strength of copper mold solidified Al-Si alloys before and after various melt treatment

Alloy\UTS (MPa)	Untreated	Sr/P	Ce	Ce +P/Sr
Al-8Si (0.4Sr+1.5Ce)	108±6	151±5	164±10	198±2
Al-13Si (0.06Sr+1.5Ce)	160±2	211±9	185±15	247±7
Al-14Si (0.05P+1%Ce)	136±13	159±2	189±2	192±5
Al-22Si (0.1P+1.5%Ce)	146±4	157±5	176±1	163±10

5.8 Role of Ce in Simultaneous Refinement and Modification of Al-Si Alloys

The addition of Ce had a varying effect on Al-Si alloys. It simultaneously refined and modified aluminum and eutectic Si in hypoeutectic and eutectic alloys, whereas, it refined only primary silicon in Al-22Si alloys. However, the addition of Ce modified eutectic silicon and refined primary silicon in Al-14Si alloys. For grain refinement, the nucleation of grains would either occur directly on the substrate by epitaxial growth or by some invariant reaction [Mohanty and Gruzleski 1996]. But, the addition of Ce to Al-Si alloys was not found to form any heterogeneous nucleation agent for aluminum or primary silicon. Previous studies on Al-Ce-Si system reveal that at low concentrations of Ce only of two phases of Ce (Γ_1 or Γ_2) are stable [Gröbner et al. 2004]. For heterogeneous nucleation, a near perfect epitaxy between the nucleant and substrate should exist. In the case of α -Al (0.405 nm), Si (5.45nm) and Γ_1 or Γ_2 no such match is observed in the lattice parameters and hence Ce phases did not heterogeneously nucleate α -Al. The presence of Ce based particle along the grain boundaries is a proof that Ce intermetallic did not nucleate α -Al. Hence, the refinement obtained should be due to some invariant reaction involving Al, Si and Ce. The mechanism of Ce refinement can be explained with help of Al-Ce-Si ternary phase diagram and liquidus surface of Al-Ce-Si system as shown in the Figure 5.97 (a and b).

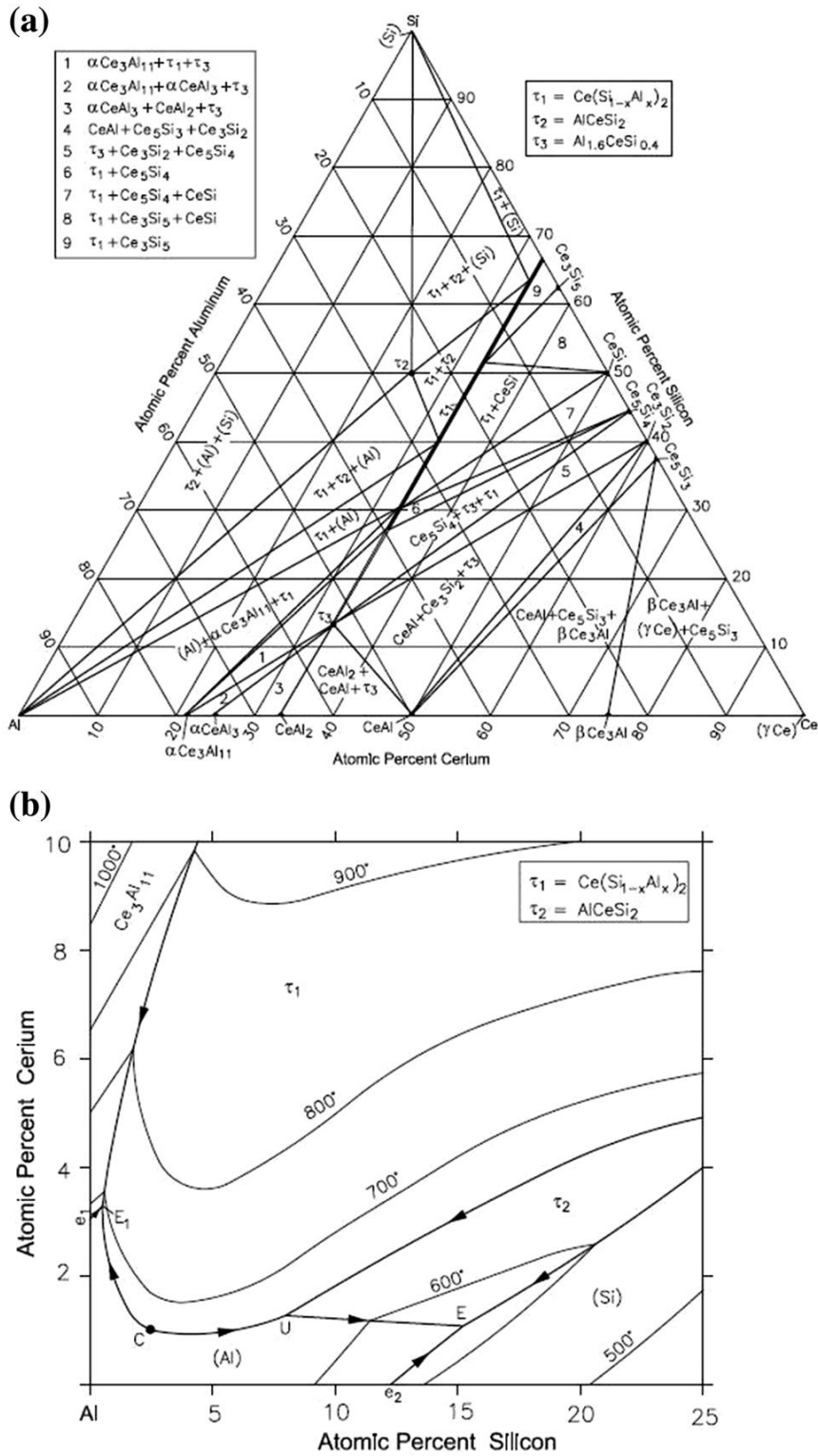


Fig 5.97 (a) Al-Ce- Si ternary phase diagram (b) Calculated Al corner of Al–Ce–Si liquidus surface [Gröbner et al. 2004]

According to the phase diagram, the Ce intermetallic formed varies with Ce content and Si content in the alloy. The addition of Ce to hypoeutectic alloy would result in the formation of Γ_1 at higher temperatures and as the temperature decreases T_1 would transform into α -Al and Γ_2 . Similarly, in the present study, the finer α -Al would have precipitated from Γ_1 , formed at higher temperatures. As the silicon content increases the Ce intermetallic formed changes and Γ_2 is formed at higher temperatures in alloys with silicon content above 10 wt. %. More specifically, in alloys having silicon content higher than 15wt. % would result in the precipitation of Si from Γ_2 during solidification. According to the phase diagram, the Γ_2 would be retained in the near eutectic alloys. This variation in the Ce intermetallic formed is the prime reason for the variation in the effect of Ce in Al-Si alloys. Figures 5.98, 5.99, 5.100 and 5.101 shows the composition of Ce intermetallic formed in the present Al-Si alloys. The composition of the Ce intermetallic was more or less same in Al-8Si, Al-13Si and Al-14Si alloys and varied in Al-22Si alloys. Hence, it was concluded that the refinement of primary silicon with the addition of Ce was due to the formation of Γ_2 and subsequent precipitation of finer primary silicon during solidification. The addition of Ce to hypoeutectic alloys results in the precipitation of α -Al and Γ_2 phase from Γ_1 phase and addition of Ce to the near eutectic alloys (Al-13Si and Al-14Si alloy) resulted in the formation of Γ_2 phase. However, in high silicon content alloys, the Γ_2 precipitates as primary silicon and Γ_3 phase. Hence, the Γ_2 phase was responsible for the modification of eutectic silicon in Ce melt treated alloys.

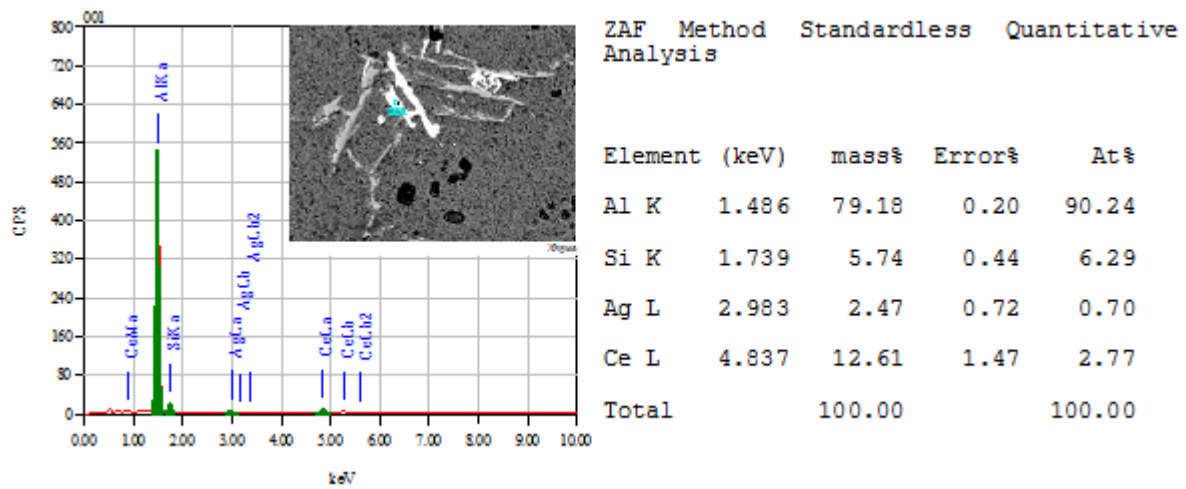


Fig. 5.98 EDAX analysis of Ce intermetallic in Al-8Si alloys

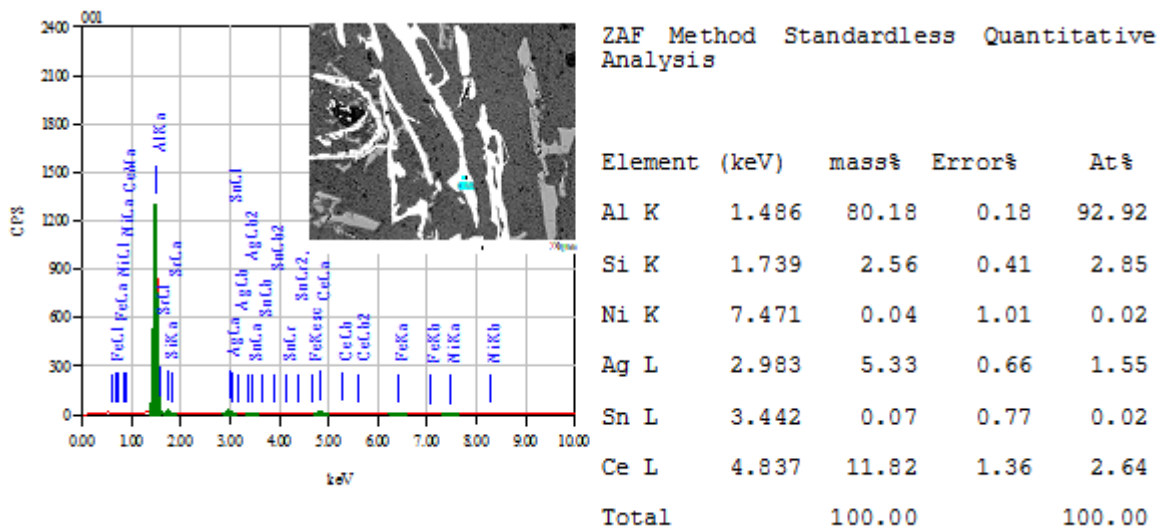


Fig. 5.99 EDAX analysis of Ce intermetallic in Al-13Si alloys

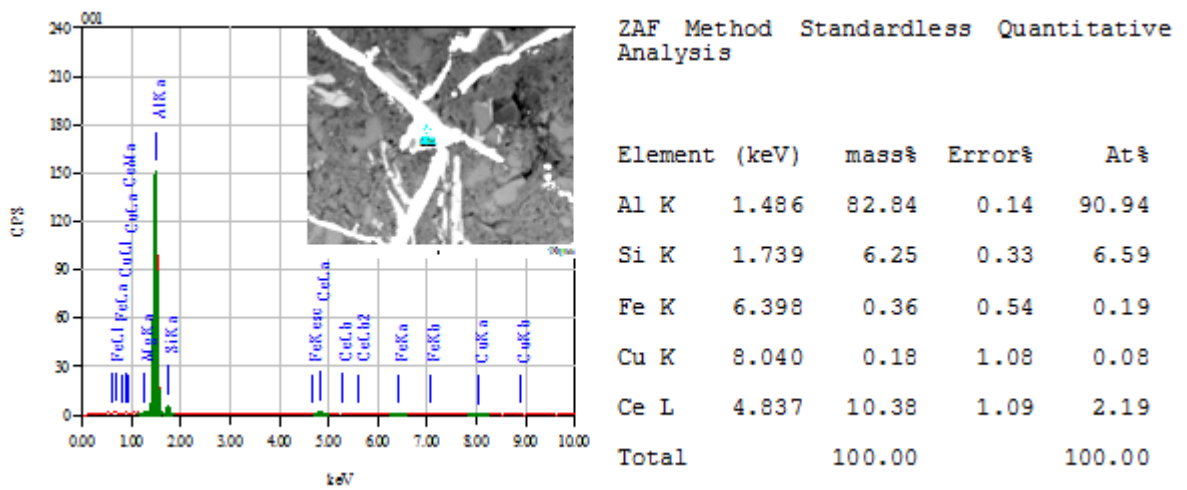


Fig. 5.100 EDAX analysis of Ce intermetallic in Al-14Si alloys

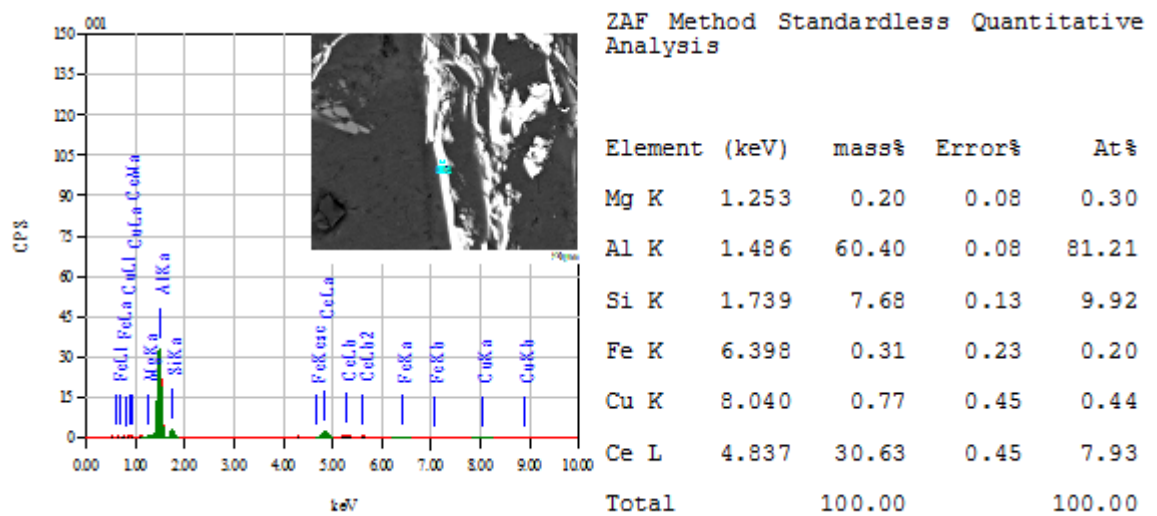


Fig. 5.101 EDAX analysis of Ce intermetallic in Al-22Si alloys

CHAPTER 6

CONCLUSIONS

The effect of Ce, Sr and P melt treatment on microstructure, thermal analysis parameters and mechanical properties of Al-8% Si, of Al-12Si, Al-14Si and Al-22Si alloys at varying cooling rates were studied. Based on the results and discussion, the following conclusions were drawn.

1. The addition of Ce to Al-8Si alloy resulted in the refinement of aluminum grains by decreasing the nucleation undercooling of primary aluminum, whereas, Sr additions did not show any significant effect on the undercooling of aluminum. The degree of eutectic undercooling increased significantly with both Sr and Ce additions to chilled alloys accompanied by modification of the eutectic Si.
2. The Ce and Sr melt treatment of Al-13Si alloy, depressed the eutectic temperature to lower temperatures. The depression was more significant with Sr addition. The addition of Ce to chilled alloys yielded better modification than the slowly cooled alloys. The additions also led to the shift in eutectic point towards high silicon content, making the alloy behave as a hypoeutectic alloy and changing the mechanism of eutectic silicon nucleation.
3. The addition of Ce and P to Al-14Si alloy resulted in the depression of primary silicon nucleation. However, the addition of 0.05% P to unchilled alloy showed a higher nucleation temperature. The decrease in nucleation temperature with high P content was due to the addition above the optimum level of 0.05%P. However, both the kinds of additions decreased the undercooling required for the nucleation of

primary silicon. The Ce melt treatment significantly depressed the eutectic temperature and increased the undercooling for the eutectic nucleation, whereas, with P melt treatment the eutectic temperature and undercooling remained unchanged.

4. The nucleation temperatures of primary and eutectic silicon increased with addition of Ce and P for all cooling conditions, except for Ce treated unchilled alloys. The undercooling for the nucleation of primary silicon decreased with additions. The effect of Ce was more significant under chilled conditions. The eutectic undercooling increased with Ce addition and decreased on addition of P.
5. The thermal analyses data of Al-8Si alloys was used to determine the dendrite coherency point (DCP) and fraction solid at DCP. The DCP temperature of the alloy decreased with addition of Ce and increased with Sr. The fraction solid at DCP increased to 14.5% with addition of 1.5% Ce, due to the refinement of aluminum grains.
6. The latent heat and solid fraction during solidification of the metal/alloy are predicted using Fourier and Newtonian analyses techniques based on the fitting data base line to the derivative curve. The latent heat calculated using Fourier analysis was found to be more reliable than Newtonian analysis. The latent heat evolved during solidification of untreated Al-8Si, Al-13Si, Al-14Si and Al-22Si alloys were 407, 510, 517 and 607 J/g and with 1.5% Ce, the latent heat of the alloys decreased to 351, 270, 493 and 538 J/g respectively.
7. Thermal diffusivity and specific heat of alloys were computed using the fraction solid obtained from the Fourier method. The melt treatment had varying effect on the thermal diffusivity, specific heat

and latent heat of an alloy. Ce and Sr melt treatment of Al-8Si alloy resulted in an increase in the diffusivity and decrease in the specific heat of the alloy. The latent heat of the alloy decreased significantly with Ce treatment and increased marginally with the addition of Sr. The melt treatment of Al-13Si alloy with Ce and Sr showed an opposite trend. The diffusivity decreased and specific heat increased on additions.

8. The diffusivity and specific heat of Al-14Si alloy increased with all concentrations of Ce and with 0.05% P. The values decreased on further addition of P. The latent heat evolved increased with P addition and decreased with Ce treatment. The decrease in the latent heat with Ce addition was due to the formation of Ce based intermetallics. The diffusivity of Al-22Si alloy decreased with Ce and P melt treatment. The decrease was more significant with P additions. The specific heat and latent heat evolved decreased with Ce addition and increased with P addition.
9. The melt treatment of Al-8%Si, Al-13Si and Al-14Si alloys using Ce and Sr resulted in an increase in the interfacial heat flux for all chilling conditions. The melt treatment of Al-22Si alloy with P resulted in the decrease of interfacial heat flux. The increase in heat flux was mainly due to the eutectic silicon modification achieved on Ce and Sr melt treatment.
10. Microstructure study of hypoeutectic alloys revealed that the addition of Ce resulted in fine equiaxed grains along with the modification of eutectic Si. The grain size increased with the addition of Sr. The addition of elemental cerium to the unchilled alloys did not modify the eutectic silicon although the additions refined the eutectic silicon. The eutectic Si in chilled alloys was completely modified due to the synergistic effect of chilling and Ce addition.

11. The simultaneous refinement and modification of primary and eutectic silicon in Al-14Si alloys was obtained on addition of Ce to hypereutectic alloys solidified against chills. The degree of eutectic modification increased with increase in Ce content. Refined and well distributed primary silicon particles were obtained with the addition of P to hypereutectic Al-Si alloys. The addition of P resulted in nucleation of acicular silicon.
12. A dimensionless thermal analysis parameter $\Delta T_G / \Delta T_N$ was proposed to assess the roundness factor of eutectic silicon in Al-8Si, Al-13Si and Al-14 Si alloys, A good correlation was observed between the roundness factor and the dimensionless thermal analysis parameter. In the case of Al-22 Si alloy, a good fit was obtained between ΔT_G and the characteristic parameter of the primary silicon. The primary silicon characteristic parameter was defined as the ratio of equivalent diameter of the refined primary silicon to the equivalent diameter of the unrefined primary silicon. The characteristic parameter could be used to assess the extent of refinement of primary silicon.
13. The mechanical properties of alloys were significantly improved on melt treatment with Ce, P and Sr. Ce treated alloys showed higher UTS values than Sr or P treated alloys.
14. The mechanical properties of the untreated alloys were significantly improved by T6 heat treatment process. The improvement was mainly due to the spheroidization of eutectic silicon during solution treatment. The heat treatment had negative impact on the mechanical properties of Ce and Sr melt treated alloys. The tensile strength of the Ce and Sr treated alloys decreased significantly with heat treatment.

REFERENCES

- Abu-Dheir, N., Khraisheh, M., Saito, K., and Male, A. (2005). "Silicon morphology modification in the eutectic Al–Si alloy using mechanical mold vibration." *Mater. Sci. Eng. A* 393, 109–117.
- Anasyida, A.S., Daud, A.R., and Ghazali, M.J. (2010). "Dry sliding wear behavior of Al–12Si–4Mg alloy with cerium addition." *Mater. Des.* 31, 365–374.
- Aparicio, R., Barrera, G., Trapaga, G., Ramirez-Argaez, M., and Gonzalez-Rivera, C. (2013). "Solidification kinetics of a near eutectic Al-Si alloy, unmodified and modified with Sr." *Met. Mater. Int.* 19, 707–715.
- Asmael, M.B.A., Ahmad, R., Ourdjini, A., and Farahany, S. (2013). "Effect of elements cerium and lanthanum on eutectic solidification of Al-Si-Cu near eutectic cast alloy." *Adv. Mater. Res.* 845, 118–122.
- Backerud, L., Chai, G., and Tamminen, J. (1990). "Solidification characteristics of aluminum alloys, Foundry Alloys." *Foundry Alloys*, AFS Des Plaines, IL, 2, 71-229
- Bernardin, J.D., and Madawar, I. (1995) "Validation of the quench factor technique in predicting hardness in heat treatable aluminum alloys." *Inter. J. Heat and Mass Transfer*, 38, 863-873.
- Ceylan, M., Kuzucu, V., and Balo, S.N. (1997). "The influence of the cooling rate on the microstructure of Al-Cu-Si, Al-Si and Al-Zn alloys." *J. Mater. Process. Technol.* 65, 41–51.
- Chai, G. and Backerud, L. (1992). "Factors affecting modification of Al-Si alloys by adding Sr-containing master alloys." *AFS Transactions*, 100, 847-857.
- Chang, J. (2001). "Crystal morphology of eutectic si in rare earth modified Al-7wt% Si alloy." *J. Mater. Sci. Lett.* 20, 1305–1307.

Chang, J., Moon, I., and Choi, C. (1998). "Refinement of cast microstructure of hypereutectic Al-Si alloys through the addition of rare earth metals." *J. Mater. Sci.* 33, 5015–5023.

Chang, J.Y., Kim, G.H., Moon, I.G., and Choi, C.S. (1998). "Rare earth concentration in the primary Si crystal in rare earth added Al-21wt.% Si alloy." *Scr. Mater.* 39, 307–314.

Chavez-Zamarripa, R., Ramos-Salas, J.A., Talamantes-Silva, J., Valtierra, S., and Colas, R. (2007). "Determination of the dendrite coherency point during solidification by means of thermal diffusivity analysis." *Metall. Mater. Trans. A* 38, 1875–1879.

Chen, C., Liu, Z., Ren, B., Wang, M., Weng, Y., and Liu, Z. (2007). "Influences of complex modification of P and RE on microstructure and mechanical properties of hypereutectic Al-20Si alloy." *Trans. Nonferrous Met. Soc. China* 17, 301–306.

Chen, X., Geng, H., and Li, Y. (2006). "Study on the eutectic modification level of Al-7Si alloy by computer aided recognition of thermal analysis cooling curves." *Mater. Sci. Eng. A* 419, 283–289.

Chen, Z., Hao, X., Zhao, J., and Ma, C. (2013). "Kinetic nucleation of primary α (Al) dendrites in Al-7%Si-Mg cast alloys with Ce and Sr additions." *Trans. Nonferrous Met. Soc. China* 23, 3561–3567.

Chen, Z., Wang, T., Gao, L., Fu, H., and Li, T. (2012). "Grain Refinement and tensile properties improvement of aluminum foundry alloys by inoculation with Al-B master alloy." *Mater. Sci. Eng. A* 553, 32–36.

Cisse, J., Bolling, G.F., and Kerr, H.W. (1975). "Simultaneous refinement of primary and eutectic silicon in hypereutectic Al-Si alloys." *Metall. Mater. Trans. B* 6, 195–197.

Closset, B, Pirie, K, and Gruzleski, J E (1984). "Comparison of thermal analysis and electrical resistivity in microstructure evaluation of Al-Si foundry alloys." AFS Trans. 92, 123–133.

Closset, B., and Gruzleski, J.E. (1982). "Structure and properties of hypoeutectic Al-Si-Mg alloys modified with pure strontium." Metall. Trans. A 13, 945–951.

Colligan, G. A., and Gunes M. A. (1973). "Some experimental observations of Al-Si hypereutectic alloys." AFS Trans. 81, 359–365.

Conley, J.G., Huang, J., Asada, J., and Akiba, K. (2000). "Modeling the effects of cooling rate, hydrogen content, grain refiner and modifier on microporosity formation in Al A356 alloys." Mater. Sci. Eng. A 285, 49–55.

Crowell, N., and Shivkumar, S (1995). "Solution Treatment Effects in Cast Al–Si–Cu Alloys." AFS Trans. 103, 721–726.

Dahle, A.K., Nogita, K., McDonald, S.D., Dinnis, C., and Lu, L. (2005). "Eutectic modification and microstructure development in Al–Si alloys." Mater. Sci. Eng. A 413-414, 243–248.

Dai, H., and Liu, X. (2009). "Effects of individual and combined additions of phosphorus, boron and cerium on primary and eutectic silicon in an Al-30Si alloy." Rare Met. 28, 651–655.

Djurdjevic, M., Jiang, H., and Sokolowski, J. (2001). "On-line prediction of aluminum–silicon eutectic modification level using thermal analysis." Mater. Charact. 46, 31–38.

Djurdjevic, M.B., Huber, G., and Odanovic, Z. (2012). "Synergy between thermal analysis and simulation." J. Therm. Anal. Calorim. 111, 1365–1373.

Djurdjevic, M.B., Sokolowski, J.H., and Odanovic, Z. (2012). "Determination of dendrite coherency point characteristics using first derivative curve versus temperature." J. Therm. Anal. Calorim. 109, 875–882.

Dobrzański, L.A., Maniara, R., and Sokolowski, J.H. (2006). "The effect of cast Al-Si-Cu Alloy Solidification Rate on Alloy Thermal Characteristics." *J. Achiev. Mater. Manuf. Eng.* 17, 217–220.

Dwivedi, D.K., Sharma, A., and Rajan, T.V. (2005). "Influence of silicon morphology and mechanical properties of piston alloys." *Mater. Manuf. Process.* 20, 777–791.

Emadi, D., Gruzleski, J. E. and Toguri, J. M. (1993). "The effect of Na and Sr modification on surface tension and volumetric shrinkage of A356 alloy and their influence on porosity formation." *Metall. Mater. Trans. B*, 24B, 1055-1063.

Faraji, M., Todd, I., and Jones, H. (2009). "Effect of phosphorus and strontium additions on formation temperature and nucleation density of primary silicon in Al-19 wt pct Si alloy and their effect on eutectic temperature." *Metall. Mater. Trans. A* 40, 1710–1715.

Fatahalla, N., Hafiz, M., and Abdulkhalek, M. (1999). "Effect of microstructure on the mechanical properties and fracture of commercial hypoeutectic Al-Si alloy modified with Na, Sb and Sr." *J. Mater. Sci.* 34, 3555–3564.

Flood, S.C., and Hunt, J.D. (1981). "Modification of Al-Si eutectic alloys with Na." *Met. Sci.* 15, 287–294.

Gafur, M. A., Haque, M. N. and Prabhu, K. N. (2003). "Effect of chill thickness and superheat on casting/ chill interfacial heat transfer during solidification of commercially pure aluminum." *J. Mater. Process. Tech.*, 133, 257-265.

Ghadimi, H., Nedjhad, S.H., and Eghbali, B. (2013). "Enhanced grain refinement of cast aluminum alloy by thermal and mechanical treatment of Al-5Ti-B master alloy." *Trans. Nonferrous Met. Soc. China* 23, 1563–1569.

Ghomashchi, R. (2004). "Factors influencing the modification and refinement of hypereutectic Al-Si alloys for production of automotive pistons." 133rd Annual

Meeting & Exhibition of The Minerals, Metals & Materials Society, A. T. Tabereaux (ed.), 851-855

Gigliotti, M.F.X., and Colligan, G.A. (1972). "The effects of sodium on the growth velocity and growth morphology of silicon in Al-Si alloys." *Metall. Trans.* 3, 933–940.

Glenister, S.M.D., and Elliott, R. (1981). "Strontium modification of Al-12.7wt-%Si alloys." *Met. Sci.* 15, 181–184.

Golbahar, B., Samuel, E., Samuel, A.M., Doty, H.W., and Samuel, F.H. (2014). "On thermal analysis, macrostructure and microstructure of grain refined Al–Si–Mg Cast alloys: role of Sr addition." *Int. J. Cast Met. Res.* 27, 257–266.

Grobner, J., Mirkovic, D., and Schmid-Fetzer, R. (2004). "Thermodynamic aspects of the constitution, grain refining, and solidification enthalpies of Al-Ce-Si Alloys." *Metall. Mater. Trans. A* 35, 3349–3362.

Gruzleski, J.E. and Closset, B.M. (1990). "The treatment of liquid aluminum-silicon alloys." *American Foundrymen's Society, Des Plaines, IL*, 12-21.

Hamilton, D.R., and Seidensticker, R.G. (1960). "Propagation mechanism of germanium dendrites." *J. Appl. Phys.* 31, 1165–1168.

Han, Y.M., Samuel, A.M., Samuel, F.H., and Doty, H.W. (2008). "Dissolution of Al₂Cu phase in non-modified and Sr modified 319 type alloys." *Int. J. Cast Met. Res.* 21, 387–393.

Han, Y.M., (2008). "Effect of solution heat treatment type on the dissolution of copper phases Al-Si-Cu-Mg type alloys." *AFS Trans.*, 116, 79-90.

Hanna, M.D., Lu, S. Z., and Hellowell, A. (1984). "Modification in the aluminum silicon system." *Metall. Trans. A* 15, 459–469.

- He, K., Yu, F., Zhao, D., and Zuo, L. (2010). "Effect of phosphorus modification on the microstructure and mechanical properties of DC cast Al-17.5Si-4.5Cu-1Zn-0.7Mg-0.5Ni alloy." *Trans. Indian Inst. Met.* 62, 367–371.
- Hegde, S., and Prabhu, K.N. (2008). "Modification of eutectic silicon in Al–Si alloys." *J. Mater. Sci.* 43, 3009–3027.
- Hegde, S., Kumar, G., and Prabhu, K.N. (2006). "Effect of section thickness and modification on thermal analysis parameters of A357 alloy." *Int. J. Cast Met. Res.* 19, 254–258.
- Hernández, F.R., and Sokolowski, J.H. (2005). "Novel image analysis to determine the si modification for hypoeutectic and hypereutectic Al-Si alloys." *JOM* 57, 48–53.
- Hosseini, V.A., Shabestari, S.G., and Gholizadeh, R. (2013). "Study on the effect of cooling rate on the solidification parameters, microstructure, and mechanical properties of LM13 alloy using cooling curve thermal analysis technique." *Mater. Des.* 50, 7–14.
- Jolly, M. (2005). "Prof. John Campbell's ten rules for making reliable castings." *JOM*, May, 19-27.
- Kang, H.S., Yoon, W.Y., Kim, K.H., Kim, M.H., and Yoon, Y.P. (2005). "Microstructure selections in the undercooled hypereutectic Al–Si alloys." *Mater. Sci. Eng. A* 404, 117–123.
- Kashyap, K.T., and Chandrashekar, T. (2001). "Effects and mechanisms of grain refinement in aluminium alloys." *Bull. Mater. Sci.* 24, 345–353.
- Kasprzak, W., Sokolowski, J. H., Yamagata, H., Sahoo, M. and Kurita, H. (2009). "The effect of the melt temperature and the cooling rate on the microstructure of the Al- 20%Si alloy used for monolithic engine blocks." *International Journal of Metal casting*, 3(3), 55-73.

Kim C. B. and Heine P. W. (1963) "Fundamentals of modification in the aluminum-silicon system." *J. Inst. Metals*, 92, 367-376.

Kim, M. (2007). "Electron back scattering diffraction (EBSD) analysis of hypereutectic Al- Si alloys modified by Sr and Sc." *Met. Mater. Int.* 13, 103–107.

Kores, S., Vončina, M., Kosec, B., Mrvar, P., and Medved, J. (2010). "Effect of cerium additions on the AlSi17 casting alloy." *Mater. Tehnol.* 44, 137–140.

Kori, S.A., Murty, B.S., and Chakraborty, M. (2000). "Development of an efficient grain refiner for Al–7Si alloy and its modification with strontium." *Mater. Sci. Eng. A* 283, 94–104.

Korojy, B., and Fredriksson, H. (2009). "On solidification of hypereutectic Al-Si alloys." *Trans. Indian Inst. Met.* 62, 361–365.

Kowata, T., Hoire, H., Hiratsuka, S. and Chida, A. (1994). "Influence of rare-earth elements on refinement of primary silicon crystals in a hypereutectic Al-Si alloy." *IMONO*, 66, 803-808.

Kumar, G., Hegde, S., and Prabhu, K.N. (2007). "Heat transfer and solidification behaviour of modified A357 alloy." *J. Mater. Process. Technol.* 182, 152–156.

Kumar, T.S.P. and Prabhu, K.N. (1991). "Heat flux transients at the casting/chill interface during solidification of aluminium base alloys." *Metallurg. Trans. B*, 22, 717-727.

Kyffin, W.J., Rainforth, W.M., and Howard, J. (2001). "Formation of primary silicon during cooling and solidification of Al-20%Si alloy." *Mater. Trans.* 42, 2098–2101.

Kyffin, W.J., Rainforth, W.M., and Jones, H. (2001). "Effect of phosphorus additions on the spacing between primary silicon particles in a bridgman solidified hypereutectic Al-Si Alloy." *J. Mater. Sci.* 36, 2667–2672.

- Lasa, L., and Rodriguez-Ibabe, J.M. (2002). "Characterization of the dissolution of the Al₂Cu phase in two Al–Si–Cu–Mg casting alloys using calorimetry." *Mater. Charact.* 48, 371–378.
- Lee, P.D., and Sridhar, S. (2000). "Direct observation of the effect of strontium on porosity formation during the solidification of aluminium-silicon alloys." *Int. J. Cast Metal Res.* 13(4),185-198.
- Lescuyer, H., Allibert, M., and Laslaz, G. (1998). "Solubility and precipitation of AlP in Al–Si melts studied with a temperature controlled filtration technique." *J. Alloys Compd.* 279, 237–244.
- Li, J.G., Zhang, B.Q., Wang, L., Yang, W.Y., and Ma, H.T. (2002). "Combined effect and its mechanism of Al–3wt.% Ti–4wt.% B and Al–10wt.% Sr master alloy on microstructures of Al–Si–Cu alloy." *Mater. Sci. Eng. A* 328, 169–176.
- Li, Q., Xia, T., Lan, Y., Zhao, W., Fan, L., and Li, P. (2013). "Effect of rare earth cerium addition on the microstructure and tensile properties of hypereutectic Al–20%Si alloy." *J. Alloys Compd.* 562, 25–32.
- Li, W., Zhang, Y., Yi, D., Kong, F., and Chen, X. (2011). "Thermodynamics calculation of reactions between phosphorus and main elements in Al-Si-Cu alloys." *JOM* 63, 42–44.
- Liao, H., and Sun, G. (2003). "Mutual poisoning effect between Sr and B in Al–Si casting alloys." *Scr. Mater.* 48, 1035–1039.
- Liao, H., Zhang, M., Wu, Q., Wang, H., and Sun, G. (2007). "Refinement of eutectic grains by combined addition of strontium and boron in near-eutectic Al–Si alloys." *Scr. Mater.* 57, 1121–1124.
- Liao, H.C., Zhang, M., Bi, J.J., Ding, K., Xi, X., and Wu, S.Q. (2010). "Eutectic solidification in near-eutectic Al-Si casting alloys." *J. Mater. Sci. Technol.* 26, 1089–1097.

Lijia, H., Jianzhong, W., Jingang, Q., Huiling, D., and Zuofu, Z. (2010). "Influences of electric pulse on solidification structure of LM-29 Al-Si alloy." *China Foundry*, 7(2), 153-156

Liu, L., Samuel, A.M., Samuel, F.H., Doty, H.W., and Valtierra, S. (2003). "Influence of oxides on porosity formation in Sr-treated Al-Si casting alloys." *J. Mater. Sci.* 38, 1255–1267.

Liu, Y., Ding, C., and Li, Y. (2011). "Grain refining mechanism of Al-3B master alloy on hypoeutectic al-si alloys." *Trans. Nonferrous Met. Soc. China* 21, 1435–1440.

Lu, L., and Dahle, A.K. (2006). "Effects of combined additions of Sr and AlTiB grain refiners in hypoeutectic Al–Si foundry alloys." *Mater. Sci. Eng. A* 435-436, 288–296.

Lu, L., Nogita, K., McDonald, S.D., and Dahle, A.K. (2004). "Eutectic solidification and its role in casting porosity formation." *JOM* 56, 52–58.

Lu, S. Z., and Hellawell, A. (1987). "The mechanism of silicon modification in aluminum-silicon alloys: impurity induced twinning." *Metall. Trans. A* 18, 1721–1733.

Lu, S. Z., and Hellawell, A. (1995). "Modification of Al-Si alloys: microstructure, thermal analysis, and mechanisms." *JOM* 47, 38–40.

Ludwig, T.H., Schaffer, P.L., and Arnberg, L. (2013). "Influence of phosphorus on the nucleation of eutectic silicon in Al-Si alloys." *Metall. Mater. Trans. A* 44, 5796–5805.

Ma, Z., Samuel, E., Mohamed, A.M.A., Samuel, A.M., Samuel, F.H., and Doty, H.W. (2010). "Influence of aging treatments and alloying additives on the hardness of Al–11Si–2.5Cu–Mg alloys." *Mater. Des.* 31, 3791–3803.

- Ma, Z., Samuel, E., Mohamed, A.M.A., Samuel, A.M., Samuel, F.H., and Doty, H.W. (2010). "Parameters controlling the microstructure of Al–11Si–2.5Cu–Mg alloys." *Mater. Des.* 31, 902–912.
- Mandal, P., Saha, A. and Chakraborty, M. (1991). "Size of primary silicon particles and mechanical properties of as-cast high. Silicon Al alloys." *AFS Trans.* 99, 643–651
- Marchwica, P., Sokolowski, J.H., and Kierkus, W.T. (2011). "Fraction solid evolution characteristics of AlSiCu alloys-dynamic baseline approach." *J. Achiev. Mater. Manuf. Eng.* 47, 115–136.
- McDonald, S.D., Dahle, A.K., Taylor, J.A., and St. John, D.H. (2004). "Modification-related porosity formation in hypoeutectic aluminum-silicon alloys." *Metall. Mater. Trans. B* 35, 1097–1106.
- McDonald, S.D., Nogita, K., and Dahle, A.K. (2004). "Eutectic nucleation in Al–Si alloys." *Acta Mater.* 52, 4273–4280.
- Miresmaeili, S.M., Campbell, J., Shabestari, S.G., and Boutorabi, S.M.A. (2005). "Precipitation of Sr-rich intermetallic particles and their influence on pore formation in Sr-modified A356 alloy." *Metall. Mater. Trans. A* 36, 2341–2349.
- Mohamed, A.M.A., and Samuel, F.H. (2012). "A review on the heat treatment of Al-Si-Cu/Mg casting alloys." *Conv. Nov. Appl.* 229, 55-72
- Mohanty, P.S., and Gruzleski, J.E. (1996). "Grain refinement mechanisms of hypoeutectic Al-Si alloys." *Acta Mater.* 44, 3749–3760.
- Moldovan, P., Popescu, G., and Buțu, M. (2007). "Heat treatment of Al-7Si-0.3 Mg alloy previously inoculated with a new type of quaternary master alloy." *UPB Sci Bull Ser. B* 69, 91–98.
- Moller, H., Govender, G., and Stumpf, W.E. (2007). "Natural and artificial aging response of semisolid metal processed Al–Si–Mg alloy A356." *Int. J. Cast Met. Res.* 20, 340–346.

Mondolfo, L.F. (1976), "Aluminum Alloys: Structure and Properties." Butterworths, London-

Moustafa, M.A., Samuel, F.H., and Doty, H.W. (2003). "Effect of solution heat treatment and additives on the microstructure of Al-Si (A413.1) automotive alloys." *J. Mater. Sci.* 38, 4507–4522.

Nguyen, H. (2005). "The effects of solidification rates on porosity formation and cast microstructure of aluminum alloy A356." Thesis, Gd. Val. State Univ. Allendale.

Niklas, A., Abaunza, U., Fernandez-Calvo, A.I., Lacaze, J., and Suarez, R. (2011). "Thermal analysis as a microstructure prediction tool for A356 aluminium parts solidified under various cooling conditions." *China Foundry*, 8(1), 89-95.

Nogita, K., and Dahle, A.K. (2003). "Effects of Boron on eutectic modification of hypoeutectic Al-Si alloys." *Scr. Mater.* 48, 307–313.

Nogita, K., McDonald, S.D., and Dahle, A.K. (2003). "Effects of boron-strontium interactions on eutectic modification in Al-10 mass% Si alloys." *Mater. Trans.* 44, 692–695.

Nogita, K., McDonald, S.D., and Dahle, A.K. (2004). "Eutectic modification of Al-Si alloys with rare earth metals." *Mater. Trans.* 45, 323–326.

Nogita, K., Yasuda, H., Yoshiya, M., McDonald, S.D., Uesugi, K., Takeuchi, A., et al. (2010). "The role of trace element segregation in the eutectic modification of hypoeutectic Al-Si alloys." *J. Alloys Compd.* 489, 415–420.

Ogris, E., Wahlen, A., Lüchinger, H., and Uggowitzer, P.J. (2002). "On the silicon spheroidization in Al-Si alloys." *J. Light Met.* 2, 263–269.

Ojha, K.V., Tomar, A., Singh, D., and Kaushal, G.C. (2008). "Shape, microstructure and wear of spray formed hypoeutectic Al-Si alloys." *Mater. Sci. Eng. A* 487, 591–596.

Onyia, C.W., Okorie, B.A., Neife, S.I., and Obayi, C.S. (2013). "Structural modification of sand cast eutectic al-si alloys with sulfur/sodium and its effect on mechanical properties." *World J. Eng. Technol.* 1, 9–16.

Osório, W.R., Garcia, L.R., Goulart, P.R., and Garcia, A. (2007). "Effects of eutectic modification and t4 heat treatment on mechanical properties and corrosion resistance of an Al–9 wt% Si casting alloy." *Mater. Chem. Phys.* 106, 343–349.

Ouyang, Z., Mao, X., and Hong, M. (2007). "Multiplex Modification with rare earth elements and P for hypereutectic Al-Si alloys." *J. Shanghai Univ. Engl. Ed.* 11, 400–402.

Parkhutik, V.P., Glinenko, L.K., and Labunov, V.A. (1983). "Kinetics and mechanism of porous layer growth during N-type silicon anodization in hf solution." *Surf. Technol.* 20, 265–277.

Pei, Y. T. and De Hosson, J. Th. M. (2000). "Materials produced by laser cladding. " *Acta Mater.* 48, 2617-2624.

Pei, Y.T., and Hosson, J.Th.M. De (2001). "Five-fold branched si particles in laser clad al-si functionally graded materials." *Acta Mater.* 49, 561–571.

Prabhu, K. N, Jayananda and Hegde, S. (2012). "Effect of chemical modification of Al-Si alloys on thermal diffusivity and contact heat transfer at the casting/chill interface." *Journal of ASTM International*, 9(2), DOI:10.1520/JAI104057, Paper ID: JAI104057, pages 10.

Prabhu, K.N., and Ravishankar, B.N. (2003). "Effect of modification melt treatment on casting/chill interfacial heat transfer and electrical conductivity of Al–13% Si alloy." *Mater. Sci. Eng. A* 360, 293–298.

Prasad B. K., and Dan, T. K. (1991). "Influence of solutionizing temperature and duration on the microstructure and properties of a hypereutectic Aluminum-Silicon alloy-graphite composite." *J. Mater. Sci. Lett.* 10, 1412–1414.

Prasada Rao, A.K., Das, K., Murty, B.S., and Chakraborty, M. (2006). "Microstructural and wear behavior of hypoeutectic Al–Si alloy (LM25) grain refined and modified with Al–Ti–C–Sr master alloy." *Wear* 261, 133–139.

Qiyang, L., Qingchun, L., and Qifu, L. (1991). "Modification of Al-Si alloys with sodium." *Acta Metall. Mater.* 39, 2497–2502.

Ransley, C. E., and Neufeld, H. (1947/1948). "The solubility of hydrogen in liquid and solid aluminum." *J. Inst. Metals*, 74, 599-620.

Reif, W., Yu, S., Dutkiewicz, J., Ciach, R., and Król, J. (1997). "Pre-ageing of AlSiCuMg Alloys in relation to structure and mechanical properties." *Mater. Des.* 18, 253–256.

Robles Hernández, F.C., and Sokolowski, J.H. (2006). "Thermal analysis and microscopical characterization of Al–Si hypereutectic alloys." *J. Alloys Compd.* 419, 180–190.

Rometsch, P., Arnberg, L., and Zhang, D.L. (1999). "Modelling dissolution of Mg₂Si and homogenization in Al-Si-Mg casting alloys." *Int. J. Cast Met. Res.* 12, 1–8.

Rometsch, P.A., Schaffer, G.B., and Taylor, J.A. (2001). "Mass balance characterisation of Al-7Si-Mg alloy microstructures as a function of solution treatment time." *Int. J. Cast Met. Res.* 14, 59–69.

Samuel, A M, Ouellet, P, Samuel, F H, and Doty, H W (1998). "Microstructural interpretation of thermal analysis of commercial 319 Al alloy with Mg and Sr additions." *Trans. Am. Foundrymens Soc.* 105, 951–962.

Samuel, E.H., Samuel, A.M, and Doty, H.W (1996). "Factors controlling the type and morphology of Cu-containing phases in 319 Al alloy." *AFS Trans* 30, 893–301.

Samuel, F.H. (1998). "Incipient melting of Al₅Mg₈Si₆Cu₂ and Al₂Cu intermetallics in unmodified and strontium-modified Al–Si–Cu–Mg (319) alloys during solution heat treatment." *J. Mater. Sci.* 33, 2283–2297.

Sebaie, O.E., Samuel, A.M., Samuel, F.H., and Doty, H.W. (2008). "The effects of mischmetal, cooling rate and heat treatment on the eutectic si particle characteristics of A319.1, A356.2 and A413.1 Al–Si casting alloys." *Mater. Sci. Eng. A* 480, 342–355.

Shabestari, S.G., and Ghodrat, S. (2007). "Assessment of modification and formation of intermetallic compounds in aluminum alloy using thermal analysis." *Mater. Sci. Eng. A* 467, 150–158.

Shabestari, S.G., and Malekan, M. (2005). "Thermal analysis study of the effect of the cooling rate on the microstructure and solidification parameters of 319 aluminum alloy." *Can. Metall. Q.* 44, 305–312.

Shabestari, S.G., and Malekan, M. (2010). "Assessment of the effect of grain refinement on the solidification characteristics of 319 aluminum alloy using thermal analysis." *J. Alloys Compd.* 492, 134–142.

Shabestari, S.G., and Moemeni, H. (2004). "Effect of copper and solidification conditions on the microstructure and mechanical properties of Al–Si–Mg alloys." *J. Mater. Process. Technol.* 153-154, 193–198.

Shabestari, S.G., Keshavarz, M., and Hejazi, M.M. (2009). "Effect of strontium on the kinetics of formation and segregation of intermetallic compounds in A380 aluminum alloy." *J. Alloys Compd.* 477, 892–899.

Shabestri, S. G. and Ghodrat, S. (2007). "Assessment of modification and formation of intermetallic compounds in aluminum alloy using thermal analysis." *Mater. Sci. Engg. A*, 467,150-158.

Shankar, S., Riddle, Y.W., and Makhlof, M.M. (2004). "Eutectic solidification of aluminum-silicon alloys." *Metall. Mater. Trans. A* 35, 3038–3043.

Shivkumar, S., Ricci, S., Keller, C., and Apelian, D. (1990). "Effect of solution treatment parameters on tensile properties of cast aluminum alloys." *J. Heat Treat.* 8, 63–70.

Sigworth G.K., and Guzowski M. M. (1985). "Grain refining of hypo-eutectic Al-Si alloy." *AFS Trans.* 93, 907–912.

Sigworth, G. (2014). "Fundamentals of solidification in aluminum castings." *International Journal of Metal Casting*, 8 (1), 7-21

Sjolander, E., and Seifeddine, S. (2010). "The heat treatment of Al–Si–Cu–Mg casting alloys." *J. Mater. Process. Technol.* 210, 1249–1259.

Sritharan, T., and Li, H. (1997). "Influence of titanium to boron ratio on the ability to grain refine aluminium-silicon alloys." *J. Mater. Process. Technol.* 63, 585–589.

Sterner-Rainer, R. (1933). "Aluminium silicon alloy with a phosphorus content of 0.001 to 0.1%." US Patent, 1940922.

Suárez-Peña, B., and Asensio-Lozano, J. (2006). "Microstructure and mechanical property developments in Al–12Si gravity die castings after Ti and/or Sr additions." *Mater. Charact.* 57, 218–226.

Sulzer J, *Mod Castings* 39 (1960) 38." *J. Mater. Process. Technol.* 203, 333–341.

Suresha, K. M. and Prabhu, K. N. (2004). "Effect of superheat, mold and casting materials on the metal/mold interfacial heat transfer during solidification in graphite lined permanent molds." *J. Mater. Engg. Perfor.*, 13 (5), 619-626.

Tang, D., and Mao, X. (2000). "A new approach to refining and modifying cast aluminum alloys with rare earth alloys." *J. Shanghai Univ. Engl. Ed.* 4, 167–170.

Tanner, D.A and Robinson, J.S. (2004). "Effect of precipitation during quenching on the mechanical properties of the aluminium alloy 7010 in the W-temper." *J. Mater. Process. Tech.* 153–154, 998–1004.

Tash, M., Samuel, F.H., Mucciardi, F., and Doty, H.W. (2007). "Effect of metallurgical parameters on the hardness and microstructural characterization of as-cast and heat-treated 356 and 319 aluminum alloys." *Mater. Sci. Eng. A* 443, 185–201.

Tenekedjiev, N., D, A., and J E, G. (1989). "Sodium, strontium and phosphorus effects in hypereutectic Al-Si alloys." *AFS Trans.* 97, 127–136.

Totten, G.E., Webster, G.M. and Bates, C.E. (2003). "Chapter 20-Quenching, Handbook of Aluminum: Volume 1 – Physical Metallurgy and Processes." CRC Press, Boca Raton, FL, 971-1062.

Velasco, E., Talamantes, J., Cano, S., Valterra, S., Mojica, J. E. and Colas, R. (1999). "Casting-chill interface heat transfer during solidification of an aluminum alloy." *Metall. Mater. Trans. B*, 30B, pp.773-778.

Veldman, N.L., Dahle, A.K., StJohn, D.H., and Arnberg, L. (2001). "Dendrite coherency of Al-Si-Cu Alloys." *Metall. Mater. Trans. A* 32, 147–155.

Voncina, M., Mrvar, P., Petric, M., and Medved, J. (2012). "Microstructure and grain refining performance of Ce on A380 Alloy." *J. Min. Metall. Sect. B Metall.* 48, 265–272.

Wang, G., Bian, X., Wang, W., and Zhang, J. (2003). "Influence of Cu and minor elements on solution treatment of Al–Si–Cu–Mg cast alloys." *Mater. Lett.* 57, 4083–4087.

Wang, T., Fu, H., Chen, Z., Xu, J., Zhu, J., Cao, F., et al. (2012). "A novel fading-resistant Al–3Ti–3B grain refiner for Al–Si alloys." *J. Alloys Compd.* 511, 45–49.

Winegard, W.C., Majka, S., Thall, B.M., and Chalmers, B. (1951). "Eutectic solidification in metals." *Can. J. Chem.* 29, 320–327.

Wu, Y., Liu, X., Jiang, B., and Huang, C. (2010). "Eutectic nucleation in Al-25wt.%Si alloy through DSC." *Rare Met.* 29, 62–65.

Wu, Y., Wang, S., Li, H., and Liu, X. (2009). "A new technique to modify hypereutectic Al–24%Si alloys by a Si–P master alloy." *J. Alloys Compd.* 477, 139–144.

Xiao, B., Wang, Q., Jadhav, P. and Li, K. (2010). "An experimental study of heat transfer in aluminum castings during water Quenching." *J. Mater. Process. Tech.*, 210, 2023–2028.

Xiaowu, H.U., Fanrong, A.I., and Hong, Y.A.N. (2012). "Influences of pouring temperature and cooling rate on microstructure and mechanical properties of casting Al-Si-Cu aluminum alloy." *Acta Metall. Sin. Engl. Lett.* 25, 272–278.

Xing, P., Gao, B., Zhuang, Y., Liu K And Ganfeng, T.U. (2010). "On the modification of hypereutectic Al-Si alloys using rare earth Er." *Acta Metall. Sin. (Engl. Lett.)* 23, 327-333

Xiufang, B., Weimin, W., Shujuan, Y., and Jingyu, Q. (2001). "Structure factors of modified liquid Al–Si Alloys." *Sci. Technol. Adv. Mater.* 2, 19–23.

Xu, C.L., and Jiang, Q.C. (2006). "Morphologies of primary silicon in hypereutectic Al–Si alloys with melt overheating temperature and cooling rate." *Mater. Sci. Eng. A* 437, 451–455.

Xu, C.L., Wang, H.Y., Liu, C., and Jiang, Q.C. (2006). "Growth of octahedral primary silicon in cast hypereutectic Al–Si alloys." *J. Cryst. Growth* 291, 540–547.

Yamagata, H., Kasprzak, W., Aniolek, M., Kurita, H., and Sokolowski, J.H. (2008b). "The effect of average cooling rates on the microstructure of the Al–20% Si high pressure die casting alloy used for monolithic cylinder blocks." *J. Mater. Process. Technol.* 203, 333–341.

Ying, Z., Dan-Qing, Y., Wang-Xing, L., Zhi-Sen, Ren., Qun, Z., and Jun-Hong, Z., (2007). "Transformation of microstructure after modification of A390 alloy." *Trans. Nonferrous Met. Soc. China* 17, 413–417.

Yu, F., Pei, J., He, K., Zhao, D., and Zuo, L. (2009). "Solidification microstructure and temperature field during direct chill casting of Al-16Si alloy." *Trans. Indian Inst. Met.* 62, 347–351.

Zhang, H., Duan, H., Shao, G., And Xu, L. (2008). "Microstructure and mechanical properties of hypereutectic Al-Si alloy modified with Cu-P." *Rare Met.* 27, 59–63.

Zhang, H., Duan, H., Shao, G., Xu, L., Yin, J., And Yan, B. (2006). "Modification mechanism of cerium on the Al-18Si Alloy." *Rare Met.* 25, 11–15.

Zhongwei, C., and Ruijie, Z. (2010). "Effect of strontium on primary dendrite and eutectic temperature of A357 aluminum alloy." *China Foundry*, 7(2), 149-152.

Zhou, J., and Duszczuk, J. (1990). "Fracture features of a silicon-dispersed aluminium alloy extruded from rapidly solidified powder." *J. Mater. Sci.* 25, 4541–4548.

Zhu, M., Jian, Z., Yang, G., and Zhou, Y. (2012). "Effects of T6 heat treatment on the microstructure, tensile properties, and fracture behavior of the modified A356 Alloys." *Mater. Des.* 36, 243–249.

Zhu, M., Jian, Z., Yao, L., Liu, C., and Yang, G. (2011). "Effect of mischmetal modification treatment on the microstructure, tensile properties, and fracture behavior of Al-7.0%Si-0.3%Mg foundry aluminum alloys." *J. Mater. Sci.* 46, 2685–2694.

Zuo, M., Liu, X., and Sun, Q. (2009). "Effects of processing parameters on the refinement of primary Si in A390 alloys with a new Al–Si–P master alloy." *J. Mater. Sci.* 44, 1952–1958.

Zuo, M., Liu, X., Dai, H., and Liu, X. (2009). "Al-Si-P master alloy and its modification and refinement performance on Al-Si alloys." *Rare Met.* 28, 412–417.

LIST OF PUBLICATIONS (Based on this Ph.D research work)

Peer Reviewed Journals

1. Vijeesh, V., and Prabhu, K.N. (2014). "Review of microstructure evolution in hypereutectic Al-Si alloys and its effect on wear properties". Transactions of the Indian Institute of Metals 67 (1), 1-18
2. Vijeesh, V., and Prabhu, K.N. (2014). "Computer aided cooling curve analysis and microstructure of cerium added hypereutectic Al-Si (LM29) alloy". Transactions of the Indian Institute of Metals, 67(4), 541-549
3. Vijeesh, V., and Prabhu, K.N. (2015). "The effect of chilling and cerium addition on the microstructure and cooling curve parameters of Al-14%Si alloy". Canadian Metallurgical Quarterly, 54, 66-76.
4. Vijeesh, V., and Prabhu, K.N. (2015). "Effect of varying cooling rate and cerium melt treatment on thermal analysis parameters and microstructure of hypoeutectic Al-Si alloy". Light Metals-2015, 403-407.
5. Vijeesh, V., and Prabhu, K.N. "The effect of Ce addition on casting/chill interfacial heat flux and casting surface profile during solidification of Al-14% Si alloy". , IOP Conf. Series: Materials Science and Engineering, 117 (2016) 012034 doi:10.1088/1757-899X/117/1/012034
6. Vijeesh, V., and Prabhu, K.N. (2015). "Assessment of latent heat and solid fraction of Al-22Si alloy using Newtonian and Fourier analysis techniques". Materials Science Forum, Materials Science Forum, 830-831, 321-324.
7. Vijeesh, V., and Prabhu, K.N. (2015). "The effect of addition of Ce and Sr on the solidification path of Al-8Si-2Cu alloy". Transactions of the Indian Institute of Metals, 68 (6), 1119-1123.
8. Vijeesh, V., and Prabhu, K.N. "Simultaneous refinement and modification of Al-8%Si alloy by the addition of cerium". International Journal of Cast Metal Research DOI 10.1080/13640461.2016.1144698

Conference Proceedings

1. Vijeesh, V., and Prabhu, K.N. "The effect of Sr modification on casting/chill interfacial heat flux and casting surface profiles during solidification of Al-7Si

alloy". CRT 2013 Conference, SDM Institute of Technology, Ujire, access through <http://ieeexplore.ieee.org/>

Conference Presentations

1. Vijeesh V and K.N. Prabhu, Effect of cooling rate on microstructure and thermal analysis parameters of hypereutectic Al-14% Si alloy". International Conference on Advanced Functional Materials, Trivandrum, India, 19-21, February 2014.
2. Vijeesh, V., and Prabhu, K.N. "Effect of varying content of Sr addition on dendrite coherency of near eutectic Al-11% Si alloy". NMD ATM 2014, November 2014, 12-15, Pune.

BIODATA

Name : VIJEESH V
Date of birth : 3rd January 1985
Permanent Address : 'Thayyil Thekathil, Panmana Puthenchanda,
Chavara, Kollam, Kerala-691583
Email : vijeesh3@gmail.com

Academic Qualifications

B. E (Mechanical) : St. Joseph Engineering College Mangalore (2007)
M.Tech (Process Metallurgy) : National Institute of Technology Karnataka
Surathkal, Mangalore-575025
Work Experience : 2 years of Industrial and Teaching